Synthesis and Characterisation of molecular materials

Davies, Hazel

Award date:
2008

Awarding institution:
University of Bath

Synthesis and Characterisation of molecular materials.

Volume 1 of 1

Hazel Mary Davies

A thesis submitted for the degree of Doctor of Philosophy

University of Bath

Department of Chemistry

December 2008

Copyright

University of Bath, 22nd December 2008

Acknowledgments

Firstly I would like to thank my Supervisors Paul and Andy for their encouragement, patience and support over the past four years, you have both been fantastic.

Thank you to the Daresbury Laboratories and EPRSC for funding.

I would also like to thank the entire Raithby/Johnson group present and past, it has been a real pleasure to be part of the group. Thanks to John Lowe and Simon Brayshaw for help with their help with the NMR machines, John I'm sorry for the number of times I crashed the machine. Also thanks to Anneke Lubben, Alan and Robert for all their help, samples they have run for me and equipment they have provided over the years. Also thanks to Dr Frank Marken for his valuable electrochemistry help.

Thank you to Dr Stuart Reid for his support and encouragement.

Thank you to my MChem students Chris and Mike who helped to me to explore many synthetic routes I would never have had time to do myself. Also for keeping me smiling and introducing me to new bands.

The past four years in Bath have been challenging and full of highs and lows but a massive thank you to all my friends for providing chocolate, hugs, alcohol and general support without you I would have gone mad!

Declaration

The work described in this thesis was conducted by the author at the University of Bath between January 2005 and March 2008. It represents the author's original and independent work, except where specific reference is made to the contrary. Neither the whole nor any part of this thesis has been submitted previously in support of a degree at this or any other university. It does not exceed the prescribed limit, including tables, references and appendices.

Abstract

Chapter 1 contains a brief background into subjects such as Robin-Day classes, binary code, logic gates and electrochemistry in order to aid understanding of the rest of the chapter. The unique paradigm of Molecular Quantum Cellular Automata (MQCA) is presented along with the advantages it offers to traditional silicon based electronics. A summary of the existing modelled and synthesised MQCA systems is included along with an explanation of the characteristics required for materials to be suitable for MQCA.

The subject of chapter 2 is cyclopentadiene cobalt cyclobutadiene complexes for the application of MQCA. The introduction examines the mechanism for the formation of cyclopentadiene cobalt cyclobutadiene complexes and the bonding in these compounds. A range of acetylenes were prepared for the formation of cyclopentadiene cobalt cyclobutadiene complexes were examined and characterised. Metal fragments including $\{Ru(dppe)_2Cl\}$ and $AuPPh_3Cl$ were attached to a cyclopentadiene cobalt cyclobutadiene core and these materials were characterised.

The subject of chapter 3 is benzene based materials for the application of MQCA. 1,2,4,5-*tetrakis*(ferrocenylethynyl)benzene was prepared, characterised and the electrochemistry was examined for electronic communication between the ferrocene sites. A range of two metal centre compounds were examined for solubility and electrochemical stability with the view of preparing four metal centre compounds with a benzene core.

The subject of chapter 4 is porphyrin based materials. This was the first area of work for this thesis and was discontinued. A brief summary of the synthetic work carried out is described, along with some literature work that was published whilst this work was being carried.

Chapter 5 contains the experimental information for chapters 2-4.

Abbreviations

E_a	Activation barrier
A	Acceptor
A	Alpha
Å	Angstrom
E_{pa}	Anodic potential
Ar	Aromatic
AFM	Atomic Force Microscopy
β	Beta
br	Broad
BuLi	Butyl Lithium
E_{pc}	Cathodic potential
v_0	Change of free energy ΔG (cm^{-1})
K_c	Comproportionation constant
J	Coupling constant
i	Current
i_{pf}	Current of the forward peak with respect to the baseline.
i_{pf}	Current of the reverse peak with respect to the baseline.
Cb	Cyclobutadiene
Cp	Cyclopentadienyl
[CpCoCb]	Cyclopentadiene Cobalt Cyclobutadiene
β'	Damping factor
°	Degree
DCPA	DC Potential Amperometric
DCM	Dichloromethane
DDQ	4,5-dichloro-3,6-dioxo-1,4-cyclohexadiene-1,2-dicarbonitrile
Depe	1,2-*bis*(diethylphosphino)ethane

ΔE	Difference between the peak potentials
DMF	Dimethylformamide
Dmpe	1,2-*bis*(dimethylphosphino)ethane
Dppe	Diphenylphosphinoethane
Dppm	1,2-*bis*(diphenylphosphino)methane
r	Distance between the two sites
D	Donor
D-B-A	Donor-Bridge-Acceptor
d	Doublet
α^2	Electronic Coupling Parameter
ET	Electron Transfer
EPR	Electron Paramagnetic Resonance
eq.	Equivalents
EtOH	Ethanol
ε	Extinction Coefficient
F	Faradays constant
Fc	Ferrocene
Fc/Fc^+	Ferrocene/Ferrocenium couple
$[FcH][PF_6]$	Ferrocenium hexafluorophosphate
$\Delta E^{\circ\prime}$	Formal electrode potential of the couple Ox/red
G	Free energy
TFA	Trifluoroacetic acid
fwhm	Full width at half maximum
$\Delta\nu_{1/2}$	Full width at half height (cm^{-1})
HF	Hartree-Fock
Tp*	hydrotris(3,5-dimethylpyrazolyl)borate
HOMO	Highest Occupied Molecular Orbital

IP	Ionisation potential
IVT	Intervalence transfer
IVCT	Intervalence charge transfer
IR	Infra-red
KS	Kohn-Sham
L	Ligand
LUMO	Lowest Unoccupied Molecular Orbital
M.p.	Melting point
MMCT	Metal-to-Metal Charge Transfer
MeOH	Methanol
mV	Millivolt
MQCA	Molecular Quantum Cellular Automata
m	Multiplet
NIR	Near Infrared
NMR	Nuclear Magnetic resonance
n	Number of electrons
N	Number of hopping steps
Ox	Oxidant
ppm	Parts Per Million
ΔE_p	peak separation between the forward and the reverse peak.
Ph	Phenyl
Pdma	1,2-phenylenebis(dimethyl)arsine
hν	Photon
E_{pa}	Potential of the anodic peak

E_{pc}	Potential of the cathodic peak.
E_{pf}	Potential of the forward peak
E_{pr}	Potential of the reverse peak
QCA	Quantum Cellular Automata
Red	Reductant
v	Scan rate
s	Singlet
SOMO	Singly Occupied Molecular Orbital
SPS	Solvent Purification System
$TBAPF_6$	Tetrabutylammonium hexafluorophosphate
TCE	Tetracyanoethylene
Bu_4NF	Tetra-*n*-butylammonium fluoride
THF	Tetrahydrofuran
H_2TFCP	5,10,15,20-tetraferrocenylporphyrin
TPP	5,10,15,20-*tetra*-pyridin-4-yl-porphyrin
TLC	Thin Layer Chromatography
α’	Transfer Coefficient
ν_{max}	Transition energy (cm^{-1})
OTf	Trifluoromethanesulfonate
TMS	Trimethylsilyl
TIPS	Triisopropylsilyl
t	Triplet
EE	Two one electron transfers
UV-Vis	Ultraviolet-visible
V	Volts

v/v	Volume per Volume
XPA	X-ray Bragg Profile analysis
XPS	X-ray Photospectroscopy

1. Chapter 1: Introduction

The principle of electronic devices has changed little over the past fifty years utilising binary code and switches for the storage and transfer of data. However, the main driving force for the electronics industry is the desire to manufacture smaller and faster devices, which requires sophisticated manufacturing techniques. With the miniaturisation of silicon-based electronic devices many problems have been encountered including spiralling manufacturing costs, quantum mechanical effects and huge quantities of heat generated. In the 1970s one alterative to current silicon-based electronics was proposed, this being molecular electronics. This is the concept of utilising a single molecule or a group of molecules as the fundamental units for electronic components such as wires, switches, memories or transistors.[1] While many areas of molecular electronics aim to be compatible with silicon-based electronics there are a few areas which are completely new concepts, one of these is Molecular Quantum Cellular Automata (MQCA). The synthesis and characterisation of new materials for the utilisation in MQCA applications is the focus of this thesis.

By a way of an introduction to this new concept, chapter 1 will firstly discuss Moore's law and the future of the electronics industry. An explanation of some definitions and fundamentals of subjects such as binary code, Robin-Day classifications and electrochemistry has been included to aid understanding of a relatively new area of research. The concept and existing research into MQCA will then be presented.

1.1 The future of the electronics industry

In 1965 Gordon Moore published a ground breaking paper observing 'that the functional area of a transistor was halving approximately every eighteen to twenty-four months'.[2] This observation has become known as Moore's law and has become one of the driving forces behind development in the electronics industry. This law is represented by the

graph shown in Figure 1 which shows the increasing number of transistors in an integrated circuit over time.

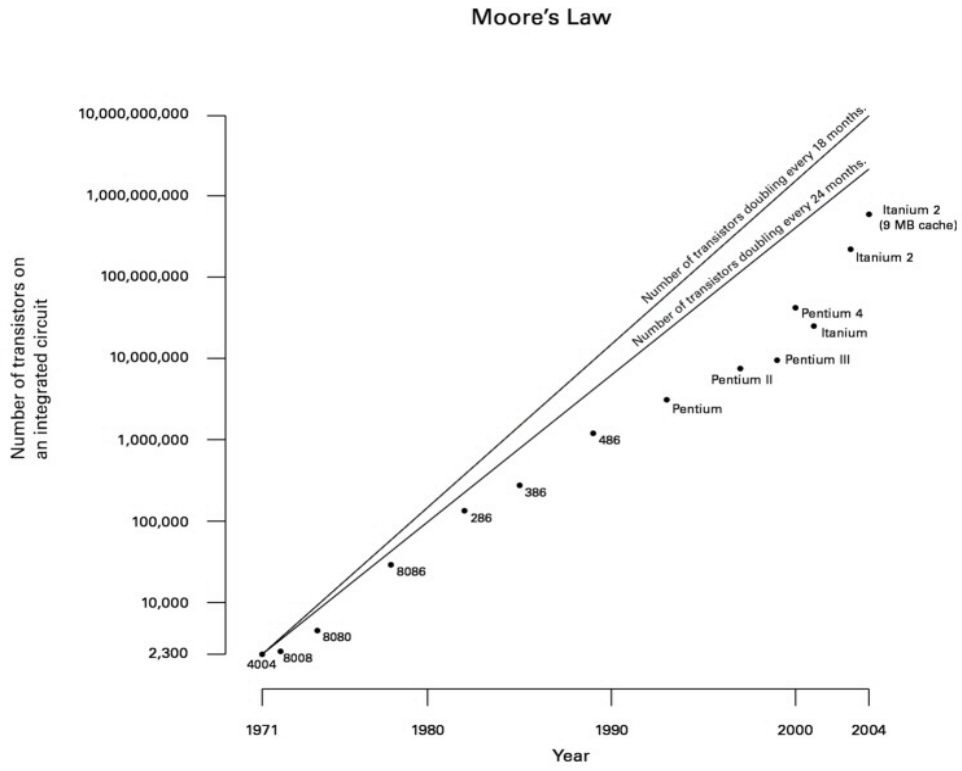

Figure 1. Plot of the increasing number of transistors in an integrated circuit over time. Black dots represent Intel processors. Taken from [3].

Moore believed that his prediction would be true for 10 years, however it has remained true for over forty years and it is believed that it will continue to be relevant until approximately 2012. It has been predicted that around 2012 silicon-based devices will reach their smallest possible size because of limits in manufacturing technology and quantum effects. Charge leakage has already become a problem due to the insulating silicon oxide layers being only 3 atoms thick.[1] In 2001 Intel's new fabrication facility cost $2 billion to construct, it is estimated that by 2010 this cost will have risen to $15-30 billion due to the sophisticated equipment required.[1] While the electronics industry battles to improve lithography techniques and solve the problems that silicon-based devices are beginning to experience, researchers have been looking at alternatives to silicon in areas such as molecular devices.

1.2 Robin-Day Classes and electronic communication

In order for compounds to be suitable for MQCA it is necessary for them to fulfil a number of criteria. Prior to the discussion of MQCA and the selection criteria it is important to explain some relevant background so that the unique solution that MQCA offers can be appreciated and also to understand the relevance of the criteria and the existing research.

1.2.1 Robin-Day Classes

Robin-Day classes are classifications of mixed valence compounds, which are compounds that contain ions of the same element in two different oxidation states.[4] A classic example of a mixed-valence compound is the 'Creutz-Taube ion' $[(NH_3)_5Ru\text{-}(N_2C_4H_4)\text{-}Ru(NH_3)_5]^{5+}$ which contains Ru^{II} and Ru^{III}. There are three classes of mixed valence compounds in the Robin-Day system, the characteristics are summarised in Table 1.

	Class I	Class II	Class III
Geometry	Metal ions in ligand fields are of very different symmetry and/or strength. *i.e.* tetrahedral compared to octahedral.	Metal ions in ligand field have nearly identical symmetry, differing only ~0.10-0.20 Å.	Metal ions are indistinguishable.
Interaction between sites	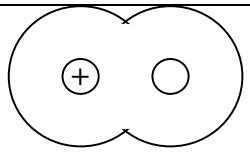 No interaction between sites, the charge is localised on one site.	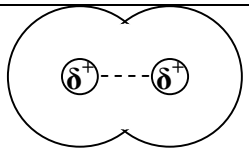 Interaction between sites, the charges are distinguishable but with slight delocalisation.	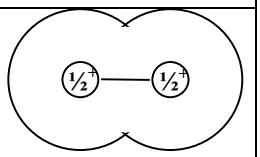 Complete delocalisation over sites.
Properties	Optical and electronic properties are equal to the sum of the components.	New optical and electronic properties are observed as well as those for the constituent components.	New optical and electronic properties

Table 1. Summary of some keys features of the three different Robin-Day classes.[4,5]

In Class I compounds the charge is located on one site and there is a high barrier to electron transfer between the two sites. In Class III the charge is localised over the molecule and electron transfer has no barrier, and Class II is an intermediate between these two states. The potential energy surfaces for the different classes and the energy barriers are shown in Figure 2.

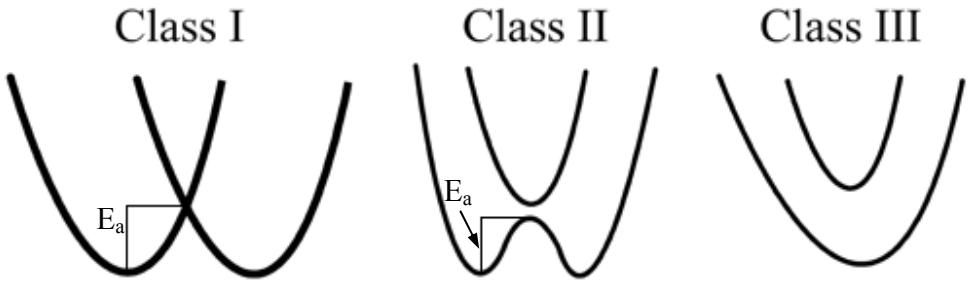

Figure 2. Potential energy surfaces for the Robin-Day mixed-valence classes. E_a is the energy barrier to electron transfer. Adapted from [6]

There are two main values used to determine the Robin-Day classes, these are the comproportionation constant K_c and the electronic coupling parameter α^2.

The comproportionation constant K_c can be measured electrochemically and is a measure of the stability of the mixed-valance state.[7] For the following reaction:

$$M^n + M^{(n-2)} \rightleftharpoons 2M^{(n-1)}$$

$$\text{at } 25°C \quad K_c = 10^{\Delta E/59mV} = [M^{(n-1)}]^2/[M^n][M^{(n-2)}]$$

As a general indication:[8]

- Robin Day class I $K_c < 10^2$
- Robin Day Class II $10^2 < K_c < 10^6$
- Robin Day Class III $K_c > 10^6$

Another measure of the effectively of the electron transfer is the electronic coupling parameter α^2 which can be obtained by examination of the intervalence charge transition (IVCT). The Hush equation is shown below

$$\nu_{max} - \nu_0 = (\Delta\nu_{1/2})^2 / 2310 \text{ cm}^{-1}$$

ν_{max} = transition energy (cm^{-1}), $\Delta\nu_{1/2}$ = full width at half height in cm^{-1}, ν_0 = change of free energy ΔG (cm^{-1}).[9]

Leading to

$$\alpha^2 = (4.2 \times 10^{-4})(\varepsilon_{max}\Delta\nu_{1/2})/ \nu_{max}r^2$$

ε ($Mol^{-1}cm^{-1}$) and r = distance between redox sites (Å).

Another common indication of the class of complex is given by the ratio $\Delta\nu_{1/2obs}/ \Delta\nu_{1/2calc,}$ for class III this is often found to be considerably greater than 1,[10] and for class II compounds it is typically reported to be between 1.1 and 1.4.[11-13]

1.2.2 Electron transfer

A Robin-Day mixed-valence system can be thought of as consisting of an electron donor site and an electron acceptor site connected by a bridging ligand though which electrons can pass as shown in Figure 3.

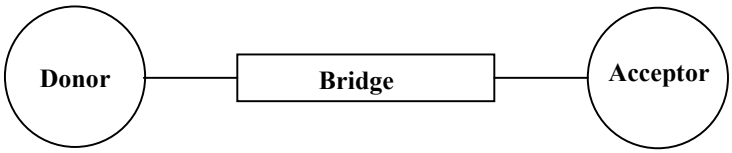

Figure 3. Donor-bridge-acceptor system.

Even though in a symmetrical system both the sites are identical apart from the extra electron, the presence of this electron causes the equilibrium intramolecular and solvent configurations to be different at the two sites. This causes inequivalence between the two sites and there to be a barrier to their interconversion. Energy conservation requires that before the electron transfer can take place the nuclear configurations of the reactants

and the surrounding medium must adjust from their equilibrium values to an intermediate configuration as shown in Figure 4. This means that there is no energy change when the electron transfer occurs. When the distance between the sites is large or their interaction is symmetry or spin forbidden then the electron interaction will be weak and the electron transfer will be slow.[14]

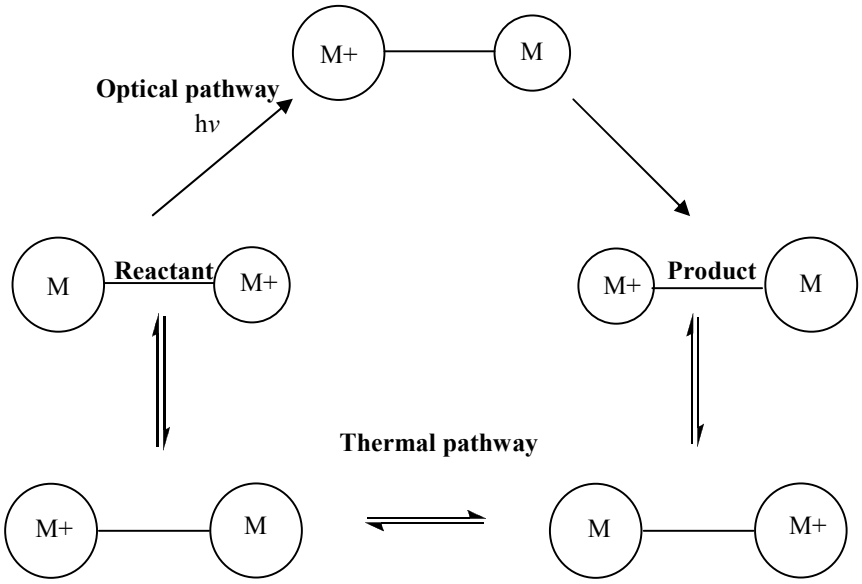

Figure 4. Optical and thermal electron transfer processes in a symmetric binuclear mixed valence complex. Adapted from [14].

Whilst thermal electron transfer can not occur without rearrangement of the complex, optical electron transfer can occur as shown in Figure 4. This pathway occurs when absorption of the correct frequency of light provides sufficient energy for the formation of the excited state. This process gives rise to intervalence transfer (IVT) absorption which is also known as metal-to-metal charge transfer (MMCT) absorption.[15]

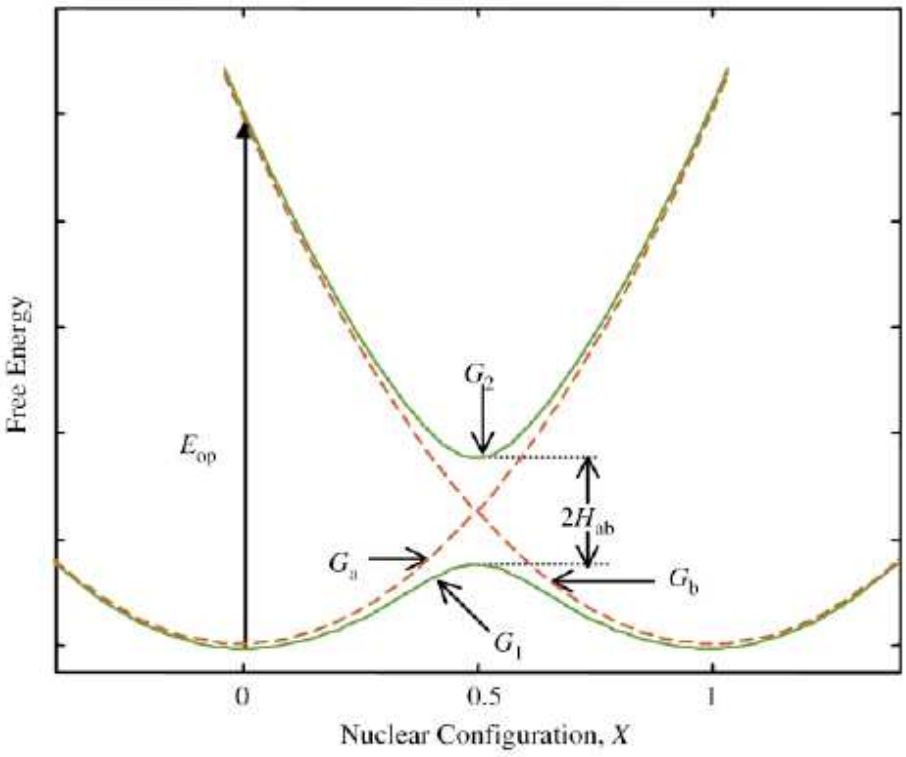

Figure 5. Plot of the free energies of the initial (left-hand parabola, G_a) and final (right hand parabola, G_b) states of a symmetric mixed-valence system *vs.* the reaction co-ordinate. Taken from[14].

Figure 5 shows the free energy curves for a mixed-valence system, where E_{op} is the energy of the donor-acceptor (MMCT or IVCT) charge-transfer transition; the top curve is the optical electron transfer pathway. The lower curve is the thermal electron transfer pathway, the barrier to this process is the energy difference between x=0 and x=0.5. H_{ab} is the electronic coupling matrix element between the states.

1.2.2.1 Mechanisms for electron transfer

There are three basic mechanisms for molecular charge-transfer. The first is super-exchange – this is where an electron or hole is transferred in a single step from the donor to the acceptor and the bridge is the medium for the electronic coupling. In this process the redox state of the bridge does not change and the probability of transferring an electron/hole from donor to acceptor generally decreases exponentially with distance.[16]

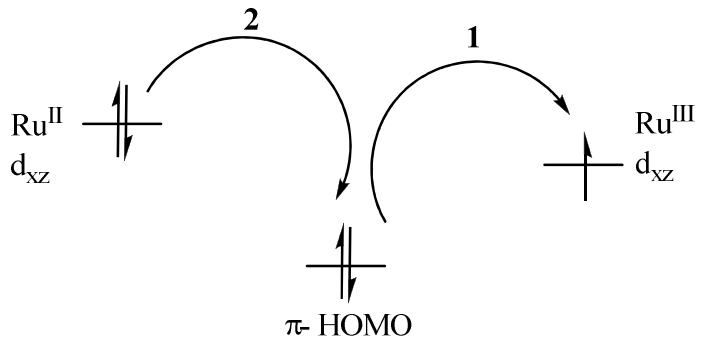

Figure 6. Schematic diagram representation of the hole transfer super-exchange process, showing a concerted process as two sequential electron transfers between the bridging ligands π-HOMO and the acceptor (Ru^{III}) and the donor (Ru^{II}). Adapted from [17].

The hole transfer super-exchange process is shown in Figure 6, the first electron transfer is from the π-HOMO of the bridging ligand to the acceptor (Ru^{III} d_{xz} orbital). A second electron transfer then occurs from the donor (Ru^{II} d_{xz} orbital) to the π-HOMO orbital. It is termed as a hole transfer process as the concerted event is the movement of the electron hole across the molecule. When the metal-to-metal charge transfer is mediated by the bridging ligand LUMO, the process is known as electron transfer as the electron transfers from the donor to the LUMO and then to the acceptor.

For super-exchange the rate is given by[18]

$$k_{ET} \alpha e^{(-\beta' r)}$$

Where r = distance between the two sites and β' is the damping factor based on distance effects, free energy and reorganisation barriers.

The second mechanism is tunnelling where an electron or hole tunnels under successive energy barriers from one side to the next until it reaches a charge trap. Because this occurs through the barrier and not over the barrier, nuclei rearrangement does not occur before the electron transfer.[16]

Both these mechanisms have a weak temperature dependence arising from the coupling between the donor and acceptor sites or between adjacent sites.[16]

The third mechanism is charge-hopping; this is when the charge is injected from the donor into a bridge which consists of a series of weakly coupled units between which the charge hops until it reaches the acceptor as shown in Figure 7. The rate k_{ET} is dependant upon the number of hopping steps (N) and is given by [18]

$$k_{ET} = N^{-\eta} \text{ where } \eta \approx 1\text{-}2$$

The critical factor is the injection of charge from the donor into the bridge and hence the energy gaps between the donor and bridge must not be too large. If the energy gap is too large then the super-exchange mechanism can also occur.

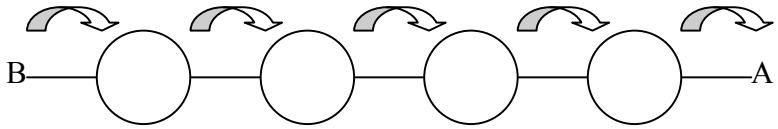

Figure 7. Schematic diagram representation of charge hopping from B to A. Adapted from [18].

It is thought that in complex systems charge transfer is a combination of three mechanisms.

The key requirement of the bridging ligand is that it has the correct symmetry empty orbital to overlap with that of the metal, so that an electron can transfer from the metal to the empty ligand orbital. It is also necessary for there to be a barrier so that the electron could not transfer freely. The second metal in the molecule will need an empty d-orbital to accept the electron. Any spectator ligands on the bridge or metals can also affect the energies of the orbitals depending upon their electronic properties.

In a donor-bridge-acceptor (DBA) system there are three main factors that effect the electron transfer rates these are ; the structure of the bridge, the energy gap in the DBA system and the bridge length or the distance between D and A.

1.2.2.2 Electrochemistry

Electrochemistry is a very valuable tool for evaluation of electronic communication between metal centres. Calculation of the comproportionation constant by electrochemical measurements gives a good indication of the communication within the sites.

A cyclic voltammogram of a fully reversible system is shown in Figure 8 showing the common electrochemical parameters which are often referred to the electrochemical results.

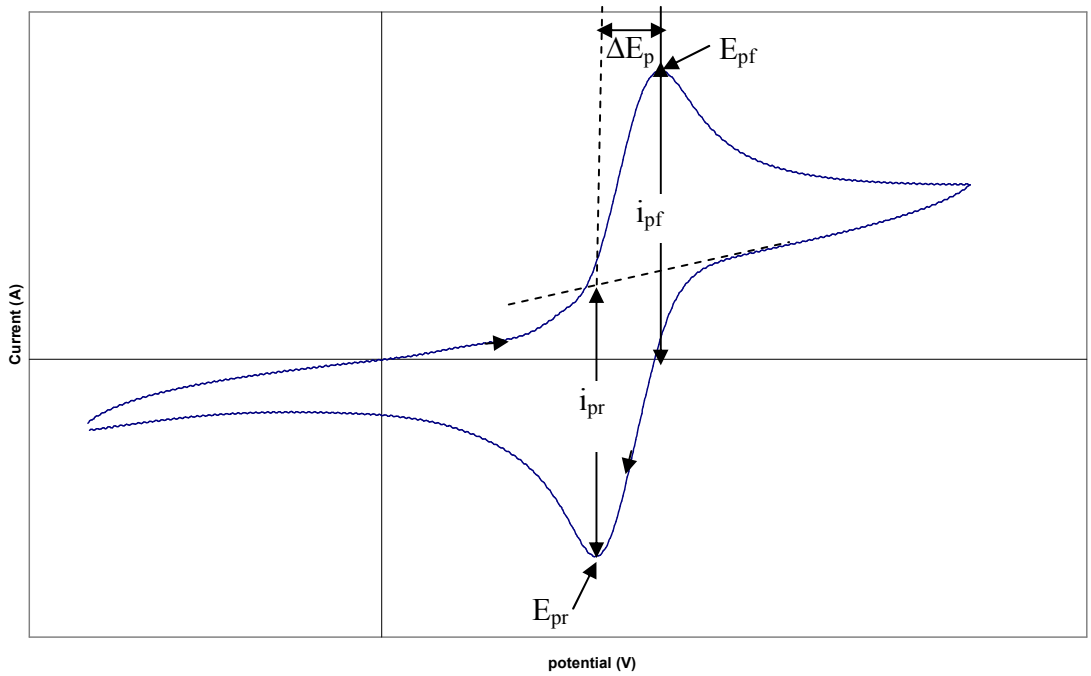

Figure 8. Cyclic voltammogram of a reversible process which in this case is of ferrocene showing the different electrochemical parameters. E_{pf} = potential of the forward peak, E_{pr} = potential of the reverse peak, ΔE_p = the peak separation between the forward and the reverse peak. i_{Pf} = current of the forward peak with respect to its baseline and i_{Pr} = current of the reverse peak with respect to its baseline.

Whilst Figure 8 shows a fully reversible redox couple such as ferrocene, this is not always the case in electrochemistry; redox processes can also be irreversible or quasi-reversible. The key features that classify the processes are summarised in Table 2.

Reversible process	Irreversible process	Quasi-reversible process
E_{pf} is independent of the scan rate.	E_{pf} shifts with scan rate	E_{pf} shifts with scan rate
ΔE_p(mV) = 59/n at 25°C. This value remains constant with changes in scan rate	Generally no reverse reaction	$\Delta E_p > 59/n$ at 25°C
$i_{pr}/i_{pf} = 1$	-	$i_{pr}/i_{pf} = 1$ when $\alpha' = 0.5$ $i_{pr}/i_{pf} < 1$ when $\alpha' > 0.5$ $i_{pr}/i_{pf} > 1$ when $\alpha' < 0.5$
$i_{pf}/\sqrt{v}$ is constant with scan rate	$i_{pf}/\sqrt{v}$ is constant with scan rate	$i_{pf}/\sqrt{v}$ non linear dependence

Table 2. Summary of the features of different electrochemical processes. Where n = number of electron exchanged per molecule of Ox for Ox + *n*e- $\rightleftharpoons$ Red, *α'* = transfer coefficient which is a measure of the symmetry of the energy barrier and *v* = scan rate.

An example of a cyclic voltammogram showing an irreversible process is shown in Figure 9, which shows three irreversible reduction processes with no reverse waves.

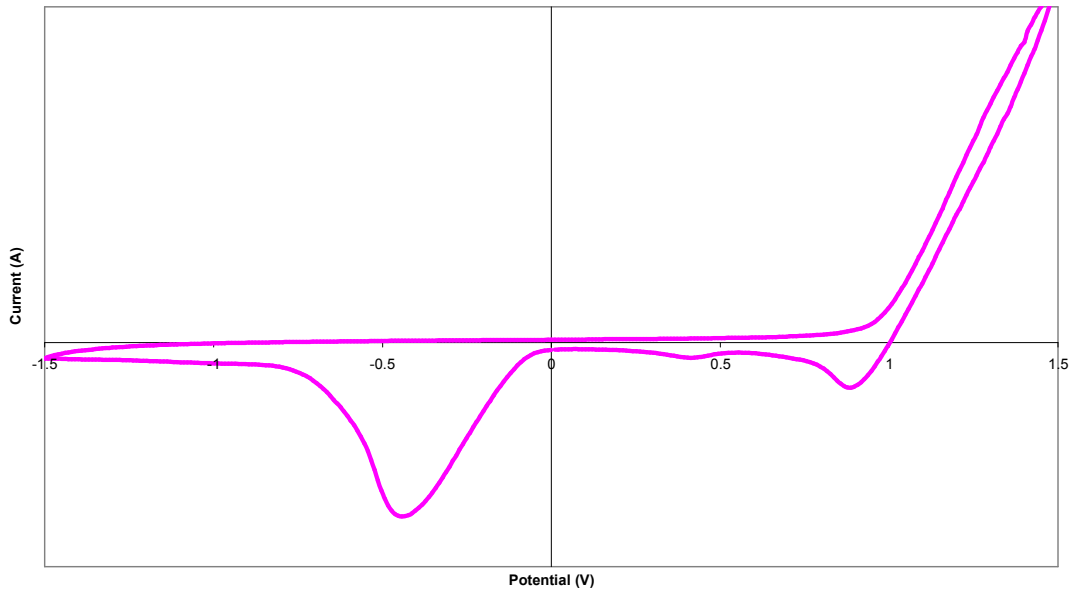

Figure 9. CV of irreversible reduction processes.

1.2.2.2.1 Two reversible one-electron transfers

The simplest form of two reversible one electron transfer reactions is two one-electron transfers (EE mechanism).[8]

If the process is fully reversible then the process is:

$$Ox + e^- \rightleftharpoons Red_1 \quad E^\circ{}_1'$$

$$Red_1 + e^- \rightleftharpoons Red_2 \quad E^\circ{}_2'$$

When $E^\circ{}_1' >> E^\circ{}_2'$ (by a minimum of 120 mV) meaning that Ox is more easily reduced than Red_1 then two discrete reversible peaks will be observed in the cyclic voltammetry. As the difference $\Delta E^\circ{}'$ between $E^\circ{}_1'$ and $E^\circ{}_2'$ decreases, overlap between the two peaks occurs and it appears as one peak.[8]

If the electron transfers occur successively then electrostatically the addition of the second electron will be unfavourable, unless a molecular rearrangement occurs leaving a non-bonding orbital available for the second electron.[8]

In solution for an EE mechanism the comproportionation reaction is

$$Ox + Red_2 \rightleftharpoons 2Red_1$$

The equilibrium constant in general terms is given by

$$K_c = e^{(n1n2\,\Delta E^\circ{}'F/RT)}$$

Where n_1 and n_2 are the number of electrons transferred in each reaction.

and for one electron transfers at 25°C simplifies to

$$K_c = 10^{(\Delta E^\circ/59mV)}$$

1.3 Binary code and logic gates

A brief overview of binary code and logic gates is now presented so that it can be seen how QCA will perform these functions.

1.3.1 Binary Code

Conventional arithmetic operates around a base ten or decimal system, however computers operate and store information in binary code or a base two system. Binary code is formed from combinations of 0s and 1s and is the simplest number system possible. Binary numbers form a bridge between arithmetic and electronics; many electronic features can be represented by the binary system. For example, a wire can be a binary circuit, by describing current flow as "1" and no current flow as "0", other devices such as switches can also be represented in this manner.[19]

These binary digits 0 and 1 are often referred to as 'bits', which are regarded as the basic building block of information. Every number, letter and picture can be represented as a series of binary digits.[19, 20] Decimal numbers can be broken down into units of tens, hundreds, thousands etc. To understand how binary numbers are generated it is necessary to think how many units of 1s, 2s, 4s, 8s, 16s *etc* the number is made up of. For example 13 can be considered as $(1x2^3) + (1x2^2) + (0x2^1) + (1x2^0) = 8+4+0+1$ which in binary is written as 1101. The binary equivalent for the first 15 decimal numbers is illustrated in Table 3.[19]

Etc.	32 (2^5)	16 (2^4)	8 (2^3)	4 (2^2)	2 (2^1)	1 (2^0)	Decimal Number
						1	1
					1	0	2
					1	1	3
				1	0	0	4
				1	0	1	5
				1	1	0	6
				1	1	1	7
			1	0	0	0	8
			1	0	0	1	9
			1	0	1	0	10
			1	0	1	1	11
			1	1	0	0	12
			1	1	0	1	13
			1	1	1	0	14
			1	1	1	1	15

Table 3. Binary equivalents of the decimal numbers 1-15. Adapted from [19].

Bits can then be bundled into groups of eights called 'bytes', and are used to represent letters, numbers and colours in what is known as binary notation. The binary notation for each letter of the alphabet is shown in Table 4. More complex information such as graphics, audio and video are created using a combination of binary code and the on/off action of the transitors.[20]

Letter	Binary Notation	Letter	Binary Notation
A	0100 0001	N	0100 1110
B	0100 0010	O	0100 1111
C	0100 0011	P	0101 0000
D	0100 0100	Q	0101 0001
E	0100 0101	R	0101 0010
F	0100 0110	S	0101 0011
G	0100 0111	T	0101 0100
H	0100 1000	U	0101 0101
I	0100 1001	V	0101 0110
J	0100 1010	W	0101 0111
K	0100 1011	X	0101 1000
L	0100 1100	Y	0101 1001
M	0100 1101	Z	0101 1010

Table 4. The binary notation used for the letters of the alphabet. Adapted from [20].

1.3.2 Logic gates

Boolean algebra can be used to determine whether something satisfies a certain criteria which is the basis for logic gates such as AND or OR in computers.[19] Logic gates are defined as "digital circuits with one or more inputs, and an output which depends logically on the input signal combinations".[21] NOT is often not considered a true logic gate as it only has one input.[19] The 0 input of a logic gate is when the voltage is low (approximately 0 V) *i.e.* no current flows through the device and the 1 input is when the voltage is high (approximately +5 V) *i.e.* the current flows through the device. There are seven basic logic gates: AND, OR, XOR, NOT, NAND, NOR, and XNOR which are shown in Table 5.[19, 22] Logic gates are formed by transistors and other components joined together and are used to perform all the internal operations of a computer.[19] The role binary code plays in logic is primarily to establish whether a current flows in the gate or not depending on the input into the gate.[22]

Symbol	Name	Input 1	Input 2	Output	Description
	AND	0	0	0	Both inputs are required in order to get an output.
		0	1	0	
		1	0	0	
		1	1	1	
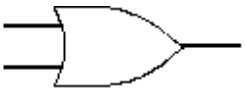	OR	0	0	0	An output occurs if either or both inputs are present.
		0	1	1	
		1	0	1	
		1	1	1	
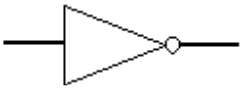	NOT	1		0	Also known as an inverter. No input is required to get an output and vice versa.
		0		1	
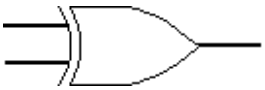	XOR (exclusive OR)	0	0	0	The output occurs only when one input occurs. Two inputs produce no output.
		0	1	1	
		1	0	1	
		1	1	0	
	NAND	0	0	1	Opposite of AND. When both inputs occur there is no output. Both inputs must be off to get an output.
		0	1	1	
		1	0	1	
		1	1	0	
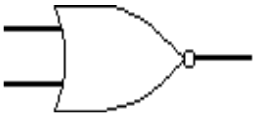	NOR (NOT OR)	0	0	1	Opposite of OR. Only get an output when both inputs are off.
		0	1	0	
		1	0	0	
		1	1	0	
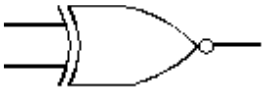	XNOR (exclusive NOR)	0	0	1	Output occurs only when both inputs are off or both inputs are on.
		0	1	0	
		1	0	0	
		1	1	1	

Table 5. The symbols for the seven basic logic gates and their truth tables.[19,22]

1.4 Quantum Cellular Automata (QCA)

Whereas molecular electronics aims to be compatible with existing electronic technology, there is one area which is a completely new paradigm. The main principle of this new paradigm, quantum dot cellular automata (QCA) is that the binary information is encoded in binary notion just as in modern microelectronics. However, this binary information is stored in the charge configuration of the cell rather than in the on/off state of a current switch.[23]

1.4.1 The principle of QCA

The simplest QCA cell is two quantum dots, with a mobile electron which can move within the cell but cannot leave the cell. A more versatile cell is one with four quantum dots and two mobile electrons within the cell. The term quantum dot is used to refer to a region where charge is localised. These quantum dots can be either metal islands coupled by capacitors and tunnel junctions or redox sites within a molecule, examples of both systems are shown in Figure 10.[24] When the quantum dots are redox sites it is known as molecular quantum cellular automata (MQCA) which is the area of interest of this thesis.

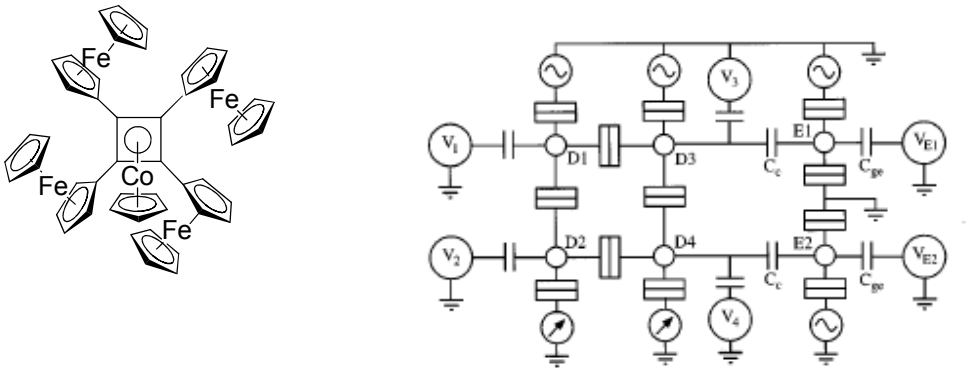

Figure 10. Examples of four dot cells left) example of MQCA cell and right) simplified QCA cell formed from alumina dots and capacitors taken from [25].

Due to columbic repulsion the two mobile electrons will sit in antipodal sites within the cell, as this can occur in two different arrangements as shown in Figure 11 which leads to two degenerate states. These two degenerate states can represent the two binary states

used in electronics. The cell can be switched to the other configuration by application of a potential.

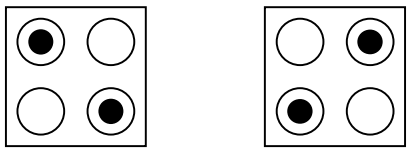

"0" **"1"**
P = -1 **P = +1**

Figure 11. Schematic diagram of the two degenerate ground states of a simple QCA cell and the binary states they represent. The white dots represent the quantum dots and the black dots represent the mobile electrons. The polarisation (P) of each state is also shown.

It has been proposed if two cells are placed adjacent to each other then they will adopt the same polarisation due to Coulombic repulsion. Computational studies have shown that application of a potential to one cell causes switching which will induce switching in the neighbouring cell as shown in Figure 12. Cell 2 is said to demonstrate highly bistable switching, as it switches polarisation rapidly as the polarisation of cell 1 is changed linearly from 0 from 1.[26] It is a key feature necessary for QCA to operate, that interaction between cells occurs in a non-linear manner and that a small change in the polarisation of one cell induces switching in the adjacent one.[24]

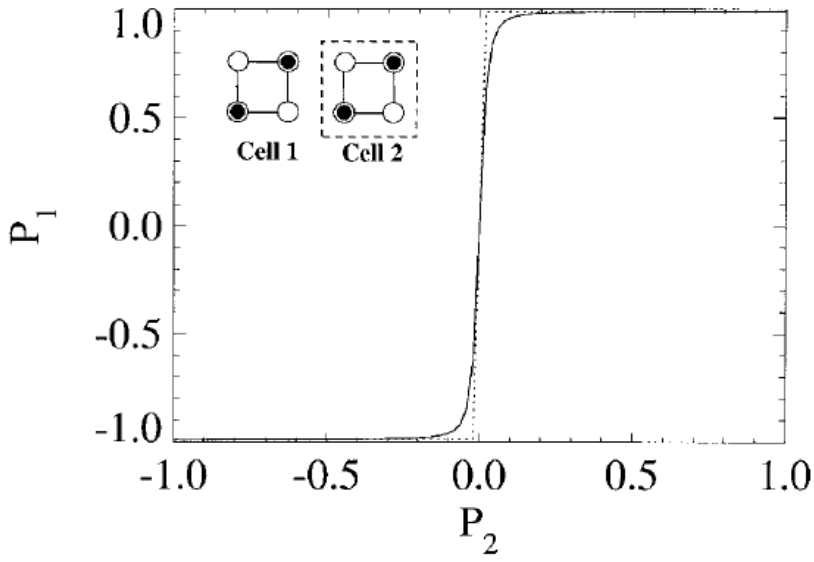

Figure 12. Schematic diagram showing the non-linear switching response exhibited by cell 2 in response to a change in polarisation of cell 1.Taken from [27].

A QCA wire can be formed by a linear array of cells, as shown in Figure 13. By flipping the polarisation of the left hand cell, the line of cells can be switched so that the input and the output are the same.[10,28] One of the key attractions of QCA is that each cell only communicates with its neighbours and only the ends of each line need to be connected to the computer which makes connecting the system up much simpler than traditional electronics.[25]

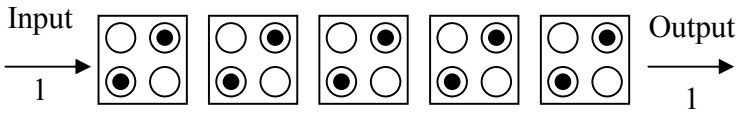

Figure 13. Diagram of basic wire of QCA cells.

1.4.2 Logic Gates and Majority gates

Computer stimulation of two electrons in a box has produced logic gates and majority gates by arranging several QCA cells. Through this arrangement basic logic functions AND, OR and NOT can be achieved as shown in Figure 14. These logic gates could then be arranged in series to map more complicated systems.[29]

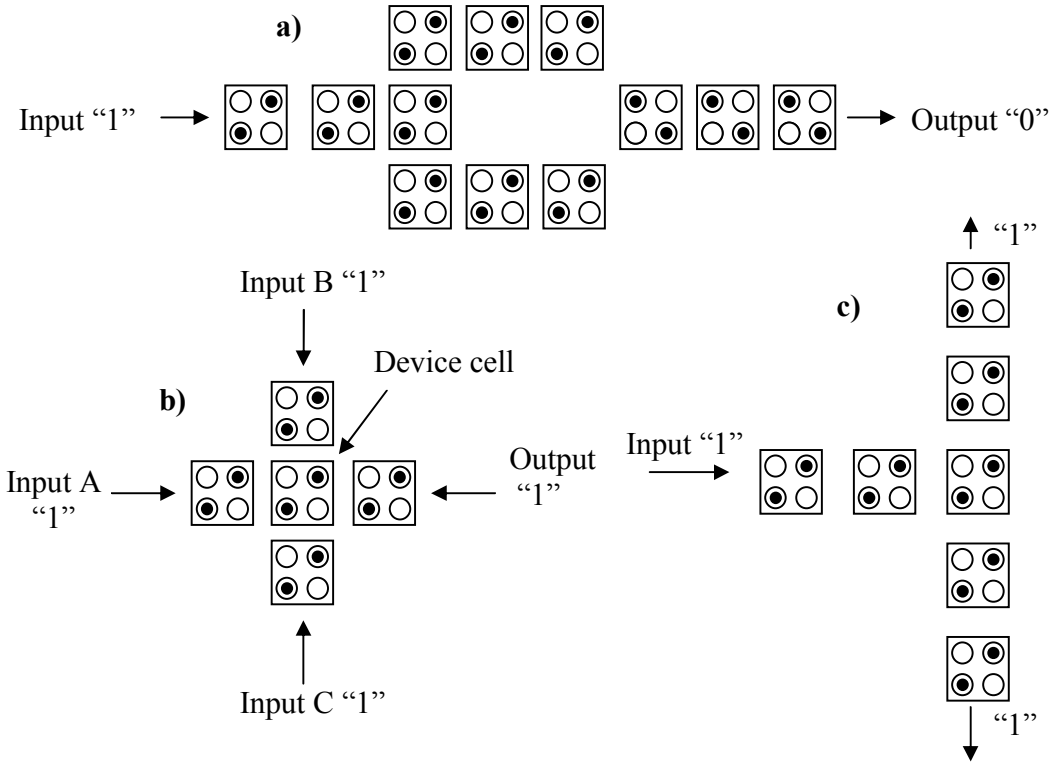

Figure 14. (a) QCA NOT gate. (b) QCA AND or OR majority gate (c) QCA fan-out. Adapted from [27].

In the NOT gate shown in Figure 14(a) the polarisation of the input is inverted by the 45° placement of the cell, resulting in the opposite output. The output of the AND or OR gate shown in Figure 14(b) is dependant on the input of all three cells, the majority input wins. When the input is programmed as 1 then the gate is an OR and when the input is 0 then the gate is AND. In the QCA fan-out shown in Figure 14(c) when the input on this structure is flipped, the new ground state of the system is achieved by flipping all of the cells in both branches.[27] It has also been shown that these logic gates can be combined to form more complex components of circuits.

1.4.3 Clocking

As information moves from stage to stage, energy in the signal path is lost due to unavoidable dissipative processes. Unless the signal is replenished it will eventually be lost in the thermal noise. In conventional electronics the signal is automatically supplemented by energy from the power source at each stage. In a QCA system it has been proposed by Lent *el al.* that the signal could be replenished using clocking.[24,30] In a clocked QCA cell, there are now three states of the cell; two active states "1" and "0" and an inactive state "null" which contains no information. These three different states are shown in Figure 15 where a clocked signal is applied to the middle dots and controls the energy of these relative to the other dots.

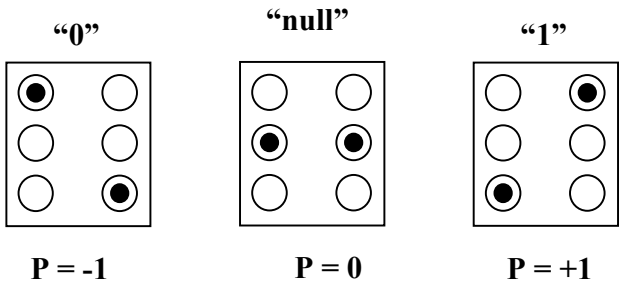

Figure 15. A clocked QCA cell. Adapted from [30].

When the clocked signal makes the energy of the null dot energies lower than the active dot energies then the electrons will be drawn to the null state regardless of the state of the adjacent cells. When the energy of the null dots is raised then the electrons move to the active state, whether this is 0 or 1 is determined by the neighbouring cell.[30]

The clocking signal can be applied in two different ways depending on the system. As metal-dot cells are large compared to molecular cells it is possible to apply a time varying voltage to a lead capacitively coupled to the middle dot islands. For molecular cells it is not possible to connect each cell to the clocking voltage. Instead an electric field is applied perpendicular to the plane of the molecules which provides the clocking signal. Therefore the middle dots must be at a different height to the active dots giving a V configuration.[30]

A line of clocked cells allows the transfer of a signal down the row in a controlled manner; this is known as a shift register. As the clocked signal is increased on the first cell creating an active state, then the same state will be created in the adjacent cell. The original cell can then bought back to the null state and the next bit can be generated. By using continuously varying clocking potential, information can be moved along a line.[30]

In a shift register the target cell will receive energy flow from the cell to its left (E_{in}) and will transfer energy flow to a cell on its right (E_{out}) as shown in Figure 16. The target cell will also lose energy due to dissipative processes (E_{diss}) and gain energy from the clock signal (E_{clock}). In steady state for a well functioning shift register these energies are in balance *i.e.* $E_{out} = E_{in}$ and $E_{diss} = E_{clock}$ and the power gain is one. However when E_{in} is weak because of cell alignment or fabrication error then $E_{out} > E_{in}$ and $E_{diss} > E_{clock}$ and the clock supplies the additional energy to the signal and the power gain is greater than one.[30]

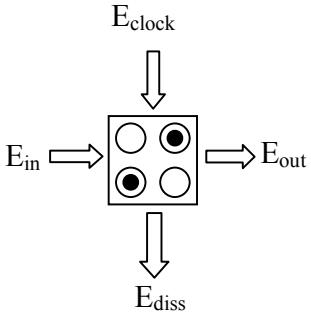

Figure 16. Schematic diagram of the energy transfer within a clocked QCA cell. Adapted from [30].

1.4.4 Advantages of MQCA

A Pentium 4 Chip contains 42,000,000 transistors in an area several cm^2 and operates on a nanosecond scale emitting 40 watts of heat. By comparison it is believed that due to the nm scale of the QCA lines, QCA circuits could produce device densities of 100,000,000,000 devices per cm^2.[23] MQCA also allows for the synthesis of large numbers of identical molecules in a single round bottomed flask. As the electrons only move within the MQCA cell then the amount of heat generated is much smaller than in traditional electronics.[1]

A prototype QCA cell has been fabricated from aluminium islands and aluminium oxide tunnel junctions on an oxidized silicon wafer. However in order for a QCA system to operate, the state energy difference must be greater than kT, and with the 60 nm scale dots and tunnel junctions used in the experiments, extremely low temperatures of 10 mK were required.[29]

It has been predicted that if the QCA cell was smaller at roughly 20-30 Å a side then the device could function at room temperature. This is due to the particle in a box theory which states as the box gets smaller the difference in the energy levels becomes larger and hence the barrier to switching becomes larger. Whilst it is difficult to produce identical metal clusters of this size, the synthesis of identical molecules is much more straight forward.[31,32]

1.4.5 Criteria for materials suitable for MQCA

Molecular sized QCA cells are mixed valence complexes, however not all mixed-valence complexes are suitable for this application.

Complexes for a diad QCA molecule must have; [10,28]

1. A stable mixed valence state with a comproportionation constant* greater than or equal to 10^3.
2. A strong coupling between the redox centres to allow rapid exchange of the charge between the sites.
3. The capability of functionalisation to allow surface binding in ordered arrays.
4. A complex that can by made by a good preparative route from accessible starting materials.
5. A complex that is kinetically stable and ideally neutral species to remove the need for counter ions.

For a tetrad system the requirements are slightly different, these are;[33]

1. A metal complex with two stable redox states,
2. The complex must be planar with a four fold symmetry axis.
3. The complex must also have good through space or through bond interactions so that the 2+ state is stable with respect to the comproportionation constant for 1+ and 3+ states.
4. Robin Day type II or III mixed-valence behaviour.
5. Easily isolated pure products from readily accessible starting materials.

1.4.6 MQCA Systems

1.4.6.1 Modelled systems

Both metal QCA and MQCA systems have been the subject of many modelling studies and theoretical studies. Whilst the results are important to the understanding of systems it is not possible to summarise the huge amount of information here. Two different modelled systems are presented in this section in order to gain an understanding of how a MQCA system would function and why the criteria of MQCA are necessary. The first

* The comproportionation constant is a measure of the ability of the mixed valence state to form a product which is more stable which in the case of the diad cell is the +1 state and in the tetrad system is the 2+ state.

model is of the implementation of a clocked MQCA system whilst the second study examines the interactions of the orbitals of different Robin-Day classes.

1.4.6.1.1 Clocked system

A 1,4-diallyl butane radical cation was first proposed by Aviram as a gate for a molecular current switch,[34] and later studied by Hush.[35] The structure of this molecule is shown in Figure 17. Aviram thought this molecule a potential candidate due to the potential electron localisation in the allyl end groups and the σ bridging ligand which offered a tunnelling barrier. One of the allyl groups is neutral with a doubly occupied bonding level and a singly occupied non-bonding orbital, the allyl cation has an empty non-bonding orbital. Whilst this molecule is only suitable for a model system it offers computational tractability and exhibits key features of more complex mixed valence systems. Lent *et al.*[28] also felt that this molecule would provide a model system for a diad MQCA cell or by placing two cells together a tetrad cell. However this molecule does not fulfil the criteria for MQCA as it lacks the functional groups that would allow surface-binding.

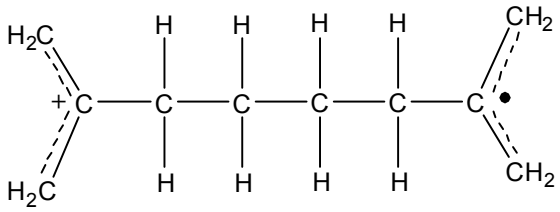

Figure 17. Structure of the diallyic system modelled.

Modelling using quantum chemistry was carried out and revealed that the molecule is capable of QCA bistability and molecule to molecule communication. Application of an applied field (driver cell) showed abrupt switching from one sign to another as shown in Figure 18 hence meeting the non-linear response requirement of MQCA. It was also found that the presence of a dipole moment in one molecule could induce a dipole moment in an adjacent molecule in a non-linear manner. Arrays of these molecules were found to function as wires and majority gates within the quantum chemistry calculations.[28]

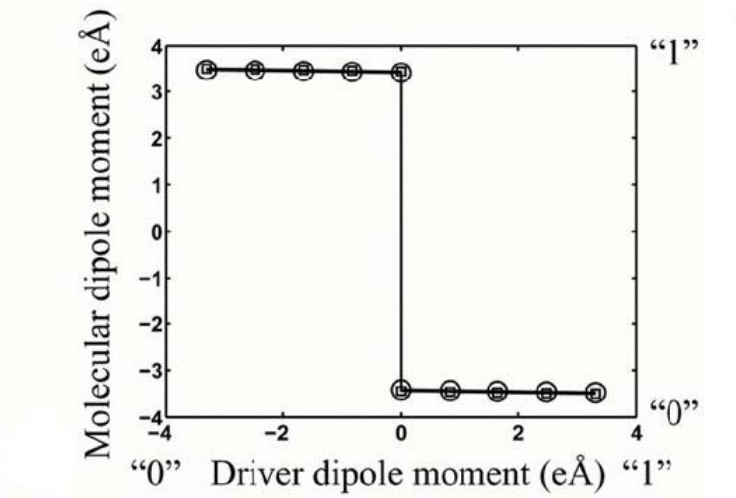

Figure 18. Plot of the calculated response of the molecule to the driver cell. Taken from [28].

By adding a third allyl dot to the Aviram molecule as shown in Figure 19, the first example of clocking in MQCA was demonstrated. Two of the allyl groups are now neutral and one has a positive charge. Calculations confirmed that application of a perpendicular field could switch the molecule from the null state to the active state.[24]

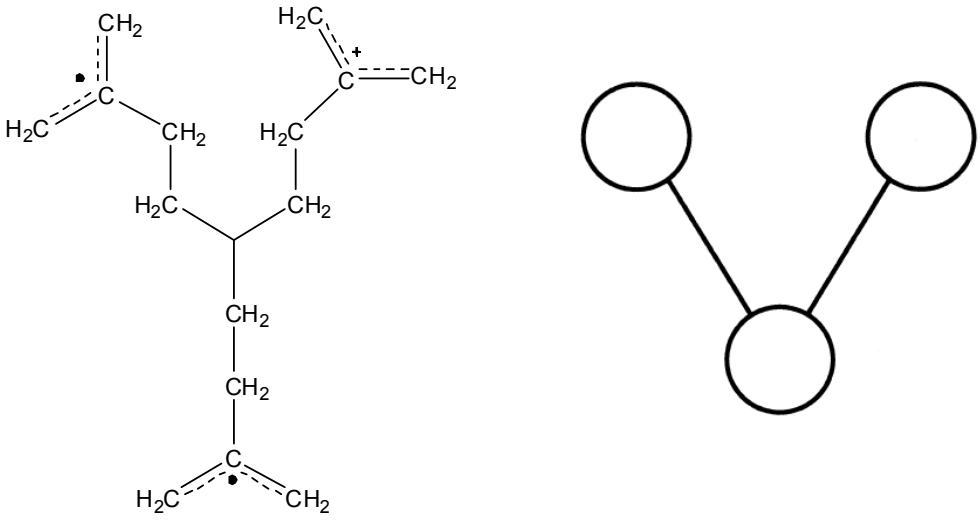

Figure 19. Left) Structure of the three allyl group molecule adapted from [24]. Right) Simple representation for the molecule. Taken from [24].

The three charge configurations of the three allyl group molecule are shown in Figure 20; note that in this study the green circle represents the positive charge (hole) not an

additional electron. The hole can occupy either of the top dots which represents the two active states “1” and “0”, occupation of the lower dot is the “null state” of the cell. For an isolated molecule the two active states are degenerate but application of a field from a driver cell or the presence of another cell breaks this degeneracy. In this system the energy of the “null” state is lower than the energy of the two active states. The clocking field controls whether the hole is in either the lower or upper dots. Which active site the hole occupies is determined by adjacent cells.[25]

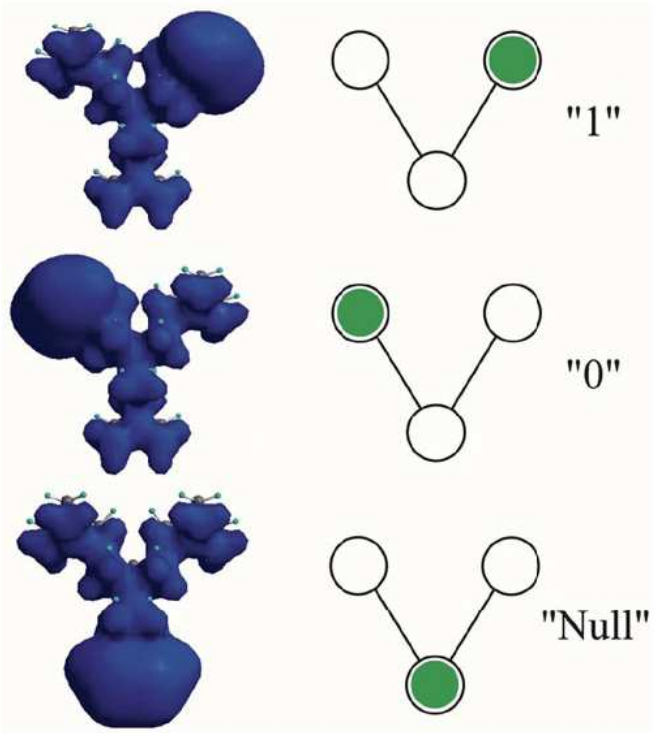

Figure 20. Schematic diagram for the three different states of the clocked cell. The calculated isopotential surfaces of the three states are shown on the left. Note the positive charge (hole) is represented by a green circle. Also note that the presence of this hole on an allyl groups causes a bulge in the *iso*-potential surface around this group. Taken from [24].

As for the two allyl group molecule a non-linear response was seen by applying a field through a driver cell. The effect of varying the clocking field was also examined. It was seen that when the field was greater then 1.1 V/nm then a non-linear response was observed. However when the field was less than 0.6 V/nm the dipole moment of the molecule was zero for all values of the driver dipole moment. This means when the clocking field is lower than 0.6 V/nm then the molecule is in the “null” state and does

not respond to the driver cell. This is the desired action of a clocked cell. The field controls whether the molecule is in the active state where it responds in a non-linear way or in the null state where it is unresponsive to inputs. It is proposed by Lent *et al*. that by changing the nature of the lower dot, molecules can be designed to be either in an default active state or default null state.[28]

Lent *et al.* also modelled a six dot clocked cell using two molecules positioned as Figure 21. The driver cell is the third molecule. In a clocking field of 2.6 V/nm a strong non-linear response was observed with changes in the driver dipole. This shows that there is communication between the two molecules as the second switch is induced by the first molecule switching in response to the driver cell.[24]

The clocking current in Figure 21 is produced by the buried conductors, when the clocking field is positive the hole is drawn into the null state (top right hand picture). When the clocking field is negative then the hole is pushed into the active state (top left hand picture). By applying a shifted sinusoidal clocking phase to successive wires a continuously varying clocking signal is created which causes the information to move along the line.[36]

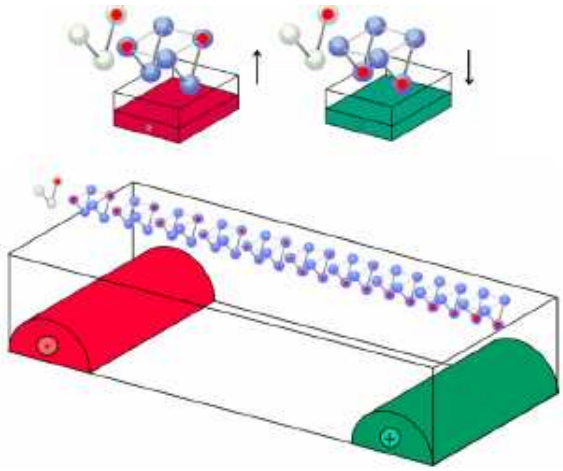

Figure 21. Schematic diagram of a clocked MQCA array. The clocking field is produced by buried conductors. The electric field in the y direction controls the state of the cell (active/null/switching). Wires perpendicular to the layer of QCA induce a field when a voltage is applied. Taken from [36].

1.4.6.1.2 Modelling of Different Robin-Day Classes

Braun-Sand *et al.*[6] have carried out a series of calculations for three ruthenium compounds which represent different Robin-Day classes, the structure of these compounds are shown in Table 6. Note that compounds **2** and **3** are known in the literature whilst **1** is not known. Compound **1** was selected as it is analogous to **3** but with only σ bonds and therefore believed to be a Class I compound. The first aim of their study was to examine the ability of the computational methods to predict the molecular geometries and also to analysis the molecular orbitals. The molecules were calculated using a B3LYD level of theory with a 3-21G basis set, which has been demonstrated previously to perform well with difficult models.

Robin Day Class (Compound number)	Structure
I **(1)**	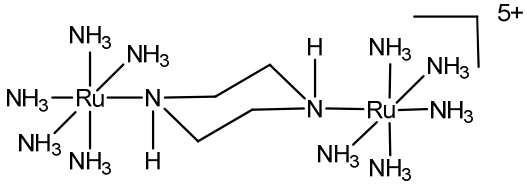
II **(2)**	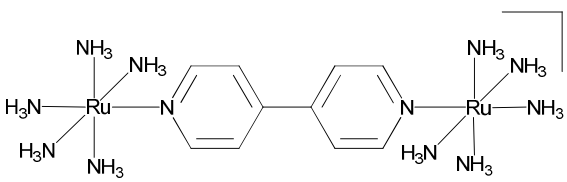
III **(3)**	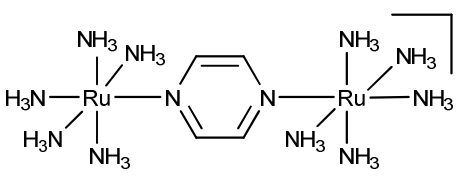

Table 6. Structures and Robin-Day class for the three molecules modelled by Braun-Sand *et al.*[6]

This work also explores the effect of perturbing the potential surface by adding an extra electron into the system. When an extra electron is added the potential energy surface is perturbed as shown in Figure 22, so that the electron is energetically favoured to occupy one site in the molecule.

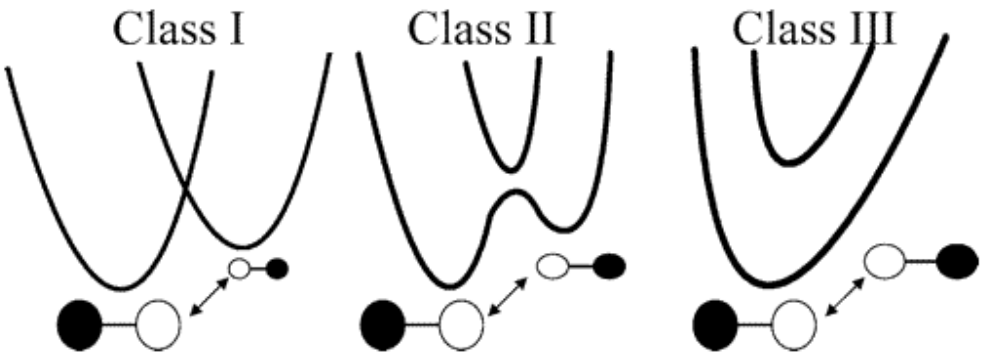

Figure 22. Schematic diagram potential energy surfaces for electron transfer in Robin-Day classes I, II, and III where an extra electron has been added to the molecule. Taken from [32].

Two key requirements for QCA are the ability to bias a system so that one configuration is more favourable and also the ability for the system to switch back and forth between states. Class II and III compounds could be suitable for QCA applications as they have a fast rate of electron transfer suitable for computation. However it is also necessary for there to be a small energy barrier to electron transfer otherwise random switching maybe occur at room temperature. The energy barrier for electron transfer in Class I compounds is too high for QCA applications causing the electron to be fixed in one position.[32]

It is thought that electron transfer between two metal sites occurs via the ligand, therefore the energy gap between the singly occupied molecular orbital (SOMO) and the molecular orbital centred on the bridging ligand is a good indication of the barrier to electron transfer. Studies on ruthenium dimers have suggested that when the energy gap between the molecular orbital on the ligand and the dπ-orbitals on the ruthenium is small then there is stronger coupling between the two metal sites. Table 7 shows the orbitals obtained from the calculations, although both Kohn-Sham (KS) orbitals and Hartree-Fock (HF) orbitals were obtained the HF orbitals only were considered in the discussion as they are better understood.[6]

Compound No.	Orbital	Energy gap (eV)
2	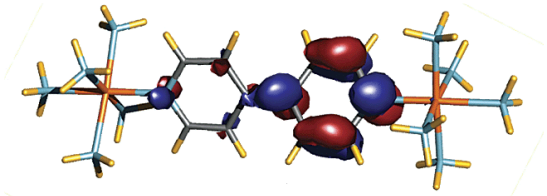 LUMO	9.25
	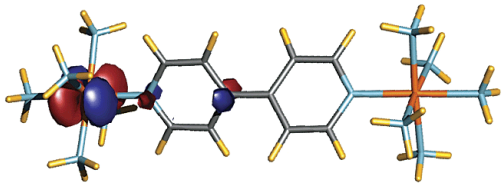 SOMO	
3	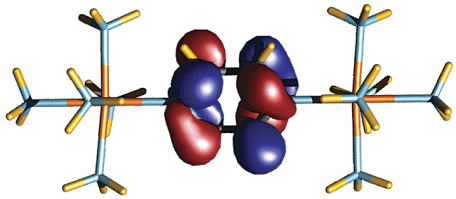 LUMO	8.16
	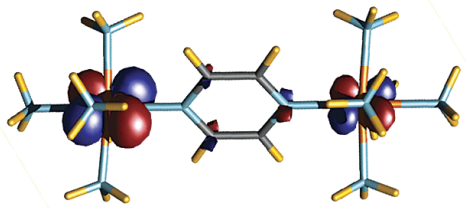 SOMO	

Table 7. HF orbitals for the LUMO and SOMO of compounds 2 and 3 and the energy gaps. Taken from [6].

As seen in Table 7 the SOMO of compound **2** is located on one ruthenium atom whilst the SOMO on **3** is located on the both the ruthenium atoms. This suggests that the structure of **3** is more delocalised than in **2**. The LUMO of **2** is localised on the bridging ligand, however due to the break in π conjugation in this bridging ligand the orbital is not evenly spread across the ligand. This is also seen in the difference in spin densities and charges on the two ruthenium atoms summarised in Table 8, which shows a much larger difference for compound **2** than for compound **3**. These observations are in

agreement with that expected from a Robin-Day class II compound compared to a class III compound.

Compound Number	Mulliken Charge on Ruthenium	Mulliken spin density on Ruthenium
1	0.93 on each	0.54 on each
2	0.00, 1.14	0.86, 1.18
3	-0.03, 0.05	0.85, 0.86

Table 8. Summary of the calculated charges and spin densities for the two ruthenium atoms in each compound.

Compound **1** was found to be very different as the bridging ligand is non-conjugated leading to the SOMO being on the bridging ligand. The highest occupied metal- centred orbital is lower than the SOMO and is denoted SOMO-1. The energy gap between the SOMO-1 and bridging ligand molecular orbital (BLMO) was found to be very large at 19.3 eV. Because the piperazine bridging ligand in this molecule has no π^* orbitals and the σ^* orbitals are much higher in energy, this leads to the large energy gaps. This also means that the BLMO is no longer the LUMO and is denoted LUMO +12 in Figure 23. LUMO +5 is the lowest lying molecular orbital on the other ruthenium atom. Because of these large energy gaps between the orbitals it means that coupling between the ruthenium atoms was found to be weak as expected for a Class I compound.[6]

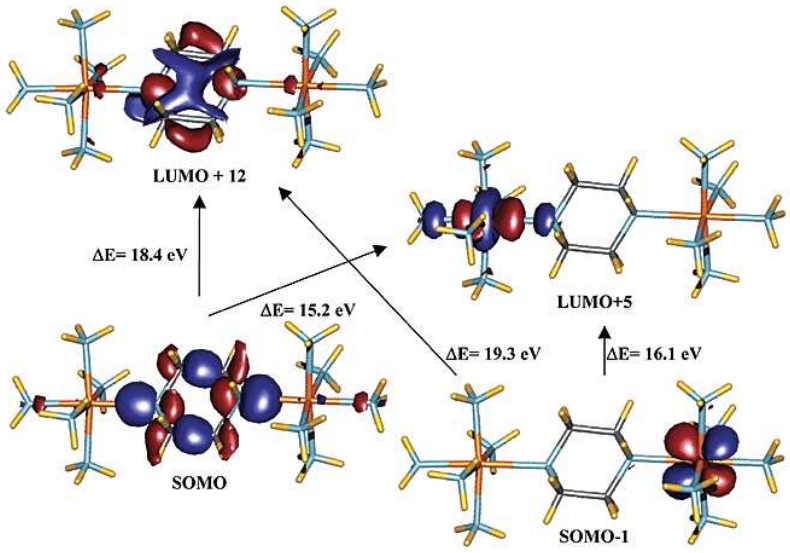

Figure 23. HF orbitals of compound 1 taken from [6].

It was concluded from this study that the orbital calculations showed a difference between the three Robin-Day classes if the electron transfer occurs through the bridging ligand. The energy gap between the SOMO and LUMO increased with increased localisation within the molecule and is believed to be able to provide a measure of electron communication within the molecule.

The study also highlights the fact that for MQCA applications the bridging ligand must be fully conjugated to allow for efficient electron transfer between the metal centres. When selecting materials for study for MQCA utility the choice of the bridging ligand is the most important factor to be considered.

1.4.6.2 Synthesised MQCA Systems

1.4.6.2.1 Diad systems

While MQCA has been well modelled there are very few diad or tetrad systems that have been synthesised and exhibit the required characteristics. Fehlner *et al.*[10] carried out the synthesis of a diad system following scheme 1. Compound **4** had been previously synthesised by another group[37,38] but the electrochemistry that was reported was different to that observed by Fehlner *et al.*

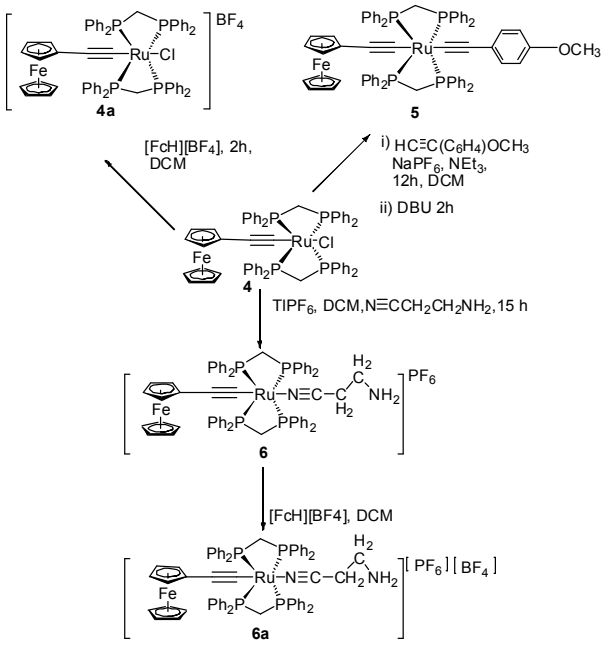

Scheme 1. Compounds prepared by Fehlner starting from the simple starting material *trans*-RuCl(dppm)$_2$(C≡CFc) Fc = ferrocene.

Compounds containing ferrocene are very attractive as the electrochemistry of ferrocene is well known and understood. Introduction of a second metal such as ruthenium adjacent to the ferrocene centre provides a wide diversity of oxidation states and ligands, which increase the potential architectural flexibility and fine tuning of the properties necessary for electronic devices.[39] Whilst a symmetrical molecule is required for a MQCA wire and logic gates, Fehlner examined an unsymmetrical system to examine whether mixed-valence systems are suitable for MQCA.

Spectroscopy was carried out on the compounds **4a** and **6a** to obtain some parameters for comparison to other known mixed-valence compounds. The values of $(\Delta\nu_{1/2})_{obs}/(\Delta\nu_{1/2})_{calc}$ for **4a** and **6a** shown in Table 9 are considerably higher than the 1.1-1.3 which are typical of a Class II system. The delocalisation parameter α^2 for **4a** is 1.2 x 10^{-2} which is larger than other known class II systems[10] but **6a** has a more typical α^2 value at 3 x 10^{-3}.

Complex	$\Delta\nu_{1/2}$	α^2	$(\Delta\nu_{1/2})_{obs}/(\Delta\nu_{1/2})_{calc}$
4a	2200	1.2×10^{-2}	1.83
6a	2730	3×10^{-3}	2.4

Table 9. Summary of spectroscopic values for complex 4a and 6a.

Electrochemistry was carried out on compounds **4**, **5** and **6** and an osmium analogue of **4** in order to assess the use of these in molecular QCA and the results are summarised in Table 10.

Complex	$E_{1/2}(1)$ (V)	$E_{pa}(1)$ (V)	$E_{pc}(1)$ (V)	$E_{1/2}(2)$ (V)	$E_{pa}(2)$ (V)	$E_{pc}(2)$ (V)	$\Delta E_{1/2}{}^{c}$ (V)	Ref
4	-0.40	-0.34	-0.46	0.30	0.35	0.25	0.70	[10]
4	-0.39	-	-	0.37	-	-	0.76	[37]
Fc(C≡C)(Os(dppm)$_2$Cl)	-0.44	-	-	0.21	-	-	0.65	[37]
5	-0.43	-0.38	-0.48	0.06	0.11	0.01	0.49	[10]
6	-0.20	-0.15	-0.25	~0.78^{b}	0.86	0.70	~0.98	[10]

Table 10.[10] Cyclic Voltammetry data for *trans*-RuCl(dppm)$_2$(C≡CFc) 4, *trans*-Ru(dppm)$_2$(C≡CFc)(C≡C(C$_6$H$_4$)OCH$_3$) 5 and [*trans*-Ru(dppm)$_2$(C≡CFc)(N≡CCH$_2$CH$_2$NH$_2$)][PF$_6$] 6.[10]

[a] Electrolyte 0.1 M [NBu$_4$][BF$_4$] in CH$_2$Cl$_2$; Pt electrode, 25°C, scan rate 100 mV/s. $E_{1/2}$ values are referenced to ferrocene in the same system.[b] $E_{1/2}(2) = (1/2)[E_{pa}(2) + E_{pc}(2)]$ (irreversible for 6).[c] $\Delta E_{1/2} = E_{1/2}(2) - E_{1/2}(1)$.

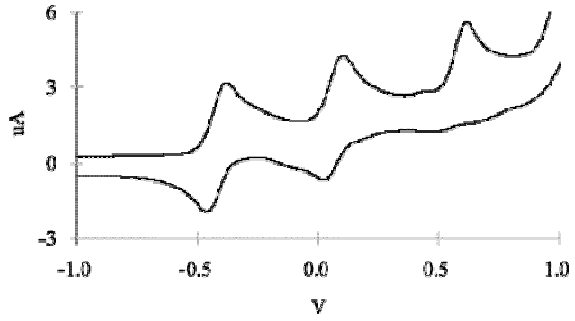

Figure 24. CV of *trans*-Ru(dppm)$_2$(C≡CFc)(C≡C(C$_6$H$_4$)OCH$_3$) 5 taken from [10].

The CV for compound **5** is illustrated in Figure 24, showing two quasi-reversible waves at -0.43 V and -0.06 V. For both these waves the peak separation ΔE_p = 0.1 V, the first

peak has a current ratio i_{pa}/i_{pc} ~1 but for the second peak i_{pa}/i_{pc} ~0.6. The oxidation wave at 0.57 V was assigned as the oxidation of the ligand (-C≡C(C_6H_4)OCH_3).[10]

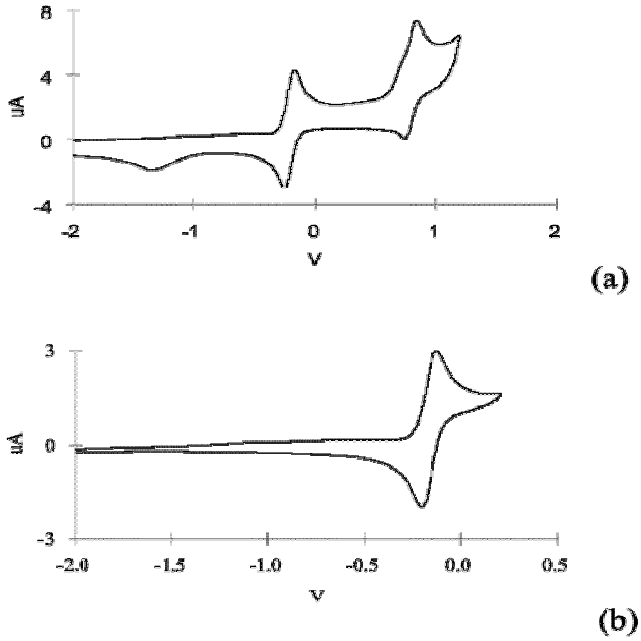

Figure 25. CV of [*trans*-Ru(dppm)$_2$(C≡CFc)(N≡C$CH_2CH_2NH_2$)][PF_6] 6 in CH_2Cl_2: (a) scan from -2.0 to 1.2 V (scan rate 100 mV/s, referenced to Fc/Fc$^+$); (b) scan from -1.8 to 0.2 V (scan rate 50 mV/s, referenced to Fc/Fc$^+$).Taken from [10].

The CV of compound **6** is shown in Figure 25, **6** exhibited one quasi-reversible wave at -0.20 V with $\Delta E_p(1)$ = 0.1 V and i_{pa}/i_{pc} ~ 1. In addition there is one irreversible wave at ~0.98 V with $\Delta E_p(2)$ = 0.16 V and i_{pa}/i_{pc} ~ 0.5. An additional wave was observed at E_{pc} = -1.38V , this wave was not observed on a further scan as seen in Figure 25(b) and is believed to reflect the instability of the double oxidised species.[10] Fehlner *et al.* also found that the current of the reduction wave at -0.70 V decreased with cycling of the potential. However when the maximum positive potential scanned to was limited to 0.20 V the current of the wave at -0.20 V did not change after several scans.

As QCA use only requires access to the mixed-valence state, Fehlner *et al*. propose that the chemical instability of the tailed, doubly oxidised complex should not be a problem.

Previous work [38] based on similar heterobimetallic *bis*(acetylide)ferrocene complexes lead to the assignment of the first wave in Figure 24 and Figure 25, as being due to the oxidation at the ferrocene centre and the second being due to the oxidation at the ruthenium centre.[10]

It is also possible to see the effect of ligand substitution from this series of compounds comparing values from Table 10 for compounds **4** and **5**. It can be seen that there is little effect on the first redox wave but there is a 0.24 V shift to negative potential for the second wave with substitution of a chloride atom for -C≡ $C(C_6H_4)OCH_3$. Comparison of the data for **4** and **6** shows a 0.20 V positive shift for the first redox wave after introduction of a cation into the molecule. Comparison of the second redox wave shows a positive shift by 0.48 V by substituting the chloride for the $N{\equiv}CCH_2CH_2NH_2$ ligand. It can be seen that ligand substitution of an electron donating ligand caused a negative shift in potential at the ruthenium centre. Whilst substitution for a ligand that can back bond shifts the peak the other way. Ligand substitution had little effect on the ferrocene redox potential. Comparison of **4** and the osmium analogue shows little difference in the first redox wave and only a slight shift in the second redox peak, this suggests that again the ferrocene centre oxidises first and that substitution of ruthenium by osmium has very little effect.

The conclusion of this work was that the presence of the two well-separated oxidations indicates significant stabilisation of the mixed-valence species. However the separation of the two peaks could be due to the unsymmetrical nature of the molecule rather than metal-metal interaction. It has also been demonstrated by Fehlner *et al*. that **4** could be functionalised with groups suitable for surface binding such as OCH_3 and NH_2 without significant change in the mixed-valence properties of the coupled ruthenium-iron centres.[10]

1.4.6.2.1.1 Attachment to Gold surface

Continuing the work with the systems discussed in the previous section Fehlner *et al.*[40] then attached a thiol group to compound **6** and then bound it to a gold surface as shown in Scheme 2.

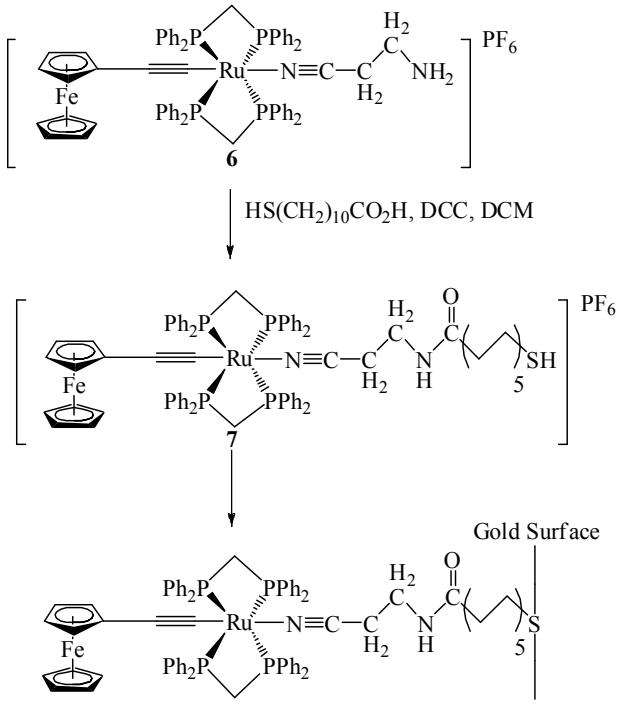

Scheme 2. Preparation of 7 for attachment to the Au surface adapted from [40].

Addition of a thiol tail to **6** had little effect on the electrochemistry as seen comparing Figure 26 of **7** before attachment to the surface and the CV of **6** shown in Figure 25. There was a small peak at E_{pa} = 1.1 V in Figure 26a which is proposed by Fehlner *et al.* to be due to the oxidation of the thiol tail.[40]

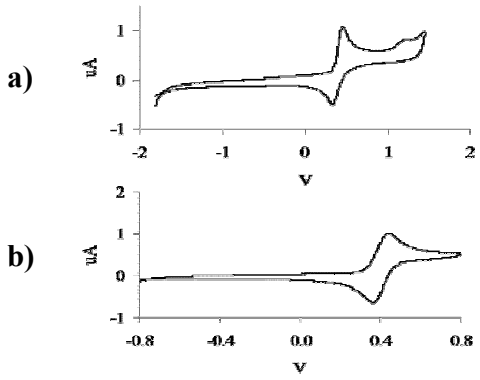

Figure 26. CV of $[Ru(dppm)_2(C{\equiv}CFc)(N{\equiv}CCH_2CH_2NHC(O)(CH_2)_{10}SH)]][PF_6]$ 7, in CH_2Cl_2: a) first scan from -1.8 to 1.5 V, and b) scan from -0.8 to 0.8 V (*vs.* Pt wire) (0.1 M $TBAPF_6$ in CH_2Cl_2 as electrolyte, scan rate 25 mV/s).Taken from [40].

The CV of **7** after it is bound to the gold surface is shown in Figure 27. When the voltage scan was limited to a maximum of 0.8 V then the first wave was reversible: E_{pa} = 134 mV, E_{pc} = 132 mV and the peak width at half the height of the maximum (fwhm) was 90 mV. It is expected for a strongly bound surface-bound species where the electron transfer from complex to electrode is not rate limited that E_{pc} and E_{pa} would be equal and the fwhm would be 90.6 mV.[41] As the E_{pc} and E_{pa} are very similar and the peak width is very close to ideal, combined with the profile having no asymmetric or broad peaks; Fehlner *et al.* reports this as evidence for the presence of isolated, tethered **7** in homogeneous environments relative to redox properties.[40]

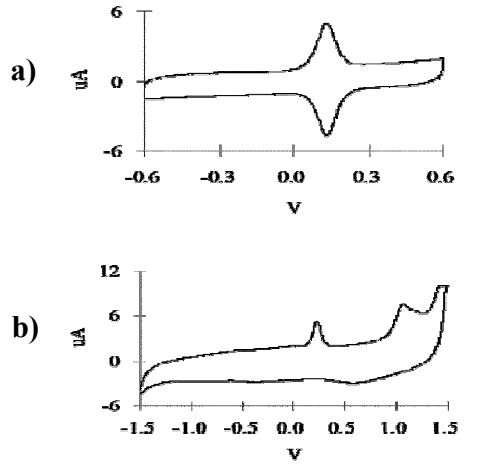

Figure 27. CV after molecule 7 is attached to Au surface from a 1 mM solution in CH_2Cl_2(0.1 M $TBAPF_6$ in CH_2Cl_2 as electrolyte) (scan rate 50 mV/s): a) from -0.6 V to 0.6 V: b) from -1.5 V to 1.5 V first scan. Taken from [40].

A single shift to more negative potential was seen for **7** as a film (Figure 27) compared to solution (Figure 26). When the film was swept to 1.5 V, non reversible behaviour was observed as seen in Figure 27b), the return scan showed no peak which combined with further scans suggests the destruction of the film.[40] Fehlner *et al*. suggest that is because the gold-thiol bond is redox active and its oxidative cleavage takes place at a lower potential than the second oxidation of the compound that this is the cause of the destruction of the film.

Integration of the redox peaks can be used to calculate the total charge which is equal to the total number of electroactive tethered complex **7** on the electrode. Taking into consideration the area of the electrode, the area of the counterion and the surface roughness given by AFM data Fehlner *et al.* estimate the surface coverage to be ~67%. Electrochemical techniques were used to measure the coverage of the gold substrate as a function of deposition time and it was found that 30% of the maximum coverage occurs rapidly and soaking beyond 60 min provided little additional coverage.

Current measurements at different scan rates showed a non-linear relationship which allowed comparison to literature data and suggested that the rate of electron transfer from a tethered complex to the electrode is very slow relative to electron exchange in a type II mixed-valence complex. This suggests that saturated tethers could make substrate driven clocking rates very slow and therefore are not ideal for such applications.

For a surface bound complex to be suitable for QCA applications it must be robust and stable. Cycling of the film of **7** between -0.3 V and 0.8 V lead to a 10% loss of current after 40 cycles and the peak potential shifted by ~100 mV. Holding the film at a negative potential for an hour produced very little degradation in the film but holding the film at a positive potential produced a 25% drop in current after 30 minutes. However the unoxidised film was found to be stable after a month in air and even when the electrolyte was $NaClO_4/H_2O$ electrochemistry could be carried out on the film.

Chemical oxidation of **7** with [FcH][PF_6] produced *trans*-[Ru(dppm)$_2$(C≡CFc)(N≡$CCH_2CH_2NHC(O)$-$(CH_2)_{10}SH$] $^{2+}$ **7a** as a film. Cyclic voltammetry of the resulting film showed that the complex remained intact and that application of a reducing potential converted the surface bound **7a**, the mixed-valence complex, into **7**. Repeated oxidation of this film showed deterioration in the CV signal but that the surface-bound complex still remained intact. Comparing the data from amperometric experiments for unoxidised and oxidised films suggested that only 10% of the surface was chemically oxidised. The explanation for this low conversion suggested by Fehlner *et al*. was that there may be problems with the oxidising agent reaching the surface bond molecules.[40]

These results show that it is possible to generate a film containing mixed-valence complexes and demonstrates that charged, two-dot QCA cells can be bound to a metal surface.[40]

1.4.6.2.1.2 Attachment to Silicon Surface

Following the production of films on the gold surface, Fehlner *et al.*[31] then attached the same complex [*trans*-Ru(dppm)$_2$(C≡CFc)($NCCH_2$-CH_2NH_2)][PF_6] **6** to a silicon surface. Problems were found when obtaining measurements for the gold films which were believed to be due to degradation of the gold-thiol bond, so it was proposed by Fehlner *et al.*[31] that an amine-silicon bond will be less reactive. These films were then used to investigate switching of the divalence mixed valence metal complex between its oxidation states ($Ru^{II}Fe^{III}$ *vs.* $Ru^{III}Fe^{II}$) using an electric field. To carry out this work an assembly of biased, vertically orientated, two-dot cells sandwiched between two electrodes were fabricated. The capacitance of the parallel plate device as a function of applied voltage across the plates was measured.[31] The complex **6** was bound to the silicon surface in a similar manner to the gold surface, as shown in Scheme 3.

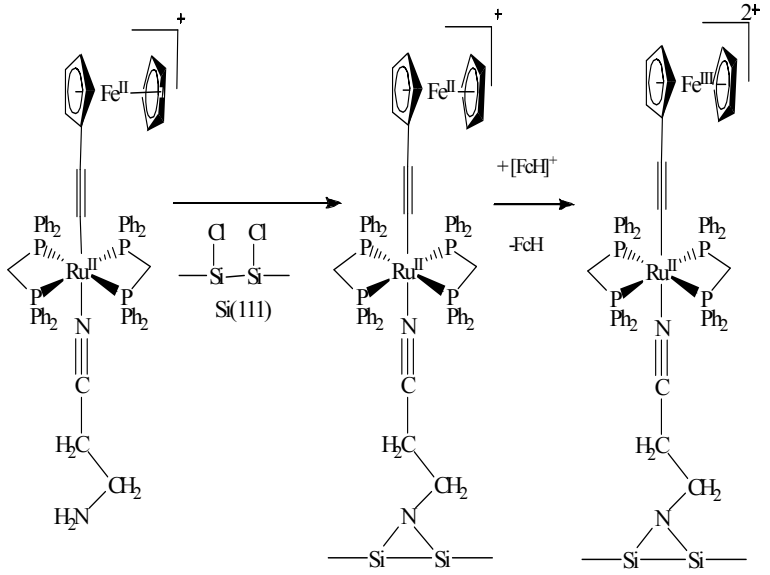

Scheme 3.Reaction of 6[PF_6] with a chlorinated Si(111) surface to produce surface bound 6^+ and, subsequently, the mixed-valence state.Taken from [31].

The complex was bound to the silicon substrate as a monolayer and the top electrode was created using liquid mercury. The use of mercury as an electrode has been found to minimise distribution of the monolayer. A schematic diagram of the experimental procedure is shown in Figure 28; a control experiment was also carried out with the equivalent inactive cell containing Fe^{II}- Ru^{II}.

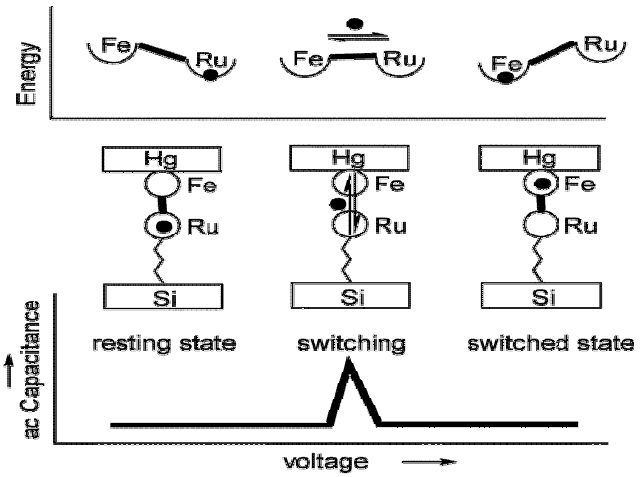

Figure 28. Schematic diagram representation of the experiment showing, from the top, the relative energies of the Fe and Ru wells, the parallel plate capacitor containing the mixed-valence complex, and the capacitance as a function of the voltage imposed across the Hg and Si plates. Taken from [31].

In the experiment a dipole is created between the moving electron and the stationary counter-ion as the electron moves from the ruthenium atom to the iron atom. This dipole is responsible for the increased capacitance that is measured at the DC voltage, which is where the dipole is created and destroyed in response to the small AC voltage. As the applied DC voltage is increased further; the stable dipole no longer affects the capacitance. Examination of the capacitance data enabled an estimation of the number of molecules per unit area that form dipoles. [31]

It is important that the QCA cell must be orientated perpendicular to the plane of the surface with the molecule dipoles in the same direction. Variable angle XPA provided strong evidence of a perpendicular orientation and thickness measurements of the film gave an average thickness of 15-19 Å which was more consistent with the height of **6** than its width. It was also possible to tell that the iron centre is further from the surface than the ruthenium centre.

During the experiment the active, mixed valence complex is formed by chemical oxidisation of the bound species with the ferrocenium complex [FcH][PF_6], and the ferrocene produced can then be washed away. Sonication as part of the washing process improved washing but only a small fluorine signal was observed by XPS after washing which suggested that the majority of [PF_6]$^-$ counterions were lost. Fehlner *et al.* suggested that for the oxidised form there were two surface species: [**6**][Si-O][PF_6] and [**6**][Si-O]$_2$ present and after extensive washing the second species is the most common one.

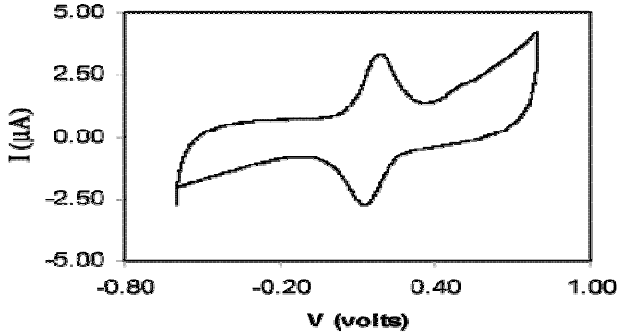

Figure 29. CV of 6^+ bound to a highly doped Si surface (10 mV/s, 0.1 M $TBAPF_6$ in CH_2Cl_2). Taken from [31].

The CV of the bound material $\mathbf{6}^{+}$ is shown in Figure 29, which is very similar to the CV of the molecule bound to a gold surface shown in Figure 27. It can be seen that the fwhm peak is 140 mV and E_{pc} and E_{pa} were spilt by ~60 mV, which Fehlner *et al.* believes is a sign of good uniformity and redox centres that interact to a measurable extent. It is also believed by Fehlner *et al.* that the non-zero splitting between the peak maxima here compared to that in Figure 27 indicates that there was a lower electrode to complex electron transfer rate than on the gold surface. Integration of either peak in Figure 29 gave a density of redox sites as 4×10^{13} cm^{-2} which was equivalent to 45% coverage. It was estimated that the rate of electron transfer between **6** and the silicon surface was about 4.3 s^{-1} which is slower than the rate between **6** and the gold surface.

The stability of the films of $\mathbf{6}^{+}$ was examined in the same manner as those on the gold surface and it was found that the film could be reduced and reoxidised without degradation. Integration of the charge suggests that only 10-20% of the film was oxidised by the ferrocenium ion. As with the film on the gold surface it was found that the oxidised films were modestly air sensitive but the unoxidised film did not degrade after several weeks.

Capacitance measurements of the chemically oxidised $\mathbf{6}^{+}$ showed two peaks at 0.7 and -0.4 V Hg which disappeared on reduction of the film and were attributed to the presence of the mixed valence $\mathbf{6}^{2+}$. This enhanced capacitance was believed to be due to the rapid flipping of the dipole as the electron transfers between the ruthenium and the iron centres at the potential where the two metal wells are equalised. From integration of the peak at 0.7 V the maximum density of 8×10^{11} cm^{-2} for $\mathbf{6}^{2+}$ was obtained. The fact that there are two signals was attributed to the presence of [**6**][Si-O][PF_6] and [**6**][Si-O]$_2$. Assignment of the two signals was carried out by washing a piece of oxidised film several times before measurement. This time the signal at -0.4 V was much smaller than the peak at 0.7 V and XPS found a decrease in the amount of PF_6^- present leading to the peak at -0.4 V to being assigned as [**6**][Si-O][PF_6]. Films oxidised using [$N(Bu)_4$][PF_6] as the electrolyte instead of chemical oxidation produced the same results.

All the measurements obtained suggest that the system exhibits switching between the two metal sites caused by changing electric field, which means that this material is a candidate for molecular QCA.[31]

Whilst this work showed that electron transfer can be generated by an electron field it was also found that this study raised several questions which were

a) The dependence of the intensity of the dipolar response to switching on the distance between the two metal centres.
b) The effect of removing the dissymmetry between the metal centres.
c) The effects of counter-ions on the switching potential.

In an extension to this work a symmetrical diad system was then used to provide answers to the questions. The systems chosen for the examination was *trans*-$[Cl(dppe)_2Ru(C{\equiv}C)_6Ru(dppe)_2Cl]$ which was modified by the addition of an amine tail to allow attachment to the silicon surface. This molecule was selected as it is a representative of the class of symmetrical Robin Day Class III compounds. It was thought that these compounds would be unsuitable for MQCA applications as the ground state is when the electron is delocalised between the metal centres and this does not provide the two binary states required. However it is thought that changes caused by binding a Class III molecule to the surface, the effect of counter-ions or the applied electric field might localise the electron and could make such a system suitable of MQCA.[42]

The starting material *trans*-$[Cl(dppe)_2Ru(C{\equiv}C)_6Ru(dppe)_2Cl]$ has been shown prior to this study to afford two reversible oxidation waves which correspond to the formation of the mixed valence monocation and dication. The splitting of the oxidation waves was 230 mV which corresponds to a comproportionation constant of 10^4 which is sufficient for MQCA criteria.[43]

The functionalisation for attachment to the surface was carried out as shown in Scheme 4.

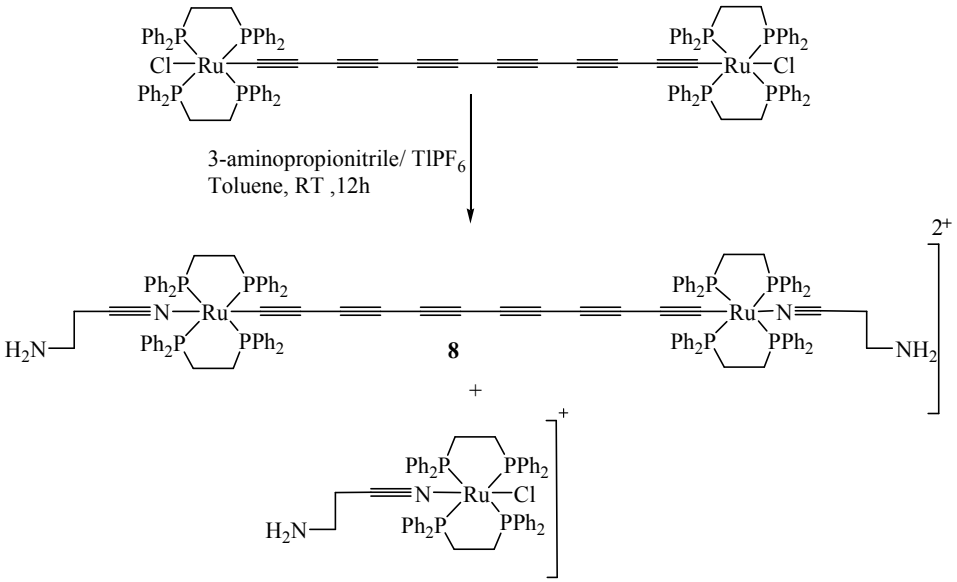

Scheme 4.Functionalisation of *trans*-[Cl(dppe)$_2$Ru(C≡C)$_6$Ru(dppe)$_2$Cl]. Adapted from [42].

The first oxidation process of **8**[PF_6]$_2$ was found by Fehlner *et al.* to be shifted by 0.2 V with respect to the neutral compound. However as with the earlier studies replacement of a chloride by an amine linker caused the second oxidation peak to become irreversible. Repetitive scanning and scanning at higher positive potentials lead to degradation in solution.[42]

The mixed valence **8**$^{3+}$ state was studied using quantum chemical calculations, replacing the phenyl rings with hydrogens denoted **8**$^{3+}$**(H)** to enhance high-quality calculations. The optimised structure shows the charge to be localised between the two metals with no overall dipole moment as shown in Figure 30.

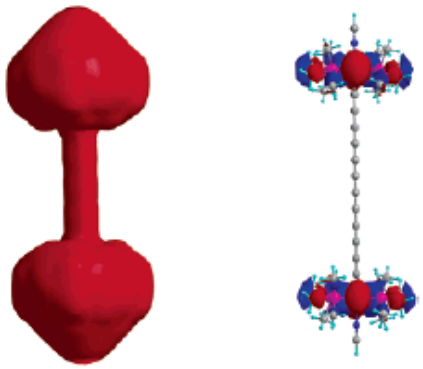

Figure 30. Left) Electrostatic potential surface and Right) charge distribution in the HOMO for 8^{3+}(H). Taken from [42].

A uniform field was then applied between the two redox centres to see whether an external field can cause localisation. It was seen that the dipole moment of **8^{3+}(H)** increased with increasing external field, when the electric field was at 1 V/nm the dipole moment was 8.4 Å. The charge distribution showed +1.1 at one ruthenium and +1.9 at the other ruthenium compared to +1.5 on both rutheniums in no field. The charge distribution and electrostatic potential surface are shown in Figure 31.

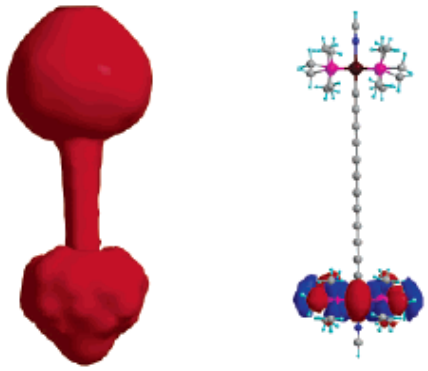

Figure 31. Left) Electrostatic potential surface and right) charge distribution in the HOMO for 8^{3+}(H) in a uniform electric field of 1 V/nm. Taken from [42].

This modelling shows that although compound **8^{3+}** is a class III compound it should still be suitable for MQCA applications along as the field of the adjacent molecule can localise the electron by breaking the symmetry of the two quantum wells.[42]

The complex was attached to the silicon surface as before, apart from the solvent had to be changed from DCM to acetonitrile due to a decrease in solubility of **8**$[PF_6]_2$ compared to **6**. However Fehlner *et al*.[42] reported that after 72h only 15% coverage was achieved compared with 45% coverage of **6** after 30 h. It is not possible for both ends of **8**$[PF_6]_2$ to bind to the surface due to the rigid nature of the bridging ligand.[42]

The compound **8**$[PF_6]_2$ was found by Fehlner *et al.*[42] to be more air sensitive than **6**$[PF_6]$ so the films were prepared in a drybox and no sonication was used. This time, variable angle XPS could not be used due to the symmetry of the molecule so film thickness was relied on as an experimental indicator of orientation of the complex. An average film thickness was measured as 27.7 ±0.8 Å, which was closer to the length of the molecule **8**$[PF_6]_2$ (28 Å) than the width (13 Å).

Square wave voltammetry on films of **8**$[PF_6]_2$ on a boron doped substrate gave reversible waves with a 143 mV fwhm and a peak separation of 30 mV compared to a 140 mV fwhm and 40 mV peak separation for **6**$[PF_6]$. The density of the redox sites was calculated at 1.6 x 10^{13} cm^{-2} which is 15% coverage.

Whilst the mixed valence state of **6**$[PF_6]$ was shown to be generated electrochemically and chemically using [FcH]$[PF_6]$, the oxidation potential of **8**$[PF_6]$ was higher and electrolysis was thought to be a better choice. An oxidising potential of 750 mV was applied to the supporting electrolyte in acetonitrile. The net yield of mixed-valence complex was obtained by dc potential amperometric (DCPA) and it was found 11% of the oxidised molecules survived a 2s oxidation. Increasing the oxidation time to 10 s lead to 5% yield of oxidised molecules and after 30 s the chemical activity of the film was completely destroyed. So a 2s oxidation time at 750 mV was adopted by Fehlner *et al.* as the best conditions.[42]

A single wafer of **8**$[PF_6]_2$ was cut in half, one half was oxidised to **8**$[PF_6]_3$ and the other half was used unoxidised. Capacitance measurements were carried out on both wafers and even after 2 h in air the signals did not degrade significantly. As there may have

been redox processes occurring between the silicon and mercury electrodes, the unoxidised film was used as a baseline. The activity due to the mixed valence species is thus the capacitance of the oxidised film – the capacitance of the unoxidised film and the switching potential of the **8**$[PF_6]_3$ was found to be -0.2 V. Integration of the peak at the switching potential showed the density of the mixed valence state to be 1.8 x 10^{12} cm^{-2}. As for **6** the switching potential value is lower than the value given by the electrochemical measurement of the density.[42]

Fehlner *et al.*[42] used the switching potentials and surface densities of the mixed-valence complexes to propose that the dipolar response increased with an increased distance between the metal centres. This suggests that the dipolar field generated can be tuned by adjusting the length of the conjugated bridge in a diad system. In a MQCA system this dipolar field would be responsible for inducing switching in a neighbouring cell and therefore transferring a signal down a row of cells. Being able to tune the dipolar field would be a distinct advantage as the distance between two MQCA cells is dictated by the steric bulk of the ancillary ligands.[42]

Whilst it is not clear what the differences between symmetrical and unsymmetrical systems are, Fehlner *et al.* have demonstrated that the switching occurs in the same manner in **6**$[X]_2$ and **8**$[PF_6]_3$.[42]

Further investigation was carried out with the more robust **6**$[PF_6]$ to look at the effect of the counter-ion. Compound **6** was oxidised with a range of oxidising agents to generate $\mathbf{6}^+$ with the counter-ions $[SO_3CF_3]^-$,$[PF_6]^-$ and $[Cl]^-$ and the switching potentials of these compounds were measured. Fehlner *et al.* found that the larger the size of the counter-ion the less effect it had on the switching potential. Overall it was suggested that the counter-ion causes perturbation of the potential at which the energy of the electron is independent of metal site location. The effect appeared to be more dominating than the identify of the metal sites, hence, the switching potentials of **6**$[Cl][PF_6]$ and **8**$[PF_6]_3$ are similar despite one being a symmetrical complex and the other not.[42]

1.4.6.2.2 Tetrad ferrocene systems for MQCA

One of the problems with four-metal centres systems is that the metals must be arranged in a square since a rectangular or tetrahedral arrangement would not be suitable. In 1978 Rausch *et al.* synthesised a cyclobutadiene complex containing four ferrocene units.[45,46] Whilst the reported electrochemistry was not encouraging with a wave at 0.29 V and then the remaining three waves merging to form a broad wave, Fehlner *et al.* felt that it would be a system worthy of closer examination.[33] The complex $\{(\eta^5\text{-}C_5H_5)Fe(\eta^5\text{-}C_5H_4\}_4(\eta^4\text{-}C_4)Co(\eta^5\text{-}C_5H_5)\}$ **9** was synthesised from diferrocenylacetylene and $CpCo(CO)_2$ and the structure is shown in Figure 32.[33]

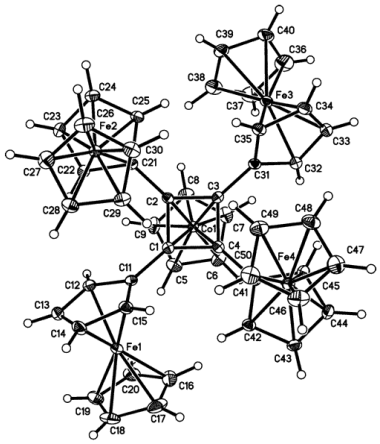

Figure 32. Molecular structure of $\{(\eta^5\text{-}C_5H_5)Fe(\eta^5\text{-}C_5H_4\}_4(\eta^4\text{-}C_4)Co(\eta^5\text{-}C_5H_5)\}$ 9.Taken from [47].

Oxidation of **9** was carried out with $[FcH][PF_6]$ resulting in $[\mathbf{9}][PF_6]$. Generation of $[\mathbf{9}][PF_6]_2$ required several attempts with different reagents but was achieved with acyl-substituted ferrocene and $[\mathbf{9}][X]_2$ X= PF_6, BF_4 and triflate were isolated. Attempts were also made by Fehlner *et al*. to synthesise the +3 and +4 ions but while spectroscopic data suggested that the ions were obtained it was not possible to isolate them.

It was found that solvent choice for electrochemistry was important and that a 1:1 DCM:acetonitrile provided good resolution. Cyclic voltammetry and square voltammetry is illustrated in Figure 33 and shows three distinct redox waves. It is proposed by Fehlner *et al*. that the broad peak at the most positive potential suggests the presence of a fourth peak.

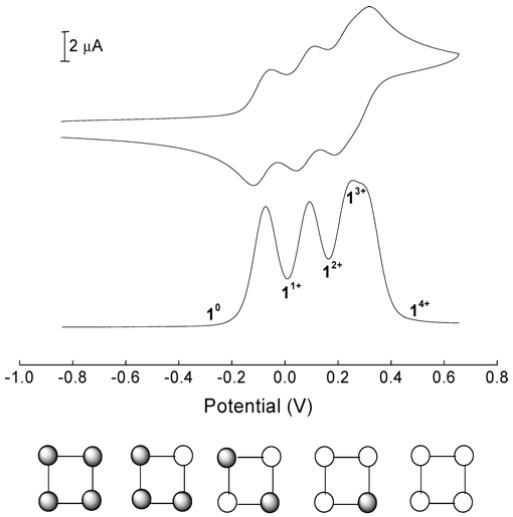

Figure 33.Cyclic and square voltammetry of {(η^5-C_5H_5)Fe(η^5-C_5H_4}$_4$(η^4-C_4)Co(η^5-C_5H_5) 9^0, at 100 mV s-1 in CH_2Cl_2/CH_3CN mixed solvent. The five oxidation states (Fe^{II} grey, Fe^{III} white) are represented at the bottom of the figure, and the numbers on the square wave data indicate the potentials at which each is stable. Taken from [44].

The $E_{1/2}$ potentials have been measured as $\mathbf{9^0/9^{1+}}$ = -0.085 V, $\mathbf{9^{1+}/9^{2+}}$ = 0.075 V, $\mathbf{9^{2+}/9^{3+}}$ = 0.225 V and $\mathbf{9^{3+}/9^{4+}}$ = 0.283 V relative to the ferrocene/ferrocenium couple. This gives a potential difference between the redox waves of 160, 150 and 58 mV which generated the following comproportionation equilibria as:

$$\mathbf{9^0} + \mathbf{9^{2+}} \rightleftharpoons 2(\mathbf{9^{1+}}) \qquad K_c = 510$$

$$\mathbf{9^{1+}} + \mathbf{9^{3+}} \rightleftharpoons 2(\mathbf{9^{2+}}) \qquad K_c = 346$$

$$\mathbf{9^{2+}} + \mathbf{9^{4+}} \rightleftharpoons 2(\mathbf{9^{3+}}) \qquad K_c = 10$$

Fehlner *et al.* suggest that from these comproportionation equilibria shown above that it is likely that $\mathbf{9^{1+}}$, $\mathbf{9^{2+}}$ and $\mathbf{9^{4+}}$ can be isolated but not $\mathbf{9^{3+}}$.

Mid-range IR spectroscopy has been proven to be a good indicator of whether a mixed-valence complex is electron delocalised or not within the time scale of molecular vibrations. Also it was noted that a change in the frequency of the perpendicular C-H bending vibration in the IR is observed upon oxidation of ferrocene to ferrocenium changing from 815 cm^{-1} to 851 cm^{-1}. $[BF_4]^-$ salts were prepared as $[PF_6]^-$ salts exhibit a band in a similar region to the ferrocene/ferrocenium band. The IR spectra for the **9**, $\mathbf{9^{1+}}$,

$\mathbf{9}^{2+}$ and $\mathbf{9}^{3+}$ are shown in Figure 34, where it can be seen that **9** has a single band characteristic of ferrocene, $\mathbf{9}^{1+}$, $\mathbf{9}^{2+}$ and $\mathbf{9}^{3+}$ have two bands consistent with ferrocene and ferrocenium in varying ratios.

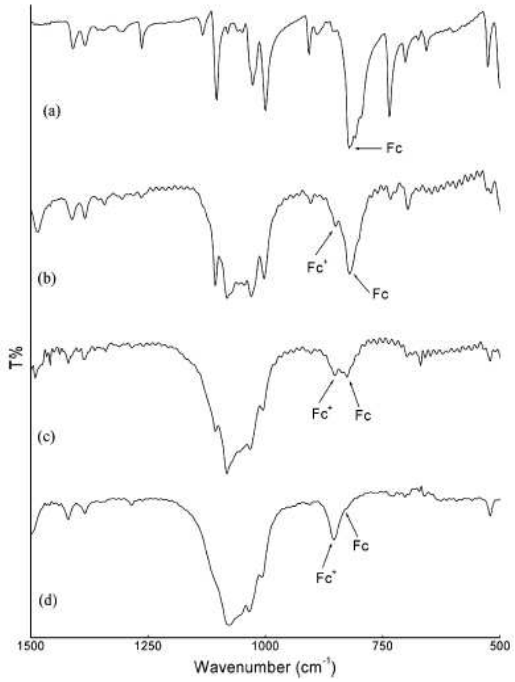

Figure 34. FT-IR spectra in KBr pellets of a) $\mathbf{9}^{0}$ b) $\mathbf{9}^{1+}$ c) $\mathbf{9}^{2+}$ and d) $\mathbf{9}^{3+}$.Taken from [44].

The IR data showed each complex had localised Fe^{II} and Fe^{III} ferrocene species on the IR time scale which means the electron exchange rate must be $<10^{12}$ s^{-1} at room temperature in the solid state. This data also suggests that the $\mathbf{9}^{3+}$ is formed and that disproportionation is not rapid in solid state but occurs in solution.

Electron paramagnetic resonance (EPR) measurements were made for $\mathbf{9}^{1+}$ and $\mathbf{9}^{2+}$ and comparison with mixed valence biferrocene complexes suggested that the cations are localised on the EPR time scale. Magnetic spin measurements were also made on $\mathbf{9}^{1+}$ and $\mathbf{9}^{2+}$; the results were consistent with one and two unpaired electrons respectively. Mössbauer spectroscopy results for **9** showed a quadrupolar doublet very similar to ferrocene and characteristic of low spin Fe^{II} in a highly distorted environment. $\mathbf{9}^{1+}$ and $\mathbf{9}^{2+}$ also exhibited this doublet and a smaller doublet was also observed for both

complexes consistent with Fe^{III} in a highly distorted environment. This data also suggested that there is no electron delocalisation between the Fe^{II} and Fe^{III} sites in $\mathbf{9}^{1+}$ or $\mathbf{9}^{2+}$ and that on the Mössbauer timescale (10^{-7} s) the complexes behave as Robin Day class II localised discrete valence compounds. It is known that for a mixed-valence biferrocene compound with an electron exchange rate > 10^{7} s^{-1} a single averaged quadrupole is observed.[48,49]

Mössbauer spectroscopy also showed that for $\mathbf{9}^{1+}$ one out of four Fe^{II} of the sites had been oxidised to Fe^{III} rather than the other alternative which is that in a quarter of the molecules all the four sites are Fe^{III}.

IR was used to look for the presence of IVCT bands in the near IR region which is a characteristic of class II and class III mixed-valence compounds. As expected the neutral compound $\mathbf{9}^{0}$ showed no bands in UV-Vis and near IR spectroscopy. The near IR spectra of $\mathbf{9}^{1+}$ and $\mathbf{9}^{2+}$ showed a band which was assigned to the transfer of an electron between the ferrocene and ferrocenium centres. $\mathbf{9}^{3+}$ showed one broad band at 922 nm which shifted to lower energy with time. This is thought to be due to disproportionation into $\mathbf{9}^{2+}$ and $\mathbf{9}^{4+}$ which is expected following the comproportionation constants obtained from the electrochemistry results. The impure $\mathbf{9}^{4+}$ shows no bands in the near IR region. From this data $(\Delta\nu_{1/2})_{obs}/(\Delta\nu_{1/2})_{calc}$ were obtained which was found to be an average of 1.3 for $\mathbf{9}^{1+}$ and 1.1 for $\mathbf{9}^{2+}$ which is consistent with Robin-Day class II complexes. The delocalisation parameter α^2 was found to be ~5-6 x 10^{-3} for $\mathbf{9}^{1+}$ and ~6 x 10^{-3} for $\mathbf{9}^{2+}$ which also fits in with literature Robin-Day class II compounds. Hush theory also allowed Fehlner *et al*. to estimate the electron transfer rate at 10^{8} s^{-1} for $\mathbf{9}^{2+}$ (compared to 10^{7} s^{-1} in solid state calculated from EPR, Mössbauer) in the absence of an electric field. The thermal free energy barrier corresponded to 6.6 kcal/mol but Fehlner *et al.* hope that in the presence of an electric field that the electron transfer rate will increase.

It is important that the extra electrons are *trans* to each other, Variable temperature NMR was used by Fehlner *et al.* to examine the position of the electrons and holes in the molecules.

NMR spectroscopy of $\mathbf{9^0}$ showed that at room temperature free rotation around the C-C bonds occurred and all the ferrocene protons were equivalent. However at 233 K this rotation ceased and two of the ferrocene rings were up and two were down as seen in the X-ray structure.

The NMR spectra for $\mathbf{9^{1+}}$ and $\mathbf{9^{2+}}$ were more complicated than $\mathbf{9^0}$ due to paramagnetism. If electron transfer was rapid then one signal would be observed for the ferrocene/ferrocenium groups however for $\mathbf{9^{1+}}$ and $\mathbf{9^{2+}}$ several signals were observed. Fehlner *et al.* interpretated this as the presence of a thermal barrier causing electron transfer to be slow. However in the spectrum for $\mathbf{9^{1+}}$ at low temperatures the Co-η^5-C_5H_5 ring signal was split into two resonances which would be expected if the ferrocenium group can be either above or below the cyclobutadiene plane. In previous mixed-valence biferrocene cation complexes it has been found that the electron transfer rate is different for coplanar and non-coplanar arrangements of the ferrocene.[50] So the slow electron transfer may be due to in the solid state the π-systems of the cyclobutadiene and the ferrocene groups not being aligned. It was not possible from the spectra for $\mathbf{9^{2+}}$ obtained to determine whether the two electrons were *trans* or *cis* to each other.

Although the data suggests that the electron is localised in the structures and that electron exchange is slow, Fehlner *et al.* believe that much of this is due to the misalignment of the ferrocene groups and the cyclobutadiene linker. As it is necessary for the molecules to be attached to a surface for MQCA applications they hope that this would force the ferrocene groups to all be *trans* to the Co-η^5-C_5H_5 ring and hence faster electron transfer will occur.

1.5 Summary and Objectives

To summarise, the miniaturisation of electronic devices can not continue at its current rate and problems are already being encountered. The use of molecules in electronics is an attractive choice because of their size and their diverse range of functional groups which could provide a wide range of applications. Whilst most molecular electronics are designed to be compatible with silicon technology, QCA is a completely new paradigm. Whilst QCA is well modelled there are very few real systems that have been researched which are suitable for such applications. A brief overview of the existing research carried out in the area of MQCA has been summarised here.

The objectives of this thesis were to synthesise and characterise new materials suitable for application in MQCA. The electrochemistry of these materials will be presented and compared to previous research in order to assess the compounds suitability for MQCA applications.

2. Chapter 2: Cyclobutadiene cobalt complexes

2.1 Introduction to cyclobutadiene cobalt complexes

In chapter 1 one of the focuses of the discussion was that for molecular materials to be suitable for MQCA applications they must have a square symmetry. There are only a limited number of possibilities for creating such an arrangement and one such arrangement is with a cyclopentadiene cobalt cyclobutadiene [CpCoCb] linker to connect the redox centres. These compounds are known to be very stable and Fehlner *et al.*[47] have already proven that ferrocene centres linked by this ligand have potential as MQCA materials. Whilst there are many [CpCoCb] compounds known in the literature there are none containing four redox active groups other than ferrocene.[45] With this is mind it was felt that [CpCoCb] systems would be worth investigating as there is literature evidence to suggest communication through the cyclobutadiene linker.[47]

In this Chapter the proposed mechanism for cyclisation of acetylenes leading to the formation of squares is presented along with discussion of the possible products from the reaction. Modelling of the bonding of the [CpCoCb] system from literature is described along with additional modelling that has been carried out as part of this study. Discussion of [CpCoCb] systems known in the literature that are of interest for MQCA applications concludes the introduction.

2.1.1 Metal mediated cyclisation

Cyclisation of acetylenes has been carried out using a range of metal fragments including {CpRuCl},[51] $[CpRu(PH)_3]^+$,[52] {CpCo}[53-55] and {Cp*Rh}.[56] However {CpCo} is the classic alkyne cylisation catalyst and is the focus of this discussion. Understanding of the cobalt mediated cyclisation mechanism is limited and experimental results are often hard to explain.

Since the 1960s a huge range of [CpCoCb] compounds have been prepared and studies of the reactivity of the products been carried out. Yet it is still not clear what controls the

distribution of the products obtained and the precise nature of the mechanism. Dicobalt compounds with bridging acetylenes have been isolated from reactions and have been suggested as possible intermediates.[57] However, the mechanism proposed by Rausch *et al.* featuring a metallocyclopentadiene intermediate is more widely accepted and is shown in Scheme 5.

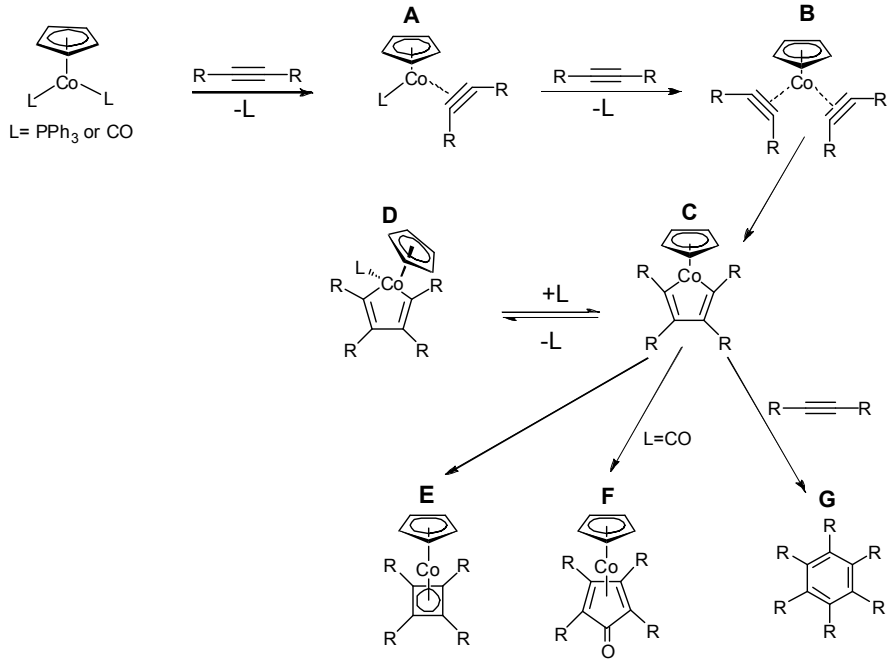

Scheme 5. Schematic diagram of Rausch's mechanism for cobalt mediated cyclocylisation.[58]

The first step of Rausch's proposed mechanism is the stepwise exchange of the ligand (L) which is either PPh_3 or CO, on the cobalt with the alkynes which leads to **A** and **B**. From **B** then **C** can form which is equilibrium with **D**. Then the products **E**, **F** and **G** can be obtained from **C** depending on the reaction conditions used. Evidence to support this mechanism is found by the isolation of complexes **A** and **D** and whilst **B** and **C** can not be isolated there is experimental data to support their existence. Veiros *et al*.[59] have modelled two different pathways *via.* asymmetric intermediates between **B** and **E** which show a large activation barrier to formation of **E** by either pathway. Because of this high barrier to formation of **E** the other products **F** and **G** are often formed in preference.[59]

Studies have been carried out to investigate the effect of steric bulk on converting [CpCoCb] **E** into the cyclopentadienecobalt cyclopentadienone product **F** but there have been no systematic studies examining the formation of the cyclobutadiene product.[58]

Computational studies have also been used to calculate the energetics for the reaction pathways for the intermediates in [CpCoCb] formation. These energetics for the formation of **C** and **E** are shown in Figure 35.

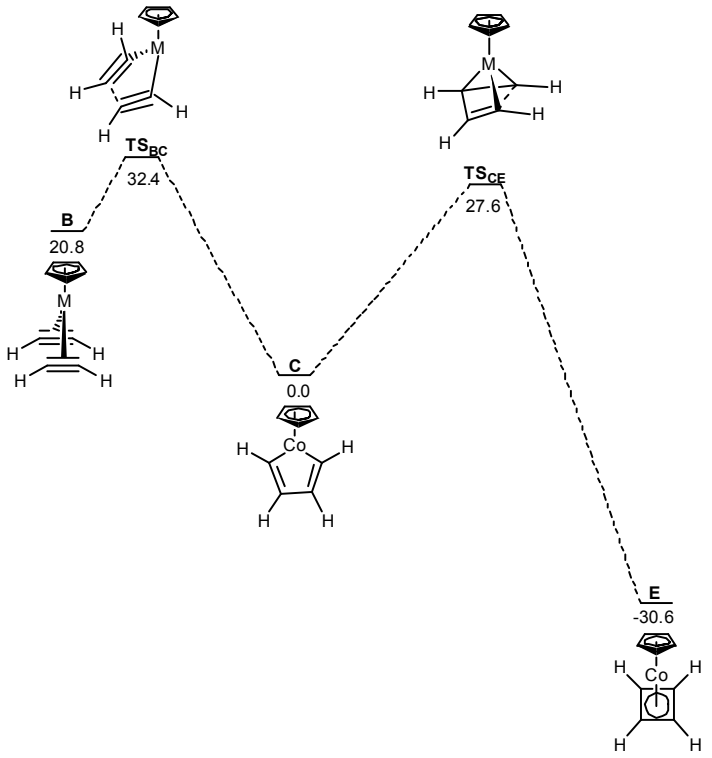

Figure 35. Energetics for the conversion of B to C (left) and C to E (right) for {CpCo} , energies in kcal/mol.[59]

It can be seen from Figure 35 that the formation of the transition state between **B** and **C** (**TS_{BC}**) has a much lower energy barrier than the transition state between **C** and **E** (**TS_{CE}**). In a similar system to that shown in Figure 35 Veiros *et al*.[59] found that for the reaction of {CpRuCl} with HC≡CR the barrier to the transition states varies as the R group changes H≈Ph>Me>>$SiMe_3$. Veiros *et al*. also speculate that the steric bulk of the acetylene substituent could block the approach of a third acetylene preventing trimerisation. From the studies of the reaction pathways for the different metal fragments[59] it has been shown that the reaction mechanisms of {CpCo}, {CpRh} and {CpRuCl} are very similar. Hence the steric bulk of the acetylene substituent is likely to

have the same effect on the barrier to the transition state in {CpCo} as it does in {CpRuCl}. However, when the reagent is $CpCo(CO)_2$ there is also the added complication of formation of the cyclopentadienone product **F** as shown in Figure 35. It has been found that when $[CpRu(Ph_3)]^+$ is used as a catalyst, phosphane migration occurs into the metallocyclopentadiene leading to the formation of η^3-allyl carbene products.[52] A range of acetylenes have been studied and it was found that the only system that formed the cyclobutadiene product was diphenylacetylene. All the carbene products were formed very rapidly at room temperature, but it was necessary to heat the diphenylacetylene to 80°C for a reaction to occur.[52] It has been suggested from the DFT calculations that were carried out, in conjunction with the experimental observations that the cyclobutadiene complexes are thermodynamically favoured but kinetically unfavoured.[52] From these studies it is believed that formation of cyclobutadiene complexes occurs when all the other alternatives are inhibited. [59]

2.1.2 Bonding in Cyclobutadiene cyclopentadiene cobalt compounds

Cyclobutadiene as an isolated non-coordinated species is predicted by Hückel's rule to be anti-aromatic† as it does not fulfil the (4n+2) π electrons criteria. Cyclobutadiene is not very stable and tends to dimerise easily, unless it is stabilised *e.g.* trapped in a matrix at low temperature. Molecular orbital calculations and experimental data have shown that cyclobutadiene is a rectangle not a square and it rapidly interconverts between two forms which are shown in Figure 36.[60]

Figure 36. The two interconverting forms of cyclobutadiene. Adapted from [60].

However cyclobutadiene can be stabilised by coordination of a metal such as cobalt to form very stable compounds.[60] Single crystal X-ray diffraction experiments performed

† Anti-aromaticity is the destabilisation of a compound by a closed ring of electrons.[60] J. March, Advanced Organic Chemistry, 4th, Wiley Interscience, New York, 1992.

on these cobalt stabilised compounds have shown that the cyclobutadiene ring is a square with 4 equal bond lengths and angles.[45,55,61]

Whilst the bonding in homoleptic compounds such as ferrocene and cobaltocene is well known and understood, this is not true for heteroleptic systems such as $(C_5H_5)Mn(C_6H_6)$, $(C_5H_5)Cr(C_7H_7)$ and $(C_5H_5)Co(C_4H_4)$. Complications arise when considering heteroleptic systems, as the energies of conjugated cyclic ligands vary with ring size.

It is know that for conjugated cyclic ligands with increasing ring size the energies of the e_1 and e_2 ligand orbitals become more negative,[62] as shown in Figure 37. Assuming that the d-orbitals of the metal remain lower in energy than the ligand e_2 set, this means that as the ring size increases the interaction between the 3d and e_2 orbitals should increase and the interaction between the 3d and e_1 decreases. For the purpose of this diagram it was assumed that the ligand a_1 orbital energy is unaffected by a change in ring size and that the 3d a_1 level does not make a significant contribution to the bonding.[62]

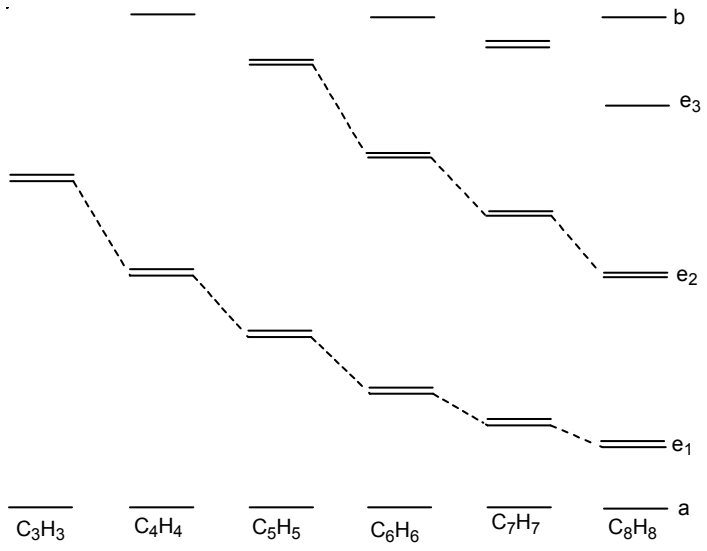

Figure 37. Plot showing the ligand π-orbital energies on ring size.

Clack and Warren have carried out INDO SCF molecular orbital calculations on a range of homoleptic and heteroleptic metal systems[62,63] which include the only molecular

orbital considerations of the [CpCoCb] system to date. In these calculations the 4s and 4p orbitals are ignored as the extent of their contribution to the bonding is not fully understood. The contribution of 3d orbitals to bonding is much better understood and in sandwich systems the main interaction occurs between the π-orbitals and the 3d metal orbitals.

To supplement the calculations by Clack *et al*.[62,63] complimentary calculations[64] were carried out by us as part of these studies using the Gaussian program suite.[65] The molecular orbital diagrams obtained from our calculations shown in Figures 38 and 39 were in agreement with those of Clack *et al*. but provide additional information on the contributions of the different orbitals into forming the [CpCoCb] orbitals. These calculations do not form part of this thesis but some information is provided here to gain clarity on the bonding of [CpCoCb].

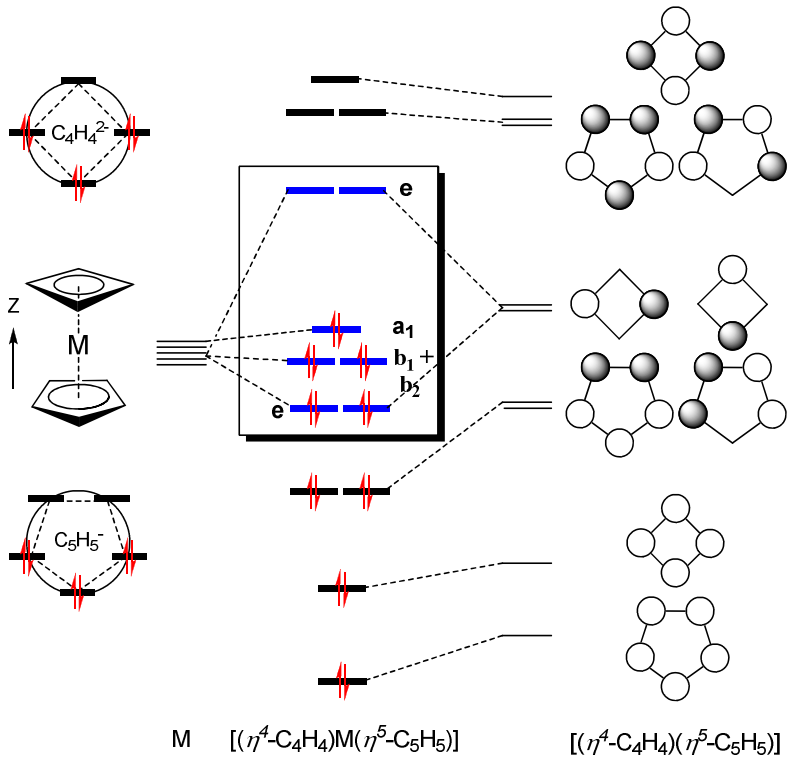

Figure 38. Molecular orbital diagram of cyclobutadienecobaltcyclopentadiene. The highlighted orbitals are the frontier orbitals.

The calculations for the frontier orbitals show that the three highest occupied orbitals shown in Figure 39 are all almost entirely metal-based in their character. As these are all filled the metal centre has a d^6 configuration and results in an oxidation state of III for cobalt. Cyclopentadiene is now Cp^- as it has 6 electrons and the cyclobutadiene ring is denoted Cb^{2-} as it also has 6 electrons.

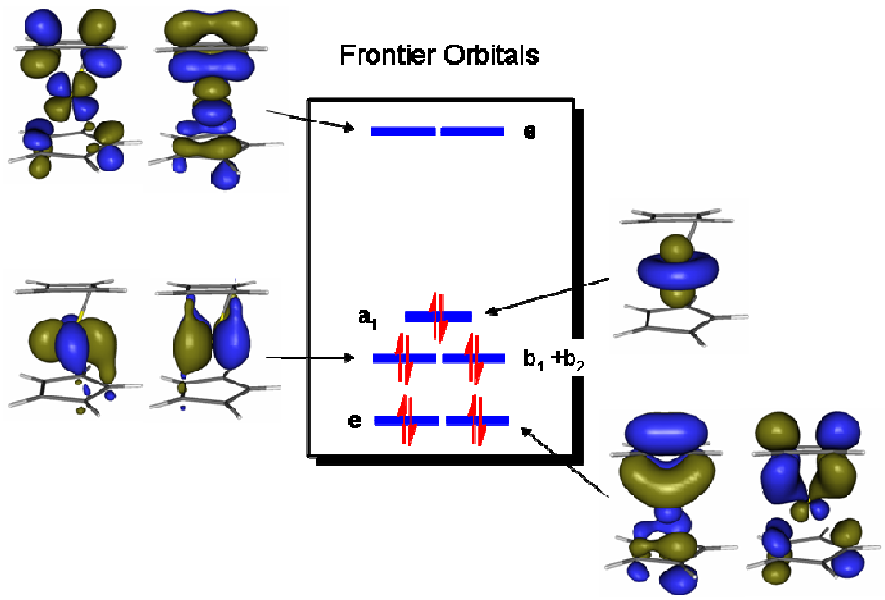

Figure 39. Frontier orbitals in [CpCoCb].

The e orbital was found to be mainly cyclobutadiene in nature with a ~20% contribution from the 3d orbitals which shows a powerful effect of the e, $3d_{xz},d_{yz}$-π-Cb interaction on the bonding. There is little interaction between the π-Cp orbitals and the 3d orbitals on cobalt as the π-Cp orbital lies at a lower energy than the π-Cb orbital. The π-Cp orbital is however at the correct energy to interact with the s and p orbitals of the cobalt and form strong bonds. Clack *et al.*[62] studies of the free $Cb^{2-}Cp^-$ moiety showed that the π-donation from the cyclobutadiene ligand is roughly twice as great of that of cyclopentadiene.

The molecular orbital diagram [CpCoCb] generated by the modelling shows that the compound is an 18 electron compound which explains its stability. Because of the higher energy of the Cb orbitals it can be expected that the Co-Cb bond is kinetically

labile compared to the Co-Cp bond. It can also be seen from the molecular orbital diagram that [CpCoCb] is diamagnetic which is in agreement with the NMR spectroscopy observed for these compounds.

2.1.3. Synthesis of aromatic substituted [CpCoCb] complexes.

In general the synthesis of [CpCoCb] complexes can follow two approaches as shown in Scheme 6. Route 1 is building up the desired linear monomer and then carrying out the dimerisation at the metal centre.[66] Route 2, requires dimerisation to be carried out at the metal centre followed by build up of the desired branch by methods such as Sonogashira coupling.[67]

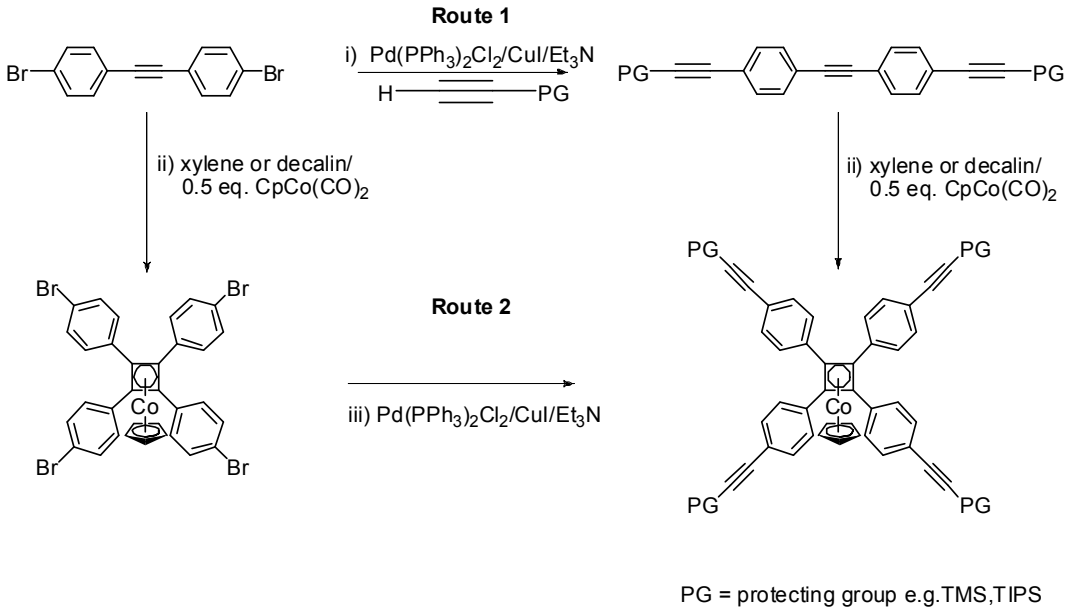

Scheme 6. Two different approaches to synthesising aromatic substituted [CpCoCb] compounds. Route 1 building up the linear chain first then dimerisation or Route 2 dimerisation first and then further functionalisation.

Harrison *et al.*[67] have prepared a series of aromatic substituted [CpCoCb] complexes. Their interest in these compounds was for the development of uniform 2D grids from the cyclobutadiene squares and then functionalisation of the cyclopentadiene ring to allow surface attachment. The range of [CpCoCb] complexes synthesised during their work is shown in Scheme 7.

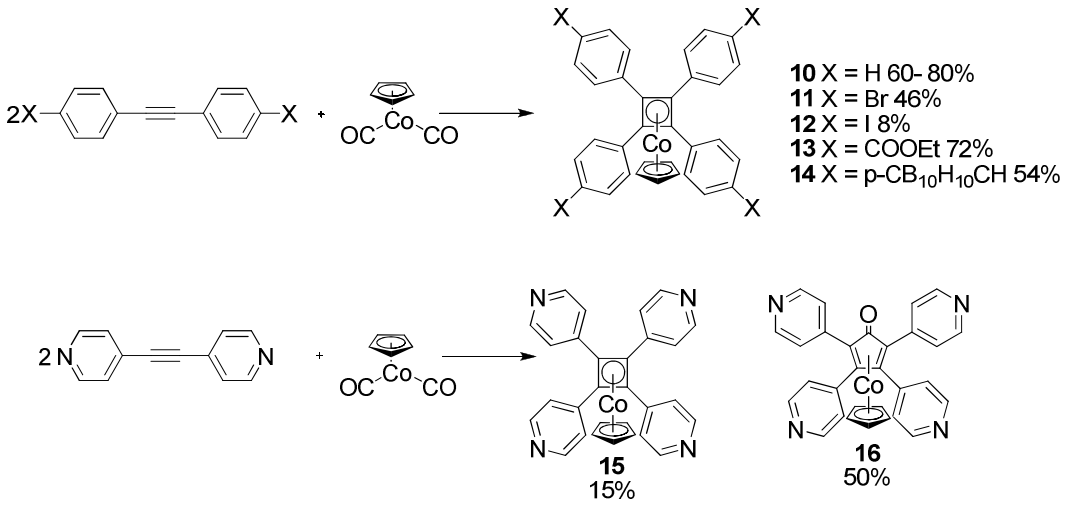

Scheme 7. Reaction scheme for compounds produced by Harrison *et al.* Percentage yields are shown in the key.

The complexes of interest for MQCA applications are **11** and **15**. Compound **11** is of interest because it has the potential for branch modification using Sonogashira coupling to form more extended acetylene systems. Compound **15** is of interest for MQCA applications as it has the potential to form σ bonds with groups such as ruthenium(*p*-cymene) dichloride as shown in Scheme 8.

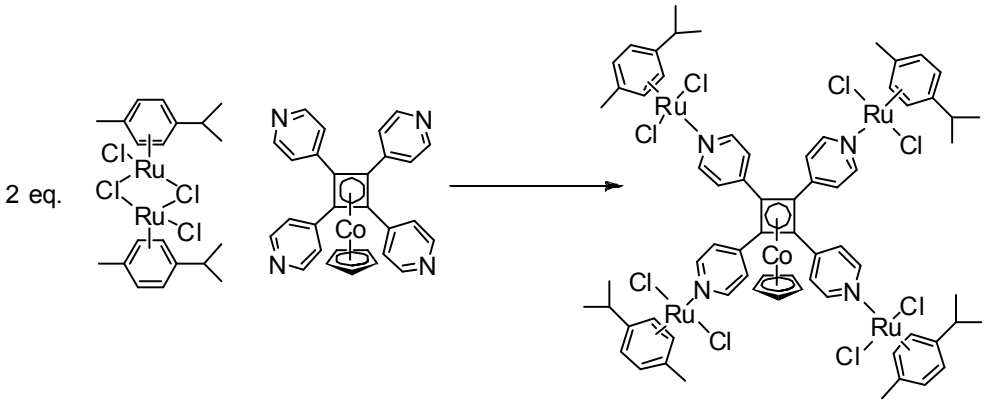

Scheme 8. Proposed reaction between 15 and ruthenium(*p*-cymene) dichloride.

Further functionalisation of compound **11** has been carried out by Harrison *et al.* using Sonogashira coupling as shown in Scheme 9.[67] However the conditions reported for the reaction are very harsh, the reaction was refluxed in total for 192 h and the catalyst and triethylsilylacetylene was added in three batches. The overall $Pd(PPh_3)_2Cl_2$ loading was 84 mol% and 42 equivalents of triethylsilylacetylene to produce **17** in 58%.[67] For a

comparison a typical Sonogashira reaction tends to use 2-5 mol% of palladium catalyst and 1.1-1.2 equivalents of trimethylsilylacetylene per coupling site. This reaction would be more favourable if the iodo derivative **12** was used however Harrison *et al*. only achieved an 8% yield of **12** so were not able to carry out this reaction.

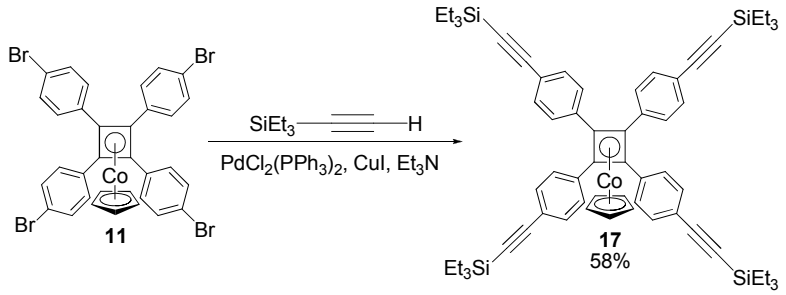

Scheme 9. Further functionalisation of 11 by Sonogashira coupling.

In a complimentary study Waybright *et al.* report the build up of the linear precursor before dimerisation which required much milder conditions than the reaction shown in Scheme 5. The range of TIPS protected [CpCoCb] complexes which Waybright *et al*. synthesised are shown in Figure 40. The starting materials **18-21** are particularly useful as they contain two types of alkynes. The outer alkyne groups are protected by the bulk of the triisopropylsilyl groups and therefore do not undergo the cyclisation reaction. However, the inner diaryl alkyne is able to undergo reaction with $CpCo(CO)_2$, and hence it was found that the reactions proceeded with high yields and with easily purified products.[66]

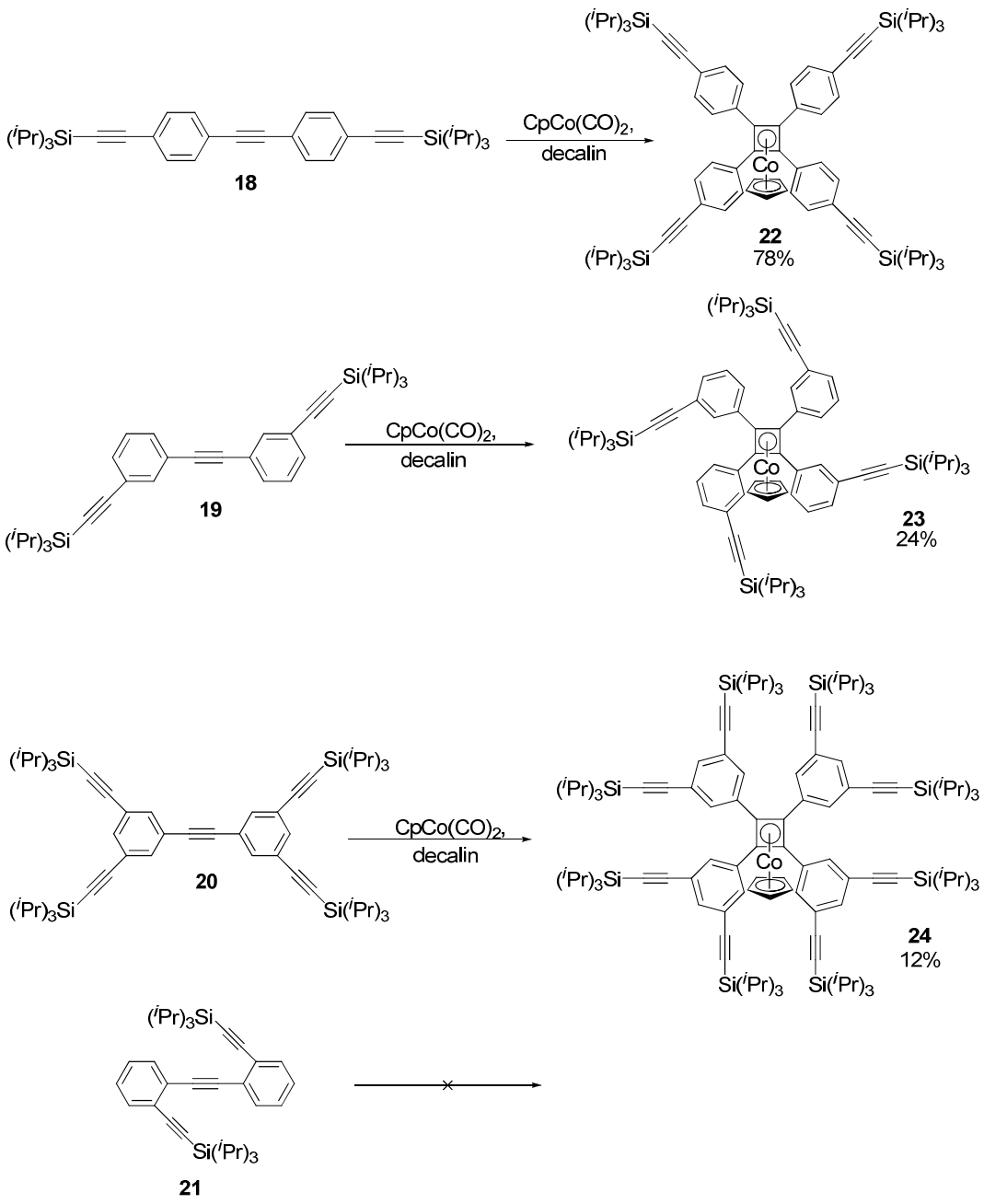

Figure 40. Summary of the [CpCoCb] compounds synthesised by Waybright.[66]

As it can be seen from Figure 40 the highest yield obtained was for **22** when the $\{Si(^{i}Pr)_3\}$ groups are *para* to each other. It has been suggested that the low yields of **23** and **24** were obtained and **21** did not react due to the steric blocking of all three alkyne groups by the arrangement of the $\{Si(^{i}Pr)_3\}$ groups.[66]

Waybright *et al.* has also reported the removal of the $\{Si(^{i}Pr)_3\}$ groups on the [CpCoCb] compounds **22**, **23** and **24** and their subsequent reaction with an excess of tetraphenylcyclopentadiene in boiling decane to give organometallic dendrimers in good yields.[66]

2.2 Results and Discussion

2.2.1. Mechanism for Sonogashira coupling.

The majority of the organic ligands throughout this work were produced by palladium catalysed Sonogashira reactions. The catalyst for this reaction is a palladium (0) complex which can either be $Pd(PPh_3)_4$ or can be generated *in situ* from Pd(II) as shown in Scheme 10. One of the advantages of using a Pd(II) complex is that they tend to be more stable, easier to synthesise and more soluble than some Pd(0) complexes.[68]

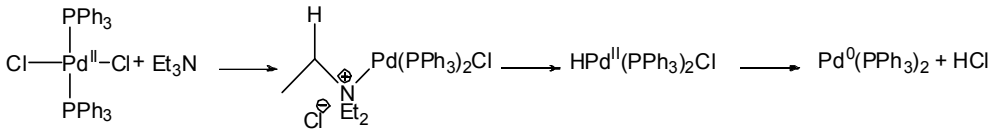

Scheme 10. Mechanism for the *in situ* generation of a Pd^0 species from Pd^{II} by Et_3N.[68]

It is also possible to generate the Pd^0 species using PPh_3, alkenes and organometallics but amine is the reagent used throughout this work. The first step in Scheme 10 is ligand exchange of the amine for a chloride on the Pd complex. The next step is *β*-hydride elimination followed by reductive elimination generating the required Pd^0 species.[68] A range of different amines can be used for Sonogashira reactions and depending on the solubility of the reagents sometimes an additional solvent is used such as THF or toluene to improve the solubility. The reaction also requires a co-catalysis which is copper iodide, which then coordinates to the alkyne and then reacts with the Pd-Ar species as shown in Scheme 11.

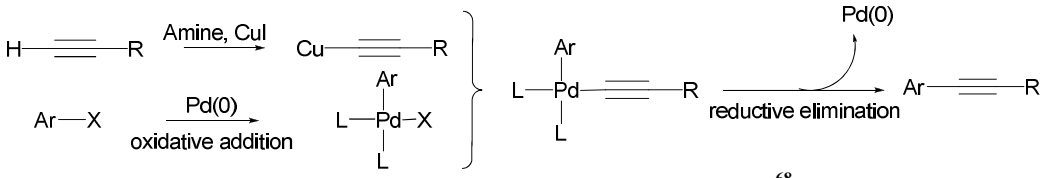

Scheme 11. General reaction pathway for Sonogashira reaction[68], Ar = aromatic and X = Br or I.

The reaction conditions required can often be mild, if X = I then the reaction will process rapidly at room temperature but if X = Br then the reaction may require a long period of heating under reflux.

2.2.2 Synthesis of tolanes

A series of Sonogashira reactions were carried out to produce 1,4-dibromotolane **27** which is a versatile intermediate. Scheme 12 shows the series of reactions and conditions used to produce 1,4-dibromotolane, syntheses were adapted from literature methods.[69] Purification of **25** and **26** was carried out by column chromatography on silica but purification of **27** was carried out by soxhlet extraction due to low solubility. Characterisation of **25**, **26** and **27** was carried out by ^{1}H and ^{13}C NMR spectroscopy and were found to be in agreement with the literature data.[70,71]

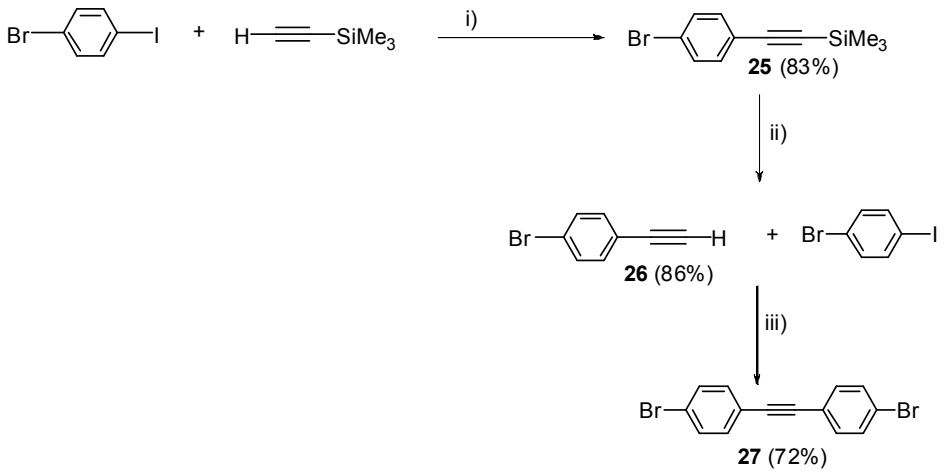

Scheme 12. Reaction scheme for the synthesis of 1,4-dibromtolane 27. i) 2.5 mol% $Pd(PPh_3)_2Cl_2$/ 5 mol% CuI/Et_3N ii) MeOH/THF/NaOH iii) 2.4 mol% $Pd(PPh_3)_2Cl_2$/5 mol% CuI/Et_2NH

1,4-dibromotolane **27** was then used to synthesise 4-4'-*bis*-(trimethylsilyl)ethynyltolane **28**, 1,4'-*bis*-(triisopropylsilyl)ethynyltolane **18** and *bis*(ferrocenylethynyl)tolane **30** v*ia* Sonogashira palladium catalysed cross coupling or [*tetrakis*(4-bromophenyl)cyclobutadiene]cyclopentadienyl cobalt **11** as shown in Figure 41.

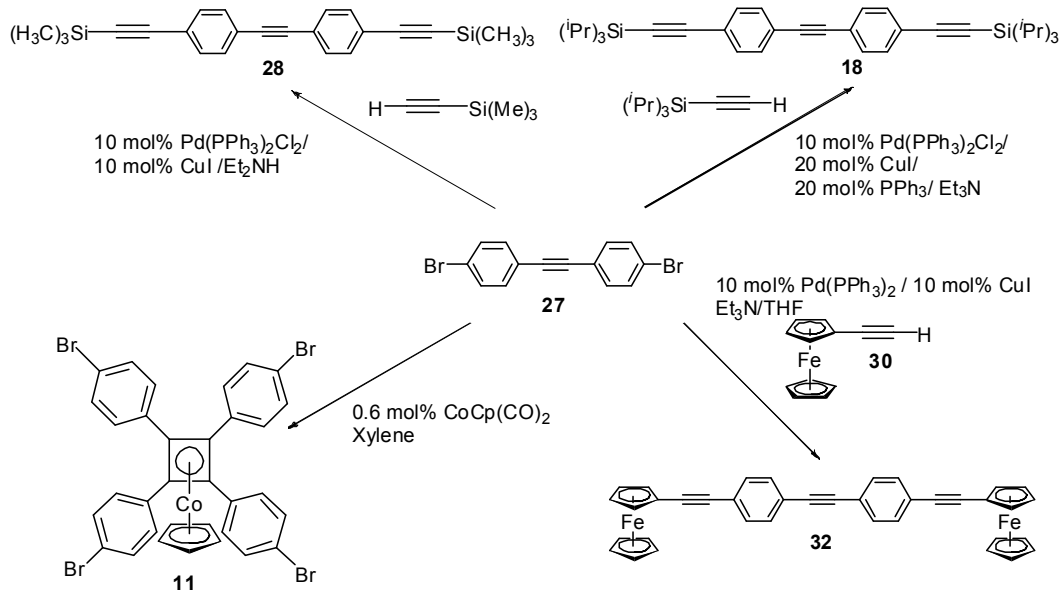

Figure 41. Further reactions of 1,4-dibromotolane 27.

Compound **28** was prepared by adaptation of the method used for compound **18** and after purification by column chromatography on silica was produced in a 55% yield.[66] ^{1}H and ^{13}C NMR spectroscopy of **28** was found to be consistent with that previously published.[72] The synthesis of *bis*(triisopropylsilyl)tolane **18** was carried out by adapting a literature preparation[73] which gave a higher yield than the method used by Waybright *et al*.[66] Column chromatography on silica yielded **18** as a yellow oil but recrystallisation of this oil yielded a pale yellow solid.

Before *bis*(ferrocenylethynyl)tolane **32** could be synthesised it was first necessary to make ethynylferrocene **30**. Two literature routes[74,75] were used for the preparation of ethynylferrocene these routes are shown in Scheme 13. Route B proved to be a very good method and produced a stable intermediate 2,2-dibromo-1-ferrocenyl ethylene **29**

which could be isolated and characterised before the final step. It was also found that the yield was higher for route B than for A.

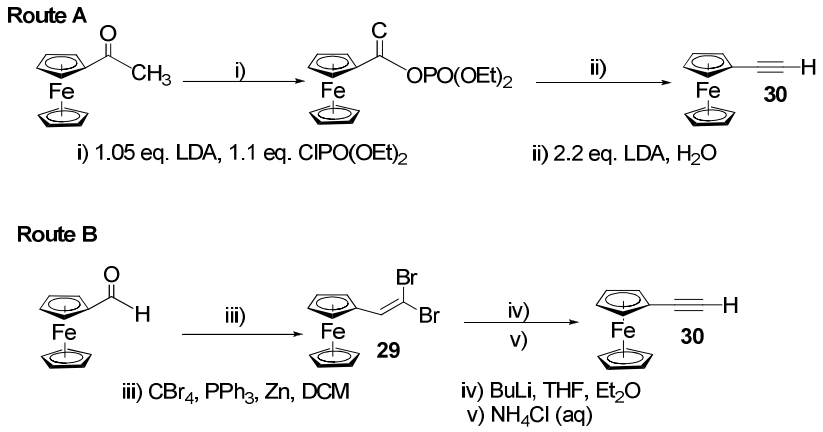

Scheme 13. Two literature routes available for the synthesis of ethynylferrocene.[74,75]

Ethynylferrocene **30** was then reacted with 1,4-dibromotolane **27** to form *bis*(ferrocenylethynyl)tolane **32**; this compound has been previously reported but was prepared *via* a monocuproferrocene intermediate which produced **32** in a 26% yield.[76] Using Sonogashira coupling conditions based on similar compounds the desired product was synthesised and isolated by column chromatography in a 59% yield. During column chromatography to purify **32** a small amount of crystalline material of the by product 4-bromo-4'-(2-ferrocenylethynyl)tolane **31** was isolated in an early fraction. The crystals were suitable for a single crystal X-ray diffraction experiment and the molecular structure obtained is shown in Figure 42.

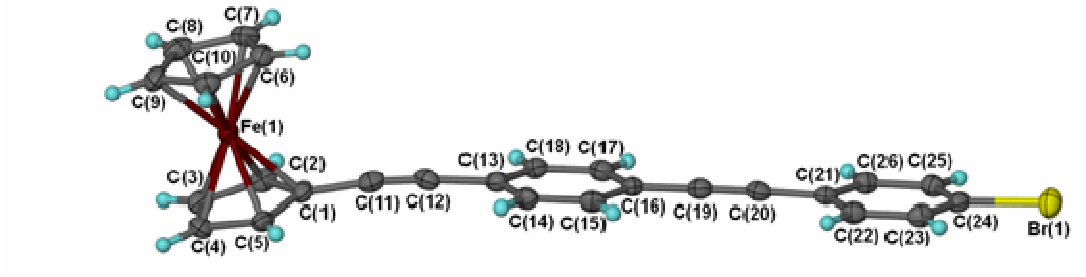

Figure 42. Molecular structure of 4-bromo-4'-(2-ferrocenylethynyl)tolane 31. Thermal ellipsoids of non-hydrogen atoms are shown at 50% probability; hydrogen atoms are shown as blue circles.

The structure of compounds **31** or **32** have not been previously published, so a comparison with a series of ethynylferrocene compounds of 1,3,5-tribromobenzene is made for the molecular structure of **31** and *bis*(ferrocenylethynyl)tolane **32**.[77] Table 11 shows selected bond lengths and angles for **31**. The average C-C bond in the cyclopentadienyl rings is 1.421(4) Å, whilst the average C-C bond in the benzene ring C(13)-C(18) is 1.398(4) Å and in C(21)-C(26) is 1.391(4) Å. These bond lengths and angles are in agreement with those of the other ferrocene systems mentioned above, the Fe-C bond lengths and angles in the ferrocene moiety are also in agreement with those in other ferrocene systems. The lengths of the C≡C bonds are 1.173(4) and 1.198(4) Å compared to those previously reported ranging from 1.145(11)-1.187 (11) Å. The dihedral angle for C(2)-C(1)-C(13)-C(18) is -3.8(3)° which shows that the ferrocene ring and the phenyl ring are slightly out of plane to each other. The dihedral angle between the two phenyl rings was measured as -0.3(3)° showing that within experimental errors the two rings are coplanar. The two cyclopentadienyl groups in the ferrocene fragment are nearly parallel as shown by the angle $C_{nt}(1)$-Fe-$C_{nt}(2)$ 179.3(12)°, where $C_{nt}(1)$ and $C_{nt}(2)$ corresponds to the centroids of the two cyclopentadienyl rings.

Fe(1)-C(1)	2.055(2)	C(9)-C(10)	1.411(4)
Fe(1)-C(2)	2.052(2)	C(6)-C(10)	1.420(4)
Fe(1)-C(3)	2.055(3)	C(1)-C(11)	1.438(4)
Fe(1)-C(4)	2.053(3)	C(11)-C(12)	1.173(4)
Fe(1)-C(5)	2.046(3)	C(12)-C(13)	1.447(3)
Fe(1)-C(6)	2.050(3)	C(13)-C(14)	1.401(4)
Fe(1)-C(7)	2.041(3)	C(13)-C(18)	1.408(4)
Fe(1)-C(8)	2.044(3)	C(14)-C(15)	1.385(4)
Fe(1)-C(9)	2.044(3)	C(15)-C(16)	1.410(4)
Fe(1)-C(10)	2.050(3)	C(16)-C(17)	1.399(4)
Fe(1)-C_{nt}(1)	1.653(3)	C(16)-C(19)	1.436(3)
Fe(1)-C_{nt}(2)	1.656(3)	C(17)-C(18)	1.387(4)
Br(1)-C(24)	1.898(2)	C(19)-C(20)	1.198(4)
C(1)-C(2)	1.438(4)	C(20)-C(21)	1.431(3)
C(2)-C(3)	1.418(4)	C(21)-C(22)	1.404(4)
C(3)-C(4)	1.418(4)	C(21)-C(26)	1.404(4)
C(4)-C(5)	1.416(4)	C(22)-C(23)	1.381(4)
C(1)-C(5)	1.436(4)	C(23)-C(24)	1.386(4)
C(6)-C(7)	1.414(4)	C(24)-C(25)	1.388(4)
C(7)-C(8)	1.419(4)	C(25)-C(26)	1.381(4)
C(8)-C(9)	1.420(4)	C_{nt}(1)-Fe-C_{nt}(2)	179.3(12)
C(12)-C(11)-C(1)	173.4(3)	C(11)-C(12)-C(13)	175.5(3)
C(20)-C(19)-C(16)	178.9(3)	C(19)-C(20)-C(21)	178.7(3)
C(2)-C(1)-C(13)-C(18)	-3.8(3)	C(17)-C(16)-C(21)-C(26)	-0.3(3)

Table 11. Selected bond lengths (Å) and angles (°) in 4-bromo-4'-(2-ferrocenylethynyl)tolane 31. C_{nt}(1) is the centroid of the C(1)-C(5) ring, C_{nt}(2) is the centroid of the C(6)-C(10) ring.

Crystals of **32** were obtained by slow evaporation of benzene solvent and a single crystal X-ray diffraction experiment was carried out allowing the molecular structure shown in Figure 43 to be obtained. In the crystal, molecules of **32** sit on a crystallographic centre of symmetry located at the mid-point of the central C≡C triple bond, C(19) and its symmetrical equivalent, and within the crystallographic asymmetric unit there are two independent half molecules. From the molecular structure of **32** shown in Figure 43 it can be seen that the two ferrocene groups in the molecule are in an up-down arrangement.

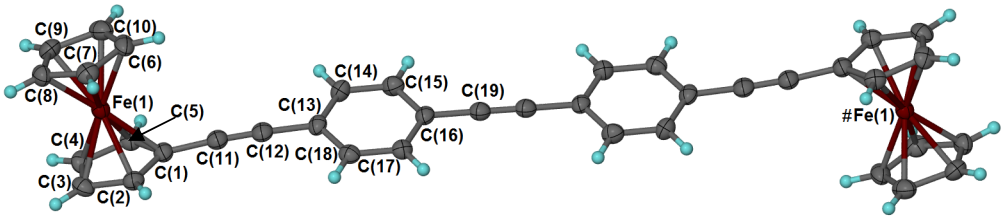

Figure 43. Molecular structure of *bis*(ferrocenylethynyl)tolane 32.[‡] Thermal ellipsoids of non-hydrogen atoms are shown at 50% probability; hydrogen atoms are shown as blue circles. # denotes atoms from the other half of the symmetrical molecule.

Selected bond lengths and angles for **32** are shown in Table 12. Full tables of bond lengths and angles for the all the molecular structures in this thesis can be found in the appendices. The average C-C bond length in the cyclopentadienyl rings is 1.428(7) Å and 1.398(6) Å in the benzene ring C(13)-C(18). The length of the C≡C bond is 1.187(6) Å, all these lengths are consistent with those found in other similar systems.[77] The two cyclopentadienyl groups in the ferrocene fragment are nearly parallel are shown by the angle C_{nt}(1)-Fe-C_{nt}(2) = 178.3(19)°. The dihedral angle C(18)-C(13)-C(1)-C(2) was measured as 14.4(4)° and shows that the cyclopentadienyl ring C(1)-C(5) and the aromatic ring are not coplanar. The dihedral angle C(15)#1-C(16)#1-C(16)-C(17) was measured as 0.0(4)° which shows that the two aromatic rings are coplanar. The bond angles C(11)-C(12)-C(13) and C(19)#1-C(19)-C(16) were measured at 177.6(4)° and 178.5(6)°. This shows that the C≡C units linked to aromatic rings are close to linear as expected. Whilst C(12)-C(11)-C(1) is 174.7(4)° which is not unexpected as the dihedral angle shows that the phenyl and the cyclopentadiene ring are not coplanar.

[‡] The asymmetric unit contains two half molecules of compound **32** and two molecules of benzene. One of the molecules of benzene is disordered, half the symmetric unit and the solvent are omitted here in Figure 43 clarity.

Fe(1)-C(1)	2.056(4)	C(5)-C(4)	1.426(6)
Fe(1)-C(2)	2.055(4)	C(5)-C(1)	1.437(6)
Fe(1)-C(3)	2.050(4)	C(6)-C(7)	1.426(6)
Fe(1)-C(4)	2.047(4)	C(8)-C(7)	1.429(6)
Fe(1)-C(5)	2.046(4)	C(9)-C(8)	1.421(6)
Fe(1)-C(6)	2.052(4)	C(10)-C(9)	1.429(7)
Fe(1)-C(7)	2.060(4)	C(6)-C(10)	1.428(7)
Fe(1)-C(8)	2.054(4)	C(13)-C(14)	1.404(6)
Fe(1)-C(9)	2.042(4)	C(14)-C(15)	1.382(6)
Fe(1)-C(10)	2.050(5)	C(15)-C(16)	1.405(6)
C_{nt}(1)-Fe	1.653 (4)	C(17)-C(16)	1.399(6)
C_{nt}(2)-Fe	1.655 (4)	C(18)-C(17)	1.387(6)
C(1)-C(2)	1.424(6)	C(13)-C(18)	1.413(6)
C(3)-C(2)	1.430(6)	C(11)-C(12)	1.187(6)
C(4)-C(3)	1.425(6)		
C_{nt}(1)-Fe-C_{nt}(2)	178.3(19)	C(12)-C(11)-C(1)	174.7(4)
C(11)-C(12)-C(13)	177.6(4)	C(19)#1-C(19)-C(16)	178.5(6)
C(18)-C(13)-C(1)-C(2)	14.4(4)	C(15)#1-C(16)#1-C(16)-C(17)	0.0(4)

Table 12. Selected bond lengths and angles for *bis*(ferrocenylethynyl)tolane 32. C_{nt}(1) is the centroid of the C(1)-C(5) ring, C_{nt}(2) is the centroid of the C(6)-C(10) ring. # denotes atoms from the other half of the symmetrical molecule.

2.2.3 Synthesis of *bis*(pyridyl)acetylenes

In order to synthesise compound **15** it was necessary first to prepare *bis*(4-pyridyl)acetylene **34** and it was also decided to prepare the 2- and 3- pyridyl acetylenes as well. Following literature preparations for *bis*(2-pyridyl)acetylene[78] and *bis*(3-pyridyl)acetylene[78] proved to be straightforward and the compounds were found to be consistent with the reported spectroscopy. However, the synthesis of *bis*(4-pyridyl)acetylene proved to be harder as the starting reagent can only be bought as a 4-bromopyridine hydrochloride and the intermediates are less stable. The two routes available are shown in Scheme 14 , route A[79] proved to be a much cleaner and higher yielding route than route B[80] so this route was used.

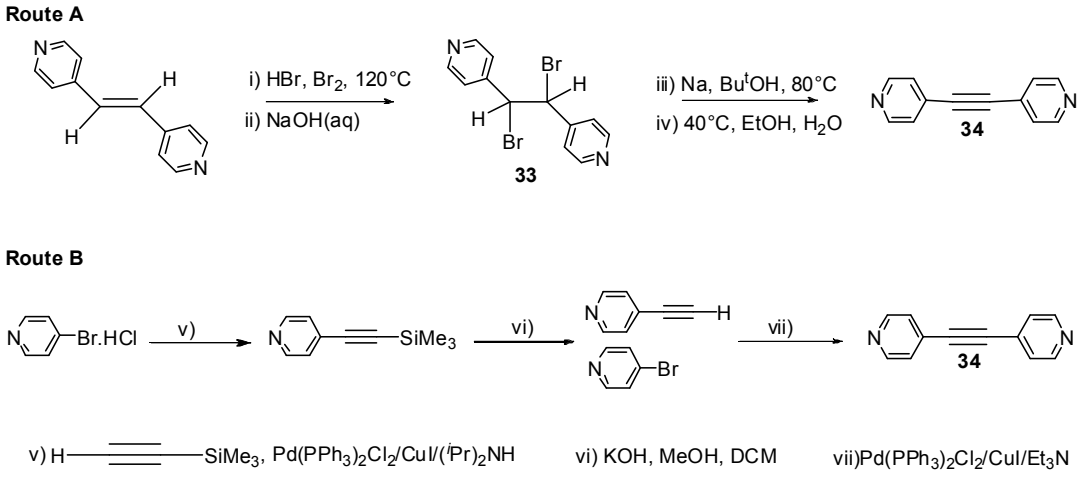

Scheme 14. Two literature syntheses for the preparation of *bis*(4-pyridyl)acetylene) 34. [79, 80]

1,2-*bis*(4-cyanophenyl)ethyne was also by literature methods.[81]

2.2.4. Cobalt mediated Coupling

2.2.4.1 $CoCl(PPh_3)_2$ coupling

It is possible to use a variety of cobalt catalysts but $CoCp(CO)_2$ is a widely used catalyst. Another common starting material is $CoCl(PPh_3)_2$ which is used to generate the catalyst *in situ* by reaction with NaCp. Whilst this method often produces low yields for some reactions, the main advantage of this starting material is that no cyclopentadienone products can be produced as there is no CO present. Therefore, it was felt that investigating different cobalt starting materials would be worthwhile.

Shown in Scheme 15 are the reactions carried out *via* the $CoCl(PPh_3)_3$ route. It was found that for the starting materials *bis*(4-pyridyl)acetylene **34** and 1,2-*bis*(4-cyanophenyl)ethyne highly insoluble materials were obtained which were not possible to characterise. Harrison *et al.*[67] also reported a failed attempt at preparing *tetrakis*(4-pyridyl)cyclobutadiene *via* $CoCl(PPh_3)_3$. Attempts with 2- and 3- *bis*(pyridyl)acetylene did not yield the desired product.

Because of the greater molecular mass of $CoCl(PPh_3)_3$ compared to $CpCo(CO)_2$, a much larger mass of $CoCl(PPh_3)_3$ is required compared to the equivalent mol% of $CpCo(CO)_2$. Using $CoCl(PPh_3)_3$ as the reagent generates a large amount of free PPh_3 in the reaction after the *in situ* generation of $CpCo(PPh_3)_2$. This free PPh_3 proved to be very hard to separate from the product. From the reaction of **27** and $CoCl(PPh_3)_3$ the ^1H NMR spectrum of the product showed a signal in the region of 4.58 ppm consistent with the cyclopentadiene ring in the desired system but the aromatic region was a broad multiplet. ^{31}P NMR spectroscopy revealed that all fractions showed strong signals at 30.34 and -4.15 ppm which are believed to be triphenylphosphine and triphenylphosphineoxide. Because of the large amount of phosphine compounds compared to the products it was not possible to separate these phosphine compounds from the product using chromatography or recrystallisation.

The ferrocene and TMS products showed very broad multiplet peaks in the correct region but as the reactions were done on a small scale it was very hard to purify the samples further.

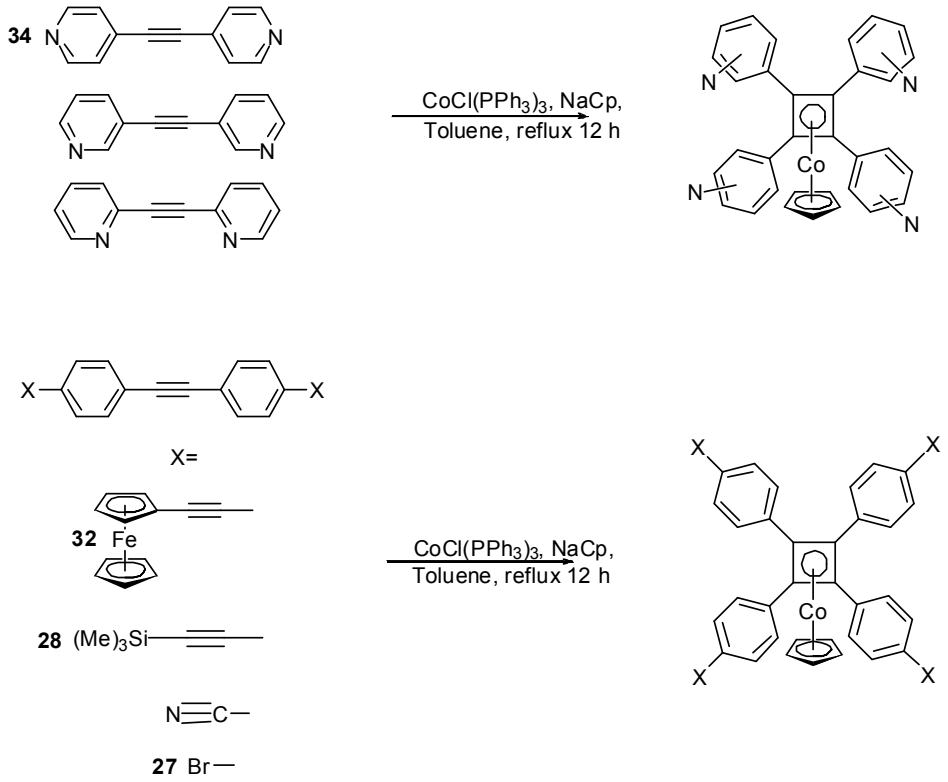

Scheme 15. Attempted cobalt mediated cyclisation using $CoCl(PPh_3)_3$.

Due to the problems isolating the desired products from these reactions it was felt that $CoCp(CO)_2$ would be a better cobalt source than $CoCl(PPh)_3$.

2.2.4.2 $CoCp(CO)_2$ coupling

The cyclisation of bromotolane **27** and *bis*(4-pyridyl)acetylene **34** were the first reactions to be carried out using $CpCo(CO)_2$ following the procedure by Harrison *et al.*[67] The yields obtained were considerably lower than that obtained by Harrison *et al.* A 12% yield for compound **11** was obtained compared to the literature value of 56% and only a 2% yield was obtained for **14** compared to the literature value of 15%. However crystals of [*tetrakis*(4-bromophenyl)cyclobutadiene]cyclopentadienyl cobalt **11** and [*tetrakis*(4-pyridyl)cyclopentadienone]cyclopentadienyl cobalt **15** suitable for single crystal X-ray diffraction experiments were obtained and molecular structures were obtained that had not been previously reported.

The molecular structure of **11** is shown in Figure 44 where it can be seen that the cyclopentadiene and cyclobutadiene ring are almost parallel to each other, with an angle between the planes of the two rings of 1.73(11)°.

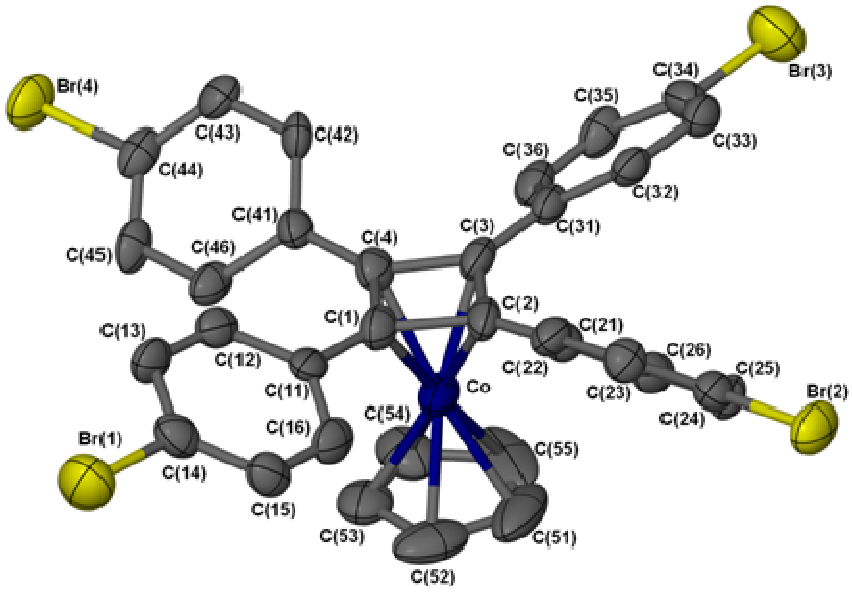

Figure 44. Molecular structure of |*tetrakis*(4-bromophenyl)cyclobutadiene|cyclopentadienyl cobalt 11. Thermal ellipsoids are shown at 50% and hydrogen atoms are omitted for clarity.

The dihedral angle between the phenyl rings and the cyclobutadiene ring are shown in Table 13 and vary between 26-42° which is consistent with values seen in similar systems.[66] From this table and Figure 44 it is clear that the phenyl rings are in a propeller arrangement and that none of the phenyl rings are in the same plane as each other.

	{C(1)-C4}	{C(11)-C(16)}	{C(21)-C(26)}	{C(31)-C(36)}
{C(11)-C(16)}	26.13	-	-	-
{C(21)-C(26)}	41.65	42.51	-	-
{C(31)-C(36)}	29.59	55.31	49.35	-
{C(41)-C(46)}	37.84	48.17	79.42	48.44

Table 13. Interplanar angles (°) of the phenyl rings and the cyclobutadiene ring in 11.

Selected bond angles and lengths are shown in Table 14. The bond lengths and angles for the cyclobutadiene and cyclopentadiene rings are consistent with those reported in other cyclobutadiene systems[45,55,61] The Co-centroid distances measured were 1.689(9) Å for the cyclobutadiene ring and 1.665(12) Å for the cyclopentadiene ring which are also typical of those reported for [CpCoCb] systems.

C(1)-C(2)	1.474(11)	C_{nt}(1)-Co-C_{nt}(2)	178.39
C(2)-C(3)	1.481(13)	C(4)-C(1)-C(2)	89.9(7)
C(1)-C(4)	1.458(12)	C(1)-C(2)-C(3)	89.0(7)
C(3)-C(4)	1.445(11)	C(3)-C(4)-C(1)	91.0(7)
C_{nt}(1)-Co	1.689(9)	C(4)-C(3)-C(2)	90.1(7)
C_{nt}(2)-Co	1.665(12)	C(52)-C(51)-C(55)	109.4(14)
C(51)-C(52)	1.39(2)	C(51)-C(52)-C(53)	104.0(14)
C(52)-C(53)	1.397(14)	C(54)-C(53)-C(52)	112.7(12)
C(51)-C(55)	1.41(2)	C(53)-C(54)-C(55)	107.5(15)
C(53)-C(54)	1.326(14)	C(54)-C(55)-C(51)	106.4(16)
C(54)-C(55)	1.396(19)		

Table 14. Selected bond angles (°) and lengths (Å) for [*tetrakis*(4-bromophenyl)cyclobutadiene]cyclopentadienyl cobalt 11.

2.2.4.2.2. Varying conditions for the synthesis of [*tetrakis*(4-pyridyl)cyclobutadiene] cyclopentadienyl cobalt 15.

The reaction with $CpCo(CO)_2$ and *bis*(4-pyridyl)acetylene **34** was also carried out using decalin rather than xylene in the hope that the increase in temperature might cause an increase in the amount of desired product. However, the increased temperature appeared to improve the yield of the cyclopentadienone product **16** to 51% and only a few milligrams of the desired product **15** was obtained.

In the literature it has been found that there are a variety of starting reagents which form the cyclopentadienone as the favoured and sometimes the exclusive product.[54] There is no clear explanation for this; it does not appear to be due to electronic factors or steric bulk. It appears that problematic starting materials contain fluorine, iodide and pyridine.[54,67] One possible explanation could be that the cobalt binds to these atoms rather to the acetylene, but there have been no schematic diagram studies to confirm

this. The cyclopentadienone product also appears to be highly favourable when the acetylene group contains methyl groups which is probably due to the small size of the methyl group.[54]

Crystals of [*tetrakis*(4-pyridyl)cyclobutadiene]cyclopentadienyl cobalt **15** suitable for X-ray diffraction experiments were obtained and found to have the same cell parameters as those obtained from single crystal X-ray diffraction experiments performed by Harrison *et al*.[67] Harrison *et al.* report the structure of **15** to have a distance of 3.36 Å between the two rings and an angle of 4° between the ring planes. The dihedral angle between the ring and the phenyl ring is reported at 35° for each arm. It is also reported that the structure has a disordered cyclopentadiene ring and that a small amount of the opposite isomer was present in the crystal.[67] The structure obtained by Harrison *et al*. is shown in Figure 45.

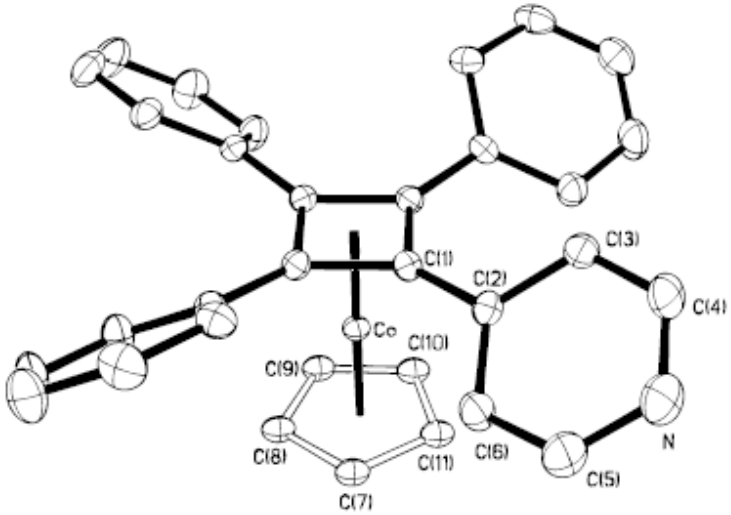

Figure 45. Molecular structure of *tetrakis*(4-pyridyl)cyclobutadiene]cyclopentadienyl cobalt 15. Taken from [67].

Selected bond lengths and angles of the structure of **15** obtained by Harrison *et al*.[67] are shown in Table 15, where it can be seen that the bond lengths in the cyclobutadiene ring and cyclopentadiene ring are all equal.

N-C(5)	1.337(2)	C(9)-C(10)	1.42
C(1)-C(2)	1.467(2)	C(10)-C(11)	1.42
C(2)-C(3)	1.399(2)	C(7)-C(8)	1.42
C(3)-C(4)	1.390(2)	C(8)-C(9)	1.42
C(7)-C(8)	1.42	C(8)-C(7)-C(11)	108.0
N-C(4)	1.345(2)	C(7)-C(8)-C(9)	108.0
C(1)-C(1)#1	1.469(2)	C(7)-C(11)-C(10)	108.0
C(2)-C(6)	1.402(2)	C(10)-C(9)-C(8)	108.0
C(5)-C(6)	1.391(2)	C(9)-C(10)-C(11)	108.0
C(7)-C(11)	1.42		

Table 15. Selected bond lengths (Å) and angles (°) of 15.[67] # denotes atoms from the other half of the symmetrical molecule.

The structure of [*tetrakis*(4-pyridyl)cyclopentadienone]cyclopentadienyl cobalt **16** is shown in Figure 46. The cyclopentadienone ring is distorted with the carbonyl group deviating away from the plane of the rest of the ring by 12.67(3)°. The cyclopentadiene and cyclopentadienone rings are eclipsed and are almost parallel with a 1.13(3)° angle between the two planes.

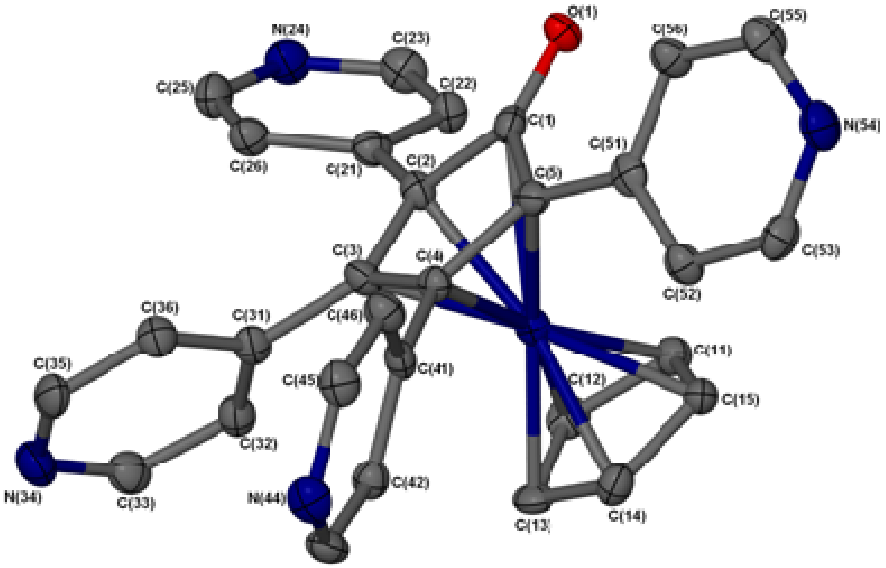

Figure 46. Molecular structure of *tetrakis*(4-pyridyl)cyclopentadienone]cyclopentadienyl cobalt 16. Thermal ellipsoids are shown at 50% and hydrogen atoms are omitted for clarity.

Selected bond lengths and angles are shown in Table 16 and it can be seen that the cyclopentadienone ring is made up of two shorter C-C bonds and two longer; the fifth

bond length is of an intermediate bond length. The cyclopentadiene ring shows very little variation in C-C bond lengths and angles and the values are consistent with those measured for Cp rings in [CpCoCb] systems.[45,55,61]

C(1)-O(1)	1.240(5)	C(3)-C(2)-C(1)	109.2(4)
C(1)-C(2)	1.474(6)	C(2)-C(3)-C(4)	107.9(4)
C(2)-C(3)	1.438(6)	C(5)-C(4)-C(3)	107.4(4)
C(3)-C(4)	1.456(6)	C(4)-C(5)-C(1)	108.9(4)
C(4)-C(5)	1.448(6)	C(2)-C(1)-C(5)	104.4(4)
C(1)-C(5)	1.478(6)	C(15)-C(11)-C(12)	107.1(4)
C_{nt}(1)-Co	1.669(2)	C(11)-C(12)-C(13)	108.9(4)
C_{nt}(2)-Co	1.650(3)	C(14)-C(13)-C(12)	107.4(4)
C(11)-C(12)	1.430(7)	C(13)-C(14)-C(15)	107.9(4)
C(12)-C(13)	1.422(6)	C(11)-C(15)-C(14)	108.7(4)
C(13)-C(14)	1.423(6)	C_{nt}(1)-Co-C_{nt}(2)	176.74(3)
C(14)-C(15)	1.429(6)		
C(11)-C(15)	1.414(6)		

Table 16. Selected bond lengths (°) and angles (Å) for [*tetrakis*(4-pyridyl)cyclopentadienone] cyclopentadienyl cobalt 16. C_{nt}(1) is the centroid for C(1)-C(5) and C_{nt}(2) is the centroid for C(11)-C(15).

There are few similar cyclopentadienone compounds known in the literature, and many of the structures were obtained the 1960s and hence the errors associated with the data obtained from the single crystals X-ray diffraction experiments are large.[82,83] Boese *et al.*[84] obtained a structure of η^5-(3-methyl-1-methoxycarbonyl-cyclopentadienyl-($\eta^4\sigma^1$-(1,3-bis(trimethylsilyl)-2-cyclopentadienone) cobalt from which a comparison with **16** can be made. Table 17 shows bond lengths and angles for the cyclopentadienone ring in η^5-(3-methyl-1-methoxycarbonyl-cyclopentadienyl-($\eta^4\sigma^1$-(1,3-*bis*(trimethylsilyl)-2-cyclopentadienone) cobalt.

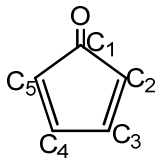

C(1)-C(2)	1.459(9)	C(5)-C(1)-C(2)	100.4(6)
C(1)-C(5)	1.451(8)	C(1)-C(2)-C(3)	108.7(6)
C(2)-C(3)	1.419(9)	C(2)-C(3)-C(4)	106.0(6)
C(3)-C(4)	1.419(9)	C(3)-C(4)-C(5)	108.5(6)
C(4)-C(5)	1.424(9)	C(4)-C(5)-C(1)	111.4(6)

Table 17. Selected bond lengths (Å) and angles (°) from η^5-(3-methyl-1-methoxycarbonyl-cyclopentadienyl-($\eta^4\sigma^1$-(1,3-*bis(*trimethylsilyl)-2-cyclopentadienone) cobalt[84] and also a diagram showing the numbering of the carbons in the cyclopentadienone fragment.[84]

From Table 17 it can be seen that the cyclopentadienone ring in η^5-(3-methyl-1-methoxycarbonyl-cyclopentadienyl-($\eta^4\sigma^1$-(1,3-*bis*(trimethylsilyl)-2-cyclopentadienone) cobalt also consists of two short C-C bonds, one intermediate and two longer bonds as seen in **16.** There is a range of angles between 100.4(5)-111.4(5)° observed within the cyclopentadienone ring for η^5-(3-methyl-1-methoxycarbonyl-cyclopentadienyl-($\eta^4\sigma^1$-(1,3-*bis*(trimethylsilyl)-2-cyclopentadienone) cobalt. The bond angles in the cyclopentadienone ring in **16** were found to be more consistent ranging from 104.4(4)-109.2(4)° ; for both systems the smallest angle was measured for the C(2)-C(1)-C(5) angle which corresponds to the angle at the carbonyl group. The Co-C_{nt}(2) distance which is the Co-Cp distance is 1.650(3) Å in **16** compared to 1.679(6) Å for the system obtained by Boese *et al*.[84] The distance between the centroid of the cyclopentadienone to the cobalt atom is 1.650(3) Å in **16** which is slightly shorter than in the system obtained by Boese *et al*.[84] which was measured at 1.702(6) Å.

Table 18 shows the interplanar angles between the pyridyl rings and the cyclopentadienone core in **16**, which shows that there is quite a wide range of angles between the pyridyl rings and the cyclopentadienone rings. From the Table 18 it can be seen that the pyridyl rings that are diagonal to each other are nearly at 90° to each other.

	{C(2)-C(5)}	{C(21)-C(26)}	{C(31)-C(36)}	{C(41)-C(46)}
{C(21)-C(26)}	36.42	-	-	-
{C(31)-C(36)}	56.70	56.17	-	-
{C(41)-C(46)}	51.47	81.31	49.78	-
{C(51)-C(56)}	39.76	67.52	86.45	62.85

Table 18. Interplanar angles (°) of the pyridyl rings and the cyclopentadienone ring in 16.

2.2.4.2.2 Trimethylsilyl protecting groups versus triisopropylsilyl.

Initially the interest was in synthesising [*tetra*(-4-trimethylsilylethynyl) phenylcyclobutadiene]cyclopentadienyl cobalt rather than using the less economical triisopropylsilyl (TIPS) protecting group. The first attempt using $CpCo(CO)_2$ and 4-4'-*bis*-(trimethylsilyl)ethynyltolane **28** was carried out in refluxing xylene and it was found

the majority of the starting material did not react. However it was possible to isolate [*tetra*(-4-trimethylsilylethynyl)phenylcyclopentadienone]cyclopentadienyl cobalt in a 6% yield. The ^{1}H NMR spectra of this material shows the cyclopentadiene signal to be a multiplet at 4.85-4.88 ppm, whereas this signal was expected to be a singlet. The signal for the methyl groups and the C_6H_4 groups were also seen as a multiplet but this is less of a surprise because of the asymmetry of the five membered cyclopentadienone ring. The ^{13}C NMR spectra confirmed that there are many more peaks than would be expected and there were at least four different cyclopentadienone environments.

Column chromatography could not separate the starting material 4-4'-*bis*-(trimethylsilyl)ethynyltolane **28** from the small amount of [tetra-(-4-trimethylsilylethynyl)phenylcyclobutadiene]cyclopentadiene cobalt product **35**. So this crude mixture was reacted again with $CpCo(CO)_2$ but using a higher boiling point solvent in the form of decalin. This time all the starting material was dimerised but ^{1}H and ^{13}C NMR spectroscopy suggests that the product is a mixture of isomers of [*tetra*-(-4-trimethylsilylethynyl)phenylcyclobutadiene]cyclopentadiene cobalt **35** in 31% yield and [*tetra*-(-4-trimethylsilylethynyl)phenylcyclopentadienone] cyclopentadiene cobalt **36** products in a overall yield of 9%. The two products were separated by column chromatography but separation of the different isomers was not possible by either preparative TLC or recrystallisation. A small amount was deprotected to investigate whether it possible to separate then, this did not prove to be any easier to achieve.

It seems likely that the trimethylsilyl protecting group is not bulky enough to block reactions at the outer C≡C bonds therefore the cyclisation reactions can occur at any of the triple bonds and a mixture of products are obtained, as shown in Figure 47. The isomers **a** and **b** in Figure 47 would be formed from the cyclisation of two end C≡C groups. Whilst isomer **c** is the desired product from the cyclisation of the two central C≡C groups and isomer **d** is the product of the cyclisation of a central C≡C and an end C≡C group. The structure of the isomers of the cyclopentadienone product **36** would be expected to be similar to those for the cyclobutadiene products.

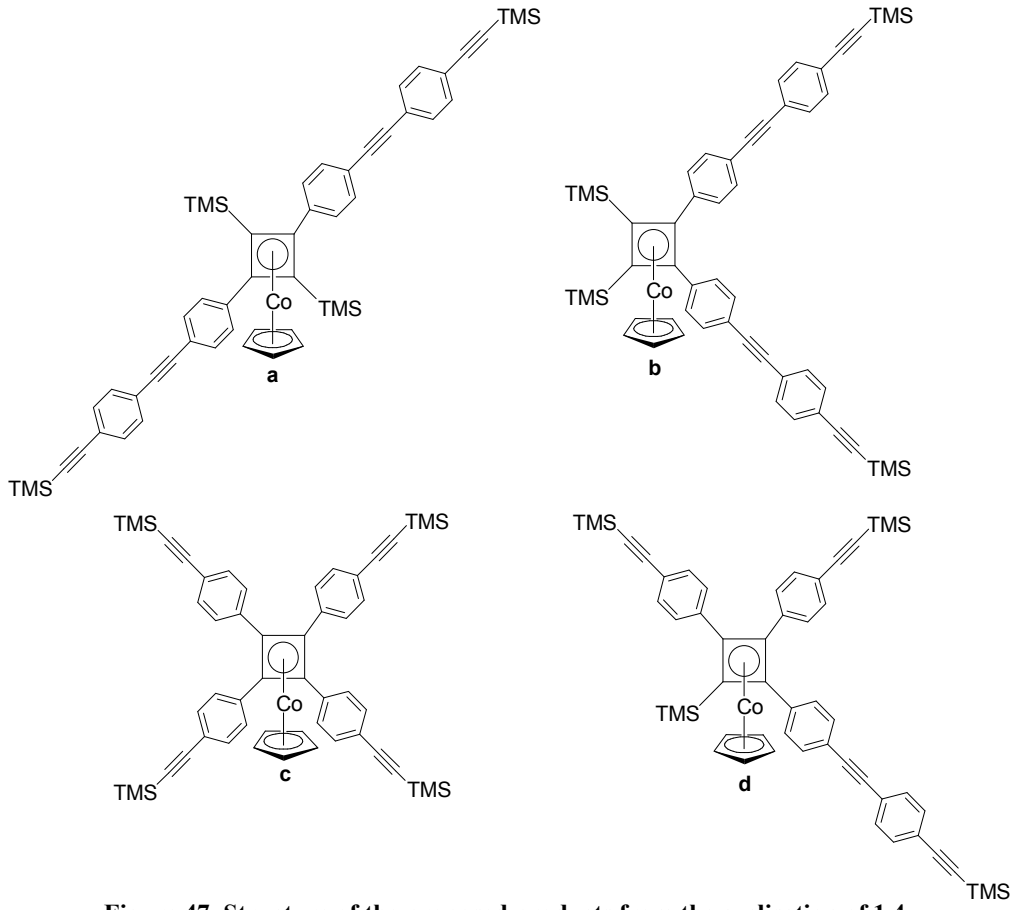

Figure 47. Structure of the proposed products from the cyclisation of 1,4-*bis*(trimethylsilyl)ethynyltolane.

Synthesis of *tetra*-(-4-triisopropylsilylethynyl)phenylcyclobutadiene]cyclopentadienyl cobalt **22** proved to be straightforward following the preparation by Waybright *et al.*[66] and the compound was isolated in a 63% yield. Isolation of the cyclopentadienone product **37** in a 12% yield was also achieved which had not be reported by Waybright *et al.* Recrystallisations of the TIPS protected products resulted in poor and disordered crystals but removal of the protection group using Bu_4NF lead to the production of X-ray quality crystals of both **38** and the cyclopentadienone product **39**.

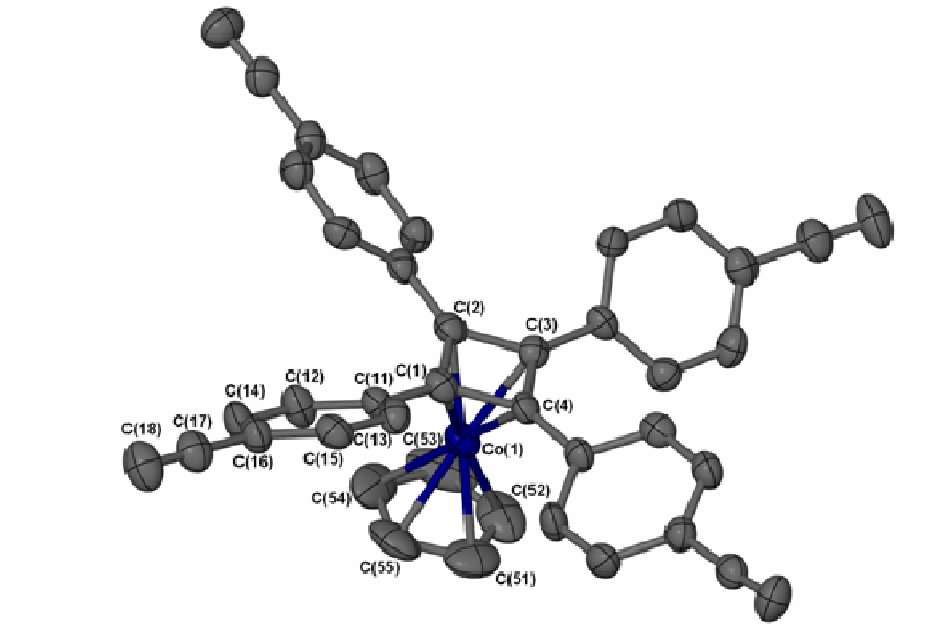

Figure 48. Molecular structure of [*tetra*(-4-ethynylphenyl)cyclobutadiene]cyclopentadienyl cobalt 38. Thermal ellipsoids are shown at 50% and hydrogen atoms are omitted for clarity.

The structure of **38** is shown in Figure 48; this structure has been previously reported by Waybright *et al.*[66] but was collected at 180 K whereas this structure was collected at 150 K. As is typical with the [CpCoCb] systems it can be seen that the cyclobutadiene and cyclopentadiene ring are nearly parallel with a 2.92° angle between the two planes. The angles between the phenyl rings and the cyclobutadiene core are shown in Table 19 and range between 27-34° which is a smaller range than for compound **11**. It can be seen that there is a wide range of angles between the phenyl rings arms and the cyclobutadiene core, giving a propeller type arrangement which is seen in all these [CpCoCb] systems with aromatic rings.

	{C(1)-C(4)}	{C(11)-C(16)}	{C(21)-C(26)}	{C(31)-C(36)}
{C(11)-C(16)}	37.90	-	-	-
{C(21)-C(26)}	27.20	49.41	-	-
{C(31)-C(36)}	37.33	74.86	45.02	-
{C(41)-C(46)}	33.67	41.77	60.81	48.44

Table 19. Interplanar angles (°) of the phenyl rings and the cyclobutadiene ring in 38.

Selected bond lengths and angles for **38** are shown in Table 20 and are typical of [CpCoCb] systems.

C(1)-C(2)	1.468(6)	C(4)-C(1)-C(2)	90.2(3)
C(2)-C(3)	1.472(5)	C(3)-C(2)-C(1)	89.7(3)
C(3)-C(4)	1.465(5)	C(4)-C(3)-C(2)	90.3(3)
C(1)-C(4)	1.470(5)	C(3)-C(4)-C(1)	89.9(3)
C_{nt}(1)-Co	1.685(4)	C(55)-C(51)-C(52)	109.6(5)
C_{nt}(2) –Co	1.669(6)	C(51)-C(52)-C(53)	109.0(6)
C(51)-C(52)	1.370(8)	C(52)-C(53)-C(54)	105.7(6)
C(52)-C(53)	1.380(9)	C(55)-C(54)-C(53)	107.1(6)
C(53)-C(54)	1.444(8)	C(51)-C(55)-C(54)	108.5(6)
C(54)-C(55)	1.382(8)	C_{nt}(1)-Co- C_{nt}(2)	176.76
C(51)-C(55)	1.352(7)		

Table 20. Selected bond lengths (Å) and angles (°) for [*tetra*-(-4-ethynyl)phenylcyclobutadiene] cyclopentadienyl cobalt 38. C_{nt}(1) is the centroid of C(1)-C(4) and C_{nt}(2) is the centroid of C(51)-C(55).

The molecular structure of [*tetra*(-4-ethynyl)phenylcyclopentadienone]cyclopentadienyl cobalt **39** is shown in Figure 49.

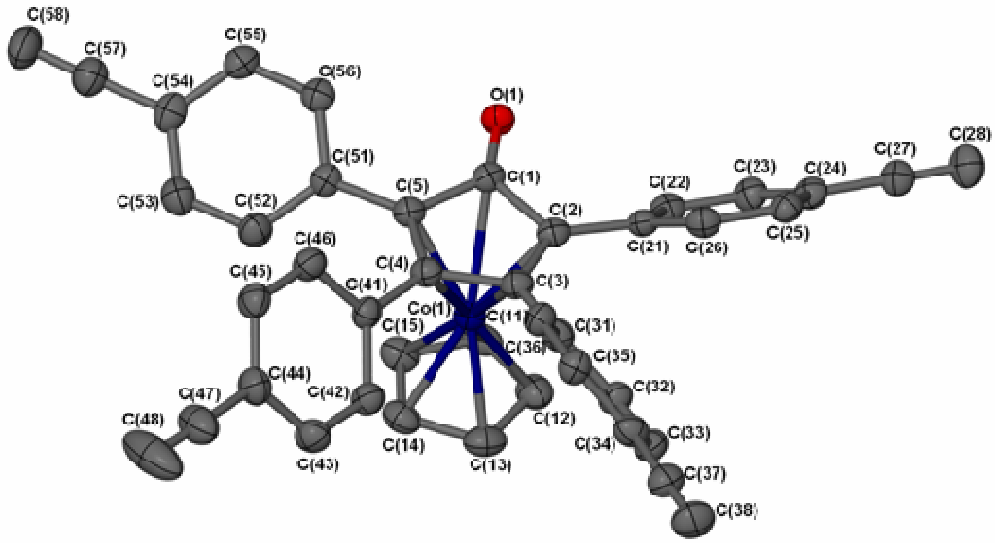

Figure 49. Molecular structure of [*tetra*-(4-ethynyl)phenylcyclopentadienone]cyclopentadienyl cobalt 36. Thermal ellipsoids are shown at 50% and hydrogen atoms are omitted for clarity.

From examination of selected bond lengths shown in Table 21 it can be seen that the Co-C(1) bond is approximately 0.2 Å longer than the other Co-C bond lengths in this cyclopentadienone ring. This causes the cyclopentadienone ring to be non-planar with the C=O group being 5.65(3)° out of the plane of the rest of the ring.

From the bond lengths shown in Table 21 it can be seen the structure is similar to **16** with the cyclopentadienone consisting of two C-C short bonds and two longer bonds and one intermediate one.

O(1)-C(1)	1.239(3)	C(2)-C(1)-C(5)	104.7(2)
C(1)-C(2)	1.476(3)	C(3)-C(2)-C(1)	108.9(2)
C(2)-C(3)	1.433(3)	C(2)-C(3)-C(4)	108.1(2)
C(3)-C(4)	1.450(3)	C(5)-C(4)-C(3)	107.9(2)
C(4)-C(5)	1.438(3)	C(4)-C(5)-C(1)	108.8(2)
C(1)-C(5)	1.477(3)	C_{nt}(1)-Co-C_{nt}(2)	174.47(12)
C(11)-C(12)	1.414(4)	Co(1)-C(1)	2.263(2)
C(12)-C(13)	1.423(4)	Co(1)-C(2)	2.052(2)
C(13)-C(14)	1.400(4)	Co(1)-C(3)	2.003(3)
C(14)-C(15)	1.421(4)	Co(1)-C(4)	2.003(2)
C(11)-C(15)	1.400(4)	Co(1)-C(5)	2.070(3)
C_{nt}(1)-Co	1.660(3)	C_{nt}(2)-Co	1.674(4)

Table 21. Selected bond lengths and angles for [*tetra*-(4-ethynyl)phenylcyclopentadienone]cyclopentadienyl cobalt 39.

The interplanar angles of the phenyl rings and the cyclopentadienone core are shown in Table 22 and as would be expected are very similar to **16** and very different from **11** and **38,** with larger angles and a larger range than for the cyclobutadiene systems.

	{C(1)-C(5)}	{C(21)-C(26)}	{C(31)-C(36)}	{C(41)-C(46)}
{C(21)-C(26)}	40.57	-	-	-
{C(31)-C(36)}	56.33	57.56	-	-
{C(41)-C(46)}	48.43	83.32	50.97	-
{C(51)-C(56)}	35.10	69.94	86.22	51.32

Table 22. Interplanar angles (°) of the phenyl rings and the cyclopentadienone core in 39.

2.2.5. ^{1}H and ^{13}C NMR spectroscopy of compounds 38 and 39.

Because of the symmetrical nature of the cyclobutadiene compound **22** the ^{1}H NMR spectra consists of only three signals at 1.14, 4.55 and 7.32 ppm in the ratio 84:5:16 corresponding to TIPS:C_5H_5:C_6H_4 groups. Removal of the TIPS group by addition of Bu_4NF to form compound **38** resulted in the disappearance of the signal at 1.14 ppm and a new signal at 3.15 ppm corresponding to four acetylene protons. These spectra are consistent with the reported values; however the literature ^{13}C spectra signals are only assigned for the TIPS groups so a carbon-proton one bond coupling and a carbon-proton through more than one bond coupling experiment were carried out to assign the signals in the deprotected system **38** to aid assignment of the [CpCoCb] systems once metals were attached**.**

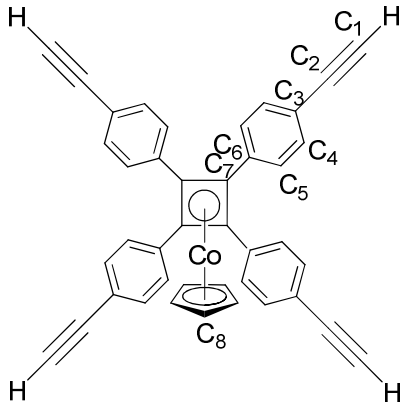

Figure 50. Schematic diagram of the carbon numbering used for the ^{13}C spectra assignment for 38.

Carbon Number	Chemical shift (ppm)	Coupling
C_1	77.8	
C_2	84.0	48 Hz C_a≡C-H_b.[85] 240 Hz C_2-C_4
C_3	120.1	
C_4	132.1	240 Hz C_2-C_4
C_5	128.7	
C_6	137.0	
C_7	74.6	
C_8	83.6	

Table 23. Assignment of the ^{13}C NMR signals to the carbons in 38.

Isolation of *tetra*-(-4-triisopropylsilylethynyl)phenylcyclopentadienone] cyclopentadienyl cobalt **38** has not been previously reported. Because of a decrease in symmetry compared to the cyclobutadiene compound the NMR spectra is more complex. In the ^{1}H NMR spectra the TIPS signal is now seen as two very similar signals giving the appearance of a doublet at 1.12-1.16 ppm. The cyclopentadiene signal is a singlet but is slightly shifted to 4.86 ppm. The aromatic region is made up of four sets of signals overlapping to form three multiplets. In the ^{13}C NMR spectra the $SiCH(CH_3)_3$ signals are seen as what appears to be two doublets at 11.9 and 19.0 ppm as the signals are so similar. Between 110-78 ppm there are 7 signals which are due to four unequivalent acetylene carbons, two signals for the cyclopentadienone ring and one for the cyclopentadiene ring. No signal is observed for the carbonyl group as these are very weak due to slow relaxation times and quadrupolar coupling. This is also consistent with the other cyclopentadienone system compound **16** reported by Harrison *et al.* where the CO signal is also not observed.[67]

2.3 Tetrametallic [CpCoCb] systems

2.3.1 Ruthenium

There are many ruthenium complexes containing C≡C-Ru moieties known in the literature, and often the metal fragment attached to the acetylene is$\{RuCp(PPh_3)_2\}$ or $\{Ru(dppe)_2Cl\}$.[7,86-89] However attaching a ruthenium group to **38** proved to be very challenging. A number of different methods were tried based on similar compounds known in the literature.

The first method for attachment of four ruthenium fragment to **38** was based on the work of Lin *et al.*[90] who synthesised a range of triaryl carbocations containing two or three $\{CpRu(PPh_3)_2\}$ groups. The proposed reaction and conditions are shown in Figure 51.

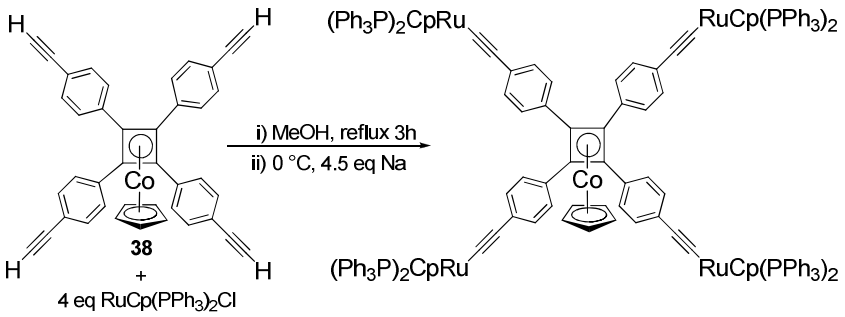

Figure 51. Proposed reaction scheme for the synthesis of (*tetrakis*RuCp(PPh$_3$)$_2$ethynylphenyl)cyclobutadiene)cyclopentadienyl cobalt.

The reaction was carried out by refluxing a mixture of 4 equivalents of RuCp(PPh$_3$)$_2$Cl with **38** in MeOH for 3 h. After cooling to 0°C, 4.5 equivalents of sodium were added and precipitation occurred. ^{31}P NMR spectroscopy of this precipitate showed the majority of the material was RuCp(PPh$_3$)$_2$Cl but there were small peaks at 51.43 and 30.35 ppm which suggested some reaction had occurred. Purification by recrystallisation with a variety of different solvent systems was attempted but was not successful. Some ruthenium acetylenes can be purified by flash chromatography on alumina, however, in the case of this crude reaction mixture, flash chromatography resulted in decomposition.[91]

As only a small amount of the RuCp(PPh$_3$)$_2$Cl appeared to react when using MeOH/Na it was decided to generate the Li salt of the ligand first and then add the RuCp(PPh$_3$)$_2$Cl.

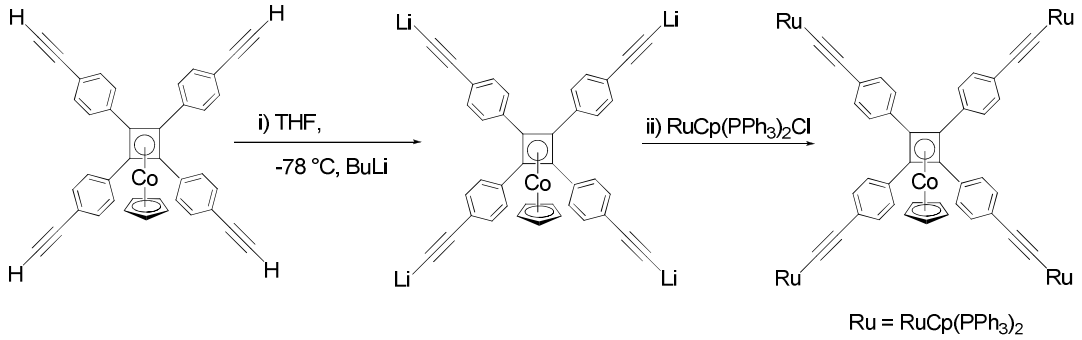

Figure 52. Proposed reaction scheme *via* lithiation of the ligand.

The proposed reaction scheme is shown in Figure 52, starting with lithiation of the ligand by cooling a solution of the ligand **38** in THF to -78 °C and adding 4 equivalents of BuLi. After leaving the mixture to react for around 10 mins, the THF solution of 4

equivalents of $RuCp(PPh_3)_2Cl$ was cooled and added to the mixture. The reaction was then left to warm up overnight and then heated to reflux. Unfortunately ^{31}P NMR spectroscopy of the crude reaction mixture indicated that the $RuCp(PPh_3)_2Cl$ had not reacted.

It is common to activate the ruthenium starting material by removing one of the chlorines by reaction with a reagent such as $AgPF_6$ or NH_4PF_6.[92,93] A solution containing a mixture of $RuCp(PPh_3)_2Cl$ and $AgPF_6$ was allowed to react for approximately 30 mins before filtering and addition to the ligand. The reaction was then carried out as in Figure 51. Again ^{31}P NMR spectroscopy showed only a small amount of $RuCp(PPh_3)_2Cl$ had reacted.

Another method used for the synthesis of ruthenium acetylides is deprotection of the acetylene *in situ*. with a fluorine source often KF in MeOH.[93] The deprotection occurs because the silicon has a strong affinity for electronegative groups such as F^- or OH^-,[68,94] so the Si-C bond is cleaved producing a reactive acetylene. Some test reactions were carried out using 4,4'-*bis*-(triisopropylsilyl)ethynyltolane **18** and a variety of conditions and reagents including Bu_4NF and KF but it was not found to be successful for this particular system.

Dixneuf *et al.* have synthesised many ruthenium-acetylides materials. This research group tends to use $Ru(dppe)_2Cl_2$ rather than $RuCp(PPh_3)_2Cl$ and the reaction goes *via* an intermediate vinylidiene. These reactions occur at room temperature and take typically around 72 h to react. The isolation of a *tris*(alkynylruthenium) compound in high yields *via* the isolation of the *tris*(vinylidineruthenium(II) complex by Dixneuf *et al.*[95] suggested that this might be a good method for reaction with [tetra(-4-ethynylphenyl)cyclobutadiene] cyclopentadienyl cobalt. The synthetic route for the *tris*(alkynylruthenium (II)) complex used by Dixneuf *et al*. is shown in Scheme 16.

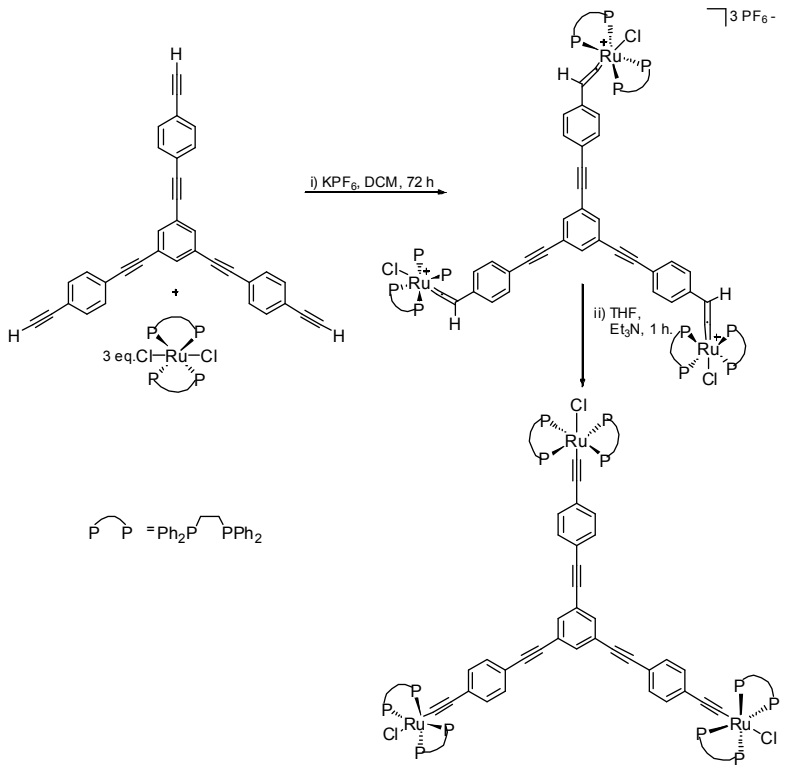

Scheme 16. Synthetic route used for the synthesis of *tris*(alkynylruthenium (II)) complex *via* a vinylidiene used by Dixneuf *et al.*[95]

A solution of **38** with 4 equivalents of $[Ru(dppe)_2Cl]OTf$ in DCM was stirred at room temperature and a slow colour change from red to yellow occurred over three days. Removal of the solvent yielded a red solid which was characterised by $^{31}P\{^1H\}$ NMR spectroscopy which showed two triplets at 85.19 and 57.09 ppm which is due to $[Ru(dppe)_2Cl]OTf$ and a strong signal at 38.90 ppm which is consistent with literature values for vinylidienes.[95]

Conversion of the vinylidiene to the alkyne compound was carried out by suspension of the solid in THF and addition of Et_3N. The solution was stirred for 1 h and the solvent was removed to yield a brown solid.

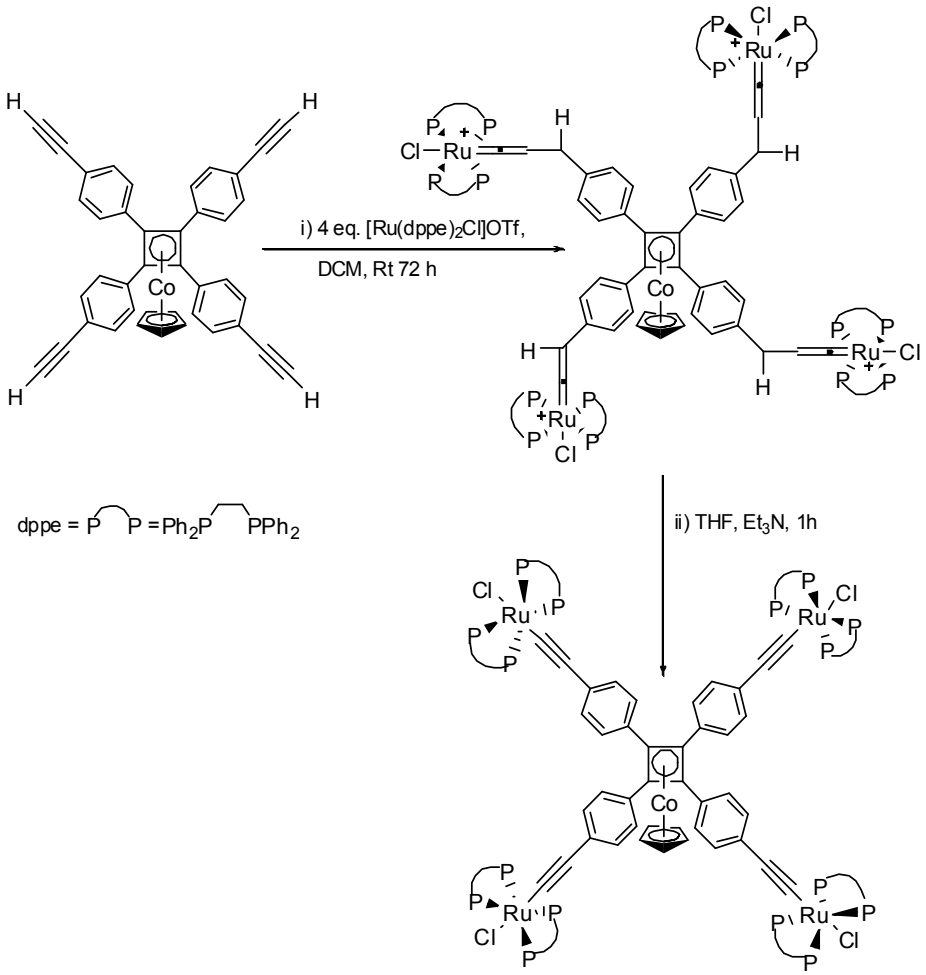

Scheme 17. Synthesis of (*tetrakis*(Ru(dppe)$_2$Cl)ethynylphenylcyclobutadiene)cyclopentadienyl cobalt 40.

^{31}P NMR spectroscopy of **40** showed a signal at 49.91 ppm which is consistent with literature values for ruthenium-acetylene compounds.[96] ^{1}H NMR spectroscopy showed a broad singlet at 2.73 due to the CH_2CH_2 group in dppe, a singlet at 4.70 ppm due to the cyclopentadienyl group and a series of overlapping multiplets between 6.90-7.60 ppm due to the aromatic protons. The relative integrations of the different regions were found to be 32:5:176 CH_2CH_2:cyclopentadienyl:arene which is consistent with the desired product.

The $^{13}C\{^{1}H\}$ spectra exhibited ^{31}P-^{13}C coupling which allowed identification of the dppe signals. The ethyl group was seen as a multiplet at 31.3 ppm as was the quaternary

phenyl carbon which was a multiplet at 137.4 ppm. The signals due to the Cp, Cb and the C_6H_4 components of the [CpCoCb] ligand showed very little variation from those of the free ligand **38** as can be seen from Table 24. The C≡C signals however showed a significant shift after attachment to the $Ru(dppe)_2Cl$ fragment shifting from 77.8 and 84.0 ppm to 114.8 and 131.8 ppm, which is consistent with the results obtained from other $Ru(dppe)_2Cl$-acetylene compounds.[88, 95, 97]

ppm	multiplicity	Assignment	coupling
31.3	m	CH_2CH_2	-
75.5	s	Cb	-
83.5	s	Cp	-
114.8	s	$C\equiv\underline{C}\text{-}C_6H_4$	-
127.7	d	C_6H_5	$^2J_{C\text{-}P}$=33.6
128.6	s	C_6H_4	-
128.8	s	C_6H_4, quaternary	-
129.5	d	C_6H_5	$^3J_{C\text{-}P}$=15.1
130.1	s	C_6H_4	-
131.8	broad s	$C\equiv\underline{C}$-Ru	too broad to measure
134.9	d	C_6H_5	$^4J_{C\text{-}P}$= 48.6
136.5	s	C_6H_4, quaternary	-
137.4	m	C_6H_5 quaternary	-

Table 24. Summary and assignment of the $^{13}C\{^1H\}$ NMR spectra of 40.

2.3.1.1 Electrochemistry of 40

The CV profile of **40** is shown in Figure 53 at varying scan rates, and shows two reversible oxidation processes at -0.14 V and +0.09 V *vs.* Fc/Fc^+, the first oxidation process blends into the second peak producing a slight shoulder. On the reverse scan two reduction peaks are observed at -0.04 V and -0.14 V *vs.* Fc/Fc^+.

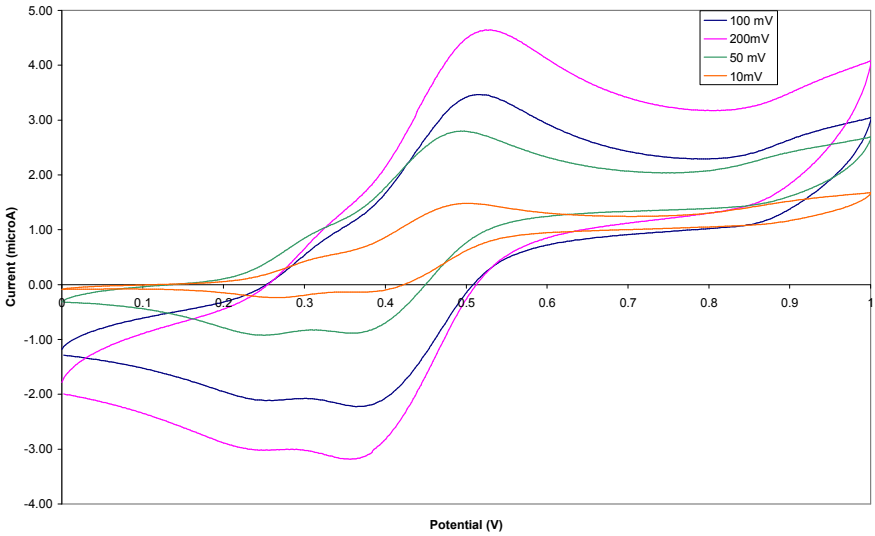

Figure 53. CV of 40 at varying scan rates. Conditions: CH_2Cl_2, 0.1M NBu_4PF_6, Working electrode Pt, Counter electrode Pt and reference electrode Pt wire.

Microelectrode experiments allowed the peaks to be identified as a 1 electron process followed by a 3 electron process. The one feasible reason for this 1 electron process followed by a 3 electron process, is that after the oxidation of the first ruthenium that an extended allenylidiene type structure is formed as shown in Figure 54. This would mean that the cyclobutadiene ring structure is lost and the three unoxidised rutheniums to become chemically equivalent hence the second redox wave is equivalent to a 3 electron process.

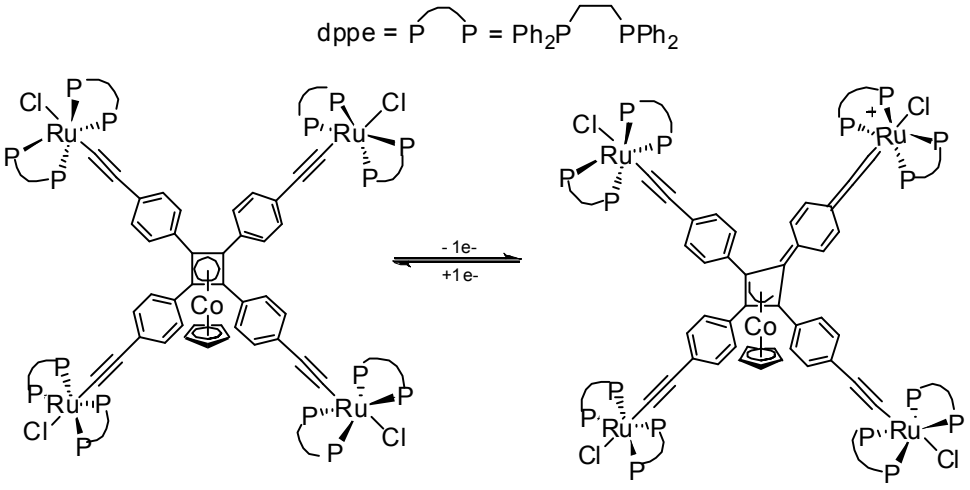

Figure 54. Proposed intermediate after first oxidation of 40.

2.3.3 Attachment of $AuPPh_3Cl$

It is known that Au(I) exhibit no oxidation process in the DCM solvent window and irreversible oxidation in other solvent windows.[98-101] However, as there are few compounds containing the ligand **38** known it was decided to investigate the synthesis of **38** with other metal fragments including $AuPPh_3$.

The method used for the synthesis of *tetrakis*(triphenylphosphinegold) ethynylphenylcyclobutadiene)cyclopentadienyl cobalt **41** was based on the synthesis of $1,3,5\text{-}C_6H_3(C{\equiv}CAu(PPh_3))_3$,[102] and previous work within the group.[103,104]

Cross *et al.*[105] reported that when a suspension of $[Au(PPh_3)Cl]$ in EtOH was treated with sodium ethoxide and phenylethyne then $[Au(C{\equiv}CPh)(PPh_3)]$ was obtained. They also report that when no acetylene was present treatment of $[Au(PPh_3)Cl]$ with sodium ethoxide produced no reaction. It is believed that the reaction starts with the removal of a proton from the acetylene by the base followed by the displacement of the chlorine from the gold by the acetylene. The formation of gold acetylides has been found to occur in methanol as well as ethanol and a variety of bases can be used including KOH and NaOMe. As very small amounts of base are required for the reaction then it was decided to try potassium butoxide as small amounts can easily be weighed out.

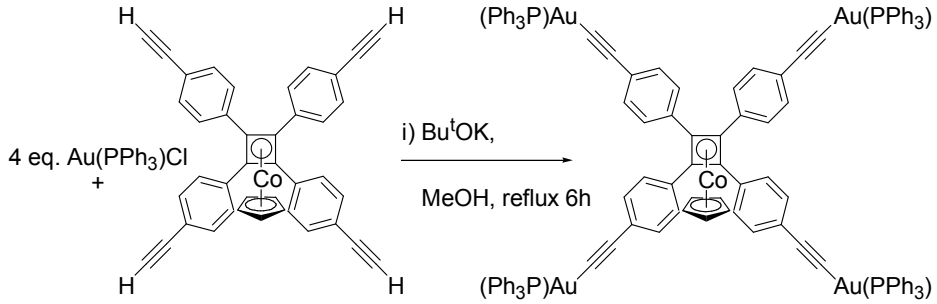

Figure 55. Synthesis of [*tetrakis*(triphenylphosphinegold)ethynylphenylcyclobutadiene] cyclopentadienyl cobalt 41.

The reaction of $AuPPh_3Cl$ and [*tetra*-(-4-ethynyl)phenylcyclobutadiene] cyclopentadienyl cobalt was carried out as shown in Figure 55. After refluxing the reaction in MeOH for 6 h, the solvent was removed and the crude residue was dissolved

in DCM and washed with deionised water. ^{31}P NMR spectroscopy showed a small amount of $AuPPh_3Cl$ remained which was removed by recrystallisation from DCM/hexane to yield pure product as a bright yellow solid. $^{31}P\{^1H\}$ NMR spectroscopy of this solid showed a peak at 43.60 ppm which is consistent with literature gold acetylidiene compounds.[103,104,106] Due to the smaller number of aromatic protons than in compound **40** it was possible to identify the C_6H_4 and the C_6H_5 signals which were seen as two doublets at 7.24 and 7.33 ppm and a broad multiplet at 7.40-7.68. These had the relative intensities of 16:60 which is consistent with four $AuPPh_3$ groups attached to the ligand **38**.

In Au(I) complexes ^{31}P-^{13}C coupling is observed for all the C-H carbons in the phenyl rings in triphenylphosphine. As would be expected the largest coupling constant is seen for the C_9 in Figure 56 as it is closest to the phosphorus. The coupling constants shown in Table 25 are in good agreement with those of similar compounds synthesised by previous members of the group.[103] Broad signals are often observed for tertiary carbons adjacent to Au due to the 100% abundance of the ^{197}Au nucleus which causes quadrupolar broading.[107] However, an overnight experiment provided a ^{13}C NMR spectrum which showed all 12 carbon signals expected for the compound **41**.

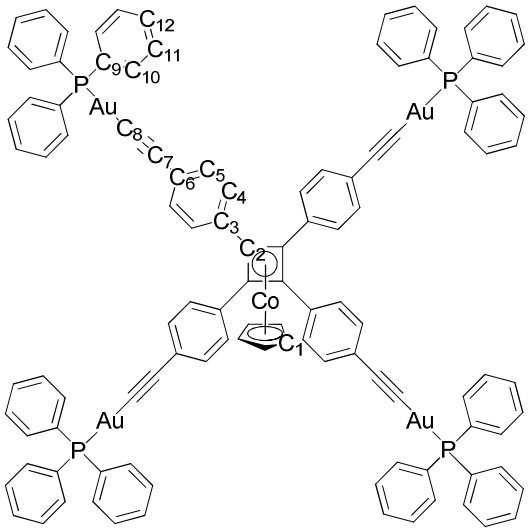

Figure 56. Labelling system for the assignment of ^{13}C spectra for 41.

^{13}C NMR signal position (ppm)	multiplicity	Coupling constant (Hz)	Assignment
75.3	s		Cb (C_2)
83.7	s		C_5H_5 (C_1)
122.9	s		C_6H_4-C≡C (C_7)
128.5	s		C_6H_4 (C_4)
128.6	d	$^2J_{PC}$ 5.0	C_6H_4-C≡C (C_8)
129.1	d	$^3J_{PC}$ 11.3	*meta*-C_6H_5
129.9	d	$^1J_{PC}$ 56.0	quaternary C_6H_5
131.5	d	$^4J_{PC}$ 2.0	*para*- C_6H_5
131.6	d	$^4J_{PC}$ 5.0	C_6H_4 (C_5)
131.7	s		quaternary C_6H_4
134.9	d	$^2J_{PC}$ 13.8	*ortho*- C_6H_5
135.5	s		quaternary C_6H_4

Table 25. ^{13}C assignment for 41.

Mass spectroscopy was carried out but the only identifiable peak was that of $[Au(PPh_3)_2]^+$, this fragment has also been observed in the mass spectroscopy of other similar gold compound.[102]

2.3.4 Attachment of Platinum.

Platinum dendrimers are highly desirable as it is believed that the introduction of a metal centre into the dendrimer could introduce functions such as catalysis, multi-redox centres and molecular recognition.[108] Because of the interest in this area there are many examples of organometallic compounds in the literature with multiple platinum centres.[108, 109]

Leininger *et al.*[110] reported the synthesis of 1,3,5-[*trans*-$I(Et_3P)_2PtC{\equiv}C]_3C_6H_3$ and 1,2,4,5-[*trans*-$I(Et_3P)_2PtC{\equiv}C]_4C_6H_2$ with yields of 56% and 44%, respectively. However three equivalents of $Pt(PEt_3)_2I_2$ per acetylene site is used for the synthesis of these materials. The reaction occurs at room temperature in 3 h and the majority of the starting material is reported as being able to be recovered. Onitsuka *et al.* have synthesised platinum-acetylene dendrimers containing up to sixty platinum atoms using careful

control utilising two different protecting groups on the terminal acetylenes.[108] The synthesis of the Pt core based on triethynylmesitylene used 0.9 equivalents of $Pt(PR_3)_2Cl_2$ per acetylene site, CuCl as the catalyst and refluxing in a 1:1 mixture of piperdine/toluene for 48 h.[111]

When building up dendrimers it is necessary to use platinum starting materials that have two chlorides or iodides so that the next organic layer can be added to the structure. However, for the application of MQCA discrete platinum materials are required at this stage so it is also possible to use platinum starting materials such as $Pt(PEt_3)_2ClPh$. The reaction of **38** with $Pt(PEt_3)_2ClPh$ was carried out as in Scheme 18 and was found to be successful using a slight excess of $Pt(PEt_3)_2ClPh$. The mixture was stirred overnight in a 1:1 mixture of $^{i}Pr_2NH$ and toluene in the presence of a catalytic amount of CuI. These reaction conditions were based on previous synthesis carried out within the group.[103,112]

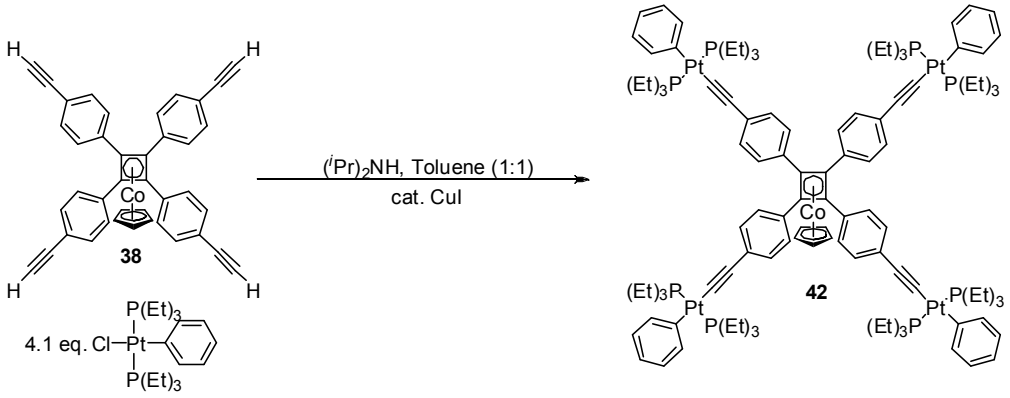

Scheme 18. Synthesis of 42.

Because of the high degree of symmetry within the compound **42** and the fact that the phosphorus are *trans* to each other gives rise to one $^{31}P\{^{1}H\}$ signal being observed. The presence of the adjacent ^{195}Pt, which has a natural abundance of 33.8% and $s=^{1}/_{2}$ gives rise to satellites either side of the central signal. The coupling constant is measured as 2646.5 Hz which is typical of *trans* Pt(II) tertiary phosphines.[113§]

§ The coupling constant for *cis* Pt(II) tertiary phosphine compounds is ~100 Hz larger than those for *trans* systems. [113] S. O. Grim, R. L. Keiter, and W. McFarlane, *Inorg. Chem.*, 1967, **6**, 1133.

The ^{1}H spectrum was a series of mainly unresolved multiplets which are summarised in Table 26, which could be identified by integration of the peaks and comparison to the starting materials and other known compounds.

Group	Chemical shift ppm	Multiplicity	coupling	Number of protons
CH_3	1.04-1.18	m	-	72
CH_2	1.66-1.86	m	-	48
C_5H_5	4.60	s	-	5
C_6H_5-*para*	6.77	t	$^{3}J_{H-H}$ 7.3	4
C_6H_5-*meta*	6.94	t	$^{3}J_{H-H}$ 7.4	8
C_6H_4	7.08-7.15	d	$^{3}J_{H-H}$ 8.3	8
C_6H_4 and C_6H_5-*ortho*	7.28-7.36	m	-	16

Table 26. Summary of the ^{1}H NMR spectra obtained for compound 42.

In $^{13}C\{^{1}H\}$ NMR spectroscopy of **42** it is possible to observe ^{31}P-^{13}C coupling in the CH_2 group of the ethyl phosphine ligand. This is a type of virtual coupling and occurs because $^{2}J_{P-P}$ is much larger than $|^{1}J_{PC} - {}^{3}J_{PC}|$ which is true for most *trans-bis*-phosphine compounds. The carbon nuclei appears to be coupled to both equivalent phosphorus centres giving an apparent triplet. If the two phosphines were *cis* then the signal would appear as two doublets because the $^{1}J_{PC}$ and $^{3}J_{PC}$ coupling would be small.[114] The coupling measured between the two outer lines in the triplet is the sum of the long and short coupling constants $|1J_{P-C} + 3J_{P-C}|$ and for *trans-bis*-phosphine complexes tends to be in the region 30-35 Hz. For this compound $|1J_{P-C} + 3J_{P-C}|$ was measured as 34.3 Hz which is consistent with the phosphines being in the *trans* positions.

Quaternary carbons adjacent to the Pt are observed as very broad signals as they are split by the ^{195}Pt, which were observed at 115.0 and 157.0 ppm corresponding to the C≡C-Pt and Pt-C_6H_5 quaternary carbons. A proton-carbon correlation experiment through one bond was carried out which enabled the assignment of the ^{13}C signals to the C_6H_4 and C_6H_5 carbons.

2.3.5 UV-Vis measurements

UV-Vis spectroscopy experiments were carried out on solutions of **40**, **41** and **42** and also of the ligand **22**. The measurements were carried out at room temperature using DCM solutions at 0.01 mmol and 0.005 mmol concentrations.

The absorption spectra of **40, 41, 42** and the ligand **22** are shown in Figure 57 and indicates that the major absorbance peak is shifted to lower wavelength in the order Au<Pt<Ru. This shift is due to the extension of conjugation of the system to the interaction of the d metal orbitals and the ligand. It also suggests that the ruthenium orbitals overlap better with the ligand than the platinum orbitals and gold orbitals. From Figure 57 it can also be seen that the onset of absorption which is an indication of the HOMO-LUMO gap is at much lower energy for **40** than for the ligand **22** or **41** and **42**.[115] The transitions observed only in compounds **40**, **41** and **42** correspond to metal to ligand charge transfer and the transition observed in all four samples corresponds to a $\pi \rightarrow \pi^*$.[108]

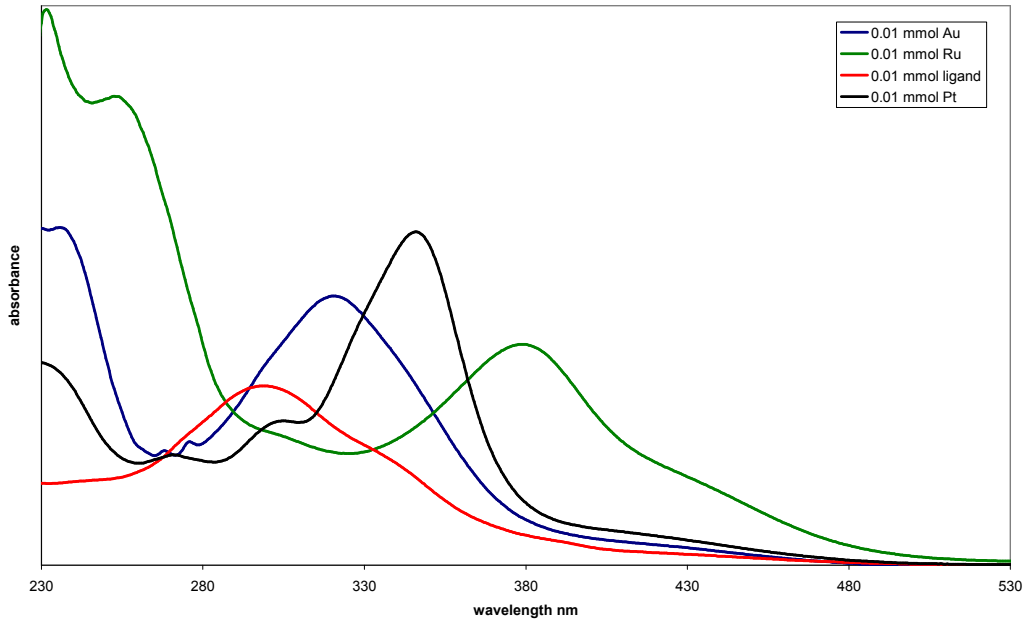

Figure 57. UV-Vis spectra of 40, 41, 42 and the ligand 22.

It can be seen from Table 27 that the extinction coefficient for **40**, **41** and **42** is of the order of 10^5 for the 0.01 mmol solution which is often seen for chromophores with a length of 10 Å.[116] From the crystal structure of **38** the distance from one arm to the opposite arm is roughly 15.6 Å.

	0.01 mmol		0.005 mmol	
M =	**Major absorption bands**	**E**	**Major absorption bands**	**ε**
$Ru(dppe)_2Cl$ **40**	252.5 378.5	167,662 78,992	253 379	174,076 80,711
$Au(PPh_2)_3$ **41**	235.5 320.5	127,123 96,273	236 320	118,258 93,552
$Pt(PEt_3)_2Ph$ **42**	346	119,205	346	128,138
22	299	64,102	299.5	65,693

Table 27. Major absorption bands and their extinction coefficients for 40, 41, 42 and 22.

2.3.5 Ferrocene Cobalt systems

Fehlner *et al.*[47] have shown that the compound $[\{(\eta^5\text{-}C_5H_5)Fe(\eta^5\text{-}C_5H_4)\}_4(\eta^4\text{-}C_4)Co(\eta^5\text{-}C_5H_5)]$ exhibits four sufficiently separated redox waves with a +1 state that can be chemically synthesised. As this is the only tetrad system known in the literature it was felt that synthesising a similar ferrocene system would be worthwhile.

The acetylene chosen to react with $CpCo(CO)_2$ was *bis*(ferrocenylethynyl)tolane **32,** the synthesis of which has been discussed in section 2.2.2. The first reaction was carried out in the same manner as that used by Fehlner *et al.*[47] which were 0.5 equivalents of $CpCo(CO)_2$ to acetylene and refluxing in xylene for 24 h. Unfortunately no reaction appeared to occur which maybe due to the low solubility of **32**. This reaction was also carried out on a small scale using $Co(PPh_3)_3Cl$ and refluxing in toluene and again no reaction seemed to occur. After finding that the reaction of **28** with $CpCo(CO)_2$ did not go to completion in refluxing xylene but did in refluxing decalin, the reaction with **32** was tried in decalin. In this third attempt the conditions were modified slightly using

0.55 equivalents of $CpCo(CO)_2$ which is the amount that Waybright *et al*.[66] use in their reactions. Compound **32** was heated in decalin to 160°C and then the $CoCp(CO)_2$ was added. After refluxing for 36 h, the solvent was removed to yield an insoluble brown solid. It is possible that the desired product is highly insoluble or that the reaction forms a polymeric material.

2.3.6 Investigations into attaching metals to *bis*(4-pyridyl)acetylene and [*tetrakis*(4-pyridyl)cyclopentadienone]cyclopentadienyl cobalt.

There are several examples in the literature of metal-ligand scaffolds using [*tetrakis*(4-pyridyl)cyclobutadiene]cyclopentadienyl cobalt and metal compounds such as $[Pd(en)((NO_3)_2)]$,[117] which is shown in Figure 58 and $[Ph_2P(CH_2)_3PPh_2]Pt^+$-$(C_6H_4)_2$-$Pt^+[Ph_2P(CH_2)_3PPh_2]$.[118]

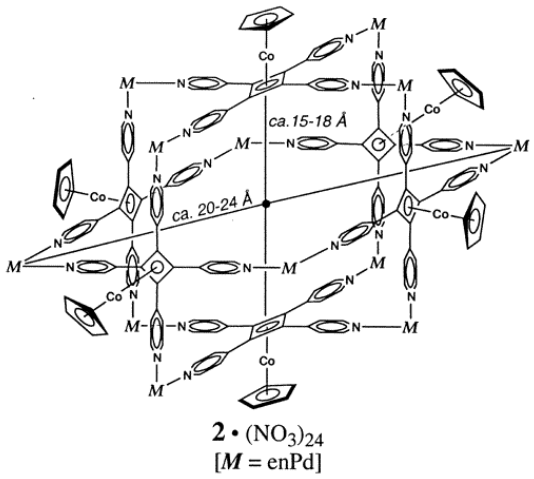

Figure 58. Example of compound obtained from reaction of 15 and $[Pd(en)((NO_3)_2)]$, [117]

Whilst compounds with structures such as this are not particularly useful for MQCA they may be useful for extended metal array formulation. It was hoped that by using metal complexes which should only bond to one ligand that materials suitable for MQCA could be obtained.

A number of compounds are known in the literature containing pyridine ligands bonded to ruthenium(*p*-cymene) dichloride.[119,120] Due to the very small amount of **15** obtained a variety of reactions were tried using **16** and *bis*(4-pyridyl)ethylene as it was felt that the reactivity of these ligands should be similar to **15**.

Therrien *et al*.[120] have carried out reactions with a range of $[Ru(\eta^6\text{-arene})Cl_2]_2$ dimers with ferrocenyl pyridine derived ligands as potential anti cancer agents. Based on the reaction conditions used, a solution of [*tetrakis*(4-pyridyl)cyclopentadienone] cyclopentadienylcobalt **16** and ruthenium(*p*-cymene) dichloride (2:1) in DCM was stirred for 24 h and then the solvent was removed. The ^{1}H NMR spectra showed that the majority of the solid was still starting material. However there was a small doublet at 8.94 ppm which was not due to the starting material which could be due to a small amount of the ligand reacting.[121]

Another test reaction attempted was the reaction of *bis*(4-pyridyl)ethylene **34** and $[Ru(dppe)_2Cl]OTf$ in a 1:2 ratio, this was initially dissolved in DCM and stirred overnight. ^{31}P NMR spectroscopy showed a small amount of $[Ru(dppe)_2Cl]OTf$ had reacted producing a new peak at 33.75 ppm but the majority was still $[Ru(dppe)_2Cl]OTf$. The solid was re-dissolved in DCM and refluxed overnight; ^{31}P NMR spectroscopy shows a slight increase in the intensity of the peak at 33.75 ppm but also several other peaks at 52.07 ppm and 46.19 ppm.

Coe *et al.*[80] have carried out reactions of *trans*-$[RuCl(pdma)_2(NO)][PF_6]$ with a range of pyridine based ligands including *bis*(4-pyridyl)ethylene. One possible explanation for why $[Ru(dppe)_2Cl]OTf$ does not seem to react very well whilst *trans*-$[RuCl(pdma)_2(NO)][PF_6]$ reacted so readily is that the triflate is very good at stabilising the $[Ru(dppe)_2Cl]^+$ complex. So the PF_6^- salt was generated by the reaction of $Ru(dppe)_2Cl_2$ and $AgPF_6$ and then added to a solution of *bis*(pyridyl)acetylene. After 24 h at room temperature ^{31}P NMR spectroscopy showed a large quantity of $[Ru(dppe)_2Cl]PF_6$ but also a large peak at 46.19 ppm plus several other peaks. Attempts at recrystallisation did not separate any of the different products.

Prismatic structures with channels filled with triflate anions have been obtained by reaction of ruthenium(*p*-cymene) dichloride with 2,4,6-tris(pyridine-4-yl)-1,3,5-triazine and silver triflate as shown in Scheme 19 by Govindaswamy *et al.*[122] It was thought that a reaction of ruthenium(*p*-cymene) dichloride with *bis*(4-pyridyl)acetylene and silver triflate might produce a similar prismatic structure to that found by Govindaswamy *et al.* It is reported[122] that whilst the final prism could be produced in one step or two steps as shown in Scheme 19 that a better yield was obtained by using two steps.

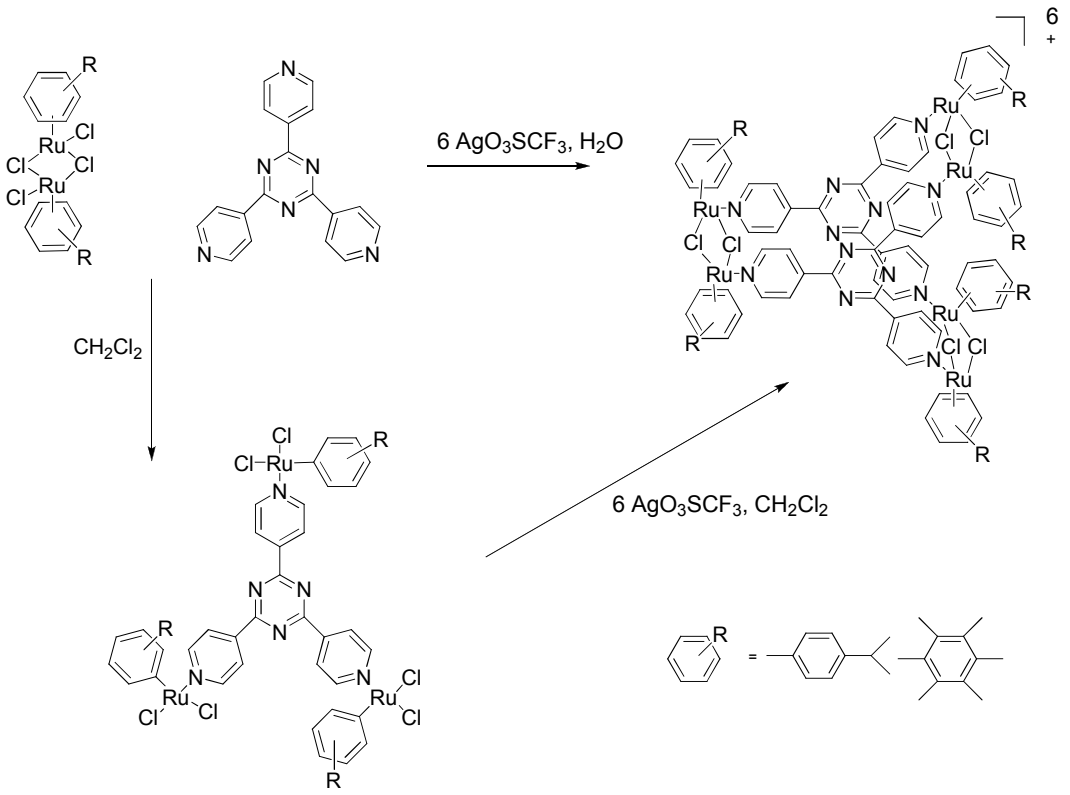

Scheme 19. Synthesis route used by Govindaswamy *et al.* to produce prismatic structures.[67]

The reaction between *bis*(4-pyridyl)ethylene and ruthenium (*p*-cymene)dichloride in a 1:1 reaction in DCM resulted in an insoluble product on which NMR spectroscopy could not be obtained. The powder was then re-dissolved in DCM with 2 equivalents of silver triflate and stirred for 4 h at room temperature. Reduction of the volume and then storage at -28°C resulted in orange crystals, however as soon as the crystals were

removed from the solvent they decomposed. The reaction was repeated as before but doing the reaction in one step and the solution was filtered through celite before reduction of the volume of the solvent. Orange crystals were formed again but as before the crystals decomposed as soon as they left the solvent.

Layering solutions of metal nitrates and pyridyl acetylene compounds such as 1,4-*bis*(4-pyridyl)butadiyne,[123] 1,2-*bis*(3-pyridyl)ethyne[78] or 1,4-*bis*(4'-pyridylethynyl) benzene[124] have been found to produce extended 1D and 2D structures sometimes containing channels. However these networks often tend to be interpenetrated,[**] a ligand with four fold symmetry such as **15** or **16** could potentially increase the channel size. Several layering experiments were carried out with [*tetrakis*(4-pyridyl) cyclopentadienone]cyclopentadienyl cobalt **16.** The metal nitrate chosen was $Cd(NO_3)_2.4H_2O$ as this has been reported to give good 2D networks in the literature. Solutions of **16** in MeOH were layered with $Cd(NO_3)_2.4H_2O$ in 4:1 and 2:1 ratios of metal:ligand and left to diffuse slowly. The solid obtained from both solutions was micro-crystalline and not suitable for single X-ray diffraction experiments. These solids were highly insoluble and therefore characterisation by mass spectroscopy or NMR was not possible.

2.4 Conclusions

The cyclisation of 4-4'-*bis*-(triisopropylsilyl)ethynyltolane to form [*tetra*-(-4-triisopropylsilylethynyl)phenylcyclobutadiene]cyclopentadienyl cobalt occurred in a good yield and could be easily purified. After removal of the TIPS groups, attachment of four $\{Ru(dppe)_2Cl\}$, $\{Au(PPh_3)_2\}$ and $\{Pt(PEt_3)_2Ph\}$ fragments was possible and a series of new compounds were obtained. The electrochemistry of (*tetrakis*$(Ru(dppe)_2Cl)$ ethynylphenylcyclobutadiene)cyclopentadienyl cobalt **40** was investigated as a potential MQCA candidate. Cyclic voltammetry experiments suggest that the oxidation process is reversible but occurs as a 1 electron process followed by a 3 electron process; the most likely explanation for this is that after the first ruthenium oxidation a delocalised

[**] Interpenetration is when a compound contains two interlocked polymers with cavities and the cavities are filled with the other polymer chain.

allenylidiene structure is formed. This allenylidiene structure would result in the loss of the cyclobutadiene structure and could cause the other three rutheniums to become chemically equivalent and hence their oxidation to occur at the same potential. Whilst it is known that the electrochemistry of Au(I) and Pt(II) centres is irreversible and hence unsuitable for a MQCA applications, compounds **41** and **42** have not been previously reported and full characterisation has been carried out.

Prior to the cyclisation of 4-4'-*bis*-(triisopropylsilyl)ethynyltolane a variety of other acetylene compounds were prepared by a series of Sonogashira reactions, for investigation in cobalt mediated cyclisation. Literature reactions have shown that the cobalt mediated cyclisation of certain acetylene compounds results in the formation of the cyclopentadienone product and sometimes the cyclisation does not occur.[54,67] For the acetylene compounds investigated though this work it was found that the reaction with *bis*(ferrocenylethynyl)tolane and 1,2-*bis*(4-cyanophenyl)ethyne produced highly insoluble products. Cyclisation of 4-4'-*bis*-(trimethylsilyl) ethynyltolane resulted in multiple [CpCoCb] and [CpCocyclopentadienone] products which is likely to be due to the cyclisation reaction occurring at all the acetylene sites. The cyclisation of 1,4-dibromotolane to form [*tetrakis*(4-bromophenyl)cyclobutadiene]cyclopentadienyl cobalt only produced a 12% yield which meant that further functionalisation of this compound was not practical.

The reaction of *bis*(4-pyridyl)acetylene with [$CpCo(CO)_2$] produced 50% of the cyclopentadienone product and only a 1% yield of the desired [*tetrakis*(4-pyridyl)cyclobutadiene]cyclopentadienyl cobalt. Altering the reaction conditions by using a higher boiling point solvent improved the yield of the [*tetrakis*(4-pyridyl) cyclopentadienone]cyclopentadienyl cobalt product **16** but not of the desired product **15**. A variety of reactions to attach metals to [*tetrakis*(4-pyridyl) cyclopentadienone]cyclopentadienyl cobalt and *bis*(4-pyridyl)acetylene were tried with very little success.

3. Chapter 3: Benzene based materials

3.1 Introduction

In the context of assembling molecular units suitable for MQCA devices, another way of arranging four connected metals with an approximate four fold symmetry is linking them to a central benzene ring which acts as the core ligand. The simplest four fold symmetrical benzene based ligand suitable for forming metal-acetylide compounds is 1,2,4,5-*tetra*ethynylbenzene, the structure of which is shown in Figure 59.

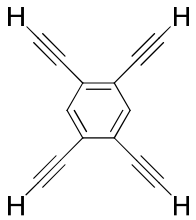

Figure 59. Structure of 1,2,4,5-tetraethynylbenzene.

Whilst there are few acetylene systems known with four metals attached, bimetallic fragments connected by a conjugated bridging ligand have been widely researched, [7, 9, 87, 125-127] several examples of which are shown in Figure 60.

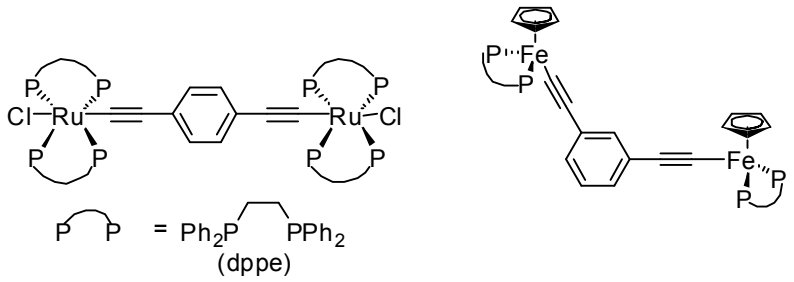

Figure 60. Two examples of bimetallic fragments connected by a conjugated bridging ligand.

Through this research, the effects on electronic communication within the complex by varying the length of the bridging ligand,[7, 125] the type of bridging ligand [7, 9, 87, 125-127] and the metal fragment[9, 87] have been closely examined and some examples are summarised in Table 28, which lists the comproportionation constants for the systems.

M—≡—S—≡—M					
Position	S=	M=			
		$Ru(dppm)_2Cl$	$Os(dppm)_2Cl$	$Fe(depe)_2Cl$	$Fe(dmpe)_2Cl$
Para	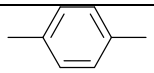	1.2×10^5	1.2×10^5	5.1×10^2	
Meta	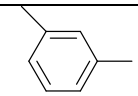	1.6×10^3	7.5×10^2		
Para	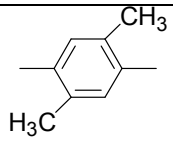	3.8×10^5	1.2×10^5		1.3×10^4
Para	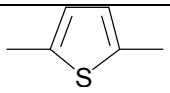	2.5×10^5	8.0×10^4		
Para	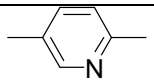	1.2×10^6	2.6×10^5		

Table 28. Comproportionation values for literature bimetallic acetylenes calculated from electrochemical measurements. Dppm = 1,2-*bis*(diphenylphosphino)methane, depe = 1,2-*bis*(diethylphosphino)ethane and dmpe = 1,2-*bis*(dimethylphosphino)ethane.

In addition to these measurements Raithby *et al.*[9] have also carried out computational studies on the energies of these systems. It was found that when the molecule is oxidised the bridge undergoes a change and is no longer aromatic but has a quinoid-like structure as shown in Figure 61. From these calculations the ionisation potential (IP_{calc}) could be obtained which showed good agreement with the first electrode potentials measured indicating that in order of ease of oxidation 2,5-thiophenediyl < 1,4-benzenediyl < 2,5-pyridinediyl < 1,3-benzendiyl. 1,3-benzenediyl cannot form the quinoid structure to stabilise the oxidised compound and hence a low K_c is observed compared to 1,4-benzenediyl.

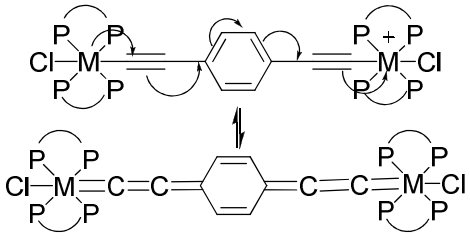

Figure 61. Delocalised allenylidiene structure that is proposed for the oxidised metal acetylene.

A study of *ortho*, *meta* and *para* substituted ferrocenes by Patoux *et al.*[128] indicates the importance of the effect of the relative substitution pattern *i.e.* 1,2, 1,3 or 1,4 of the redox centres relative to each other in determining the electronic properties of these systems.

Relative substitution pattern	**Structure** Fc= 	**K_c**	**Peak separation (mV)**
1,2 *Ortho*	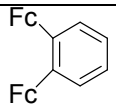	160	131
1,3 *Meta*	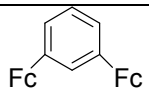	35	90
1,4 *Para*	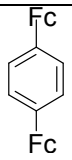	60	104

Table 29. Structure of three diferrocenylbenzene compounds and the peak separation and K_c values obtained from electrochemical measurements carried out by Patoux *et al.*[128]

As it can be seen from the Table 29, the position of the ferrocene groups relative to each other has a significant effect on the peak separation and the K_c values. The smallest through bond distance between the redox centres is when the ferrocene moieties are *ortho* to each other and this is also when the K_c value is the greatest. If the K_c value was dependant only on the distance between the redox centres then it would be expected that

the *meta* position would have the next largest K_c value however this is not observed. The explanation proposed for weak *meta* site coupling is because of a process known as quantum inference.[128] Patoux *et al*. have performed theoretical bonding calculations on the *para* and *meta* diferrocenylbenzene compounds. On the basis of these calculations it is suggested that the weak interaction in the *meta* isomer is because there are two ligand orbitals that overlap with the metal orbitals leading to molecular orbitals with different symmetries. This leads to an overall cancellation effect and produces a small coupling between sites. This substitution pattern also results in two different pathways being available for electron transfer. Weyland *et al*.[129] have observed two intervalence charge transfer bands in the NIR range for the compound $\{Cp^*(dppe)Fe(CC\text{-})\}_3(1,3,5\text{-}C_6H_3)][PF_6]_2$. This is due to an interaction between the unpaired electrons on the different sites leading to the population of both a triplet and a singlet state at room temperature which means that there are two different energy pathways for electron transfer.[129]

The nature of the metal fragment can also have an effect on the coupling between sites as shown by the different electrochemistry exhibited by various metal fragments attached to the same 1,3,5-triethynylbenzene as shown in Table 30.

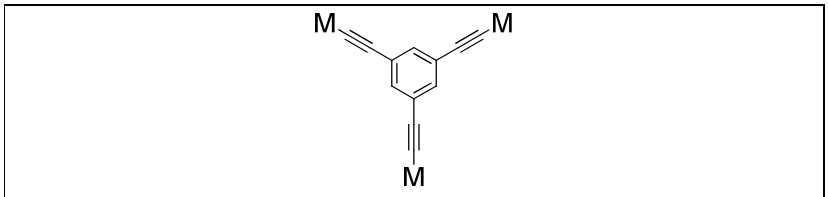

M=

	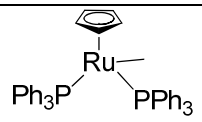	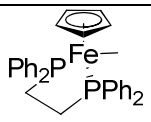
One 3e- redox wave.[77]	Three separated redox waves.[††89]	Three well separated reversible waves.[130]

Table 30. Structure and summary of the electrochemical results for a range of metal compounds linked by a 1,3,5-triethynylbenzene core.

[††] Waves are reversible on a cyclic voltammetry scale but decompose at longer time periods, resulting in a low K_c values.

The K_c and the peak separation measured by Weyland *et al*. are reported to be 130 and 0.125 V respectively for [{Cp*(dppe)Fe}(1,3,5-C_6H_3)][PF_6], [{Cp*(dppe)Fe(CC-)}$_3$(1,3,5-C_6H_3)][PF_6] and [{Cp*(dppe)Fe(CC-)}$_3$(1,3,5-C_6H_3)][PF_6]$_2$. These values are large for *meta* systems and Weyland *et al*.[129] propose that this observation is a result of linking the metal and the benzene ring *via* an acetylene linker. This linker provides a continuous orbital overlap between the metal and the ligand. This theory is also supported by the observations made by others shown in Table 30. When M = {RuCp(PPh_3)$_2$} three redox peaks are observed in the cyclic voltammetry, however, when M = ferrocene only one redox peak is observed. With M= ferrocene no continuous orbital overlap is present unlike when M = {RuCp(PPh_3)$_2$}.

During the course of the work for this thesis, three compounds containing four metal centres arranged in an approximate square have been published. The structures of these compounds and a summary of the electrochemical results observed are shown in Table 31. From the electrochemistry summary in Table 31 it can be seen that none of the compounds shown exhibit electronic communication between all the metal centres.

Compound structure	Electrochemistry results	Reference
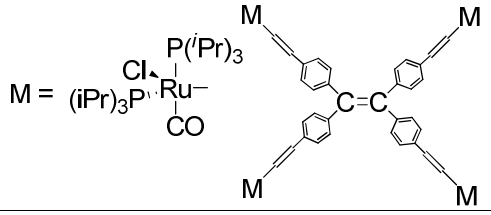	Two reversible waves at $E_{1/2}$ = -0.020 and +0.415 V *vs*. Fc/Fc^+	131
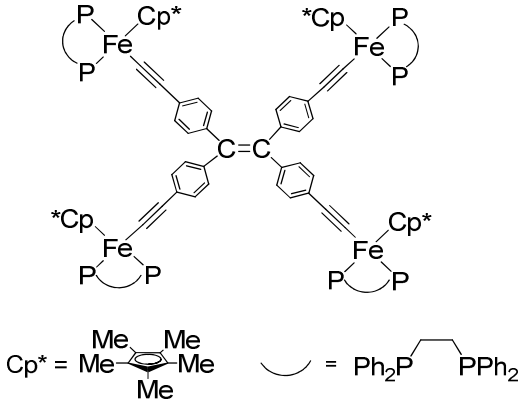	One broad and slightly unsymmetrical reversible redox wave at -0.61 V *vs*. Fc/Fc^+	132
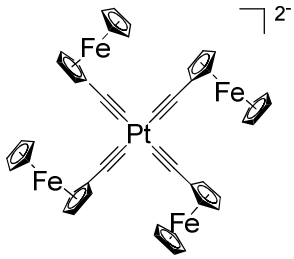	Irreversible oxidation at 0.09 V Oxidation at 0.65 V Reduction peak at 0.50 V Referenced *vs*. Ag/AgCl electrode	133

Table 31. The structure and summary of the electrochemistry for three recent compounds containing four metal centres arranged in an approximate square.

The fact that none of the compounds shown in Table 31 show electronic communication between the four metal centres suggests that compounds with the necessary properties for MQCA are very rare.

To summarise, it is known that the largest influence on the electronic communication is the distance between the metal centres; upon increasing the distance the K_c values decreases. It has also been found that the following factors also affect the electronic communication between metal centres –

a) The ability of the bridging to form a delocalised allenylidiene structure.[9]
b) The nature of the metal fragment such as its geometry and type of coligands.[134]

c) The relative energies of the metal fragment and the bridging ligand.
d) Whether the metal fragments are *ortho*, *para* or *meta* to each other.
e) The solvent and the counter-ion in the background electrolyte can also have an effect on the electron transfer process.[135]

By using 1,2,4,5-tetraethynylbenzene as a linker for metal centres, it provides *ortho*, *meta* and *para* metal positions as shown in Figure 62. For MQCA applications when the molecule is in the 2+ state the electrons should sit in antipodal (*para*) positions. This would mean that the benzene linker could form a delocalised allenylidiene structure similar to that seen in Figure 61. It is hoped that communication between the *meta* sites in the 1,2,4,5-tetraethynylbenzene core would be sufficient to induce switching in a MQCA cell.

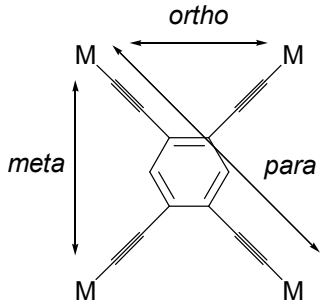

Figure 62. Relationship between the different metal sites connected to 1,2,4,5-tetraethynylbenzene core.

3.2 Results and Discussion for diad systems.

The first section of this work is focused on the synthesis of a range of known bimetallic systems which would potentially be suitable for MQCA diad applications. Examination of these systems allowed investigation of synthetic routes and also solubility of the products to evaluate whether these metal fragments and linkers would be suitable in a tetrad system.

The ligand used to investigate the diad systems was 1,4-(diethynylbenzene) **40** as this has been shown to exhibit good electronic communication through the bridging ligand.[9,

[87] This bridging ligand can also be viewed as half of the 1,2,4,5-tetraethynylbenzene core.

3.2.1 Synthesis of 1,4-*bis*(trimethylsilylethynyl)benzene 43 and 1,4-diethynylbenzene 44.

The protected ligand **43** was prepared by palladium catalysed Sonogashira coupling using an adapted literature method,[136] as shown in Scheme 20. After stirring overnight, TLC showed the reaction to have reached completion. After removal of the solvent, the crude product was extracted from the reaction residue using diethyl ether and the diethylammoniumiodide salt could be filtered off. The product was purified by column chromatography on silica to yield **43** as a white powder in a 76% yield.

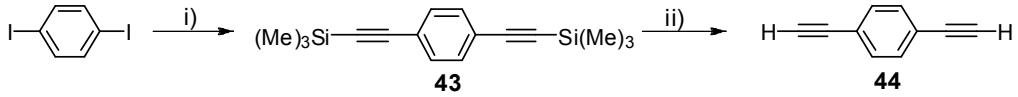

43 **44**

Scheme 20. Synthesis of 1,4-*bis*(trimethylsilylethynyl)benzene 43 and 1,4-diethynylbenzene 44. i) 4 mol% $Pd(PPh_3)_2Cl$, 2% mol CuI, Et_2NH. ii) THF/MeOH, 3 eq. K_2CO_3, RT, 12 h.

Removal of the TMS protecting group can be carried out by a variety of bases such as K_2CO_3,[137] KOH[136] and NaOH,[95] for the deprotection of **43** the base used was K_2CO_3 which is a mild deprotecting reagent. Aqueous work-up and extraction with diethyl ether yielded the crude product **44** which was purified by filtering through a short silica plug to yield a cream product that becomes brown over time.

3.2.2. $Cl(dppe)_2Ru\text{-}C{\equiv}CC_6H_4C{\equiv}C\text{-}Ru(dppe)_2$ 45.

Ruthenium complexes have been found to be a good energy match for conjugated bridging ligands and hence tend to form compounds with good electronic communication.[138] In addition to this, ruthenium σ-aryl acetylidienes have been found to have low oxidation potentials compared to organic molecules with a discernable separation between the reversible oxidation waves.[138]

The compound $Cl(dppe)_2Ru\text{-}C{\equiv}CC_6H_4C{\equiv}C\text{-}Ru(dppe)_2$ **45** was prepared as in the literature.[87] Initially *cis*-$Ru(dppe)_2Cl_2$ is reacted with $NaPF_6$ to form the complex

[Ru(dppe)$_2$Cl]PF$_6$ as this has been found to react faster with acetylenes, to form a vinylidiene intermediate as shown in Scheme 21. This vinylidiene intermediate can then be deprotonated by a base such as triethylamine to form the desired product.

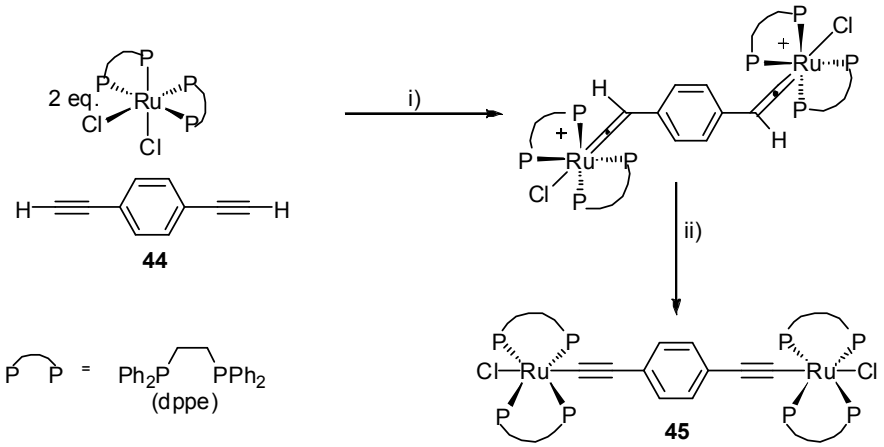

Scheme 21. Reaction scheme for the synthesis of Cl(dppe)$_2$Ru-C≡CC$_6$H$_4$C≡C-Ru(dppe)$_2$. i) 4 eq. NaPF$_6$, THF, RT, 40 h ii) THF, Et$_3$N, 16 h.

3.2.2.1 Electrochemistry of 45.

The first system studied electrochemically was that of Cl(dppe)$_2$Ru-C≡CC$_6$H$_4$C≡C-Ru(dppe)$_2$ **45** as this has already been reported by Lavastre *et al.*,[87] as showing electronic communication between the two ruthenium centres. This system was therefore used to establish that the electrochemical set-up was working correctly and to provide a comparison for the systems prepared for this thesis.

Table 31 shows a comparison between the data obtained by Lavastre *et al.* and that obtained using the cell set-up used throughout this thesis. Lavastre *et al*.[87] attributed the two successive reversible oxidation waves at E° = + 0.15 V$_{SCE}$ ($i_{p,a}/i_{p,c}$ = 1.06) and +0.55 V$_{SCE}$ ($i_{p,a}/i_{p,c}$ = 1.03) to the formation of the mono- and dications respectively.[87] The irreversible peak at 1.60 V was assigned by Lavastre *et al.* to be due to formation of Ru^{IV}. From Table 32 it can be seen that good agreement between the peak separation for the anodic and cathodic processes for both reversible redox waves and the peak potentials reported previously and observed during our work.

E_{pa} (V)	E_{pc} (V)	E° (V)	ΔE (mV)	assignment	Reference
+0.19	+0.11	+0.15	80	Ru^{II}/Ru^{III}	[87]
+0.20	+0.12	+0.16	80		This work
+0.55	+0.47	+0.51	80	Ru^{III}/Ru^{III}	[87]
+0.54	+0.47	+0.51	70		This work
+1.60	-	-	-	$Ru^{III/}Ru^{IV}$	[87]
+1.68	-	-	-		This work

Table 32. Comparison of electrochemical data for 45 obtained by Lavastre *et al.* and data obtained using the cell set-up used throughout this thesis. Lavastre *et al.* performed a ferrocene calibration prior to each measurement, for which the ferrocene couple was measured at E°'=+0.49. Measurements made for this thesis were calibrated using ferrocene and cobaltocene as internal references and calibrated to the same ferrocene value used by Lavastre *et al.*[87]

The CV profile obtained from the experiments for this thesis is shown in Figure 63, which shows a clear peak separation between the formation of the monocation and the formation of the dication.

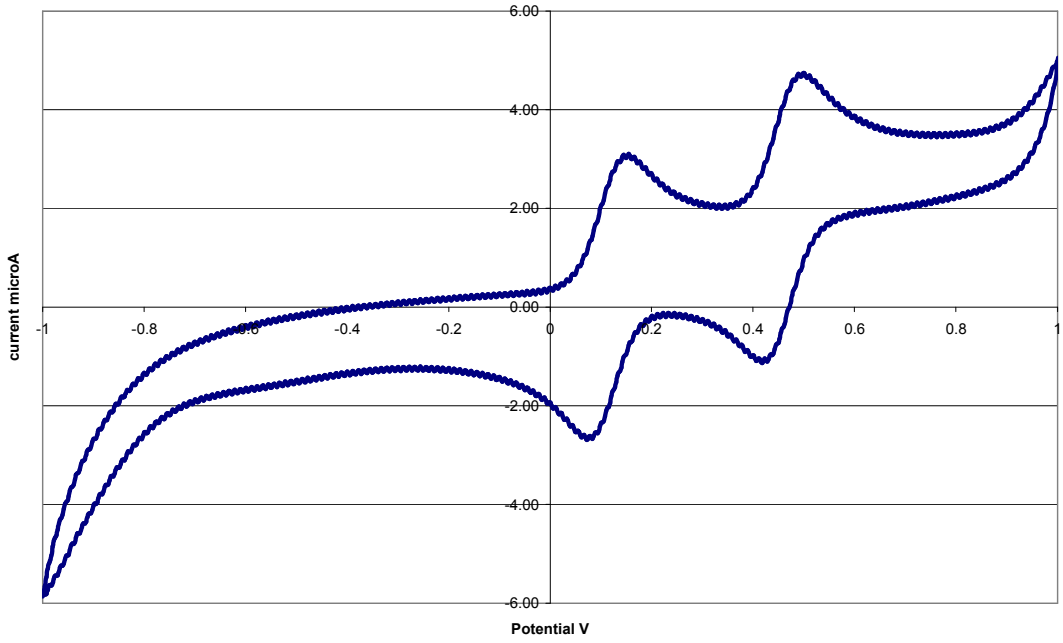

Figure 63. CV of 45. Conditions: CH_2Cl_2, 0.1M NBu_4PF_6, Working electrode Pt, Counter electrode Pt and reference electrode Pt wire.

3.2.3. {Cp(Fe(CO)$_2$)C≡CC$_6$H$_4$C≡C{Fe(CO)$_2$Cp} 46.

A second bimetallic compound of interest was {Cp(Fe(CO)$_2$) C≡CC$_6$H$_4$C≡C{Fe(CO)$_2$Cp} **46** as the metal starting reagent, CpFe(CO)$_2$I, is relatively cheap and easy to synthesise.{Cp(Fe(CO)$_2$)C≡CC$_6$H$_4$C≡C{Fe(CO)$_2$Cp} can be converted to the corresponding dppe compound {CpFe(dppe)}C≡CC$_6$H$_4$C≡C {CpFe(dppe)} which has been shown to be more stable than the corresponding dicarbonyl compound.

Firstly CpFe(CO)$_2$I was prepared by cleavage of the dimer [CpFe(CO)$_2$]$_2$ using iodine.[139] For the next step the acetylene needs to be activated in order to attach the metal, this can be done in a variety of different ways including formation of a Sn-acetylene compound,[140] lithiation of the acetylene [141] or use of a Grignard.[142]

The literature preparation[143] of {CpFe(CO)$_2$}C≡CC$_6$H$_4$C≡C{CpFe(CO)$_2$} utilising a Grignard was followed and is shown in Scheme 22.

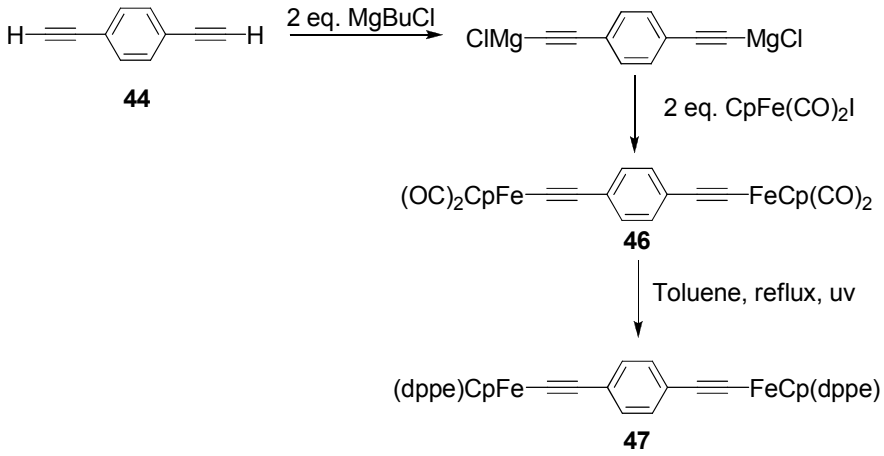

Scheme 22. Reaction scheme used for the synthesis of (CpFe(CO)$_2$) C≡CC$_6$H$_4$C≡C (CpFe(CO)$_2$) 46 and (CpFe(dppe))C≡CC$_6$H$_4$C≡C(CpFe(dppe)) 47 using a Grignard.

After the first two steps crude {CpFe(CO)$_2$}C≡CC$_6$H$_4$C≡C{CpFe(CO)$_2$} **46** was obtained as a highly insoluble solid. Purification was carried out by several cycles of dissolving in DCM and precipitation with hexane and the ^{1}H NMR spectra was found to

be consistent with that of the literature,[142,144] the solid was insufficiently soluble to obtain a ^{13}C NMR spectrum that would show the quaternary carbons.

Green *et al.*[143] reported that treating $CpFe(CO)_2C{\equiv}CPh$ with triphenylphosphine at 160 °C resulted in the formation of $CpFeCO(PPh_3)C{\equiv}CPh$. Santi *et al.*[144] also report the conversion of $\{CpFe(CO)_2\}C{\equiv}CC_6H_4C{\equiv}C\{CpFe(CO)_2\}$ **46** to $\{CpFe(dppe)\}C{\equiv}CC_6H_4C{\equiv}C\{CpFe(dppe)\}$ **47** under UV light. However the literature yield of **47** was reported as 12%, with the hope of improving the yield the conversion was carried out in refluxing toluene under UV light for 48 h. Despite using the same concentration solution as the literature, the majority of compound **46** was not soluble even in refluxing toluene. After refluxing the solution was cooled and filtered to remove un-dissolved **46** and the solvent was removed to yield a brown solid. ^{31}P NMR spectroscopy of this crude solid showed a signal at 100.7 ppm as reported in the literature for compound **47**.[144] However the largest peak was a broad peak at -10.2 ppm suggesting the majority of this solid was uncomplexed dppe ligand. The literature reported the purification of **47** by 10 cycles of dissolving in toluene and reprecipitation with hexane, this was attempted and it was found the solid was so insoluble that huge quantities of solvent were be required. Considering the insolubility of this compound containing two $\{CpFe(CO)_2\}$ groups it was decided that this would not be viable for an application requiring four metal centres.

3.2.4 Synthesis of $\{Co_2CO_6\}_2(Me_3Si\text{-}C{\equiv}C\text{-}C_6H_4\text{-}C{\equiv}C\text{-}SiMe_3)$ 48.

Coordination of $Co_2(CO)_8$ and its phosphine-substituted derivatives to acetylene compounds has been shown in the literature[145,146] to be an excellent way of obtaining crystal structures with difficult to crystallise acetylene ligands. The reaction occurs with the displacement of two carbonyl groups to produce $\{Co_2C_2\}$ clusters of the general form $Co_2(\mu\text{-}\eta^2\text{-alkyne})(CO)_4(L_2)$ (L= CO, phosphine) as shown in Scheme 23.

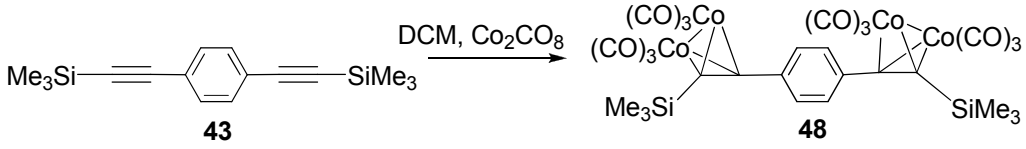

Scheme 23. Formation of cobalt clusters by reaction of 43 with $Co_2(CO)_8$.

The reaction conditions for synthesis of $Co_2(\mu\text{-}RC_2R)(CO)_6$ compounds are very straightforward. The solids are dissolved in DCM and stirred under N_2 for 6-8 h. Although this system has been previously prepared it was felt that due to the straightforward nature of the synthesis that it would be worth preparing the system to investigate the electrochemistry. The reaction of 1,4-*bis*(trimethylsilylethynyl)benzene **43** with $Co_2(CO)_8$ was carried out as in the literature.[147] After removal of the solvent and re-dissolving it in a minimal amount of dry DCM, storage at -18°C overnight resulted in the formation of red, square crystals. Single crystal X-ray diffraction structural determination found not only the desired product but the presence of unusual $Co_2(CO)_8$ compound with no bridging carbonyls as shown in Figure 64.

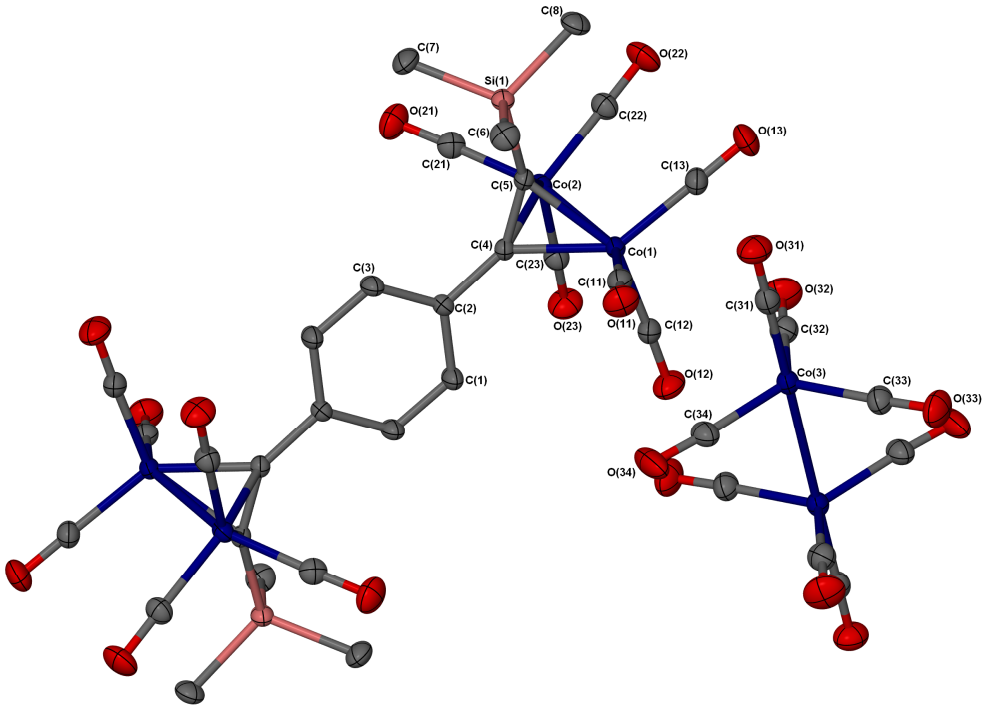

Figure 64. Structure of 1,4-μ-$Co_2CO_6(Me_3Si\text{-}C{\equiv}C\text{-}C_6H_4\text{-}C{\equiv}C\text{-}SiMe_3)$ 48 and the $Co_2(CO)_8$ moiety. Thermal ellipsoids are shown at 50% and hydrogen atoms are omitted for clarity.

The structure of **48** has been previously reported by Draper *et al*. but the structure of the $Co_2(CO)_8$ moiety with no bridging carbonyls has not reported to our knowledge. The bond lengths of the structure **48** reported by Draper *et al*.[148] showed good agreement with those from the molecular structure shown in Figure 64. The only bond length

which was not within experimental error was one Co-CO bond which Draper *et al.*[148] reported as being 1.785 (3) Å which was significantly shorter than any Co-CO bond measured in **48**. The bond angles were not available for the structure by Draper *et al.*[148] to allow comparison with the molecular structure in Figure 64.

From the molecular structure shown in Figure 64 it can be seen that the bridging cobalt cluster causes the acetylene unit to derivate from linearity to 142.2(2)° for the bond angle C(5)-C(4)-C(2). This derivation from the linearity of the starting acetylene is a feature of these kind of clusters.[149]

Co(1)-C(11)	1.806(3)	O(22)-C(22)	1.129(3)
Co(1)-C(12)	1.814(3)	O(23)-C(23)	1.140(3)
Co(1)-C(13)	1.828(2)	O(31)-C(31)	1.132(3)
Co(1)-C(4)	1.965(2)	O(32)-C(32)	1.131(3)
Co(1)-C(5)	1.996(2)	O(33)-C(33)	1.132(3)
Co(1)-Co(2)	2.4810(4)	O(34)-C(34)	1.136(3)
Co(2)-C(21)	1.802(3)	Si(1)-C(5)	1.849(2)
Co(2)-C(23)	1.811(3)	Si(1)-C(8)	1.859(3)
Co(2)-C(22)	1.831(3)	Si(1)-C(6)	1.867(3)
Co(2)-C(4)	1.982(2)	Si(1)-C(7)	1.869(3)
Co(2)-C(5)	1.986(2)	C(1)-C(3)#2	1.384(3)
Co(3)-C(31)	1.797(3)	C(1)-C(2)	1.399(3)
Co(3)-C(34)	1.806(3)	C(2)-C(3)	1.400(3)
Co(3)-C(32)	1.807(3)	C(2)-C(4)	1.456(3)
Co(3)-C(33)	1.807(3)	C(3)-C(1)#2	1.384(3)
Co(3)-Co(3)#1	2.7053(6)	C(4)-C(5)	1.347(3)
O(11)-C(11)	1.129(3)	O(13)-C(13)	1.133(3)
O(12)-C(12)	1.140(3)	O(21)-C(21)	1.128(3)
C(5)-C(4)-C(2)	142.2(2)		

Table 33. Selected bond lengths (Å) and angles (°) for 48. # denotes atoms from the other half of the symmetrical molecule.

It has been established that $\{Co_2(CO)_8\}$ exists in solution in two forms which are shown in Figure 65.[150,151] Studies of the temperature dependence of the IR spectrum in pentane have lead to Noack[150] determining that the ratio of I:II is 43:57 at room temperature and at -104°C the ratio is 84:16.

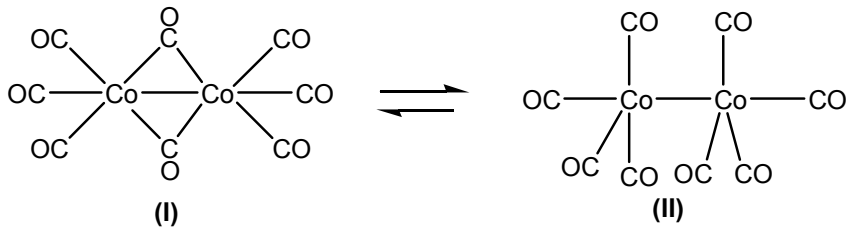

Figure 65. The two isomers of $Co_2(CO)_8$ that exist in solution.

A sample of **48** was purified to remove unreacted $Co_2(CO)_8$ by a flash column on silica and eluting with hexane/DCM, and the solution was concentrated and stored at -28°C. Needle-like crystals were obtained and the unit cell of these were found to be consistent with those reported by Draper *et al*.[148]

3.2.4.1 Electrochemistry of 48.

There are a variety of compounds containing cobalt carbonyl clusters linked by a C≡C group that exhibit electronic interaction between the clusters.[149,152] However, whilst it is known that each $Co_2(CO)_6$ cluster exhibits an one-electron, diffusion-controlled reduction, these reactions can be complicated by fast chemical reactions arising from the cleavage of the Co-Co bond.[149]

Electrochemical studies of diyne $Co_2(CO)_6$ compounds[149, 153,154] have identified the main electrochemical process as that being the reduction to form the anionic species. The anion is very reactive and can undergo fast chemical reactions or can go on to form the dianionic species depending upon the stability of the anion. The process in Figure 66 has been proposed by Duffy *et al*. for the reduction of diyne $Co_2(CO)_6$ compounds, in some systems the reduction of both clusters appears as one peak in the cyclic voltammetry.[149]

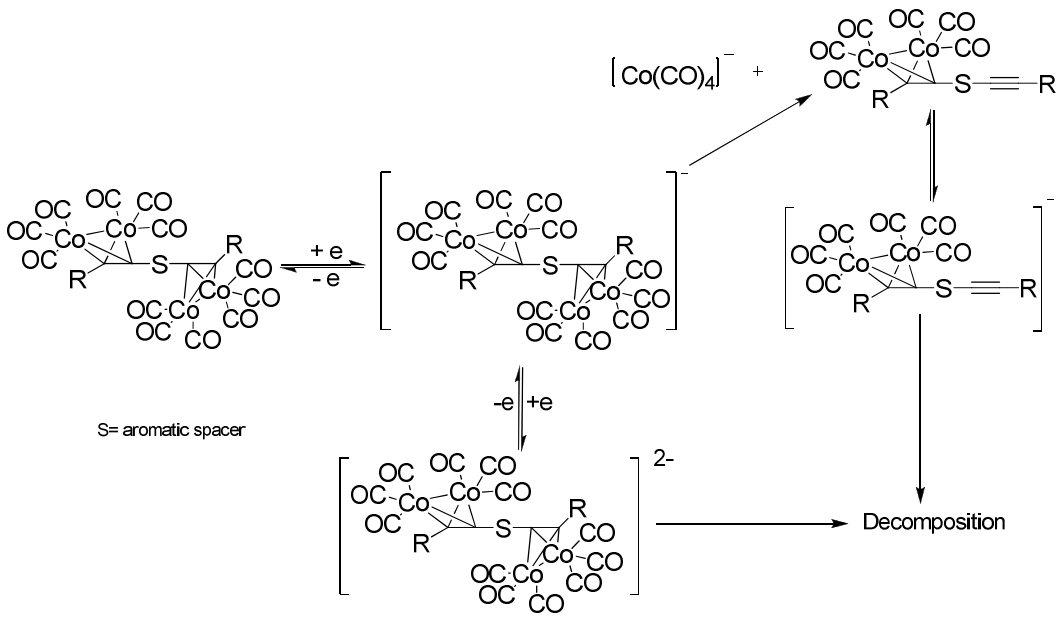

Figure 66. Proposed electrochemical process of Co_2CO_6 bridged acetylene compounds.[154]

The cyclic voltammetry of (μ^2-$Co_2(CO)_6$)$_2$ (Me_3Si-C≡C-C_6H_4-C≡C-$SiMe_3$) is shown in Figure 67 and exhibits two irreversible peaks at -0.33 V and 0.89 V with respect to the Fc/Fc^+ couple. It seems reasonable based on the systems studied by Duffy *et al.*[149] that by starting at a negative potential the dianion [(μ^2-$Co_2(CO)_6$)$_2$ (Me_3Si-C≡C-C_6H_4-C≡C-$SiMe_3$)]$^{2-}$ is generated first and the peak at -0.33 V is due to the oxidation of this material. The small peak at 0.89 V is then likely to be due to the decomposition of the compound as it increases dramatically with increasing number of scans. The large reversible peak observed in Figure 67 is due to ferrocene which is used as an internal reference.

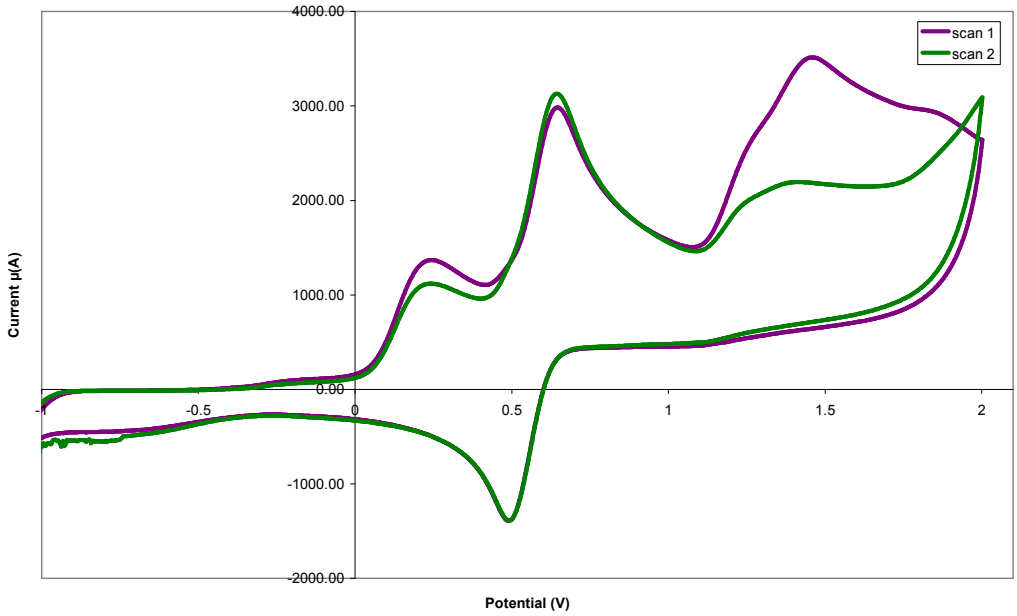

Figure 67. CV of 48.

It has been observed that the oxidation of the "$C_2Co_2(CO)_6$" cluster is not observed within accessible potentials.[152] There are several ways of tuning the compounds to improve the electrochemistry, these are:

- Introduction of electron withdrawing or bulky substituents on the acetylene to improve the reversibility of the reduction process of the radical anion.[155]
- The reversibility of the oxidation of the anion and the potential it occurs at can be tuned by the introduction of phosphine, dppm or phosphite ligands.[155]
- Carrying out the electrochemistry at -30°C in many cases causes the radical anion formation to become reversible.[153]

However the dominant process in any of these "$C_2Co_2(CO)_6$" derivatived compounds is the anion formation, often followed by fast reaction leading to decomposition, making these kind of materials unsuitable for MQCA.

3.3 Results and Discussion of Tetrad systems

3.3.1 1,2,4,5-*tetrakis*(ferrocenylethynyl)benzene 49.

Long *et al*. reported the synthesis of 1,3,5-*tri*(ferrocenylethynyl)benzene using tribromobenzene in good yield.[77] However previous attempts of the synthesis of 1,2,4,5-*tetrakis*(ferrocenylethynyl)benzene within the group suggested that a mixture of products are obtained which are very difficult to separate.[156]

The first synthesis method used for the preparation of compound **48** was adapted from that used by Long *et al*.[77] for 1,3,5-*tri*(ferrocenylethynyl)benzene. Long *et al*. used 1,3,5-*tri*-bromobenzene to synthesise 1,3,5-*tris*(ferrocenylethynyl)benzene which was exchanged for 1,2,4,5-tetraiodobenzene for the synthesis of 1,2,4,5-*tetra*(ferrocenylethynyl)benzene. However TLC after 84 h refluxing suggested that multiple products were present in the reaction mixture which could be a combination of *mono*, *bis*, *tris* or *tetra* substituted products as shown in Scheme 24 products **a-d**. Separation of these products proved unsuccessful by chromatography. One of the problems with Sonogashira coupling is that there is another reaction which can occur; this is the homocoupling of two acetylene molecules. A previous attempt to synthesis tetraethynylferrocenylbenzene within the group had isolated *bis*(ethynylferrocene) Scheme 24 product **e** as the major product from the reaction mixture.[156] It has been reported by Torres *et al*.[157] that homocoupling to produce *bis*(ethynylferrocene) as the major product, can occur instead of the desired coupling reaction. This was found to occur when ethynylferrocene was refluxed in diethylamine or triethylamine in the presence of CuI and $Pd(PPh_3)_2Cl_2$.[157] As these are the conditions that were being used for the synthesis of 1,2,4,5-*tetrakis*(ferrocenylethynyl)benzene this means that there is likely to be at least five different products possible from this reaction as shown in Scheme 24 and it was decided to examine different reactions conditions.

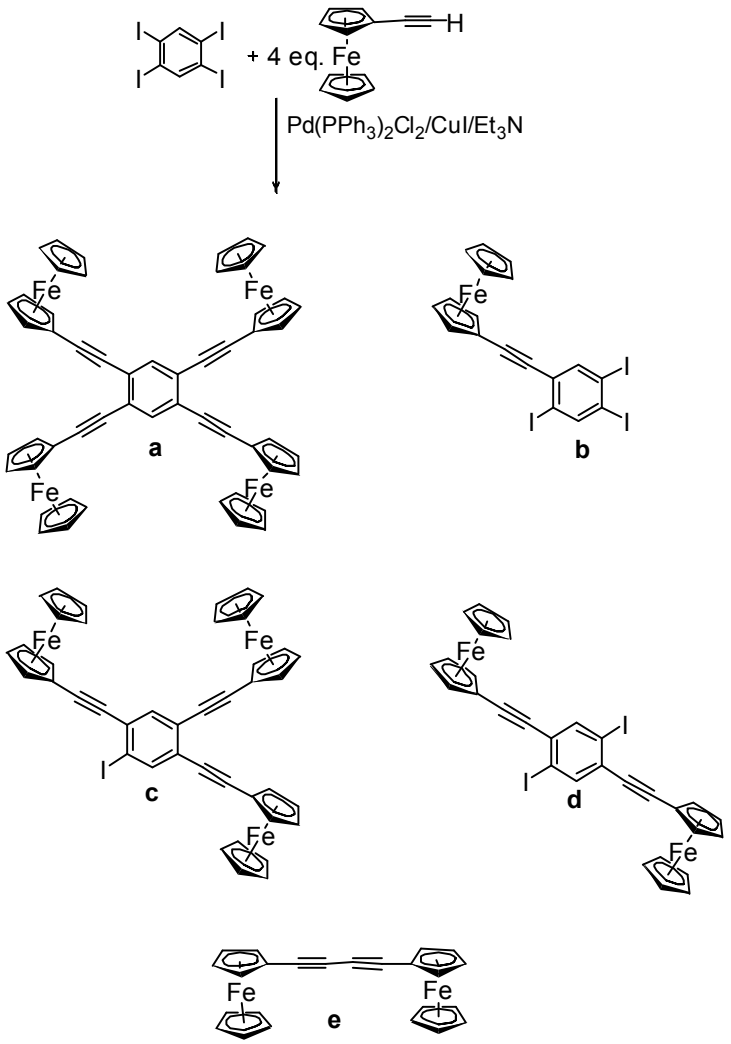

Scheme 24. Potential products from the Sonogashira palladium catalysed coupling of 1,2,4,5-tetraiodobenzene and ethynylferrocene. Note that compound d is only one of the possible *bis*-substituted possible, the ferrocene groups could be also be *meta* or *ortho* to each other.

The second attempt to synthesise this compound was made using Stille coupling[158,68] rather than Sonogashira *via* the synthesis of (tributylstannylethynyl)ferrocene, the reaction scheme is shown in Scheme 25. The synthesis of (tributylstannylethynyl) ferrocene was based on a similar literature reaction for 1,1'-*bis*(tributylstannylethynyl) ferrocene[159] and was prepared by the *in-situ* lithiation of ethynylferrocene using butyl lithium at -78°C. Followed by the reaction of the lithiated ethynylferrocene with tributyltin chloride to form the desired product. After removal of the solvent and extraction into hexane, the reaction was filtered to remove the lithium chloride and the

hexane was removed to yield (tributylstannylethynyl)ferrocene as a crude orange oil. The tributylstannylethynyl ferrocene was characterised by ^{1}H and ^{13}C NMR spectroscopy and compared to similar literature compounds prior to use in the Stille coupling.[160]

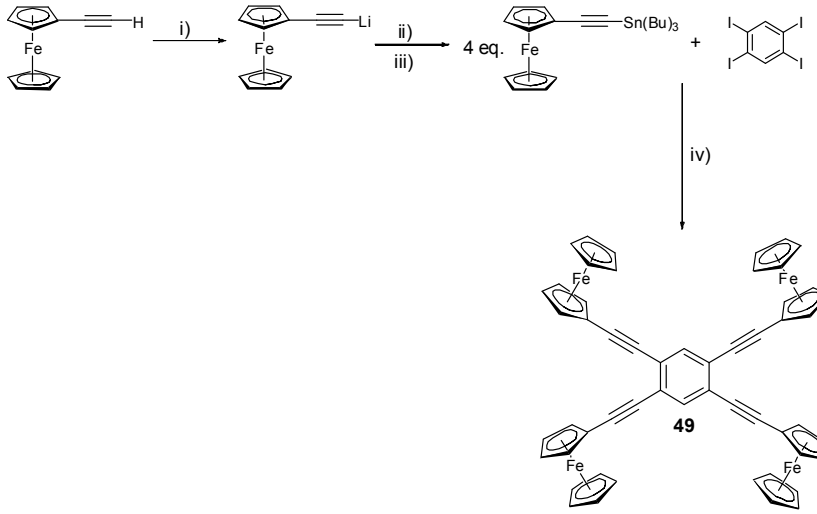

Scheme 25. Synthesis of 1,2,4,5-*tetrakis*(ferrocenylethynyl)benzene 49 using Stille coupling. Reaction conditions : i) THF,-78°C, 1 eq. BuLi, ii) 0°C, 2.5 h, iii) -78°C, 1 eq. $SnBu_3Cl$ and iv) 0.25 eq. $Pd(PPh_3)_4$, dioxane.

Tok *et al.*[160] report that any excess tributyltin chloride did not cause problems in the sequent Stille coupling so the tributylstannylethynyl ferrocene was used without further purification. The tributylstannylethynyl ferrocene was dissolved in dioxane and transferred into the reaction vessel containing 0.25 equivalents of 1,2,4,5-*tetra*iodobenzene and 10 mol% $Pd(PPh_3)_4$ as a catalyst. After refluxing for 20 h and cooling the solution a bright red precipitate had formed which was isolated by filtration and washed with hexane. ^{1}H NMR spectroscopy revealed two multiplets between 4-5 ppm and a singlet at 7.62 ppm with the ratios $1(C_6H_2):8(C_5H_4):28(C_5H_4$ and $C_5H_5)$. The product was found to be highly insoluble in most common solvents and only partially soluble in DMF and benzene. In order to obtain a sample concentrated enough for a ^{13}C NMR spectra the compound was dissolved in dichlorobenzene and then a few drops of CD_2Cl_2 was added. It was not possible to observe the signals for the arene ring of **49** due to the weak signal and the presence of a strong dichlorobenzene signal. However it was

possible to observe four signals for the ferrocene rings due to the 3 different C-H environments and one quaternary carbon and also two different C≡C signals.

However the compound **49** was fully soluble in dichlorobenzene and slow evaporation lead to formation of crystals suitable for single crystal X-ray diffraction experiments. The molecular structure derived from single crystal X-ray diffraction experiments is shown in Figure 68.

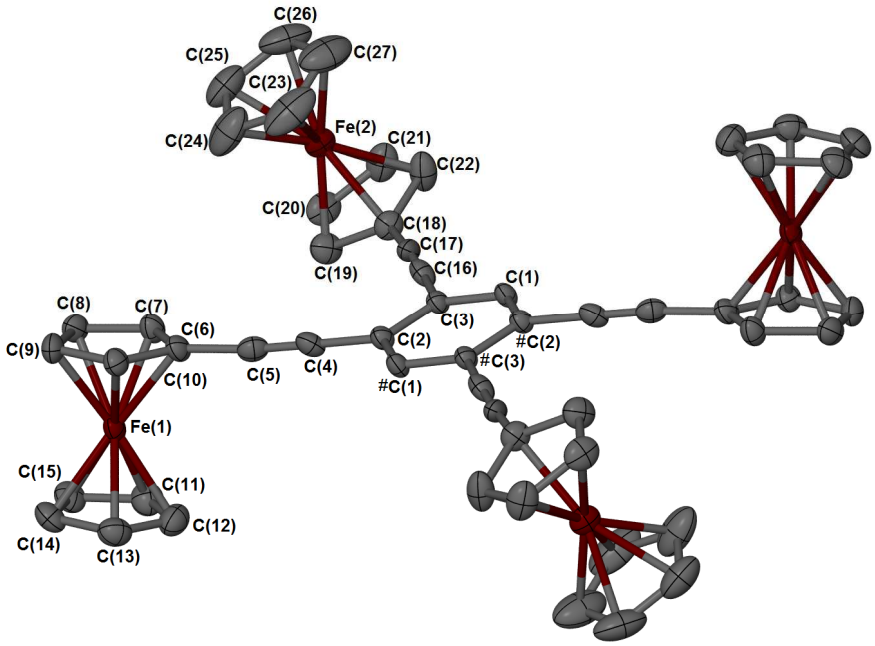

Figure 68. Molecular structure of 1,2,4,5-*tetrakis*(ferrocenylethynyl)benzene.‡‡ Ellipsoids are shown at 50% probability and hydrogens are omitted for clarity. # denotes atoms from the other half of the symmetrical molecule.

From the molecular structure of 1,2,4,5-*tetrakis*(ferrocenylethynyl)benzene **49** shown in Figure 68 it can be seen that the ferrocenes are arranged such that *ortho* ferrocenyl groups are orientated away from each other. Whereas the *meta* ferrocenyl groups project towards the same face of the arene ring in a up-down-down-up configuration about the ring. The *para* ferrocenyl groups are aligned with each other as seen by the crystallographic symmetry of the molecule. The dihedral angle for C(19)-C(18)-C(3)-

‡‡ The asymmetric unit is half of the molecular structure shown in Figure 68 and 1 molecule of disordered DCM. # corresponds to the atoms in the other half of the symmetrical unit.

C(2) is -16.3(4)° and for C(7)-C(6)-C(2)-C(3) is 10.5(4)° showing that the ferrocene moieties are not planar with the arene ring. Fehlner *et al*. reported for {(η^5-C_5H_5)Fe(η^5-C_5H_4}$_4$(η^4-C_4)Co(η^5-C_5H_5)} **9** that the ferrocenyl rings were twisted about the connecting C-C bonds with alternating torsion angles of -11° and 60°.[47] The observation of the smaller dihedral angles between the ferrocene rings and the central ring for **49** compared to **9** is likely to be due to the longer distance between the central ring and the ferrocene due to the additional C-C≡C bond. The steric clash between the cyclopentadienyl cobalt cyclobutadiene linker and the ferrocene groups also has a large influence on the large torsion angles observed by Fehlner *et al*.[47]

Selected bond lengths and angles for **49** are shown in Table 34. The average C-C bond lengths and angles in the ferrocene and benzene rings in **49** were found to be in agreement with those of 1,3,5-*tris*(ferrocenylethynyl)benzene. In **49** the geometries of the C-C≡C-C bonds are essentially linear as shown by the bond angles being between 174.5(4)° and 178.1(4)° which is similar to those obtained for 1,3,5-*tris* (ferrocenylethynyl)benzene being between 175.0(9)-178.5(10)°. The C≡C bond lengths were all 1.141(5) Å in **49**; in 1,3,5-*tris*(ferrocenylethynyl)benzene they were 1.187(11), 1.182(11) and 1.145(11) Å.

C(1)-C(2)	1.393(4)	C(5)-C(4)-C(2)	177.8(4)
C(3)-C(2)	1.422(4)	C(4)-C(5)-C(6)	174.5(4)
C(1)-C(3)#1	1.386(4)	C(17)-C(16)-C(3)	178.1(4)
C(4)-C(5)	1.141(5)	C(16)-C(17)-C(18)	176.6(4)
C(5)-C(6)	1.457(5)	C_{nt}(1)-C_{nt}(2)-C_{nt}(1#)	180.0(7)
C(16)-C(17)	1.141(5)	C_{nt}(3)-C_{nt}(2)-C_{nt}(3#)	180.0(7)
C(19)-C(18)-C(3)-C(2)	-16.32(4)	C(7)-C(6)-C(2)-C(3)	10.45(4)

Table 34. Selected bond lengths (Å) and angles(°) for 1,2,4,5-*tetrakis*(ferrocenylethynyl)benzene. # denotes atoms from the other half of the symmetrical molecule and C_{nt}(1) corresponds to C(18)-C(22). C_{nt}(2) corresponds to C(1)-C(1#),C_{nt}(1#) corresponds to C(18#)-C(22#). C_{nt}(3) corresponds to C(6)-C(10) and C_{nt}(3#) corresponds to C(6#)-C(10#).

3.3.1.1 Electrochemistry of 49.

Electrochemistry of **49** was carried out in dichloroethane and the CV obtained is shown in Figure 69. It can be seen from Figure 69 that there is only one redox wave at $E_{1/2}$ = 0.11 V versus the Fc/Fc^{+} couple for all four ferrocene moieties meaning that there is no communication between the ferrocene centres. The reduction wave observed is much larger than the oxidation wave which is due to the absorption of the oxidised species on the electrode surface, which is then reduced enhancing the reduction current.[8,161]

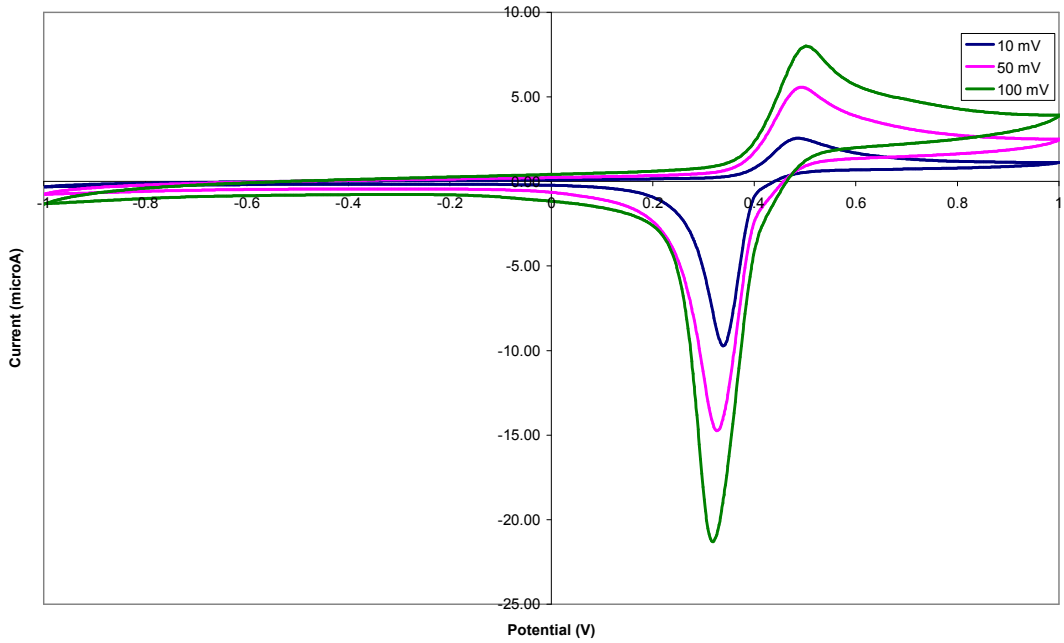

Figure 69. CV of compound 49 in dichloroethane with 0.1 M $TBAPF_6$ background electrolyte. Counter, working and reference electrode all Pt.

3.3.2 Ligand synthesis

Firstly it was necessary to prepare 1,2,4,5-*tetrakis*(ethynyl)benzene to be used as a scaffold to attach metals to through the formation of M-C σ bonds.

The synthesis of 1,2,4,5-*tetrakis*((trimethylsilyl)ethynyl)benzene **50** was carried out as shown in Scheme 26 with minor alterations to the literature preparation.[162]

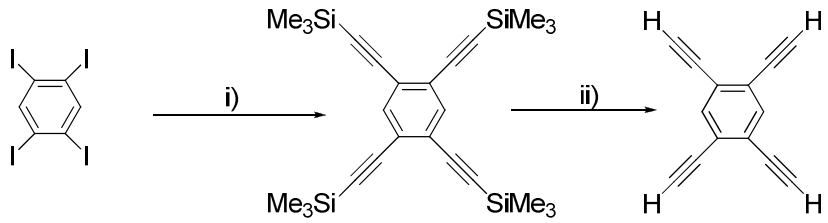

Scheme 26. Synthesis of 1,2,4,5-*tetrakis*((trimethylsilyl)ethynyl)benzene 50 and 1,2,4,5-*tetrakis*(ethynyl)benzene 51. i) 9.4 mol% $Pd(PPh_3)_2Cl_2$, 8 mol% CuI, piperdine/Et_3N, 4.9 eq. H-C≡C-$SiMe_3$, RT 4 h. ii) Et_2O/MeOH, excess KOH, RT 3 h.

By using 1,2,4,5-*tetra*iodobenzene and an excess of H-C≡C-$SiMe_3$, TLC showed the Sonogashira coupling to be complete after 4 h at room temperature. After acidified aqueous work up and column chromatography on silica, **50** was isolated as a white powder in a 64% yield. The compound 1,2,4,5-*tetrakis*(ethynyl)benzene **51** was obtained by deprotection of **52** in a diethyl ether/MeOH solution using an excess of potassium hydroxide. After extraction of the organic layer and drying, the pure compound could be isolated by evaporation of the solvent at room temperature. It has been reported in the literature that this material can detonate if heated during this process.[162]

3.3.2.1 Synthesis of $\{Co_2CO_6\}_4$(H-C≡C-C_6H_2-C≡C-H) 52.

Synthesis of $\{Co_2CO_6\}_4$(H-C≡C-C_6H_2-C≡C-H) **52** was carried out in the same manner to the diad system **48**; by stirring a solution of tetraethynylbenzene in DCM with 4 equivalents of $Co_2(CO)_8$ overnight. The solvent was removed and the compound purified by flash column chromatography on silica using 9:1 hexane/DCM as an eluent. Concentration of the fractions obtained from this column and storage at -28°C resulted in crystals suitable for single crystal X-ray diffraction experiments and the molecular structure shown in Figure 70 was obtained.

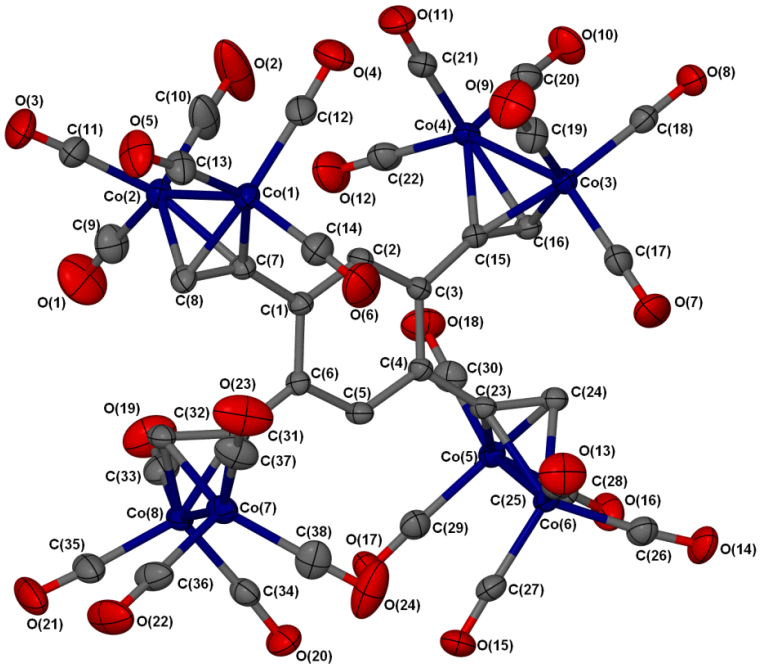

Figure 70. Molecular structure of $\{Co_2CO_6\}_4$(H-C≡C-C_6H_2-C≡C-H) 52. Ellipsoids are shown at 50% probability and hydrogens are omitted for clarity.[§§]

Selected bond lengths and angles for the molecular structure of **52** are shown in Table 35. Crystal data for this structure has not been published previously so the crystal data is compared to that of **48** published by Draper *et al*. The bond lengths for the Co-C bond in the $\{C_2Co_2\}$ clusters were found to range from 1.935(3) to 1.980(2) Å in **52** where as in the published structure of **48** the range was 1.957(2) to 1.996 (2) Å. The other bond lengths were found to be within experimental error of those reported by Draper *et al.*[148]

[§§] The asymmetric unit consists of one and half of the molecules shown in Figure 70.

Co(1)-C(14)	1.787(4)	Co(5)-C(30)	1.787(3)
Co(1)-C(12)	1.803(3)	Co(5)-C(28)	1.822(3)
Co(1)-C(13)	1.821(3)	Co(5)-C(29)	1.829(3)
Co(1)-C(8)	1.940(3)	Co(5)-C(24)	1.953(3)
Co(1)-C(7)	1.985(3)	Co(5)-C(23)	1.971(3)
Co(1)-Co(2)	2.4613(6)	Co(5)-Co(6)	2.4676(6)
Co(2)-C(9)	1.774(4)	Co(6)-C(25)	1.797(3)
Co(2)-C(10)	1.809(4)	Co(6)-C(27)	1.816(3)
Co(2)-C(11)	1.816(3)	Co(6)-C(26)	1.830(3)
Co(2)-C(8)	1.946(3)	Co(6)-C(24)	1.944(3)
Co(2)-C(7)	1.971(3)	Co(6)-C(23)	1.980(2)
Co(3)-C(17)	1.791(3)	Co(7)-C(37)	1.782(4)
Co(3)-C(19)	1.818(3)	Co(7)-C(36)	1.809(3)
Co(3)-C(18)	1.824(3)	Co(7)-C(38)	1.813(4)
Co(3)-C(16)	1.955(3)	Co(7)-C(32)	1.958(3)
Co(3)-C(15)	1.966(3)	Co(7)-C(31)	1.971(3)
Co(3)-Co(4)	2.4597(6)	Co(7)-Co(8)	2.4622(6)
Co(4)-C(22)	1.799(3)	Co(8)-C(33)	1.794(4)
Co(4)-C(21)	1.808(3)	Co(8)-C(34)	1.818(3)
Co(4)-C(20)	1.831(3)	Co(8)-C(35)	1.826(3)
Co(4)-C(16)	1.943(3)	Co(8)-C(32)	1.935(3)
Co(4)-C(15)	1.977(3)	Co(8)-C(31)	1.980(3)
C(16)-C(15)-C(3)	145.2(3)	C(24)-C(23)-C(4)	144.8(2)
C(8)-C(7)-C(1)	145.7(3)	C(32)-C(31)-C(6)	145.5(3)

Table 35. Selected bond lengths (Å) and angles (°) for (μ-$Co_2CO_6)_4$(H-C≡C-C_6H_2-C≡C-H) 52.

^{1}H NMR spectroscopy exhibited two broad peaks at 7.89 and 6.58 ppm in a ratio of 1:2 consistent with the C_6H_2 protons and the C≡C-H protons. The dramatic shift in the ^{1}H signal for the C≡C-H group from 3.42 ppm to 6.58 ppm is consistent with shifts seen in other similar compounds reported by Constable *et al*.[163] Obtaining ^{13}C NMR spectra for these kinds of materials can be very problematic as the carbonyl signals are very weak and the other peaks are often very broad. It was therefore not possible to obtain a ^{13}C spectrum for this compound.

Electrochemistry of **52** was not carried out due to the electrochemical results obtained from **48** which showed that compounds of this nature would not be suitable for MQCA applications.

3.2.2.2 Synthesis of Ruthenium compounds

As noted in Chapter 2 there are many different ways of synthesising ruthenium containing compounds. With the success of Long *et al.*[89] synthesis of a variety of ruthenium compounds based around 1,3,5-triethynylbenzene the initial aims of this project were to attach a ruthenium fragment to 1,2,4,5-*tetrakis*ethynylbenzene.

Two different methods were used to try to synthesise this system which were also tried for the [CpCoCb] system. These were 1) refluxing $CpRu(PPh_3)_2Cl$ in MeOH, followed by addition of tetraethynylbenzene and then addition of sodium. 2) lithiation of tetraethynylbenzene and then addition of $CpRu(PPh_3)_2Cl$ as shown in Scheme 27.

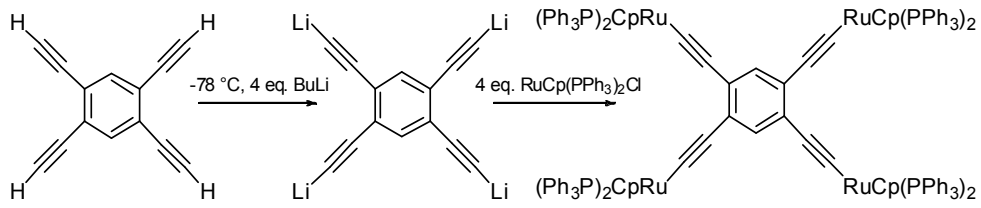

Scheme 27. Proposed reaction scheme for the synthesis of *tetrakis*(CpRu $(PPh_3)_2$ethynyl)benzene *via* the lithium salt.

In both cases, the solids obtained from both of these reactions were found to be the starting material $CpRu(PPh_3)_2Cl$. Dixneuf *et al.*[95] had previously reported that it is not possible to attach four $\{Ru(dppe)_2Cl\}$ groups to tetraethynylbenzene due to the steric demands of the ruthenium group. Whilst $\{CpRu(PPh_3)_2\}$ is not as bulky or rigid as $\{Ru(dppe)_2Cl\}$ it is possible that there is not enough space for four ruthenium groups around tetraethynylbenzene.

3.2.2.3 Synthesis of an extended tetraethynylbenzene ligand

Because of the bulk and the rigid nature of dppe Dixneuf *et al.* synthesised an tripodal polyyne from 1,3,5-*tri*bromobenzene which they then successfully attached three

{Ru(dppe)$_2$Cl} groups to as shown in Scheme 28.[95] Inspired by this work a similar ligand was synthesised but with four arms for metal attachment.

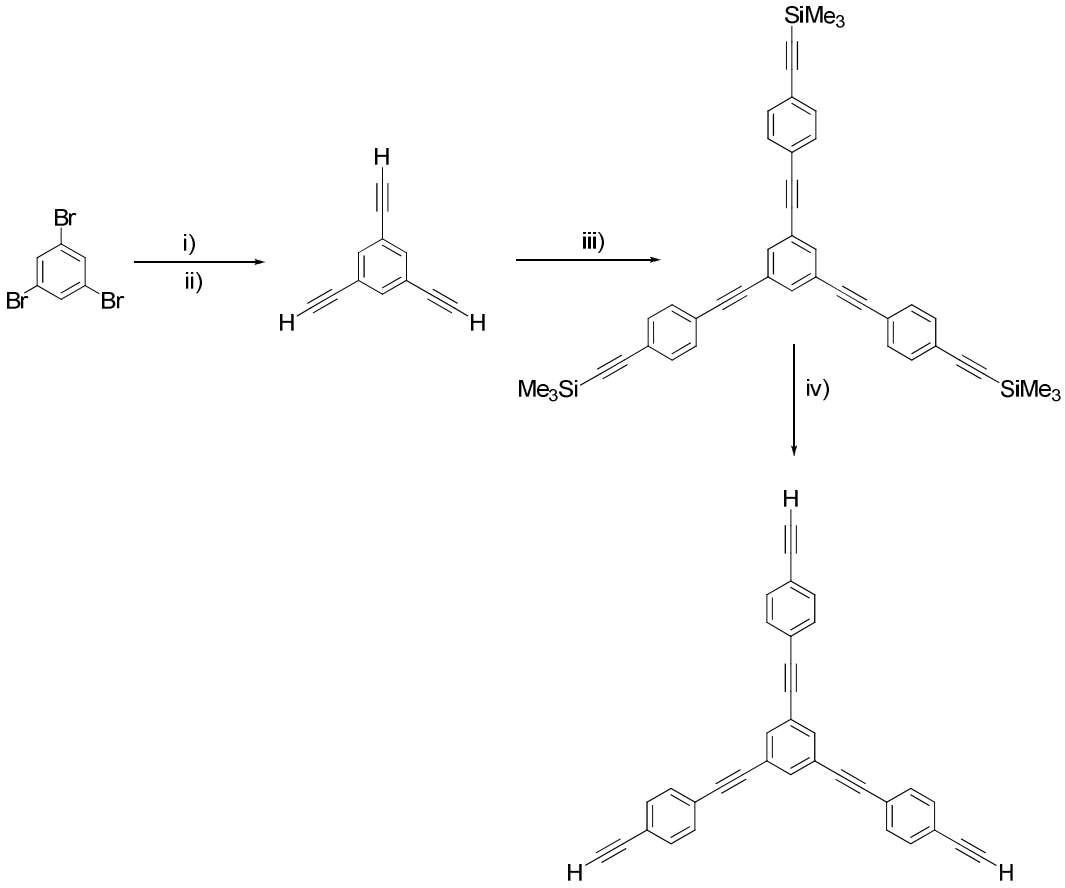

Scheme 28. Reaction scheme for the synthesis of the tripodal ligand synthesised by Dixneuf *et al.* i) HC≡CSiMe$_3$, NEt$_3$, Pd catalyst, CuI ii) NaOH (aq) iii) IC$_6$H$_4$C≡CSiMe$_3$, NEt$_3$, Pd catalyst, CuI iv) NaOH (aq).

Converting the tripodal ligand into a tetrapodal ligand by use of tetraethynylbenzene appeared to offer a solution to the steric problems encountered before. However the synthesis of a tetrapodal ligand proved to be problematic due to insolubility. The first attempt to synthesise **53** was the Sonogashira coupling of 1,2,4,5- tetraethynylbenzene with (4-bromo-phenylethynyl)trimethylsilane **25** to produce the desired product in 13% yield as shown in Scheme 29.

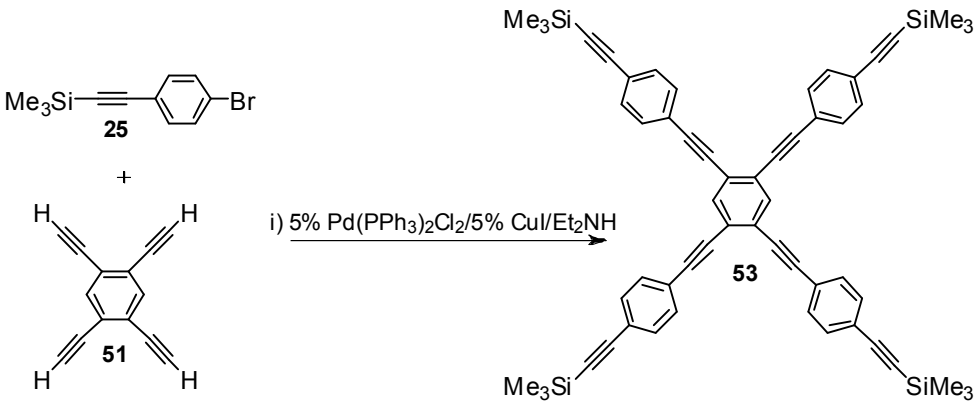

Scheme 29. First synthetic route used for the synthesis of 53.

However, it was found a higher yield could be obtained by using (4-iodo-phenylethynyl)trimethylsilane rather than the bromo derivative compound **25**. There are several different ways to synthesise (4-iodo-phenylethynyl)trimethylsilane, one of which is by conversion of the (4-bromo-phenylethynyl)trimethylsilane[69] or 4-(trimethylsilylethynyl)aniline [164] into (4-iodo-phenylethynyl)trimethylsilane **54**.

Synthesis of 4-(trimethylsilylethynyl)aniline in a 60% yield proved to be straightforward, following literature procedures.[165] With a few adjustments to a literature preparation the conversion of 4-(trimethylsilylethynyl)aniline to (4-iodo-phenylethynyl) trimethylsilane **54** in a 58% yield was achieved as shown in Scheme 30.[164]

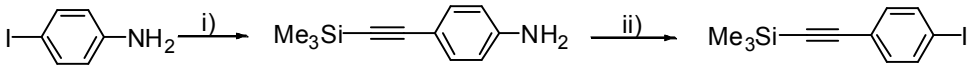

Scheme 30. Conversion of 4-(trimethylsilylethynyl)aniline to (4-iodo-phenylethynyl)trimethylsilane 54. i) 0.5% $Pd(PPh_3)_2Cl_2$, 1% CuI, 1.1 eq. H-C≡C-$SiMe_3$, Et_3N ii) HCl, 0°C, 1.2 eq. $NaNO_2$, 45 min. iii) 1.6 eq. aq. KI, DCM, 4 h, RT.

Synthesis of **53** could then be carried out using (4-iodo-phenylethynyl)trimethylsilane **54** as shown in Scheme 31 and lead to an increase of the yield to 57% from 13% using **25**. However deprotection of **53** also proved to be challenging; following the deprotection conditions used by Dixneuf *et al.*[95] which was an excess of NaOH in THF/MeOH. Unfortunately this produced a large amount of highly insoluble solid which was impossible to characterise and only a yield of 14% for the desired product **53**.

A second attempt at deprotection using Bu_4NF as a deprotecting group was made as it was hoped a milder reagent may provide a better yield of product. Use of Bu_4NF improved the yield of **52** to 42% but still produced a significant amount of insoluble material. The best deprotecting reagent was found to be K_2CO_3 giving a 57% yield of **53**, although in all cases an unidentified insoluble material was produced as a side product.

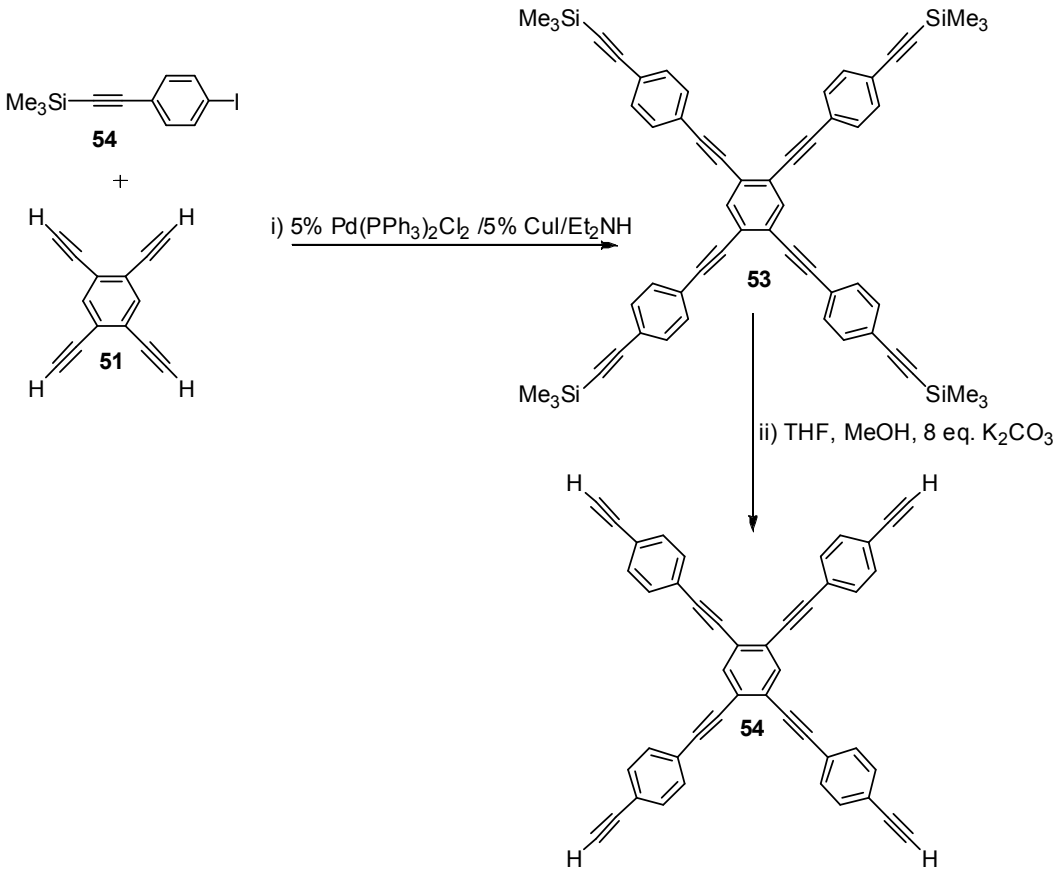

Scheme 31. Reaction scheme for the synthesis of 1,2,4,5-*tetrakis*-(trimethylsilylethynyl-phenylethynyl)-benzene 53 and 1,2,4,5-*tetrakis*(4-ethynyl-phenylethynyl)-benzene 54.

Dixneuf *et al*. attached the $\{Ru(dppe)_2Cl\}$ fragment as described in 2.3.1 which was very successful for the synthesis of **40** and these conditions were used again with ligand **54**. Isolation and ^{31}P NMR spectroscopy of the intermediate of the reaction of **54** with 4 equivalents of $[Ru(dppe)_2Cl]OTf$ revealed two triplets due to $[Ru(dppe)_2Cl]OTf$ and a singlet at 36.8 ppm consistent with a vinylidiene complex as shown in Scheme 32.

However, the protonation step using NEt_3 seemed to result in complications as the solid obtained had 7 different ^{31}P signals which could not be purified despite washing and recrystallisation.

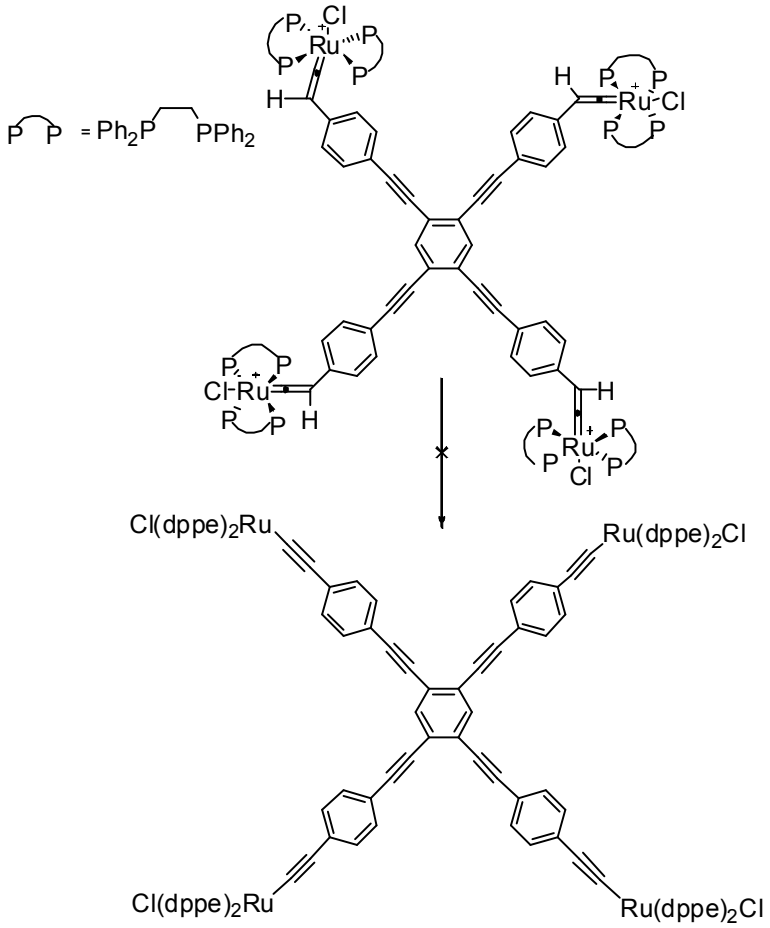

Scheme 32. Proposed conversion of the intermediate into the desired product.

Touchard *et al.*[166] have synthesised a series of $\{Ru(dppe)_2Cl\}$ compounds featuring a bound NH_3 and acetylene groups. These were obtained by the reaction of a *bis*acetylene $\{Ru(dppe)_2Cl\}$ compound with NH_4PF_6 in CH_2Cl_2, it is possible that a similar reaction could occur in the deprotonation step of the vinylidiene intermediate shown in Scheme 32. Touchard *et al.*[88] have full characterisation data for a series of their compounds and have obtained some molecular structures from single crystal X-ray diffraction experiments of the ruthenium acetylene compounds with amine bound. ^{31}P NMR spectroscopy obtained by Touchard *et al.*[88] for a variety of different *trans*

{Ru(dppe)$_2$}(C≡C-R^1)(C≡C-R^2) and *trans*{(dppe)$_2$Ru(NH$_3$)}(C≡C-R^1) compounds found a singlet at 55-53 ppm due to the triphenylphosphine group, the exact position of the peak is dependant upon the nature of R^1 and R^2. Whilst the reaction mixture from the reaction of [Ru(dppe)$_2$Cl]OTf with **54** after the deprotonation step shows several peaks in the region of 53 ppm there is also a number of other larger peaks present. Whilst ^{31}P NMR spectroscopy suggests that the intermediate vinylidiene is produced the reaction mixture obtained after the deprotonation appears to be a very complex mixture.

3.2.2.4 Synthesis of 1,2,4,5-C$_6$H$_2$(C≡CAu(PPh$_3$))$_4$.

Due to the problems experienced with attaching four {CpRu(PPh$_3$)$_2$} and {Ru(dppe)$_2$Cl} groups to the [CbCoCp] and the benzene systems, it was decided to explore a wider range of metals. The formation of Au-C≡C bonds is well known in the literature and these kinds of Au(I) compounds have been found to have interesting properties such as luminescence. So whilst 1,2,4,5-C$_6$H$_2$(C≡CAu(PPh$_3$))$_4$ was thought to be unlikely to be suitable for MQCA materials it was hoped that it would be possible to obtain novel tetrametallic compounds and crystals suitable for single crystal X-ray experiments.

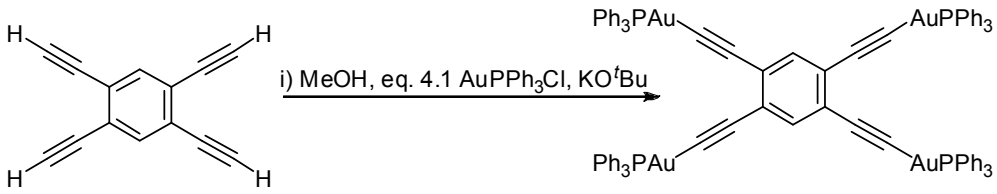

Scheme 33. Synthetic route used for the synthesis of 1,2,4,5-C$_6$H$_2$(C≡CAu(PPh$_3$))$_4$.

Tetraethynylbenzene, triphenylphosphine gold chloride and potassium *tert*-butoxide were refluxed in dry MeOH for 6 h as shown in Scheme 33. The slight excess of triphenylphosphine gold chloride was removed by recrystallisation in DCM/hexane, yielding a beige powder. ^{31}P NMR spectroscopy shows a single peak at 43.3 ppm which is consistent with other gold acetylene compounds known, studies have shown that the position of this peak shifts very little with variation in the acetylene group.[107,104] However 1,2,4,5-C$_6$H$_2$(C≡CAu(PPh$_3$))$_4$ was found to be not very stable and decomposed

over time. It is also difficult to characterise as ^{1}H NMR spectroscopy showed the aromatic region as a multiplet so it is not possible to compare integration ratios. Due to low solubility of the isolated product it was not possible to obtain a sample of suitable concentration for a ^{13}C NMR spectrum. It is common with Au(I) materials to exhibit aurophilic interactions which often results in products with low solubilities.[167]

The electrochemistry has been reported of a range of heterometallic compounds containing Au(I) centres. In all these systems the Au(I) centre is reported as exhibiting either no reversible electrochemistry or no electrochemistry within the solvent window.[98-101]

3.2.2.5 Synthesis of platinum acetylene compounds.

As with the gold systems, tetra platinum systems were examined to investigate the steric limitations of tetraethynylbenzene and also in an attempt to obtain novel tetra metallic systems.

Leininger *et al.*[110] reported the synthesis of 1,3,5-[*trans*-$I(Et_3P)_2PtC{\equiv}C]_3C_6H_3$ and 1,2,4,5-[*trans*-$I(Et_3P)_2PtC{\equiv}C]_4C_6H_2$ with yields of 56% and 44% respectively. The synthetic route used by Leininger *et al.* for 1,2,4,5-[*trans*-$I(Et_3P)_2PtC{\equiv}C]_4C_6H_2$ is shown in Scheme 34. Leininger *et al.* used three equivalents of $Pt(PEt_3)_2I_2$ per acetylene site for the synthesis of their materials. The reaction is reported to occur at room temperature in 3 h and the majority of the $Pt(PEt_3)_2I_2$ was reported to be able to be recovered.

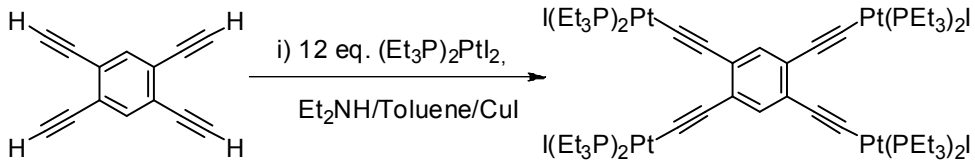

Scheme 34. Synthetic route used by Leininger *et al.*[110] for 1,2,4,5-[*trans*-$I(Et_3P)_2PtC{\equiv}C]_4C_6H_2$.

An attempt to synthesise 1,2,4,5-[*trans*-Cl(Bu_3P)$_2$PtC≡C]$_4C_6H_2$ was made using the less reactive (Bu_3P)$_2PtCl_2$ but leaving the reaction for 24 h. However the desired product could not be isolated, and alternatives conditions and reagents were investigated.

After the success of synthesising [*tetrakis*(*bis*-triethylphosphine)phenyl platinum(ethynylphenyl)cyclobutadiene] cyclopentadienyl cobalt **42** the same reaction conditions were used with tetraethynylbenzene. However it is believed that only a small amount of the Pt(PEt_3)$_2$PhCl reacted. The ^{31}P NMR spectra shows the formation of two new peaks in equal intensity with Pt satellites at 11.07 ppm with $^1J_{PtP}$ = 2658.9 Hz and 8.76 ppm with $^1J_{PtP}$ = 2718 Hz. These two peaks could be due to the incomplete formation of the tetrametallic product potentially leading to the *mono*-, *di*- or *tris*-products. In the IR spectra of the mixture a new signal is observed at 2108.0 cm^{-1} as well as the free acetylene C≡C at 2092.0 cm^{-1} which could be due to a small amount of C≡C-Pt present in the mixture.

Whilst it is very likely with adjustments of the conditions and reagent ratios that it would be possible to obtain the desired 1,2,4,5-[Ph(Et_3P)$_2$PtC≡C]$_4C_6H_2$ however due to the unsuitability of the Pt(II) centre for MQCA materials it was decided to concentrate on other parts of the work.

3.2.2.6 Pyridine based diad and tetrad systems.

As an alternative to forming M-C bonds it was decided to investigate M←N bonds by synthesising a range of pyridine-based ligands. It has been shown that pyridine- based ligands can also form extended networks by coordination to metal nitrates,[168] so these ligands could be of interest to MQCA applications as well as metal array formation.

Pyridine based ligands such as 1,4-*bis*(4'-pyridylethynyl)benzene[168] and 1,4-*bis*(4-pyridyl)butadiyne[169] have been found to form extended arrays by coordination with metal nitrates such as cadmium, cobalt and copper. A variety of different 1-D, 2-D and

3-D structures can be obtained depending upon the metal nitrate, on some occasions two different molecular structures were obtained from the same reaction mixture.[169]

The reaction of 1,4-*bis*(4'-pyridylethynyl)benzene with cadmium nitrate in a 1:1 ratio has been reported[168] to produce a structure formed from a series of layers. The pyridyl ring and the benzene rings are twisted relative to each other in 1,4-*bis*(4'-pyridylethynyl)benzene which leads to non-linear chains forming squares as shown in Figure 71a). The ligand orientation also alternates in these squares to form layers stacked in an ABAB manner which form the structure shown in Figure 71b). Variation of the ratio of the cadmium nitrate to ligand still resulted in the same interpenetrated material being obtained which are shown in Figure 71.

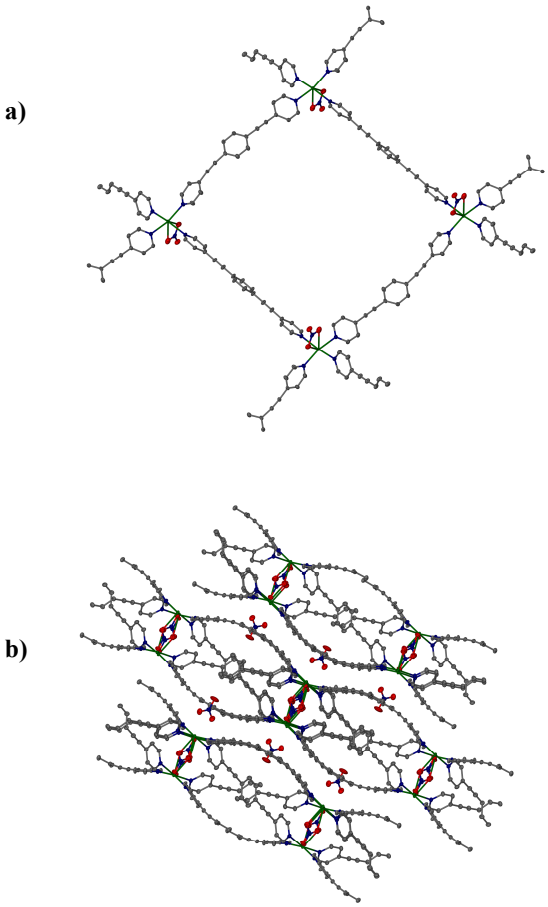

Figure 71. Structure a) of the squares and b) the extended structure formed from the reaction of 1,4-*bis*(4'-pyridylethynyl)benzene with cadmium nitrate in a 1:1.

Whilst the structure in Figure 71 has cavities these cavities are not suitable for applications such as gas storage due to the way the layers interpenetrate each other filling the cavities. Variation of the length of the ligand has been shown to affect the nature of the structure,[169] hence it was thought that the reaction of metal nitrates with a ligand with four bonding sites such as (*tetrakis*(4-pyridylethynyl)benzene) could produce an array with larger cavities.

Amoroso *et al*. [170] have prepared a large variety of *di*-, *tri*- and *tetra*-nucleating pyridyl ligands to which they have then attached {Tp*Mo(NO)Cl}[Tp* = hydro*tris*(3,5-*di*methylpyrazolyl)borate]. The electrochemistry of Mo_4(*tetrakis*(4-pyridylethynyl)benzene) where Mo = {Tp*Mo(NO)Cl} showed two well resolved one electron reversible reductions with redox separations of 240 mV, followed by two overlapping reversible reductions.[170] Bosch *et al*. also report the reaction of 1,2,4,5-*tetrakis*(2-pyridylethynyl)benzene with silver nitrate to form a silver complex.[171] Alkoxy-bridged molecular cubes have also been described by Manimaran *et al*., these cubes are [172] formed by the self-assembly of 1,2,4,5-*tetrakis*(4-pyridylethynyl)benzene and $Re_2(CO)_{10}$ in ROH , which form the structure shown in Figure 72.

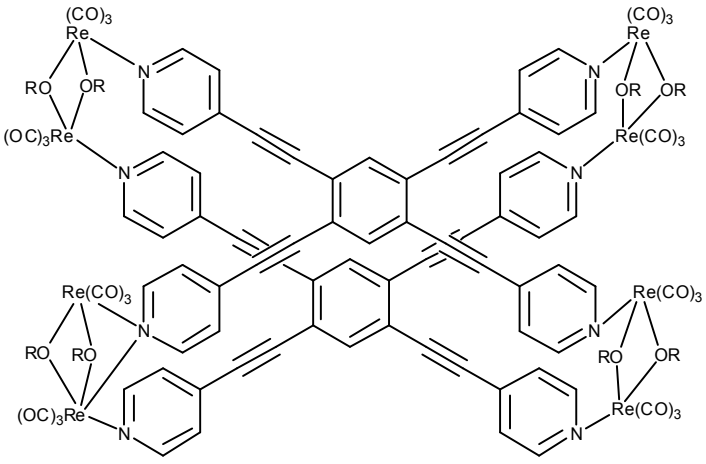

Figure 72. Structure of alkoxy-bridged molecular cubes formed from 1,2,4,5-*tetrakis*(4-pyridylethynyl)benzene and $Re_2(CO)_{10}$ in ROH. Where R =C_8H_{17}, $C_{12}H_{25}$ and C_7H_7.

All the reports of an attachment of metal fragments with ligands such as 1,2,4,5-*tetrakis*(pyridylethynyl)benzene suggested that this type of ligand would be a good multi-purpose ligand. It was hoped that it may be possible to either form extended networks or to form materials suitable for MQCA using pyridine-based ligands. A range of ligands with the pyridyl group in the 2,3 and 4 positions were prepared from literature preparations along with 1,2,4,5-*tetrakis*(cyanoethynyl)benzene and 1,2,4,5-*tetrakis*(pyrimidylethynyl)benzene by adaption of similar ligands.[173]

There are two different synthetic approaches available for the synthesis of 1,2,4,5-*tetrakis*(pyridylethynyl)benzene, these are shown in Scheme 35. The first approach has been published by Bosch *et al.*[171] whilst the second approach is reported by Amoroso *et al*.[170]

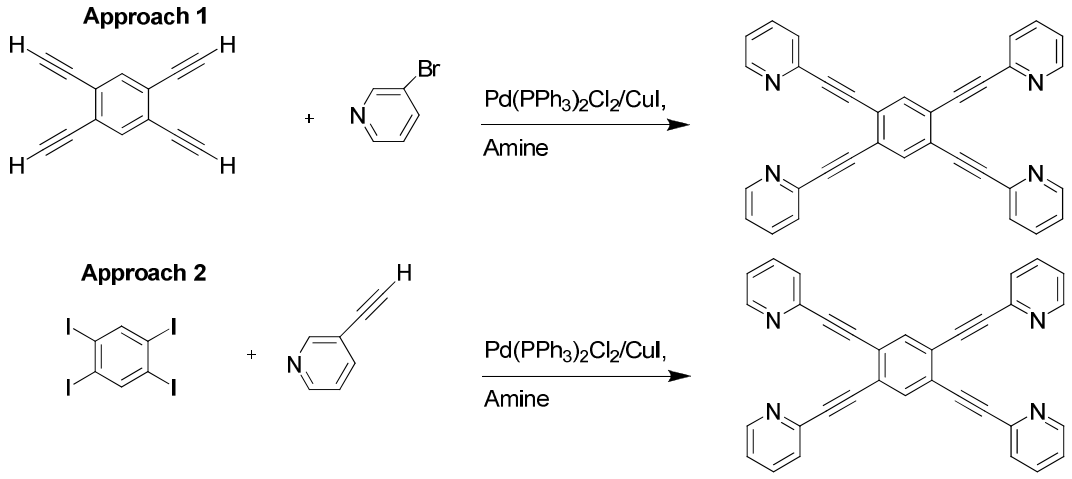

Scheme 35. The two synthetic routes available for the synthesis of 1,2,4,5-*tetrakis*(pyridylethynyl)benzene.

Attempts to prepare the ligand systems *via* both routes were attempted during this work and it was found that approach 1 was the best as it was easier to separate any excess tetraethynylbenzene from the desired product than tetraiodobenzene.

1,2,4,5-*tetrakis*(cyanoethynyl)benzene and 1,2,4,5-*tetrakis*(pyrimidylethynyl) were synthesised by following the synthesis used for *hexakis*(4-pyridylethynyl)benzene and

hexakis(5-pyrimidylethynyl)benzene.[173] Unfortunately 1,2,4,5-*tetrakis*(cyanoethynyl) benzene was too insoluble for complete characterisation to be performed.

Layering experiments between a range of metal nitrates and 1,2,4,5-*tetrakis*(pyridylethynyl)benzene or *hexakis*(5-pyrimidylethynyl)benzene resulted in the immediate formation of a microcrystalline solid. This solid proved to be insoluble and hence it was not possible to characterise it. In order to allow the two solutions to diffuse more slowly, two small vials each containing one of the ligands and a metal nitrate were placed in larger vial and the vial was filled with solvent. A variety of different solvents were tried, unfortunately over several weeks only very small amounts of solid were obtained from these vials and none of these solids were soluble or suitable for X-ray diffraction experiments. It is likely that the material produced is polymeric which makes it very hard to characterise.

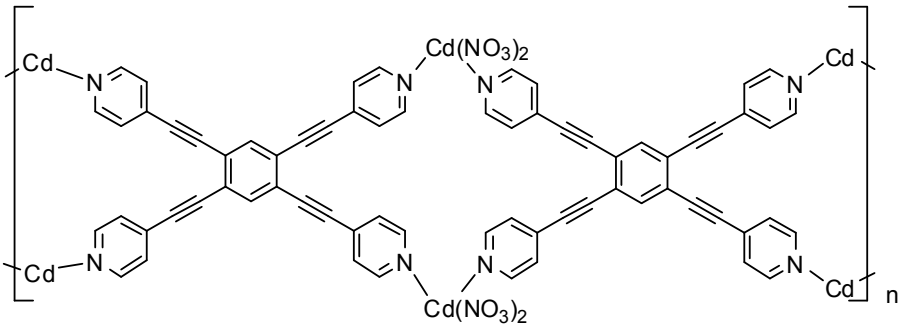

Figure 73. Possible structure formed by the reaction of 1,2,4,5-*tetrakis*(4-pyridylethynyl)benzene with Cadmium nitrate.

In an attempt to prepare materials suitable for MQCA applications the reaction of 1,2,4,5-*tetrakis*(3-pyridylethynyl)benzene with (*p*-cymene)ruthenium dichloride in DCM was carried out. Almost immediately a low solubility precipitate formed of which a ^{1}H NMR spectra was obtained suggesting that a small amount of ligand may have reacted. Due to low solubility it was not possible to obtain a more concentrated NMR sample and the reaction was abandoned.

3.3 Conclusions

This chapter has examined a series of arene based ligands to use as a linker between metal centres. Benzene based ligands were chosen as a linker between metal centres because it is known that 1,4-diethynylbenzene allows electronic communication between two metal centres. One of the main themes of this chapter is concerned with the attachment of metal fragments to 1,2,4,5-tetraethynylbenzene as this is the simplest symmetrical benzene ligand with an approximate four fold symmetry suitable for forming metal-acetylide compounds. 1,2,4,5-tetraethynylbenzene also contains all three *para*, *meta* and *ortho* relationships between the metal sites.

The work began by preparing three literature compounds based on 1,4-diethynylbenzene containing $\{Co_2(CO)_8\}$, $\{Ru(dppe)_2Cl\}$ and $\{CpFe(CO)_2\}$ to examine solubility and carry out a brief examination of the electrochemistry of the systems. From this work, two of metal fragments were ruled out for use in potential MQCA systems, the first metal fragment was $\{Co_2(CO)_8\}$ as it decomposed during electrochemical measurements. Systems containing $\{CpFe(CO)_2\}$ or $\{CpFe(dppe)\}$ were also excluded due to low solubility.

One compound of extreme interest was 1,2,4,5-*tetrakis*(ferrocenylethynyl)benzene due to the success of Fehlner *et al*. work with $\{(\eta^5\text{-}C_5H_5)Fe(\eta^5\text{-}C_5H_4\}_4(\eta^4\text{-}C_4)Co(\eta^5\text{-}C_5H_5)\}$ which suggests communication between all four ferrocene sites occurs. However, electrochemical measurements of 1,2,4,5-*tetrakis*(ferrocenylethynyl)benzene show no electronic communication between any of the ferrocene moieties.

After the success of preparing Au, Pt and Ru containing systems for the attachment to the [CpCoCb] system the same synthetic routes were applied to the 1,2,4,5-tetraethynylbenzene system. However this system proved to be more problematic, ^1H and ^{13}C NMR spectroscopy suggests that synthesis of $1,2,4,5\text{-}C_6H_2(C{\equiv}CAu(PPh_3))_4$ was successfully achieved but the compound was insufficiently soluble for a ^{13}C NMR spectra to be obtained and also decomposed over-time. The reaction of $Pt(Ph)PEt_3Cl$

and 1,2,4,5-tetraethynylbenzene did not go to completion and would require further work in order to find the correct reaction conditions. Attempts to attach a ruthenium fragment to 1,2,4,5-tetraethynylbenzene proved to be unsuccessful, which could be due to steric crowding.

This chapter has explored a wide range of different ligands and metal fragments, and several new molecular structures have been obtained. Whilst it is disappointing that 1,2,4,5-*tetrakis*(ferrocenylethynyl)benzene only has one redox wave, recent publications also found no electronic communication between tetrametallic sites in other compounds featuring a variety of metal fragments. These publications combined with this work suggests that electronic communication in tetrametallic compounds is very rare and that other strategies need to be developed to prepare materials which are suitable for MQCA applications.

4. Chapter 4: Porphyrins

4.1 Introduction

Initially it was thought that a porphyrin based compound could be suitable for MQCA applications because of the possibility of attaching four metals to the porphyrin framework and the delocalised nature of the porphyrin core.

There were two porphyrin systems that were believed to be candidates for MQCA applications; these are shown in Figure 74. The first porphyrin of interest **55** features four ferrocene rings directly attached to the porphyrin core and the second compound **56** has 4-pyridyl as the side chain which could potentially form a σ-bond to (*p*-cymene)ruthenium dichloride.

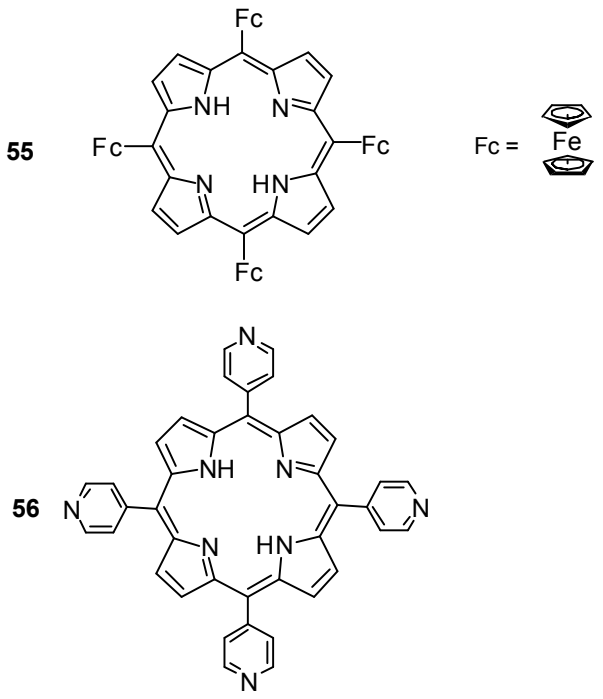

Figure 74. Two porphyrins that were of interest for potential MQCA materials.

Chronologically the work for this chapter was the first work to be carried out for this thesis but was discontinued due to later publications which suggest the oxidation of the ferrocene centres in **55** is observed as two 2 electron processes. The reaction of **56** with (*p*-cymene)ruthenium dichloride has been published as shown in Figure 75 has been

reported for potential anti-cancer applications but to our knowledge the electrochemistry has yet to be published. Solubility problems were encountered when our interest moved to the metalloporphyrin derivative of **56**, **56**.Zn and which lead to the discontinuation of this work**.**

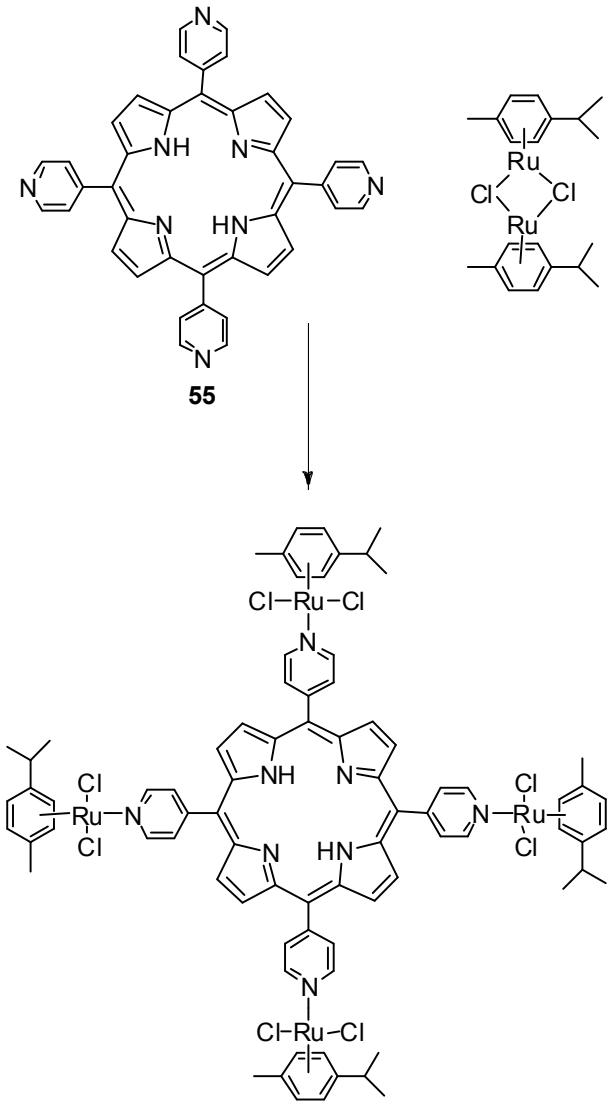

Figure 75. Proposed reaction of 55 and (*p*-cymene)ruthenium dichloride.

This chapter contains a brief discussion of the different synthetic routes used for porphyrin preparation. Following this there is an outline of the work carried out for this

thesis and a summary of the literature information that is known about the compounds of interest.

4.2 Applications and synthesis of porphyrins.

Porphyrins have proved to be highly versatile materials due to the ability to vary the side chains and have been proposed for molecular electronic functions such as switches.[174] Aromatic porphyrins and their related phthalocyanine macrocycles are well known for their use as photo-sensitisers in tumor therapy.[175,176]

Tetraphenylporphyrin was first synthesised in the 1930s by Rothemund and involved the heating of benzaldehyde and pyrrole in a sealed tube at 140°C for 24 h.[121] This however produced very low yields and was found to be largely unsuccessful for a large number of substituted benzaldehydes. This method was later modified by Alder and Longo to the reflux of benzaldehyde and pyrrole in propanoic acid for 30 minutes.[177] While this method is successful for the synthesis of some porphyrins, it produces a tar-like substance that can be very hard to purify if the desired product does not precipitate out of the reaction mixture. Also, for sensitive starting materials the harsh conditions were found to be unsuitable. In the 1980s Lindsey *et al*.[178] reported a new synthetic strategy for porphyrins which is now often referred to as the 'Lindsey protocol'. This method is based on Lindsey *et al*.[178] findings that at room temperature an equilibrium between the starting materials and an intermediate porphyrinogen is formed as shown in Scheme 36. Addition of an oxidant causes irreversible formation of the desired porphyrins in 30-40% which can be separated from the undesired products by column chromatography.

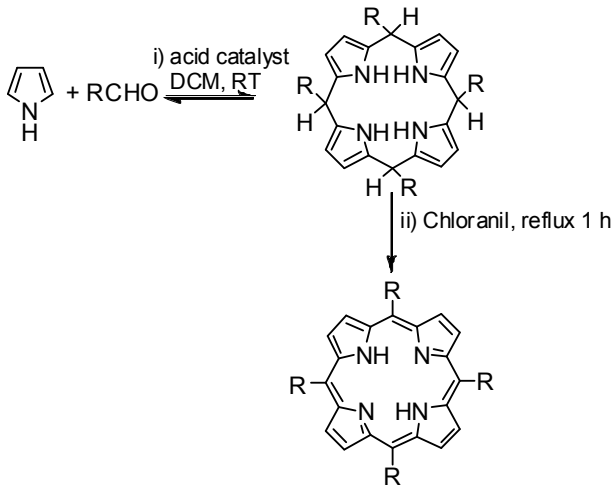

Scheme 36. Reaction scheme for the Lindsey protocol.[178]

Lindsey *et al.*[178] found that the reactant concentrations of 10^{-2} M provided optimal yields. Adaptations to this method over the years have lead to isolation of a wide variety of porphyrins.

4.2.1 Synthesis of 5,10,15,20-tetraferrocenylporphyrin (H_2TFCP) 55.

4.2.1.1 Reported synthetic routes.

The synthesis of 5,10,15,20-tetraferrocenylporphyrin **55** has been reported by various routes over the years. The first synthesis was reported by Wollmann *et al.*[179] in a 40% yield and was carried out as shown in Scheme 37.

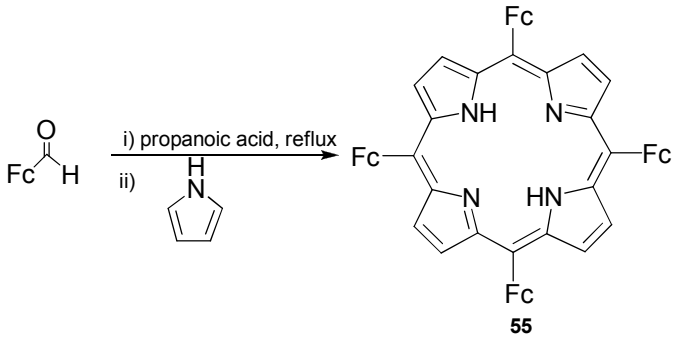

Scheme 37. Synthetic route used by Wollmann *et al.* for the synthesis of 55.

Wollmann *et al.*[179] reported that the product they obtained was a mixture of atropisomers due to the four different possible configurations (up/down) of the ferrocene

rings relative to the porphyrin ring. The ^{1}H NMR spectra was reported as showing broad multiplets where as singlets would be expected for a single atropisomer. The electrochemistry of **55** was also reported by Wollmann *et al*.[179] as a broad oxidation wave between 0.25 V to 1.05 V *vs.* SCE for the neutral compound. They investigated oxidising compound **55** and also the metalloporphyrin derivative **55.**Cu using either iodine or 4,5-Dichloro-3,6-dioxo-1,4-cyclohexadiene-1,2-dicarbonitrile (DDQ). Wollmann *et al*.[179] reported that **55** could be oxidised to $\mathbf{55}^{3+}$ but **55.**Cu could only be oxidised to [**55.**Cu]$^{2+}$. However, Wollmann *et al*.[179] could not produce the tetraoxidised form of either **55** or **55.**Cu which they speculated was due to decreased solubilities upon increased oxidation and metal complexation.

The isolation of **55** as a single atropisomer has since been reported[180] and also the synthesis of a nickel-*bis*(ferrocenyl)porphyrin that exhibits two well separated one electron redox waves.[181]

4.2.1.2 Synthesis of H_2TFCP 55.

H_2TFCP for this thesis was synthesised via the synthon *meso*-ferrocenyl dipyrromethane as shown in Scheme 38. This route was chosen because Narayanan *et al.*[180,182] suggested that by forming the synthon the orientation of the ferrocene ring is locked and they successfully used it to form a single atropisomer of H_2TFcP.

The synthesis of the intermediate *meso*-ferrocenyl dipyrromethane was carried out following the literature route as shown in Scheme 38 and gave the desired product in a 75% yield.[183]

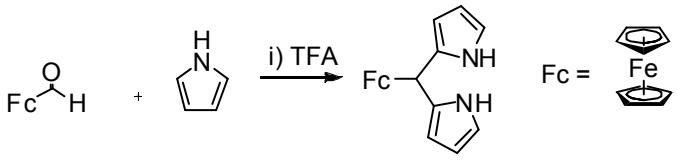

Scheme 38. Synthetic route for *meso*-ferrocenyl dipyrromethane.

The second step to synthesise **55** was carried out as shown in Scheme 39; but whilst ^{1}H NMR spectroscopy suggested that the desired product was present there was also still a significant amount of *meso*-ferrocenyl dipyrromethane remaining in the mixture.

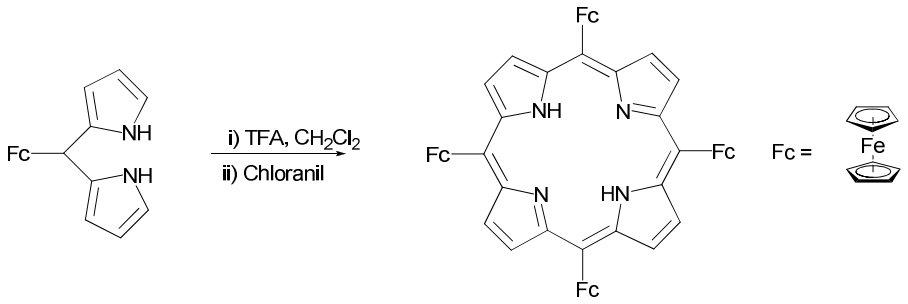

Scheme 39. Proposed synthesis of H_2TFcP 55.

Several other published routes for the synthesis of H_2TFcP were tried before the desired product could be isolated. The successful method used a 1:1 ratio of *meso*-ferrocenyl dipyrromethane and ferrocenecarboxaldehyde in DCM, in the presence of TFA as a catalyst. After stirring for 90 minutes at room temperature chloranil was added and the mixture was refluxed for a further 90 minutes. Column chromatography using ethyl acetate and DCM eluted a product in a 19% yield which had ^{1}H and ^{13}C NMR spectra consistent with those previous reported for H_2TFcP.[182] Crystals suitable for single crystal X-Ray diffraction experiments were obtained from slow diffusion of MeOH into a solution of DCM and a molecular structure was obtained as shown in Figure 76.

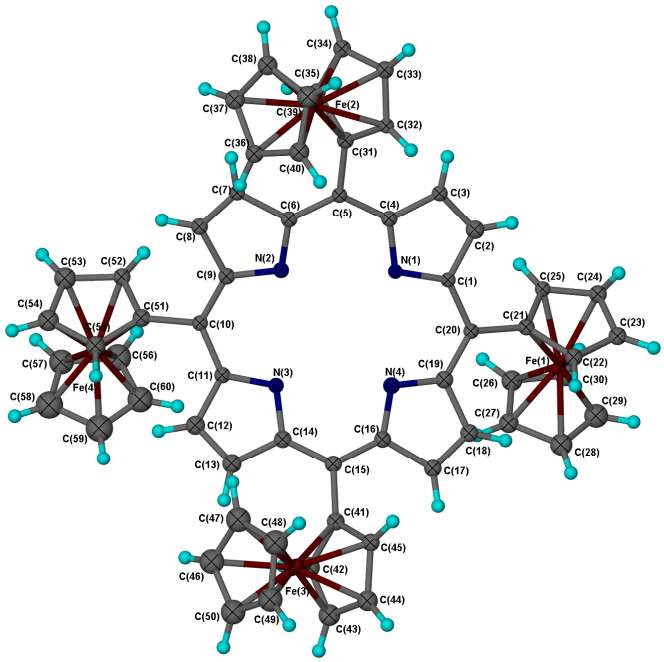

Figure 76. Molecular structure of H_2TFcP. Ellipsoids are shown at 50%.[***]

From the molecular structure shown in Figure 76 it is known that the porphyrin ring is not planar this is likely to be due to the steric bulk of the ferrocene moieties. This is a common feature in porphyrin and corrole compounds and is often referred to as having a saddle type distortion.[184] There are however many porphyrin based materials which feature metals bound in the centre of the porphyrin ring and their molecular structures suggest a planar porphyrin ring.[184, 185] Therefore it was hoped that by binding a metal into the centre of H_2TFcP that the porphyrin ring would become more planar which may improve electronic communication through the ring.

Formation of the metalloporphyrin derivatives, Zn.**55** and Ni.**55** was carried out following the method by Venkatraman *et al.*[182] as shown in Scheme 40. Comparison of the ^{1}H NMR spectra of Zn.**55** and Ni.**55** with **55** showed the disappearance of the peak at -0.48 ppm due to the inner NH protons in **55** and a slight downfield shift in the *β*-CH protons upon metallation.

[***] The asymmetric unit consists of two independent molecules of H_2TFcP and three molecules of DCM, one molecule of H_2TFcP and the solvent molecules have been omitted in Figure 76 for clarity.

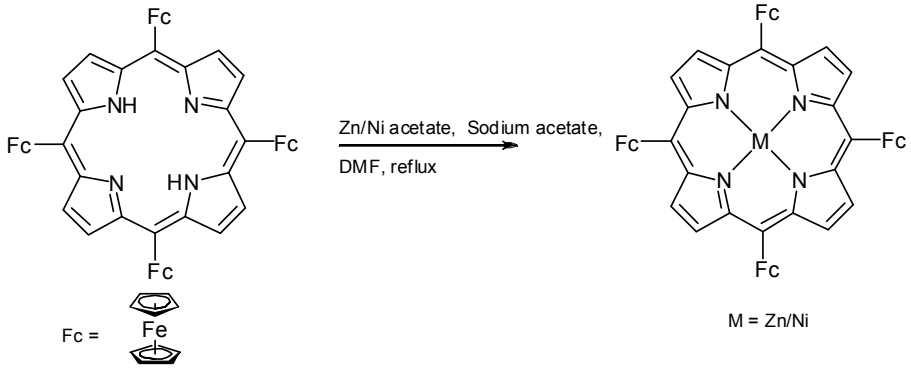

Scheme 40. Formation of the metalloporphyrin derivatives, Zn.55 and Ni.55.

Unfortunately it was not possible to obtain crystals suitable for single X-ray diffraction experiments with the metal bound inside the porphyrin ring.

4.2.2 Reported electrochemistry of H_2TFcP.

The electrochemistry of H_2TFcP has been reported several times but with different results. Venkatraman *et al*.[182] reported the porphyrin ring as exhibiting two quasi reversible oxidations which is typical of porphyrins. In addition to this two 2 electron oxidation waves were observed due to the inequivalence of the ferrocenyl moieties in the α,α and β,β positions. However Venkatraman *et al*.[182] observed that the ferrocenyl oxidation in **54** is very sensitive to factors such as supporting electrolyte, solvent and the scan rate, at faster scan rates only one oxidation wave was observed. Nemykin *et al*.[186] made a preliminary report that the electrochemistry in *o*-dichlorobenzene of **54**.Zn showed one reversible oxidation wave at 0.45 V followed by a second irreversible oxidation wave at a higher potential. Nemykin *et al*. also reported the reversible wave as being due to a three electron process which they assigned to be due to the oxidation of two ferrocene moieties but the third oxidation process to occur in the porphyrin ring.[186] Nemykin *et al*. reported the oxidation of **55**.Zn with tetracyanoethylene (TCE) but found that even when a large excess of TCE was added, that only two ferrocenyl moieties were oxidised.[186]

Recently a comprehensive study of **55** and 5,10-*bis*ferrocenyl-15,20-*bis*phenylporphyrin by Nemykin *et al.*[187] has provided a more in-depth study into the mixed-valence states

of ferrocenyl-porphyrins. They report both compounds undergo two reversible one-electron reduction processes which are due to the formation of the porphyrin anion and dianions. In addition to this **55** was found to undergo three further oxidation processes, the first two processes being two electron processes and the last one being a one electron process. Nemykin *et al.*[187] assigned the first two oxidations as being due to the oxidation of Fe^{2+} to Fe^{3+} and the second being a one electron process due to oxidation of the porphyrin ring. The corresponding reduction peak for the ferrocene groups was observed as one large sharp peak which is common in polyferrocenyl-containing phthalocyanines and due to an adsorption/desorption process on the electrode.[188] Nemykin *et al.*[187] propose that large reduction peak is due to the deposition of $\mathbf{55}^{4+}$ onto the electrode surface.

As with their preliminary report Nemykin *et al*. found that chemical oxidation of **55** using TCE oxidised only two Fe^{2+} centres to Fe^{3+} as observed by two doublets seen in the Mössbauer spectra even with a large excess of TCE.[187] It is known that the quadrupolar coupling for the ferrocene site measured by Mössbauer spectroscopy of *bis*-ferrocenyl containing compounds with prominent metal-metal coupling is lower for the *mono*-oxidised compound than in the neutral compound. This is believed to be due to electron donation from the ferrocene centre to the ferrocenium centre.[189,190] Nemykin *et al*. also observed the reduction of the quadrupolar coupling on going from the **55** to $\mathbf{55}^{2+}$ which could be due to the electron donation by the unoxidised ferrocene to the ferrocenium moiety. This observation combined with NMR spectra of $\mathbf{55}^{2+}$ shows that $\mathbf{55}^{2+}$ is formed rather than a mixture of **55** and $\mathbf{55}^{4+}$.

DFT calculations carried out by Nemykin *et al*. lead them to believe that the two oxidised ferrocenium centres are in the 5 and 10 positions i.e. *cis* rather than *trans*.[187, 191] The electrochemistry of the nickel complexed 5,15-*bis*(ferrocenyl)-2,8,12,18-tetrabutyl-3,7,13,17-tetramethylporphyrin was found by Boyd *et al*. to exhibit two one e-reversible redox waves. However 5,15-diferrocenyl-10,20-di-p-toylporphyrin shows no such coupling between the ferrocene centres.[181] It was proposed by Boyd *et al*.[181] that the coupling was observed when the *β*-pyrrolic positions have substituents attached and

no free rotation of the ferrocenes can occur.[181] Nemykin *et al*. propose that the coupling between ferrocene groups attached to porphyrin ring is dependant on distance not only on free rotation of the ferrocene groups.[187]

As Nemykin *et al*. have shown that the electrochemistry of **55** shows one two oxidation peaks and one reduction peak due to the four ferrocene centres; this suggests that this material would not be suitable for MQCA and hence the work here was discontinued.

4.2.3 Synthesis of 5,10,15,20-*tetra*-pyridin-4-yl-porphyrin.

As with **55**, the synthesis of 5,10,15,20-tetra-pyridin-4-yl-porphyrin (TPP) **56** has been reported previously by several different synthetic routes.

The synthesis of the synthon *meso*(4-pyridyl)dipyrrylmethane has been reported previously [192] but as a precursor to another porphyrin. The synthetic route shown in Scheme 41 was the first synthetic approach used for our work and whilst *meso*(4-pyridyl)dipyrrylmethane was produced and the ^{1}H and ^{13}C spectra were consistent with those reported [192] only a 20% yield was obtained.

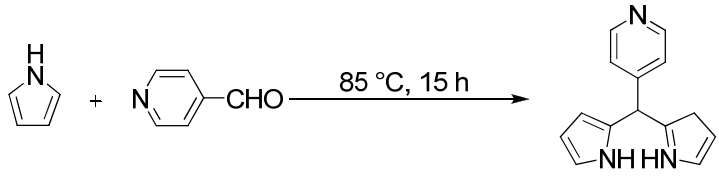

Scheme 41. Synthetic route for *meso*(4-pyridyl)dipyrrylmethane.

The next step tried is that shown in Scheme 42 based on the conditions used by Ruzié *et al*.[192] to synthesise a different porphyrin compound, however the ^{1}H NMR of the crude reaction mixture did not show any of the desired peaks and an alternative route was examined.

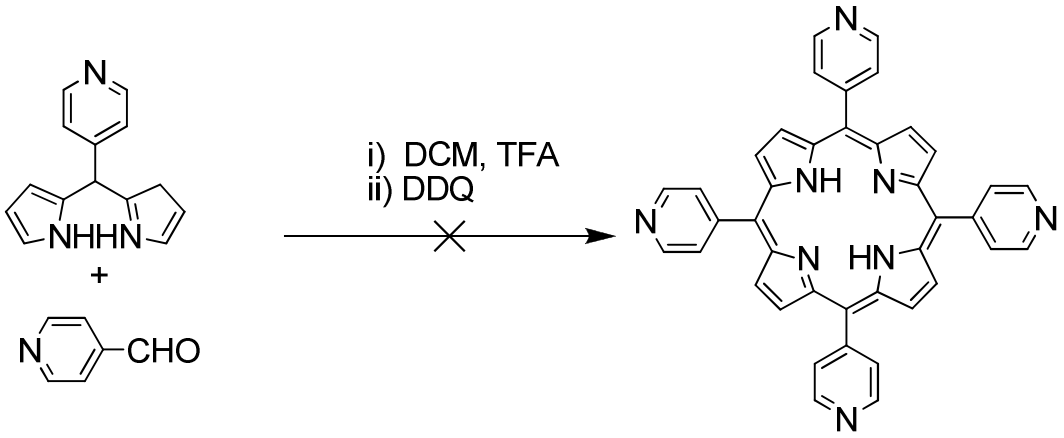

Scheme 42. Proposed synthetic route for TPP via *meso*(4-pyridyl)dipyrrylmethane.

Two papers published the synthesis of TPP via a one pot process as shown in Scheme 43. One route refluxed the pyrrole and pyridine-4-carboaxaldehdye in propanoic acid [193] whilst the other added a small amount of acetic acid to the propanoic acid.[194] By following the literature method using propanoic acid and acetic acid,[194] and purifying the crude mixture by column chromatography on alumina the desired material was obtained in a 4% yield.

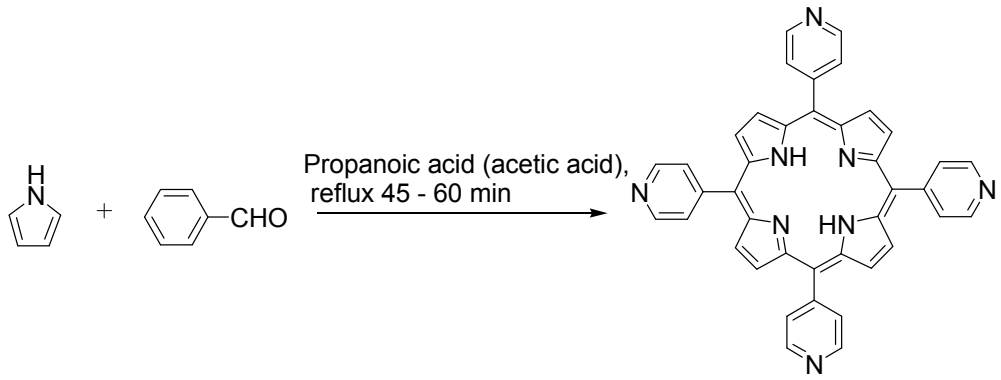

Scheme 43. Synthesis of TPP 56.

Crystals suitable for single crystal X-Ray diffraction experiments were obtained from slow diffusion of MeOH into a $CHCl_3$ solution and the molecular structure shown in Figure 77 was obtained. Bond lengths and angles obtained showed good agreement with those previously reported for 5,10,15,20-tetra-pyridin-4-yl-porphyrin *tris*(aceticacid) clathrate.[195]

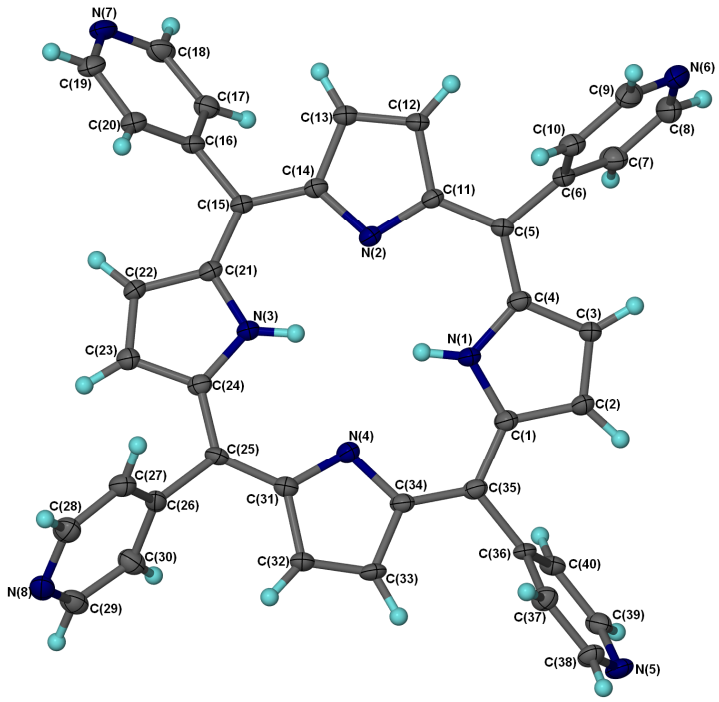

Figure 77. Molecular structure of TPP. Ellipsoids are shown at 50%.

Selected bond angles and lengths for 5,10,15,20-*tetra*-pyridin-4-yl-porphyrin are shown in Table 36.

N(1)-C(1)	1.367(4)	N(8)-C(29)	1.341(5)
N(2)-C(11)	1.379(4)	N(8)-C(28)	1.328(5)
N(2)-C(14)	1.366(4)	N(1)-C(1)	1.347(5)
N(3)-C(24)	1.370(4)	C(10)-C(6)-C(5)-C(11)	75.67(4)
N(3)-C(21)	1.365(4)	C(37)-C(36)-C(35)-C(34)	-68.02(4)
N(4)-C(34)	1.376(4)	C(20)-C(16)-C(15)-C(21)	54.29(4)
N(4)-C(31)	1.377(4)	C(27)-C(26)-C(25)-C(24)	-68.38(4)
N(5)-C(38)	1.379(4)	N(1)-C(1)-C(34)-N(4)	7.92(4)
N(5)-C(39)	1.340(5)	N(4)-C(31)-C(24)-N(3)	-9.37(4)
N(6)-C(9)	1.341(5)	N(3)-C(21)-C(14)-N(2)	8.07(4)
N(6)-C(8)	1.327(6)	N(2)-C(11)-C(4)-N(1)	-7.20(4)
N(7)-C(19)	1.336(6)		
N(7)-C(18)	1.331(5)		

Table 36. Selected bond lengths (Å) and angles (°) for 5,10,15,20-*tetra*-pyridin-4-yl-porphyrin.

As in compound **55**, the porphyrin ring is not planar which is clearer from the side view shown in Figure 78. The non-planar nature is also shown by the torsion angles shown

between the pyrrole groups such as N(1)-C(1)-C(34)-N(4) which show that all the angles range from -9.37(4) to -8.07(4) ° showing that the considerable distortion of the porphyrin ring. The torsion angles between the pyridyl rings and the porphyrin ring C(10)-C(6)-C(5)-C(11) to C(27)-C(26)-C(25)-C(24) show a range of -68.38(4) to 75.67° showing the propeller arrangement of the pyridyl rings.

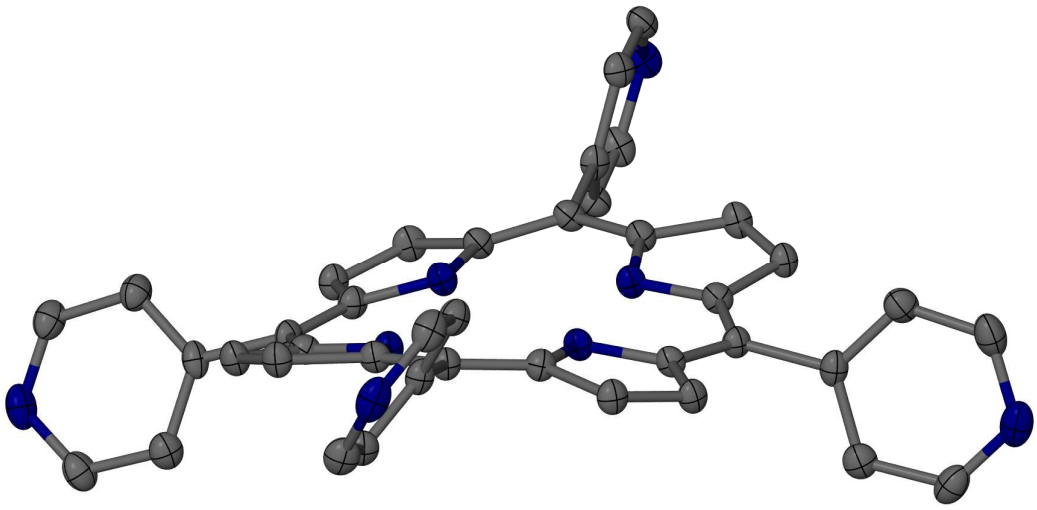

Figure 78. Side on view of TPP.

4.2.4 Metal complexation of TPP

Very recently the synthesis of $[Ru_4(\eta^6\text{-p-Pr}^iC_6H_4Me)_4(TPP)Cl_8]$ has been published by Schmitt *et al*.[196] which was carried out by refluxing (*p*-cymene) ruthenium dichloride and TPP in a 2:1 ratio in MeOH. Their interest in this material is for photodynamic therapy of cancer and the electrochemistry of this material is not reported.

Wang *et al*.[197] report the reaction with TPP with $[Cp^*IrS_2C_2(B_{10}H_{10})]$ by stirring at room temperature in DCM, these were the reaction conditions that were used for the work here to form $[Ru_4(\eta^6\text{-}p\text{-Pr}^iC_6H_4Me)_4(TPP)Cl_8]$. Excess (*p*-cymene) ruthenium dichloride was removed by washing the residue with toluene until the washings were colourless. The ^1H NMR spectra shows a shift upfield for all the signals due to the $Ru(\eta^6\text{-p-Pr}^iC_6H_4Me)Cl_2$ groups and also a shift for one of the signals due to the pyridyl groups suggesting that the $Ru(\eta^6\text{-p-Pr}^iC_6H_4Me)Cl_2$ has complexed to the pyridyl group.

Wang *et al.*[185] also report the reaction of 4 equivalents of [Cp*$IrS_2C_2(B_{10}H_{10})$] with Zn-TPP in THF at room temperature. However, when these conditions were used during our work for the reaction of (*p*-cymene) ruthenium dichloride and Zn-TPP in THF problems with solubility were encountered. Zn-TPP was found to be only slightly soluble in both THF and DCM and hence even in large quantities of solvent or refluxing the reaction mixture it was not possible to dissolve Zn-TPP. The solubility of Zn-TPP was tested in a range of solvents and was found to be highly insoluble in most of these; one possibility could be DMF.

4.3 Conclusions

Initially 5,10,15,20-*tetra*-ferrocenylporphyrin and metal fragments bound to the 5,10,15,20-*tetra*-pyridin-4-yl-porphyrin centre appeared to offer another way of arranging four metals in an approximate square structure.

However recent comprehensive studies by Nemykin *et al.*[187] have found that whilst the oxidisation of all four ferrocene moieties occurs electrochemically it does not occur as four separate oxidations. This is proposed by Nemykin *et al*. to be due to the different distances between the ferrocene moieties meaning that communication only occurs between two ferrocene centres.

A trial reaction of (*p*-cymene) ruthenium dichloride with TPP was carried out and the ^1H spectra indicated that the reaction occurs at room temperature. However, once a metal is bound into the centre of TPP the solubility dramatically decreases therefore to date it has not been possible to attach {Ru(*p*-cymene)Cl} to **55**.Zn. However even if it was possible to form the **55**.Zn[$Ru_4(\eta^6$-p-$Pr^iC_6H_4Me)_4Cl_8$] complex it seems likely that this would be high insoluble especially in its mixed-valence states, causing problems with electrochemistry. It also seems unlikely that four separate redox processes would be observed for the electrochemistry of **55**.Zn[$Ru_4(\eta^6$-p-$Pr^iC_6H_4Me)_4Cl_8$] even if there were no problems with solubility, due to the large distances between the metal centres.

5. Experimental for Chapters 1-4

5.1 General experimental

All air sensitive reactions were carried out under nitrogen or argon atmospheres using standard Schlenk line techniques. Dichloromethane, THF and MeOH were dried and degassed under an argon atmosphere over activated alumina columns using an Innovative Technology Solvent Purification System (SPS) and degassed using nitrogen or argon prior to use. All dry solvents were stored under argon or nitrogen in Young's flasks over 4 Å molecular sieves. Triethylamine, diethylamine and diisopropylamine were dried with KOH and then distilled under N_2 prior to use. Xylene and decalin were purified and distilled prior to use occurring to standard techniques.[198]

NMR spectra were recorded on Bruker AVANCE 250, Bruker AV300, AVANCE 400 or Bruker 500 spectrometers at 298 K, with the spectra referenced internally to the appropriate residual protio-solvent resonances.[199] Chemical shifts are reported in δ (ppm) and coupling constants in Hz. Assignments are supported by ^{13}C PENDANT NMR and homo- and hetero-nuclear, one- and two-dimensional experiments as appropriate.

IR spectra were recorded either as KBr discs or as a Nujol mull on a Nicolet-Nexus FTIR spectrometer in the range of 4000-400 cm^{-1} and averaged over 16 scans, and data is quoted in wavenumbers (cm^{-1}).

Electronic absorption spectra were recorded using a Perkin Elmer Lambda 650 UV-Vis Spectrometer. Samples were prepared in "Grade A" volumetric glassware and analysed in 1.0 cm path length quartz cells at 200 nm/min band pass rate. Values are quoted for Sample concentrations of 0.01 mmol unless otherwise stated.

Elemental analyses were carried out in house using an Exeter Analytical CE 440 elemental analyser.

X-ray Crystallography: The solid state molecular structures were obtained using a Nonium Kappa CCD diffractometer fitted with an area detector and Oxford Cryostream.

Unless otherwise stated chemicals were obtained commercially and used as received apart from CoCp(CO)2 which was purchased from Strem and distilled prior to use. Where it was necessary to alter the work-up or purification procedure to obtain satisfactory results or where characterisation of the materials was incomplete, full synthetic procedures and characterisation are reported here. The following compounds were synthesised following standard preparations 4-[2-(trimethylsilyl) ethynyl]benzonitrile,[200] 4-ethynylbenzonitrile,[200] 1,2-*bis*(4-cyanophenyl) ethyne,[81] *bis*(2-pyridyl)acetylene,[78] *bis*(3-pyridyl)acetylene,[78] *bis*(triphenylphosphine)palladium dichloride,[201] 4-trimethylsilylethynylaniline,[165] 1,2,4,5-tetraiodobenzene,[202] *trans*-$Ru(dppe)_2Cl_2$,[203] $[Ru(dppe)_2Cl]OTf$,[204] goldtriphenylphosphine chloride[205], *trans*-$[(Ph)(PEt_3)_2PtCl]$[206], 1,2,4,5-*tetrakis*-(2'-pyridylethynyl)benzene,[171] $FeCp(CO)_2I$,[139] $Cl(dppe)_2Ru\text{-}C{\equiv}CC_6H_4C{\equiv}C\text{-}Ru(dppe)Cl$ **45,** [87]*meso*-ferrocenyl dipyrromethane[183] and ruthenium(*p*-cymene)dichloride[207]**.**

The progress of all reactions was monitored using TLC (silica or alumina) and a suitable solvent system.

Electrochemistry for Chapter 2 and 3.

Electrochemistry was carried out using either dry degassed DCM or dichloroethane, with a 0.1 M NBu_4PF_6 supporting electrolyte. The electrochemistry cell was put under vacuum and then refilled with argon three times prior to use and was sealed under argon prior to electrochemical measurements taking place. The reference electrode used was a platinum wire, the counter electrode was a platinum electrode and the working electrode used is stated for each system. Each peak was calibrated using cobaltocenium hexafluorophosphate which had been calibrated to ferrocene, the peak potentials are quoted as the difference between the peak and the ferrocene/ferrocenium couple.

5.2 Experimental for Chapter 2

5.2.1 Calculations for Chapter 2

Calculations were performed using the Gaussian program suite.[65] The BP8 [208],[209]density functional was used with 'automatic' density fitting. For cobalt, the Stuttgart ECP and associated basis set was used.[210] The 6-31G(d) basis set was used for all other atoms.[211] Visualization of molecular orbitals was performed using the Molekel software package.

5.2.2 Synthesis for Chapter 2

Synthesis of (4-bromo-phenylethynyl)trimethylsilane 25.[69]

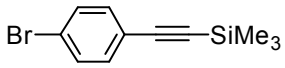

In a round bottomed flask 1-bromo-4-iodobenzene (19.88 g, 70.5 mmol), *bis*(triphenylphosphine)palladiumdichloride (1.23 g, 1.8 mmol) and copper iodide (0.67 g, 3.5 mmol) were combined and the flask was placed under an inert atmosphere. The flask was charged with diethylamine (150 ml) and trimethylsilylacetylene (9.9 ml, 70.1 mmol). The reaction was heated to reflux for 2 h and then stirred overnight at room temperature, by TLC (silica, hexane) the reaction was shown to be complete. The solvent was removed *in vacuo* to yield a crude brown which was washed with a saturated sodium bicarbonate solution and extracted with DCM.

The DCM was removed under pressure and the residue dissolved in hexane and filtered through silica yielding (4-bromo-phenylethynyl)trimethylsilane as a pale yellow solid.

Yield: 14.77 g, 58.3 mmol, 82.7%

^{1}H NMR (250.1 MHz, $CDCl_3$):
δ_H 0.24 (s, 9H, $Si(Me)_3$), 7.28-7.35 (m, 2H, C_6H_4) and 7.39-7.46 (m, 2H, C_6H_4).

$^{13}C\{^{1}H\}$ NMR (75.5 MHz, $CDCl_3$):

δ_C 0.0 ($Si(Me)_3$), 95.7, 103.7 (2C, C≡C), 122.2, 122.9 (2C, C_6H_4), 131.6 and 133.5 (4C, C_6H_4).

Synthesis of 1-bromo-4-ethynyl-benzene 26.[69]

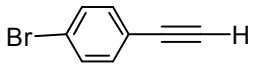

To a solution of (4-bromo-phenylethynyl)trimethylsilane **25** in THF/MeOH (50:50, 100ml, v/v) was added sodium hydroxide (4.66 g, 0.12 mol). The solution was stirred at room temperature for several hours and shown to complete by TLC (silica, hexane).

The solvent was removed and the residue washed with water and extracted into DCM. The organic layer was separated and dried with $MgSO_4$ and the solvent removed to yield pure 1-bromo-4-ethynyl-benzene **26** as a beige solid.

Yield: 9.09 g, 50.2 mmol, 86.1%

^{1}H NMR (250.1 MHz, $CDCl_3$):

δ_H 3.12 (s, 1H, C≡C-H), 7.31-7.39 (m, 2H, C_6H_4) and 7.43-7.50 (m, 2H, C_6H_4).

$^{13}C\{^{1}H\}$ NMR (75.5 MHz, $CDCl_3$):

δ_C 78.5, 82.7 (2C, C≡C) 121.2, 123.3 (2C, C_6H_4) 131.8 and 133.7 (4C, C_6H_4).

Synthesis of 4,4'-dibromotolane 27.[66]

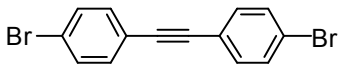

To a round bottomed flask 1-bromo-4-ethynyl-benzene **26** (8.97 g, 49.6 mmol), 1-bromo-4-iodobenzene (14.02 g, 49.6 mmol), *bis*(triphenylphosphine)palladium

dichloride (0.87 g, 1.2 mmol) and copper iodide (0.24 g, 1.2 mmol) were combined and the flask put under a N_2 atmosphere . The flask was charged with diethylamine (200 ml) and heated to reflux for 2 h and then left to stir overnight at room temperature.

The solvent was removed under reduced pressure and the residue was washed with a saturated sodium bicarbonate solution and extracted into DCM. The organic layer was acidified by adding 3M HCl until pH < 5 was achieved and then washed with ammonia solution (3 x 150 ml) followed by brine (1 x 150 ml). The organic layer was separated and dried with $MgSO_4$ and the solvent was removed under reduced pressure to yield the crude product as a brown solid. The crude product was purified by soxhlet extraction (hexane/DCM, 500 ml, 10:1 v/v) to yield a beige powder on removal of the solvent.

Yield: 12.05 g, 35.9 mmol, 72.3%.

^{1}H NMR ($CDCl_3$, 300.2 MHz):
δ_H 7.36-7.42 (m, 4H, C_6H_4) and 7.45-7.53 (m, 4H, C_6H_4).

$^{13}C\{^1H\}$ NMR ($CDCl_3$, 75.5 MHz):
δ_C 89.6 (2C, C≡C), 122.0, 122.9 (4C, C_6H_4), 131.8 and 133.1 (8C, C_6H_4).

Synthesis of 4-4'-*bis*-(trimethylsilyl)ethynyltolane 28.[72]

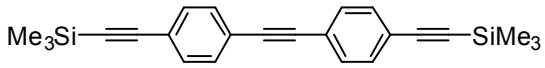

In a round bottom flask 4,4'-dibromotolane **27** (4.24 g, 12.6 mmol), *bis*(triphenylphosphine)palladiumdichloride (0.89 g, 1.3 mmol) and copper iodide (0.24 g, 1.3 mmol) were combined and the flask put under a N_2 atmosphere. The flask was charged with diethylamine (150 ml) and trimethylsilylacetylene (3.9 ml, 27.9 mmol) and the mixture heated to reflux for 8 h. The reaction was then cooled and the solvent removed under reduced pressure. The residue was dissolved in DCM and 3M HCl was added to the stirred solution until pH < 5 was reached. The organic layer was separated

and washed with conc. ammonia hydroxide (3 x 200 ml) followed by a final distilled water wash (1 x 200ml). After drying the organic layer ($MgSO_4$) the solvent was removed to yield an off white solid. The crude product was further purified by column chromatography (silica, hexane → hexane: DCM (1:2) v/v) and the solvent removed to yield the solid as an off white solid.

Yield: 2.58g, 7.0 mmol, 55.2%.

^{1}H NMR (250.1 MHz, $CDCl_3$):
δ_H 0.26 (s, 18H, $Si(CH_3)_3$) and 7.44 (s, 8H, Ph).

$^{13}C\{^1H\}$ NMR (75.5 MHz, $CDCl_3$):
δ_C 0.05 ($Si(CH_3)_3$, 6C), 91.0, 96.6, 104.7 (6C, C≡C), 123.1, 123.2 (4C, quaternary C_6H_4), 131.5 and 132.1 (8C, C_6H_4).

Synthesis of 4,4'-*bis*-(triisopropylsilyl)ethynyltolane 18.[66]

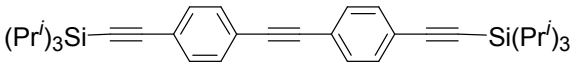

In a round bottom flask 1,4-dibromotolane **27** (5.33 g, 15.9 mmol), triphenylphosphine (0.84 g, 3.2 mmol), *bis*(triphenylphosphine)palladiumdichloride (1.14 g, 1.6 mmol) and copper iodide (0.63 g, 3.3 mmol) were combined and the flask put under a N_2 atmosphere. The flask was charged with triethylamine (200 ml) and toluene (80 ml) and heated to 50-60°C. After maintaining this temperature for ten minutes triisopropylsilylacetylene (7.8 ml, 34.9 mmol) was added dropwise and the temperature was increased to 90°C. After heating for 48 h the reaction was cooled, the solvent was removed under vacuum. The residue was dissolved in DCM (400ml) and HCl (6M) was added until a pH < 5 was achieved. The organic phase was isolated and washed with distilled water (2 x 200 ml) followed with a saturated ammonium chloride solution (2 x 200 ml) and a final distilled water wash (1 x 200 ml). The organic solution was then

dried ($MgSO_4$), and the solvent removed and the compound purified by column chromatography (silica, petroleum ether). The yellow oil obtained was recrystallised from ethanol to yield a white solid.

Yield: 4.95 g, 9.2 mmol, 61.7%.

^1H NMR (250.1 MHz, $CDCl_3$):
δ_H 1.14 (s, 42H, $SiCH(CH_3)_2$) and 7.46 (s, 8H, C_6H_4).

$^{13}C\{^1H\}$ NMR (75.5 MHz, $CDCl_3$):
δ_C 11.4 (6C, $\underline{C}H(CH_3)_2$), 18.8 (12C, $(\underline{C}H_3)_2CH$), 91.0, 93.1, 106.7 (6C, C≡C), 123, 123.7 (4C, C_6H_4 quaternary), 131.5 and 132.1 (8C, C_6H_4).

Synthesis of ethynylferrocene 30 *via* 2,2-dibromo-1-ferrocenyl ethylene 29.[75]

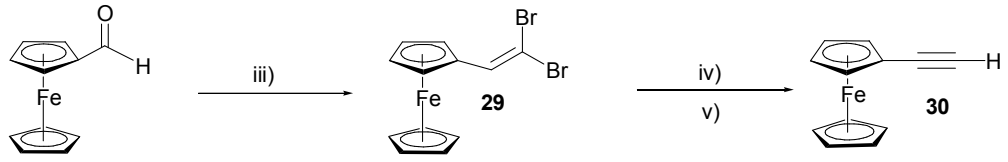

iii) CBr_4, PPh_3, Zn, DCM

iv) BuLi, THF, Et_2O
v) NH_4Cl (aq)

To a mixture of tetrabromomethane (16.61 g, 5.1 mol), triphenylphosphine (13.10 g, 5.0 mol) and zinc powder (3.30 g, 5.1 mol) under N_2 was added DCM (50 ml). After stirring the suspension at room temperature for 1.5 h, a solution of ferrocenecarboxaldehyde (5.32 g, 2.5 mol) in DCM (25 ml) was added dropwise. The deep red solution was stirred at room temperature for a further 4 h before the solvent was removed to yield a crude orange solid. The solid was purified by column chromatography (silica, hexane) to yield 2,2-dibromo-1-ferrocenyl ethylene **29** as an orange solid.

Yield: 6.38g, 17.3 mmol, 69.0%.

^{1}H NMR (250.1 MHz, $CDCl_3$):
δ_H 4.21 (s, 5H, C_5H_5), 4.31 (t, 2H, $^{3}J_{H-H}$ 1.9, C_5H_4) 4.68 (t, 2H, $^{3}J_{H-H}$ 1.9, C_5H_4) and 7.15 (s, 1H, C=C).

^{13}C{^{1}H} NMR (75.5 MHz, $CDCl_3$):
δ_C 69.2, 69.4 and 69.5 (9C, C_5H_5 and C_5H_4), 79.7 (1C, quaternary C, C_5H_4), 83.7 (1C, CH=$\underline{C}Br_2$) and 135.7 (1C, $\underline{C}H=CBr_2$).

To a solution of butyl lithium (2.5 M in hexane, 20 ml, 5.0 mol) in diethyl ether/THF (20 ml, 2:1 v/v) at -78 ˚C was added dropwise a solution of **29** (6.38 g, 17.3 mmol diethyl ether/THF, 50 ml, 2:1 v/v) under an N_2 atmosphere. The solution was stirred for 2 h at -78 ˚C and then allowed to warm to room temperature within 1 h. Stirring then continued at room temperature for a further 2 h. After cooling to -78˚C, a saturated aqueous ammonium chloride (10 ml) was added; the reaction was then allowed to warm to room temperature and stirred for a further 10 min. The mixture was then poured into a saturated ammonium chloride solution (20 ml) and the organic layer was removed from the flask. The aqueous layer was then extracted with hexane (1 x 20 ml) and the combined organic layers were dried over Na_2SO_4. Removal of the solvent under reduced pressure yielded pure ethynylferrocene.

Yield: 3.09 g, 14.7 mmol, 85.2%.

^{1}H NMR (250.1 MHz, $CDCl_3$):
δ_H 2.72 (s, 1H, C≡C), 4.20 (t, 2H, $^{3}J_{H-H}$ 1.9, Cp), 4.22 (s, 5H, Cp) and 4.46 (t, 2H, $^{3}J_{H-H}$ 2.0, Cp).

^{13}C{^{1}H} NMR (75.5 MHz, $CDCl_3$):
δ_C 64.0 (1C, C≡C), 68.9, 70.2,71.9, 73.7 (10C, C_5H_5 and C_5H_4) and 82.8 (1C, C≡C).

Synthesis of 4,4'-*bis*(2-ferrocenylethynyl)tolane 32. [76]

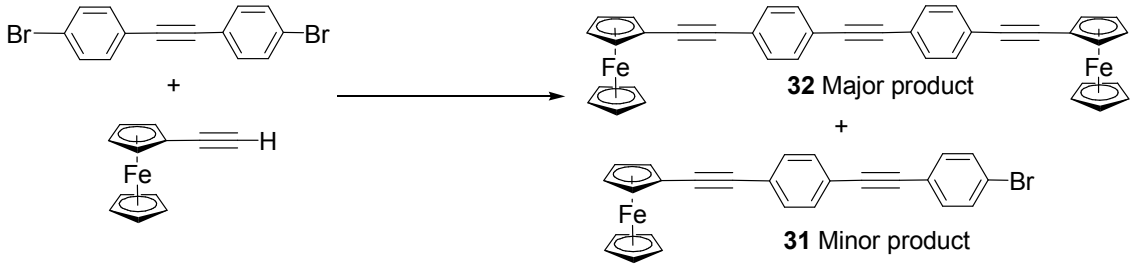

In a round bottom flask 4,4'-dibromotolane (1.6 g, 4.8 mmol), ethynylferrocene (2.01 g, 9.57 mmol), *bis*(triphenylphosphine)palladiumdichloride (0.55 g, 0.48 mmol) and copper iodide (0.09 g, 0.48 mmol) were combined and the flask put under a N_2 atmosphere. The flask was charged with THF (40 ml) and triethylamine (100 ml) and heated to reflux for 72 h. The reaction mixture was cooled to room temperature and the solvent was removed under reduced pressure. The residue was then extracted with DCM and washed with a saturated sodium bicarbonate solution (3 x 250 ml) followed by a saturated brine solution (1 x 250 ml). The organic layer was separated and dried ($MgSO_4$) and the solvent removed under reduced pressure. The product was further purified by column chromatography (silica, hexane/DCM (2:1 v/v)). The first product isolated from the column was 4-bromo-4'-(2-ferrocenylethynyl)tolane followed by the desired product .

4-bromo-4'-(2-ferrocenylethynyl)tolane 31.

^{1}H NMR (250.1 MHz, $CDCl_3$):

δ_H 4.26 (s, 7H, C_5H_5 and C_5H_4), 4.52 (s, 2H, C_5H_4), 7.28-7.40 (m, 4H, C_6H_4) and 7.44-7.54 (m, 4H,C_6H_4).

^{13}C{^{1}H} NMR PENDANT (74.3 MHz, $CDCl_3$,):

δ_C 69.3, 70.4, 71.7 (9C, C_5H_5 and C_5H_4), 83.2, 88.4, 90.8, 97.3 (4C, C≡C), 127.8, 128.4, 128.4 and 127.8 (12C, C_6H_4).

Not all quaternary C's observed due to slow relaxation time.

X-ray quality crystals were obtained from the column fraction.

4,4'-*bis*(2-ferrocenylethynyl)tolane 32.

Yield: 1.66 g, 2.8 mmol, 58.5%.

^{1}H NMR (250.1 MHz, $CDCl_3$):
δ_H 4.22-4.28 (m, 14H, C_5H_5 and C_5H_4), 4.51(t, 4H, $^{3}J_{H-H}$ 1.8, C_5H_4) and 7.46 (s, 8H, C_6H_4).

$^{13}C\{^{1}H\}$ NMR (75.5 MHz, $CDCl_3$):
δ_C 65.1, 69.2, 70.2, 71.6 (Cp), 85.7, 90.9 and 91.1 (6C, C≡C), 122.4 and 122.4 (4C, C_6H_4, quaternary), 131.5 and 131.6 (8C, C_6H_4).

X-Ray quality crystals were obtained from slow evaporation of a benzene solution.

Synthesis of *bis*(4-pyridyl)acetylene 34 via 1,2-dibromo-1,2-*bis*(4-pyridyl)ethane 33.[80]

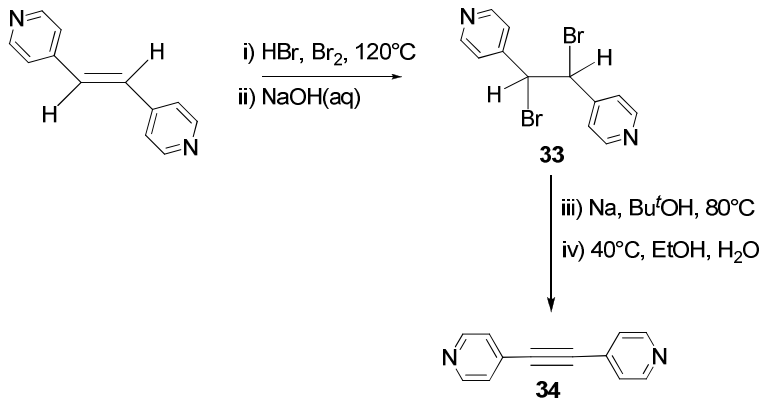

To a stirred solution of *trans*-1,2-*bis*(4-pyridyl)ethylene (7.13 g, 39.1 mmol) in conc. HBr (48%, 95 ml) at 0˚C was added dropwise Br_2 (8 ml, 24.95g, 156.1 mmol). The mixture was then heated to 120˚C and held at this temperature for 2 h before cooling to

room temperature. Standing at -5°C resulted in formation of an orange precipitate which was isolated by filtration and washed with water and then stirred in aqueous NaOH (2M, 240 ml) for 30 min. The resulting white solid, 1,2-dibromo-1,2-bis(4-pyridyl)ethane **33** was isolated by filtration and washed thoroughly with water and dried under vacuum overnight.

1,2-dibromo-1,2-bis(4-pyridyl)ethane **33**
Yield: 8.01 g, 23.5 mmol, 60.1%.

^{1}H NMR ($CDCl_3$, 250.1 MHz):
δ_H 5.28 (s, 2H, CH), 7.41 (d, 4H, $^{3}J_{H\text{-}H}$ 6.0, pyridyl) and 8.74 (br s, 4H, pyridyl).

To a flask containing ^{t}BuOH (240 ml) was added sodium pieces (2.4 g, 10.4 mol), the flask was heated under N_2 at 80 ˚C overnight to allow dissolution to occur. In portions **33** (8.01 g, 23.5 mmol) was added to the sodium butoxide solution and heated at 80˚C for 4 h. After cooling to 40˚C, EtOH (40 ml) was added followed by water (40 ml). The solution was extracted with $CHCl_3$ until the organic layers were colourless, the combined organic layers were dried (Na_2SO_4) and the solvent removed to yield a pale yellow solid **34**.

bis(4-pyridyl)acetylene **34**
Yield 4.09 g, 22.7 mmol, 58.0%.

^{1}H NMR (250.1 MHz, $CDCl_3$,):
δ_H 7.38-7.44 (m, 4H, pyridyl) and 8.60-8.71(m, 4H, pyridyl).

^{13}C{^{1}H} NMR (75.5 MHz, $CDCl_3$):
δ_C 90.8 (2C, C≡C), 125.7 (4C, pyridyl), 130.4 (2C, quaternary) and 150.1 (4C, pyridyl).

Synthesis of [*tetrakis*(4-bromophenyl)cyclobutadiene]cyclopentadienyl cobalt 11. [67]

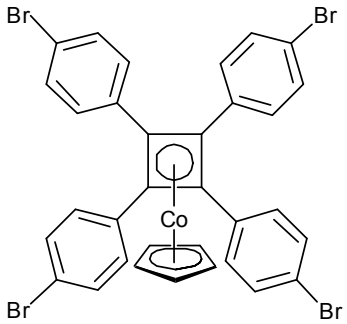

To a solution of 4,4-dibromotolane **27** (2.73 g, 8.1 mmol) in xylene (75 ml) was added a solution of $CpCo(CO)_2$ (1.02 g, 5.7 mmol) in xylene (15 ml) under N_2. The solution was then refluxed in the absence of light for 24 h before the solvent was removed by rotary evaporation. The residue was then dissolved in toluene and filtered through celite to yield a yellow-brown solution. The toluene solution was then flash filtered though a short silica column yielding crude product. The crude product was further purified by column chromatography on silica; elution with hexane removed starting material. The product was then extracted using hexane/DCM (3:1 v/v) removal of the solvent under reduced pressure yielded as a yellow solid. The product was further purified using preparative TLC (silica, hexane/DCM 3:1 v/v).

X-ray quality crystals were obtained from slow evaporation of benzene.

Yield: 0.72 g, 0.9 mmol, 12.1%.

^{1}H NMR ($CDCl_3$, 250.1 MHz):
δ_H 4.60 (s, 5H, Cp), 7.21-7.28 (m, 8H, C_6H_4) and 7.30-7.38 (m, 8H, C_6H_4).

$^{13}C\{^1H\}$ NMR ($CDCl_3$, 300.2 MHz):
δ_C 73.8 (Cb, 4C), 83.5 (Cp, 5C), 120.5, 130.3, 131.6 and 134.9 (24C, C_6H_4).

Synthesis of [*tetrakis*(4-pyridyl)cyclobutadiene]cyclopentadienyl cobalt 15 and [*tetrakis*(4-pyridyl)cyclopentadienone]cyclopentadienyl cobalt 16.[67]

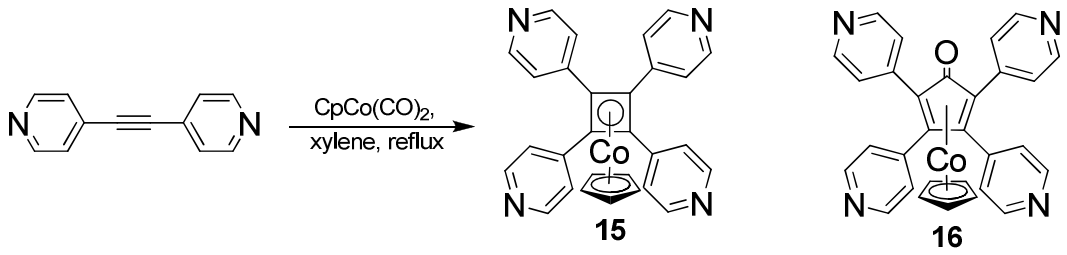

To a solution of *bis*(4-pyridyl)acetylene **34** (4.86 g, 27.0 mmol) in xylene (230 ml) was added dropwise a solution of $CpCo(CO)_2$ (2.47 g, 13.7 mmol) in xylene (10 ml). The solution was heated to reflux for 24 h in the absence of light before being cooled to room temperature and the solvent removed. The residue was washed with acetone/ pentane (10 ml, 1:1 v/v) and then the two products were separated using column chromatography on silica. Elution with $CHCl_3$ /EtOH (4:1) allowed the isolation of both **15** and **16** sequentially. [*Tetrakis*(4-pyridyl)cyclopentadienone]cyclopentadienyl cobalt was purified further by column chromatography using chloroform/ethanol (85:15 v/v) to yield [*tetrakis*(4-pyridyl)cyclobutadiene]cyclopentadienyl cobalt as a red solid.

[*Tetrakis*(4-pyridyl)cyclobutadiene]cyclopentadienyl cobalt **15**

Yield: 0.12 g, 0.2 mmol, 1.7%.

^{1}H NMR (250.1 MHz, $CDCl_3$):
δ_H 4.71 (s, 5H, Cp), 7.22-7.32 (m, 8H, pyridyl) and 8.46-8.58 (m, 8H, pyridyl).

$^{13}C\{^1H\}$ NMR (75.5 MHz, $CDCl_3$):
δ_C 73.2 (4C,Cb), 84.2 (5C, Cp), 123.0, 143.9 and 150.1 (20C, pyridyl).

[*Tetrakis*(4-pyridyl)cyclopentadienone]cyclopentadienyl cobalt **16**

Yield: 1.88 g, 3.66 mmol, 27%.

^{1}H NMR (250.1 MHz, $CDCl_3$):
δ_H 5.04 (s, 5H, Cp), 7.05 (d, 4H, $^{3}J_{H-H}$ 6.0, pyridyl), 7.50 (d, 4H, $^{3}J_{H-H}$ 6.1, pyridyl) and 8.48-8.60 (m, 8H, pyridyl).

$^{13}C\{^{1}H\}$ NMR (75.5 MHz, CD_3OD):
78.5 (quaternary C cyclopentadienone) 88.1 (Cp, 5H) and 93.2 (quaternary C cyclopentadienone), 126.7, 128.2 (8C, pyridyl), 142.0, 143.0 (4C, quaternary pyridyl), 150.1 and 150.4(8C, pyridyl).

No CO cyclopentadienone signal observed

Elemental Analysis: $C_{30}CoOH_{21}N_4.1/8(CHCl_3)$ Result % (calculated %): C = 68.6 (68.62), H = 4.26 (4.04) and N = 10.7 (10.63).

Synthesis of [*tetra*-(-4-trimethylsilylethynyl)phenylcyclobutadiene] cyclopentadienyl cobalt 35 and [tetra-(4-trimethylsilylethynyl)phenyl cyclopentadienone]cyclopentadienyl)cobalt 36.

To solution of 1.74 g of **28** in decalin (60 ml) was added $CpCo(CO)_2$ (0.47 g, 2.6 mmol) and heated at 160˚ C for 24 h. The solvent was removed under reduced pressure and the crude product was purified by column chromatography (silica, hexane/DCM (95:5 v/v) to remove **35** and the solvent system was then changed to DCM/EtOH (4:1 v/v) to remove **36**.

[*tetra*-(-4-trimethylsilylethynyl)phenylcyclobutadiene]cyclopentadienyl cobalt **35**

Yield: 1.14 g, 1.3 mmol, 37.6%.

^{1}H NMR (300.2 MHz, $CDCl_2$):
δ_H 0.24-0.28 (m, 36H, $Si(CH_3)_3$), 4.60, 4.62, 4.77 (s, 5H, Cp) and 7.24-7.42 (m, 16H, C_6H_4).

$^{13}C\{^{1}H\}$ NMR - PENDANT (75.5 MHz, CD_2Cl_2)

δ_C 0.18, 1.30, 1.60 ($Si(CH_3)_3$), 75.2 (C≡C), 81.7, 82.7, 83.8, 83.9 (Cp), 95.0, 95.3, 105.7, 105.8, 105.9 (C≡C), 121.3,121.5 (quaternary C), 129.9, 103.0, 131.0, 131.8, 132.0, 132.1 (C_6H_4) and 137.3 (quaternary C).

[*tetra*-(4-trimethylsilylethynyl)phenylcyclopentadienone]cyclopentadienyl cobalt **36**

Yield: 0.20 g, 0.22 mmol, 6.2%.

^{1}H NMR (300.2 MHz, CD_2Cl_2):

δ_H 0.22-0.28 (m, 36H, $Si(CH_3)_3$), 4.85-4.88 (m, 5H, Cp) , 7.02-7.08 (m, 4H, C_6H_4), 7.22-7.28 (m, 4H, C_6H_4), 7.29-7.36 (m, 4H, C_6H_4) and 7.50-7.58 (m, 4H, C_6H_4).

$^{13}C\{^{1}H\}$ NMR PENDANT (75.5 MHz, CD_2Cl_2):

δ_C 0.10, 0.16, 0.20 ($Si(CH_3)_3$, 81.7, 82.7, 83.8, 86.1 (C_5H_5), 93.2, 95.5, 96.3, 104.8, 105.6, 108.7 (C≡C), 122.4, 123.4 (quaternary C_6H_4), 128.4, 128.5, 129.0, 129.2, 130.0, 131.0, 131.8, 132.0, 132.1, 132.3 (C_6H_4), 133.2 and 134.2 (quaternary C_6H_4).

Synthesis of [tetra-(-4-triisopropylsilylethynyl)phenylcyclobutadiene] cyclopentadienylcobalt 22 and [tetra-(4-triisopropylsilylethynyl) phenylcyclopentadienone] cyclopentadienyl)cobalt 37.[66]

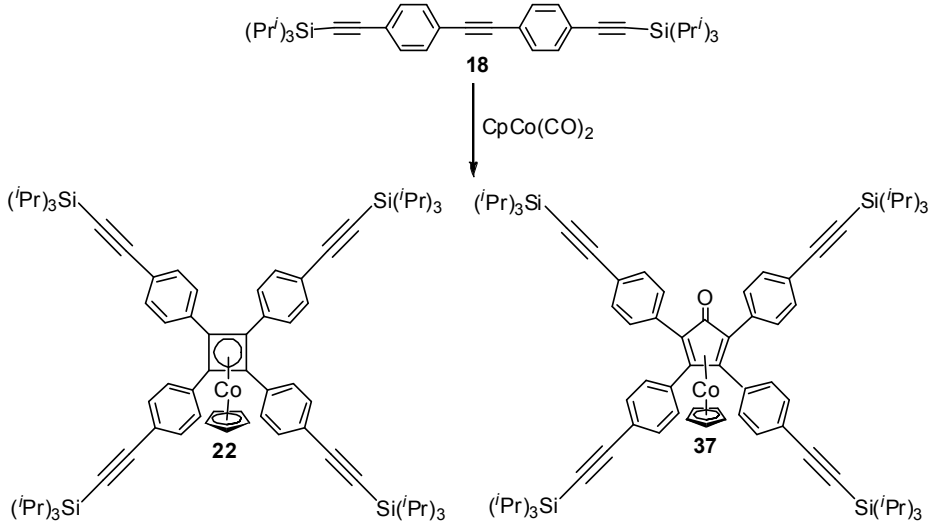

A solution of 4,4'-*bis*-(triisopropylsilyl)ethynyltolane **18** (3.39 g, 6.3 mmol) in decalin (40 ml) was heated to 140°C under N_2, $CpCo(CO)_2$ (0.65 g, 3.6 mmol) was then added dropwise to the solution. The temperature was then increased to 160°C and maintained for 6 h after which the decalin was removed under vacuum. The solid was purified by column chromatography (silica, hexane/DCM 95:5) to yield an off white solid as the first product **22**. The second product [*tetra*-(4-triisopropylsilylethynyl) phenylcyclopentadienone]cyclopentadienyl cobalt **37** was isolated from the column with DCM/EtOH (4:1 v/v). Purification of **22** was carried out by recrystallisation from diethyl ether/ ethanol.

[*tetra*-(-4-triisopropylsilylethynyl)phenylcyclobutadiene]cyclopentadienyl cobalt **22**

Yield 2.38 g, 2.0 mmol, 63.0%.

^{1}H NMR (250.1 MHz, $CDCl_3$):
δ_H 1.14 (s, 84 H, $SiCH(CH_2)_3$), 4.55 (s, 5H, Cp) and 7.32 (s, 16H, C_6H_4).

$^{13}C\{^1H\}$ NMR (75.5 MHz, $CDCl_3$):
δ_c 11.5 ($Si(\underline{C}H(CH_3)_3$), 18.8 ($Si(CH(\underline{C}H_3)_3$), 74.7 (Cb), 83.6 ($C_5H_5$), 91.4 (C≡C), 107.4 (C≡C), 120.1(4C, quaternary C_6H_4), 128.6(8C, C_6H_4), 131.9(8C, C_6H_4) and 136.6 (4C, quaternary C_6H_4).

IR(nujol): ν(C≡C) 2150.1, 1600.3 (aromatic) and 1508.7 (aromatic) cm^{-1}.

M.p.: decomposes 160°C.

[*tetra*-(4-triisopropylsilylethynyl)phenylcyclopentadienone]cyclopentadienyl cobalt **37**

Yield: 0.52 g, 0.43 mmol, 12.6%.

^{1}H NMR (300.2 MHz, CD_2Cl_2):
δ_H 1.12-1.16 (m, 84H, $(CH_3)_2CH$), 4.86 (s, 5H, C_5H_5), 7.06-7.14 (m, 4H, C_6H_4), 7.26-7.40(m, 8H, C_6H_4) and 7.52-7.58 (m, 4H, C_6H_4).

^{13}C{^{1}H }NMR-PENDANT (75.5 MHz, CD_2Cl_2):
δ_C 11.8 (apparent d, 4C, $\underline{C}H(CH_3)_2$), 19.0 (apparent d, 8C, $CH(\underline{C}H_3)_2$), 78.0, (2C quaternary cyclopentadienone,) 86.1 (5C, C_5H_5), 91.9, 92.7, 93.1, 98.9, 107.0, 107.7 (10C, C≡C and cyclopentadienone) 122.6 (2C, quaternary C_6H_4), 123.6 (2C, quaternary C_6H_4), 130.9, 131.9, 132.1, 132.3 (16C, C_6H_4), 133.1 (2C, quaternary C_6H_4) and 134.0 (2C, quaternary).

No CO cyclopentadienone signal observed.

IR(nujol): ν(C≡C) 2154.4, 1580.4 (C=O), 1508.0 (aromatic) cm^{-1}

M.p.: decomposes 232°C.

Synthesis of [*tetra*-(-4-ethynyl)phenylcyclobutadiene]cyclopentadienyl cobalt 38.[66]

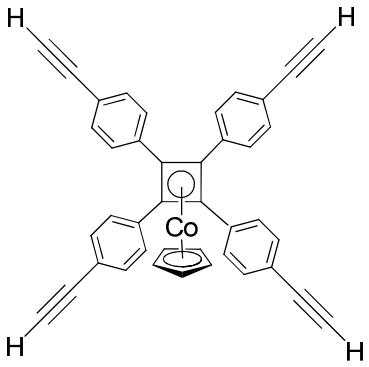

To a stirred solution of **22** in THF (50 ml) was added tetrabutylammonium fluoride (7.5 mmol, 1M in THF, 7.5 ml). The solution was stirred at room temperature overnight after which the solvent was removed. The residue was dissolved in DCM and washed with distilled water (2 x 20 ml), followed by 6 M hydrochloric acid (2 x 20 ml) and then a final wash with distilled water (1 x 20 ml). After drying ($MgSO_4$) the solution was filtered through a silica plug (hexane: DCM, 50:50 v/v) to yield the desired product.

Yield: 0.46 g, 0.8 mmol, 67.7%.

^{1}H NMR (250.1 MHz, $CDCl_3$):
δ_H 3.15 (s, 4H, C≡C), 4.60 (s, 5H, Cp) and 7.35 (s, 16H, C_6H_4).

$^{13}C\{^1H\}$ NMR (75.5 MHz, $CDCl_3$):
δ_C 74.6 (4C, Cb), 77.8 (C≡C-H), 83.6 (Cp), 84.0(Ar-C≡C), 120.1(quaternary C, adjacent to C≡C), 128.7 (Ar-H), 132.1 (Ar-H next to C≡C-H) and 137.0 (quaternary C adjacent to Cb).

Crystals suitable for X-ray diffraction were obtained by slow evaporation of chloroform/acetonitrile.

Elemental Analysis: $C_{41}CoH_{25}(CH_3Cl)_{0.5}$ Result % (calculated %): C = 82.2 (82.4), H = 4.73 (4.46).

M.p.: decomposes before melting

Synthesis of [*tetra*-(4-ethynyl)phenylcyclopentadienone]cyclopentadienyl cobalt 39.

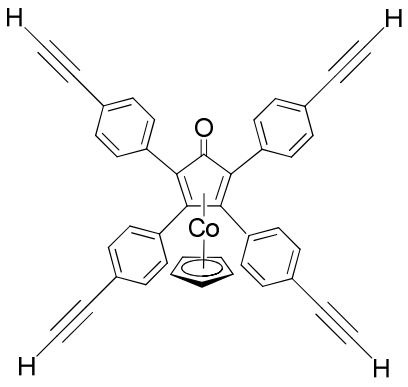

To a stirred solution of **37** (0.35 g, 0.29 mmol) in THF (20 ml) was added tetrabutylammonium fluoride (2.3 mmol, 1M in THF, 2.3 ml). The solution was stirred at room temperature overnight after which the solvent was removed. The residue was dissolved in DCM and washed with distilled water (2 x 20 ml), followed by 6 M hydrochloric acid (2 x 20 ml) and then a final wash with distilled water (1 x 20 ml). After drying ($MgSO_4$) the solution was removed under reduced pressure and recrystallisation in DCM/hexane yielded crystals suitable for X-ray diffraction.

Yield: 0.11 g, 0.19 mmol, 64%.

^{1}H NMR (250.1 MHz, $CDCl_2$):
δ_H 3.19 (2 overlapping s, 4H), 4.89 (s, 5H, Cp), 7.09 (apparent d, 4H,C_6H_4, $^3J_{H-H}$ 8.4), 7.31 (apparent d, 4H, C_6H_4, $^3J_{H-H}$ 8.4), 7.37 (apparent d, 4H, C_6H_4, $^3J_{H-H}$ 8.5) and 7.55 (apparent d, C_6H_4, 4H, $^3J_{H-H}$ 8.5).

$^{13}C\{^1H\}$ NMR (75.2 MHz, $CDCl_2$):
δ_C 77.9, 78.2, 78.8, 83.5, 84.1 (9C, C≡C and cyclopentadienone), 86.1 (5C, Cp), 91.8, 93.1 (4C, C≡C), 121.5, 122.4 (4C, quaternary, C_6H_4), 131.0, 132.1, 132.3, 132.4 (16C, C_6H_4), 133.5 and 134.5 (4C, quaternary, C_6H_4).

Elemental Analysis: $C_{41}CoOH_{25}.1/3C_4H_8O$ Result % (calculated %): C = 82.8 (82.7), H = 4.64 (4.44).

M.p.: decomposes before melting

UV-Vis absorption: λ_{max} = 299 nm, ε = 64,102 $M^{-1}cm^{-1}$.

Synthesis of [*tetrakis*((Ru(dppe)$_2$Cl)ethynylphenyl)cyclobutadiene] cyclopentadienyl cobalt 40.

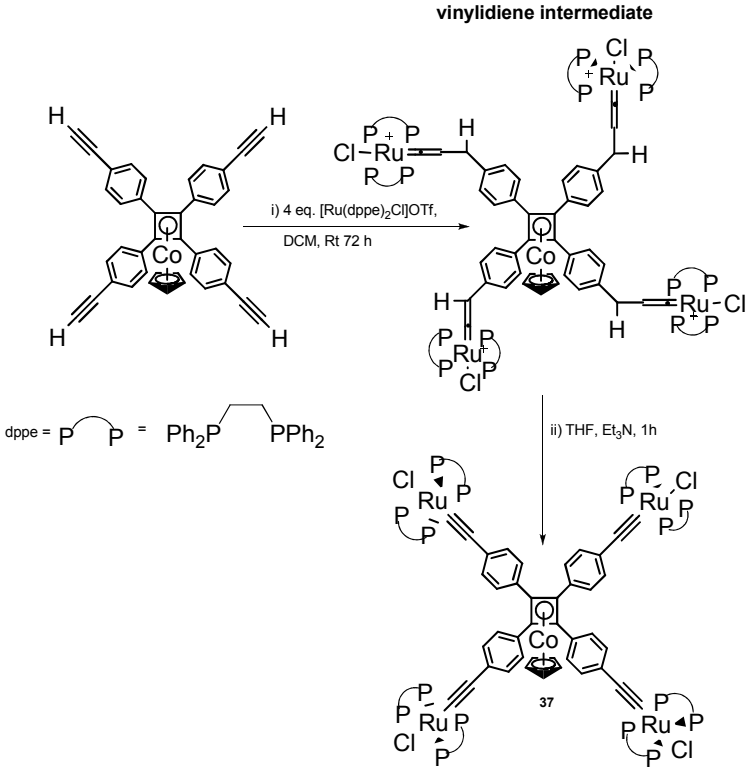

To an oven dried Schlenk was added [Ru(dppe)$_2$Cl]OTf (1.77 g, 1.7 mmol) and **38** (0.24 g, 0.4 mmol). The flask was placed under an inert atmosphere and then charged with DCM (60 ml) and stirred for 72 h. The solvent was then removed under reduced pressure and washed with diethyl ether (20 ml) followed by a mixture of hexane/DCM (25ml 4:1 v/v).

Vinylidiene intermediate

$^{31}P\{^{1}H\}$ NMR (121.5 MHz, $CDCl_3$):

δ_P 38.90

The crude product was then suspended in THF (100 ml) and Et_3N (2 ml) was added under an inert atmosphere. The suspension was stirred for 1 h at room temperature slowly becoming an orange-yellow solution. The solvent was then removed under

reduced pressure and the residue dissolved in DCM (50 ml) and washed with distilled water. The organic layer was then separated and dried and the solvent was removed under reduced pressure to yield a yellow powder. The crude product was recrystallised from DCM/hexane.

Yield: 1.34 g, 0.3 mmol, 73.6%.

$^{31}P\{^{1}H\}$ NMR (121.5 MHz, CD_2Cl_2,):
δ_P 49.91

^{1}H NMR (400.1 MHz, CD_2Cl_2):
δ_H 2.73 (br s, 32H, Et), 4.70 (5H, Cp) and 6.90-7.60 (m, 176 H, C_6H_5 and C_6H_4).

$^{13}C\{^{1}H\}$ NMR (125.8 MHz, CD_2Cl_2):

δ_C 31.3 (m, 4C, CH_2), 75.5 (4C, Cb), 83.5 (5C, Cp), 114.8 (4C, C≡C-C_6H_4), 127.7 (d, meta-C_6H_5, $^{3}J_{C-P}$=33.6), 128.6 (8C, C_6H_4), 128.8 (4C, quaternary C_6H_4) 129.5 (d, *para*-C_6H_5, $^{4}J_{C-P}$=15.1), 130.1 (8C, C_6H_4), 131.8 (4C, C≡C-Ru), 134.9 (d, ortho-C_6H_5, $^{2}J_{C-P}$= 48.6), 136.5 (4C, C_6H_4, quaternary) and 137.4 (m, C_6H_5 quaternary).

IR(nujol): ν (C-H) 3005.7, (C≡C) 2065.2, (aromatic) 1595.7 and 1502.4 cm^{-1}.

Elemental Analysis: $C_{249}H_{213}CoRu_4Cl_4P_{16}$ Result % (calculated %): C = 69.15 (69.45), H = 5.00(4.99).

M.p.: decomposes 223°C

UV-Vis absorption: λ_{max} = 378.5 nm, ε = 78,992 $M^{-1}cm^{-1}$ and λ_{max} = 252.5 nm, ε = 167, 662 $M^{-1}cm^{-1}$.

Synthesis of *tetrakis*(triphenylphosphinegoldethynylphenyl)cyclobutadiene cyclopentadienyl cobalt 41.

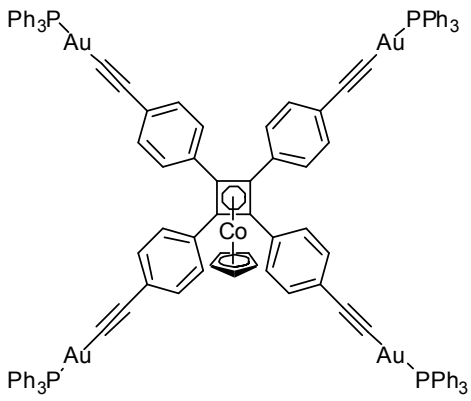

To a Youngs tube was added **38** (28 mg, 0.05 mmol) and triphenylphosphinegold chloride (98.9 mg, 0.2 mmol) and the tube was placed under an inert atmosphere. A solution of potassium *tert*-butoxide was added (1.9 mmol in 40 ml MeOH) and the tube was sealed under vacuum and heated to reflux for 7 h, and then stirred at room temperature overnight. The solvent was then removed *in vacuo* and the solid was dissolved in DCM and washed with distilled water (3 x 50 ml), dried (Na_2SO_4) and the solvent removed under reduced pressure to yield a yellow solid.

Yield: 21.9 mg, 0.0091 mmol, 18%.

$^{31}P\{^1H\}$ NMR (121.5 MHz, $CDCl_3$):
δ_P 43.60

^1H NMR (400.1 MHz, CD_2Cl_2):
δ_H 4.60 (s, 5H, C_5H_5), 7.24 (d, 8H, $^3J_{H-H}$ 7.9, C_6H_4), 7.33 (d, 8H, $^3J_{H-H}$ 7.8, C_6H_4) and 7.40-7.68 (br m, 60H, C_6H_5).

$^{13}C\{^1H\}$ NMR (125.8 MHz, CD_2Cl_2):
δ_C 75.3 (4C, Cb), 83.7 (5C, Cp), 122.9 (4C, C≡C-C_6H_4), 128.5 (4C, C_6H_4), 128.6 (d, 4C, C_6H_4-C≡C, $^2J_{PC}$ 5.0),129.1 (d, $^3J_{PC}$ 11.3, *meta*-C_6H_5), 129.9 (d, $^1J_{PC}$ 56.0, quaternary

C_6H_5), 131.5 (d, *para*-C_6H_5, $^4J_{PC}$ 2.0), 131.6 (8C, d, $^4J_{PC}$ 5.0, C_6H_4), 131.7 (4C, quaternary C_6H_4), 134.9 (d, *ortho*- C_6H_5, $^2J_{PC}$ 13.8) and 135.5 (quaternary C_6H_4)

IR(KBr): ν (C≡C) 2095.6 cm^{-1}.

M.p.: Decomposes 207°C

UV-Vis absorption: λ_{max} = 235.5 nm, ε = 127,123 $M^{-1}cm^{-1}$ and λ_{max} = 320.5 nm, ε = 96,273 $M^{-1}cm^{-1}$.

Elemental Analysis: $(C_{113}H_{81}CoAu_4P_4)(CH_2Cl_2)_2$ Result % (calculated %): C = 53.55 (53.2), H = 3.92(3.32).

Synthesis of [*tetrakis*(*bis*-triethylphosphine)phenylplatinum(ethynylphenyl) cyclobutadiene]cyclopentadienyl cobalt 42.

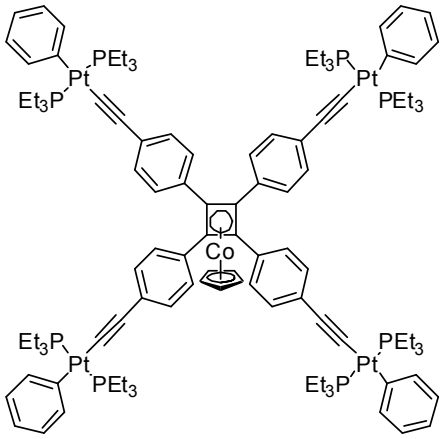

In a Youngs tube Pt(Ph)$(PEt_3)_2$Cl (0.30 g, 0.55 mmol), **38** (0.08 g, 0.14 mmol) and copper iodide (5 mg) were combined and placed under an inert atmosphere. The flask was charged with DCM/^{i}PrNH (40 ml, 1:1 v/v) and stirred in the absence of light for 48 h. The solvent was removed under reduced pressure and the residue purified by column chromatography (silica, hexane/DCM (1:1 v/v)) to yield a yellow solid. The product was further purified by recrystallisation with DCM/hexane to yield pure yellow powder.

Yield: 0.14 g, 0.05 mmol, 37.3%.

$^{31}P\{^{1}H\}$ NMR (121.5 MHz, $CDCl_3$):
δ_P 11.19 ($^{1}J_{Pt\text{-}P}$ 2646.5)

^{1}H NMR (300.2 MHz, CD_2Cl_2):
δ_H 1.04-1.18 (m, 72H, CH_3), 1.66-1.86 (m, 48H, CH_2), 4.60 (s, 5H, Cp), 6.77 (t, $^{3}J_{H\text{-}H}$ 7.7, 4H, *para*-C_6H_5), 6.94 (t, $^{3}J_{H\text{-}H}$ 7.4, 8H, *meta*-C_6H_5), 7.11 (d, $^{3}J_{H\text{-}H}$ 8.3, 8H, C_6H_4) and 7.28-7.36(m, 16H, *ortho*-C_6H_5- and C_6H_4).

$^{13}C\{^{1}H\}$ NMR (125.8 MHz, CD_2Cl_2):
δ_C 8.4 (CH_3), 15.7 (t, CH_2, $^{1}J_{PC}$ 34.3), 75.6 (Cb), 83.5 (Cp), 110.8 (C≡C-C_6H_4), 115.0 (Pt-C≡C) 121.7 (*para*-C_6H_5), 127.8 (8C, *meta*-C_6H_5),127.8 (C_6H_4, quaternary) 129.0 (8C, C_6H_4), 130.8 (C_6H_4), 133.5 (C_6H_4, quaternary), 139.8 (8C, *ortho*-C_6H_5) and 157.02 (quaternary C_6H_5).

IR(KBr): ν (C≡C) 2094.3 cm^{-1}

M.p.: decomposes 197°C

UV-Vis absorption: λ_{max} = 346 nm, ε = 119,205 $M^{-1}cm^{-1}$.

Elemental Analysis: $(C_{113}H_{161}CoPt_4P_8)(CH_2Cl_2)_3$ Result % (calculated %): C = 48.7(48.67), H = 6.33(5.88).

5.3 Synthesis for Chapter 3

Synthesis of 1,4-*bis*(trimethylsilylethynyl)benzene 43.

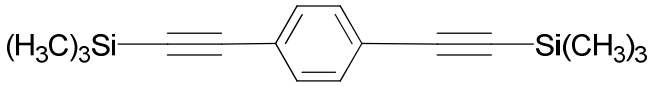

In a round bottomed flask 1,4-diiodobenzene (8.25 g, 0.03 mol), *bis*(triphenylphosphine)palladiumdichloride (0.70 g, 1.0 mmol) and copper(I) iodide (95 mg, 0.5 mmol) were combined and placed under an inert atmosphere. The flask was then charged with diethylamine (150 ml) and trimethylsilylacetylene (8.8 ml, 0.06 mol). The mixture was then stirred for 12 h at room temperature.

The solvent was then removed under reduced pressure and the residue was extracted with diethyl ether and filtered under vacuum through celite to remove insoluble catalyst residue. The solvent was then removed from the filtrate and the crude product was purified by column chromatography (silica, hexane) and eluted with a hexane/DCM gradient to yield a white product.

Yield: 6.23 g, 2.29 mol, 76%.

^{1}H NMR (300.2 MHz, $CDCl_3$):
δ_H 0.25 (18H,s, $Si(CH_3)_3$) and 7.39 (4H, s, C_6H_4).

$^{13}C\{^{1}H\}$ NMR (75.5 MHz, $CDCl_3$):
δ_C 0.05 (6C, $Si(CH_3)_3$), 96.4 and 104.7 (4C, C≡C), 123.3 (2C, quaternary C_6H_4) and 131.9 (4C, C_6H_4).

Synthesis of 1,4-diethynylbenzene 44.

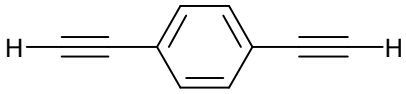

A solution of 1,4-*bis*(trimethylsilylethynyl)benzene **43** (3.79 g, 14 mmol) in THF/MeOH (100 ml, 1:1 v/v) was stirred for 8 h in the presence of an excess of K_2CO_3 (5.81 g, 0.04 mol). The mixture was extracted with diethyl ether and the organic layer dried over magnesium sulphate and the solvent removed to yield a cream solid. The crude solid was dissolved in hexane and filtered through a silica plug to yield a white solid which became pale brown/pink over time.

Yield 1.10 g, 8.7 mmol, 63%.

^{1}H NMR (300.2 MHz, $CDCl_3$):
δ_H 3.10 (2H, s, C≡C-H) and 7.37 (4H, s, C_6H_4).

$^{13}C\{^1H\}$ NMR (75.5 MHz, $CDCl_3$):
δ_C 79.2 (2C, C≡C-H), 83.2 (2C, C≡C), 122.7 (2C, quaternary C_6H_4) and 132.2 (4C, C_6H_4).

Synthesis of $(FeCp(CO)_2)C{\equiv}CC_6H_4C{\equiv}C(FeCp(CO)_2)$ 46. [143]

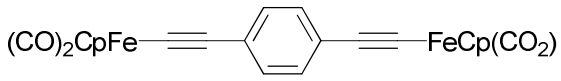

A solution of 1,4-*bis*(trimethylsilylethynyl) benzene **43** (0.63 g, 5.0 mmol) in dry THF was cooled to -78 °C and MgBuCl (5 ml,10 mmol, 2M in THF) was added drop-wise. The mixture was then allowed to warm to room temperature and then heated to reflux and leave to cool. The solution was then cooled to -78 °C and a solution of $CpFe(CO)_2I$ (3.04 g, 10 mmol) in THF (15 ml) was added, the mixture was left for 30 mins to warm up. The solvent was then removed and hexane (5 ml) was added and heated to reflux and then the solvent was removed under vacuum to remove any traces of THF, this

process was repeated twice. The solid was dissolved in DCM and filtered through celite, the crude product was purified by addition of hexane until precipitation occurred. This precipitate was then isolated and re-dissolved in fresh DCM and the cycle was repeated a further two times and then the solid was dried under vacuum.

Yield: 1.70 g, 3.6 mmol, 71.1%.

^{1}H NMR (250.1 MHz, $CDCl_3$):
δ_H 5.05 (s, 10H, C_5H_5) and 7.27 (s, 4H, C_6H_4).

$^{13}C\{^{1}H\}$ NMR (75.5 MHz, $CDCl_3$):
δ_C 84.7 (10C, C_5H_5), 132.2 (4C, C_6H_4) and 214.4 (CO).

IR(nujol): ν(C≡C) 2102.1 , ν(CO) 2034.8 and 1994.9 cm^{-1}.

Synthesis of $\{Co_2CO_6\}_2(Me_3Si\text{-}C{\equiv}C\text{-}C_6H_4\text{-}C{\equiv}C\text{-}SiMe_3)$ 48.

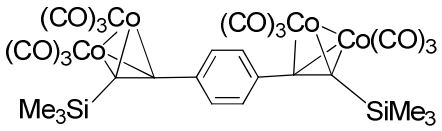

In a Schlenk flask *bis*(trimethylsilylethynyl)benzene **43** (100 mg, 0.37 mmol) and dicobaltoctacarbonyl (0.56 g, 1.64 mmol) were combined and the flask was put under an inert atmosphere. The flask was charged with dichloromethane (50 ml) and stirred at room temperature for 6 h. The solvent was removed under reduced pressure and the residue was re-dissolved in dichloromethane and filtered air sensitively through celite.

After storing at -28 °C overnight deep red squares were obtained suitable for x-ray diffraction.

^{1}H NMR (300.2 MHz, $CDCl_3$):

δ_H 0.43 (s, 18H, $Si(CH_3)_3$) and 7.46 (s, 4H, C_6H_4).

$^{13}C\{^1H\}$ NMR (75.2 MHz, $CDCl_3$):
δ_C 1.0($Si(CH_3)_3$), 80.1 (C≡C), 104.4 (C≡C), 130.6 (C_6H_4), 138.2 (quaternary C_6H_4), 200.1 (CO).

Yield: 0.03 g, 0.04 mmol, 10%.

Synthesis of 1,2,4,5-*tetrakis*(ferrocenylethynyl)benzene 49 *via* (tributylstannylethynyl)ferrocene.

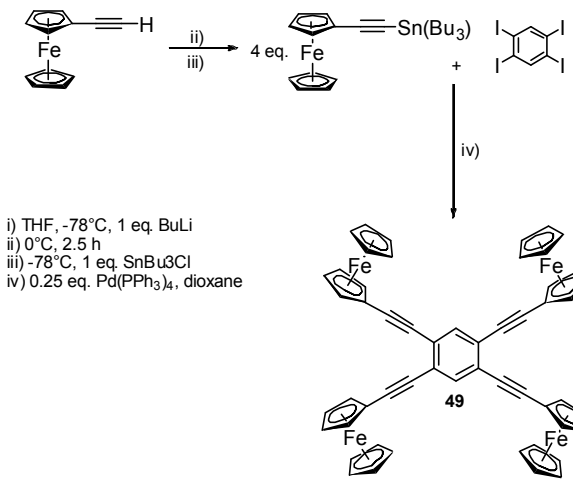

To a solution of ethynylferrocene (2.10 g, 10.0 mmol) in THF (20 ml) cooled to -78 °C was added BuLi (10.0 mmol, 4 ml, 2.5 M in hexane). The solution was then allowed to warm to 0°C and maintained at this temperature for 2.5 h. The solution was then cooled back to -78°C and tributyltin chloride (2.8 ml, 10 mmol) was added dropwise and the solution left to warm up overnight. The solution was then heated to reflux and allowed to cool, before the solvent was removed *in vacuo.,* hexane (1 x 10 ml) was then added and heated to reflux before being removed under vacuum to aid removal of THF, this process was then repeated. The product was then dissolved in hexane (20 ml) and filtered through celite to remove LiCl. Removal of the solvent *in vacuo* yielded crude (tributylstannylethynyl) ferrocene as an orange oil.

^{1}H NMR (300.3 MHz, C_6H_6):

δ_H 1.08-1.16 (m, 9H, CH_3), 1.18-1.26 (m, 6H, CH_2), 1.50-1.64 (m, 6H, CH_2), 1.82-1.94 (m, 6H, CH_2), 4.06 (t, 2H, $^{3}J_{H-H}$ 1.9, Cp), 4.29 (s, 5H) and 4.62(t, 2H, $^{3}J_{H-H}$ 1.9, Cp).

^{13}C{^{1}H } NMR (75.5 MHz, C_6H_6):

δ_C 11.4 (3C, $SnCH_2$), 14.0 (3C, CH_3), 27.4 (3C, $SnCH_2\underline{C}H_2$), 29.5 (3C, $SnCH_2CH_2\underline{C}H_2$), 67.0(1C, quaternary), 68.8 (2C, Cp), 70.5 (5C, Cp), 72.1 (2C, Cp), 89.0 (Sn-C≡C) and 109.3(C≡C).

^{119}Sn(112.0 MHz, C_6H_6):

δ_{Sn} -67.8

In a round bottomed flask tetraiodobenzene (1.45 g, 2.5 mmol) and *tetrakis*(triphenylphosphine)palladium (0.26 g, 0.23 mmol) were combined and the flask placed under an inert atmosphere. A solution of (tributylstannylethynyl)ferrocene in dioxane (5 ml) was added to the flask and dioxane (20 ml) was added. The mixture was heated to reflux and the temperature maintained for 20 h. The solvent was removed under reduced pressure and the residue was washed with hexane to remove any excess tin. The residue was then extracted with DCM and the solid filtered off was found to be the desired product.

^{1}H NMR ($CDCl_3$, 300.2 MHz):

δ_H 4.24-4.31(m, 28H, C_5H_5 and C_5H_4), 4.55-4.60 (m, 8H, C_5H_4) and 7.62 (s, 2H, C_6H_2).

^{13}C{^{1}H } NMR ($C_6H_4Cl_2/CD_2Cl_2$, 125.8 MHz):

δ_C 67.8 (4C, quaternary), 70.3 (C_5H_5), 71.2 (C_5H_5), 72.6 (C_5H_5), 85.6 (4C, C≡C) and 95.7 (4C, C≡C).

Elemental analysis: $Fe_4C_{54}H_{38}.CH_2Cl_2$ Found % (Calculated): C = 66.6 (66.4) and H = 4.27 (4.06).

IR(nujol): ν(C≡C) 2211.8 cm^{-1}.

Yield: 0.87 g, 0.95 mmol, 38%.

M.p.: decomposes at 199 °C.

Crystals suitable for single X-ray diffraction experiments were obtained from slow evaporation of a solution of 1,4-dichlorobenzene.

Synthesis of 1,2,4,5-*tetrakis*((trimethylsilyl)ethynyl)benzene 50. [162]

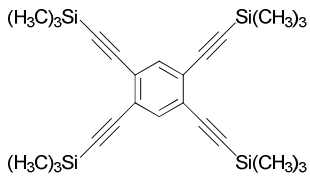

In a round bottomed flask 1,2,4,5-tetraiodobenzene (4.92 g, 8.5 mmol), *bis*(triphenylphosphine)palladiumdichloride (0.59 g, 0.8 mmol) and copper iodide (0.13 g, 0.7 mmol) were combined and placed under an inert atmosphere. The flask was charged with piperdine (80 ml), triethylamine (100 ml) and trimethylsilylacetylene (6.0 ml, 4.15 g, 42 mmol). The mixture was stirred for 4 h at room temperature after which TLC (silica, hexane) showed full consumption of the starting materials. The solvent was removed under reduced pressure and the residue extracted into DCM (150 ml) and washed with acidified distilled water (3 x 200 ml). The solution was dried ($MgSO_4$) and the solvent removed to yield a brown solid. The product was isolated by column chromatography (silica, hexane/DCM (9:1)) to yield the pure product as an off white solid.

Yield: 2.52 g, 5.4 mmol, 63.9%.

^{1}H NMR (300.2 MHz, $CDCl_3$):

δ_H 0.25 (s, 36H, $Si(CH_3)_3$) and 7.56 (s, 2H, C_6H_2).

$^{13}C\{^{1}H\}$ NMR (75.5 MHz, $CDCl_3$):

δ_C 0.05 (12C, $Si(CH_3)_3$), 101.0, 102.1 (8C, C≡C), 125.5 and 136.2 (6C,C_6H_2).

IR(nujol): ν(C≡C) 2164.6 cm^{-1}.

Synthesis of 1,2,4,5-*tetrakis*ethynylbenzene 51.

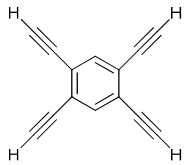

To a solution of 1,2,4,5-*tetrakis*((trimethylsilyl)ethynyl)benzene **50** (2.04 g, 4.4 mmol) in diethyl ether/MeOH (1:1 v/v 200 ml), potassium hydroxide was added (1.29 g, 2.3 mol) and the mixture was stirred for 3 h. The solution was then poured into distilled water (200 ml) and the aqueous layer was separated. The organic layer was then washed with brine (3 x 200 ml), the layers separated and the organic layer dried ($MgSO_4$). Removal of the solvent under reduced pressure yielded a pale brown solid.

Yield: 0.4264 g, 2.4 mmol, 55%.

^{1}H NMR (300.2 MHz, $CDCl_3$):

δ_H 3.42 (s, 4H, Acetylene) and 7.64 (s, 2H, C_6H_2).

$^{13}C\{^{1}H\}$ NMR (75.5 MHz, $CDCl_3$):

δ_C 80.6, 83.6 (8C, C≡C), 125.4 and 136.7 (6C, C_6H_2).

IR(nujol): ν(C≡C) 2108.0 cm^{-1}.

Synthesis of tetra((Co_2CO_6)ethynyl)benzene 52.

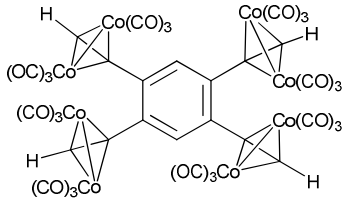

In a Schlenk flask tetraethynylbenzene **50** (100 mg, 0.6 mmol) and dicobaltoctacarbonyl (0.79 g, 2.3 mmol) were combined and the flask was placed under an inert atmosphere. The flask was charged with DCM (50 ml) and stirred for 6 h. The solvent was then removed and the residue was filtered through a silica plug using hexane/DCM (9:1 v/v). The solvent was removed under reduced pressure and the solid dissolved in minimal DCM and then stored at -28°C.

^{1}H NMR ($CDCl_3$, 300.2 MHz):
δ_H 6.58 (br s, 4H, C≡C-H) and 7.89 (br s, 2H, C_6H_2).

$^{13}C\{^1H$ NMR$\}$ unable to obtain

Yield: 5 mg.

Synthesis of 1-Iodo-4-(trimethylsilylethynyl)benzene 54.[164]

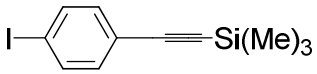

To a solution of 4-(trimethylsilylethynyl)aniline (7.17 g, 37.9 mmol) in aqueous HCl (6M, 620 ml) at 0°C was added a solution of sodium nitrite (3.13 g, 45.4 mmol). The temperature was maintained at 0-5°C and the solution was stirred for 45 min, then an ice-cold aqueous solution of potassium iodide (9.86 g, 59.4 mmol, 40 ml H_2O) and DCM (360 ml) were added. The resulting mixture was allowed to warm to room temperature and stirred for 4 h, after which the organic layer was separated. The aqueous layer was then extracted with DCM (2 x 150 ml), the combined organic layers

were washed with brine (3 x 150 ml), saturated sodium thiosulphate (2 x 150 ml) and a final distilled water wash (1 x 150 ml). After drying the organic solution ($MgSO_4$) the solvent was removed under reduced pressure and the residue was purified by column chromatography (silica, hexane) to yield a pale yellow solid.

^{1}H NMR (250. 1 MHz, $CDCl_3$):
δ_H 0.24 (s, 9H, $Si(CH_3)_3$), 7.15-7.21 (m, 2H, Ar) and 7.59- 7.67 (m, 2H, Ar).

$^{13}C\{^1H\}$ NMR (75.5 MHz, $CDCl_3$):
δ_C 0.00 (3C, $Si(CH_3)_3$), 96.0, 94.6, 104.1 (3C, 2 C≡C and quaternary C_6H_4), 122.7 (1C, quaternary C_6H_4), 133.6 and 137.5 (4C, C_6H_4)

Yield: 6.62 g, 22.1 mmol, 58.1%.

Synthesis of 1,2,4,5-*tetrakis*-(trimethylsilylethynyl-phenylethynyl)-benzene 53.

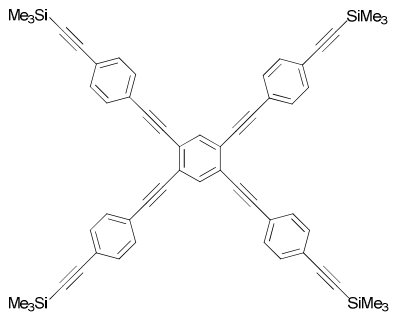

In a round bottomed flask tetraethynylbenzene **50** (0.85 g, 4.9 mmol), 1-iodo-4-(trimethylsilylethynyl)benzene (5.89 g, 19.6 mmol), *bis*(triphenylphosphine)palladium dichloride (0.17 g, 0.3 mmol) and copper iodide (47 mg, 0.3 mmol) were combined. The flask was placed under an inert atmosphere and diethylamine (100 ml) was added and the reaction was stirred for 72 h at room temperature. The solvent was removed under reduced pressure and the residue dissolved in DCM and washed with saturated sodium bicarbonate (3 x 200 ml) and the organic layer separated. The organic layer was dried

($MgSO_4$) and the solvent was removed under reduced pressure. Column chromatography (silica, hexane → hexane/DCM) initially yielded starting material and then product as a yellow solid after removal of the solvent under reduced pressure.

Yield: 2.42 g, 2.8 mmol, 57%.

^{1}H NMR (300.2 MHz, $CDCl_3$):
δ_H 0.27 (s, 36H, $Si(CH_3)_3$), 7.44-7.47 (m, 16H, C_6H_4) and 7.71 (s, 2H, C_6H_2).

$^{13}C\{^1H\}$ NMR (75.5 MHz, $CDCl_3$):
δ_C 0.06 (12C, $Si(CH_3)_3$), 89.4, 95.5, 97.0, 104.6 (16C, C≡C), 123.0, 123.7, 125.5, 131.6, 132.2 and 134.9 (30C, C_6H_4 and C_6H_2).

M.p.: 247 °C changes to brown 250°C changes to black.

Unable to obtain a satisfactory elemental analysis.

Synthesis of 1,2,4,5-*tetrakis*(4-ethynyl-phenylethynyl)-benzene 54.

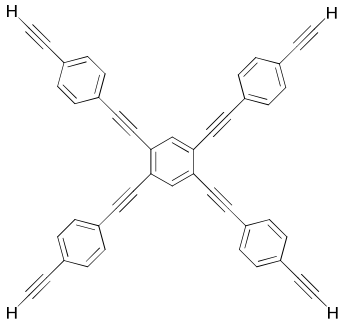

To a solution of **53** (0.81 g, 0.94 mmol) in THF/MeOH (100 ml, 50/50 v/v) was added potassium carbonate (1.14 g, 8.25 mmol). The solution was stirred overnight and then poured into distilled water (100 ml) and extracted with DCM (150 ml). The organic layer was further washed with brine (2 x 100 ml) and then dried (Na_2SO_4). The solution was further purified by filtering through a short silica plug and eluting with DCM.

Removal of the solvent under reduced pressure yielded the desired product as a yellow/ brown solid.

Yield: 0.31 g, 0.5 mmol, 57.4%.

^{1}H NMR (250.1 MHz, $CDCl_3$):
δ_H 3.21 (s, 4H, C≡C-H), 7.49 (s, 16H, C_6H_4) and 7.75 (s, 2H, C_6H_2).

$^{13}C\{^{1}H\}$ NMR (75.5 MHz, CD_2Cl_2,):
δ_C 79.9, 89.6, 95.6 and 108.8 (16H, C≡C), 123.2, 123.7, 125.8, 132.2, 132.8 and 135.6 (30H, C_6H_4 and C_6H_2).

Synthesis of 1,2,4,5-*tetrakis*($AuPPh_3$Clethynyl)benzene

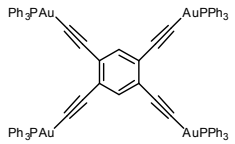

In a Youngs flask $AuPPh_3Cl$ (0.20 g, 0.41 mmol), tetraethynylbenzene (17.6 mg, 0.1 mmol) and KBu^tOH (0.43 g, 3.8 mmol) were combined and placed under an inert atmosphere. The flask was charged with dry MeOH (60 ml) and the flask was placed under a slight vacuum before sealing. The mixture was then heated to reflux and heat at this temperature for 10 h. The reaction was then cooled and the solvent was removed, the crude product was purified by recrystallising from DCM/hexane to yield a beige solid.

^{1}H NMR (300.2 MHz, CD_2Cl_2):
δ_H 7.30-7.60 (m, 62H, C_6H_5 and C_6H_2).

^{31}P NMR (121.5 MHZ, CD_2Cl_2):
δ_P 43.31

^{13}C NMR insufficiently soluble

5.4 Synthesis for Chapter 4

Synthesis of 5,10,15,20-tetraferrocenylporphyrin 55.

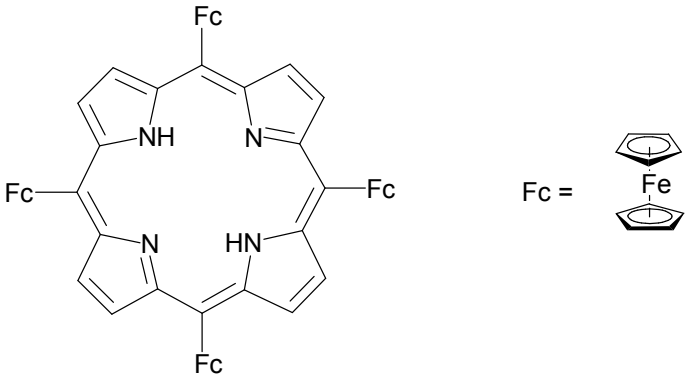

A solution of *meso*-ferrocenyl dipyrromethane (0.50 g, 1.5 mmol) and ferrocene carboxaldehyde (0.32 g, 1.5 mmol) in DCM was stirred for 5 min in the absence of light under a N_2 atmosphere. Then trifluoroacetic acid (0.06 ml, 0.8 mmol) was added and the reaction for stirred for a further 90 min. Tetrachloro-1,4-benzoquinone (0.37 g, 1.5 mmol) was added and the mixture was heated to reflux for 90 min. The reaction was then left to cool overnight and then the solvent was removed under reduced pressure. The residue was purified by column chromatography (alumina, DCM: ethyl acetate 99:11 v/v) yielding the desired product as the first green fraction

Yield: 0.30 g, 0.29 mmol, 19.3%.

^1H NMR (300.3 MHz, $CDCl_3$):
δ_H -0.48 (s, 2H, N-H), 3.97 (s, 20H, C_5H_5), 4.76 (t, 8H, C_4H_5, $^3J_{H-H}$ 1.8), 5.33 (t, 8H, C_4H_5, $^3J_{H-H}$ 1.8) and 9.61 (s, 8H, pyrrole).

$^{13}C\{^1H\}$ NMR (75.5 MHz, $CDCl_3$):
δ_C 60.5 (4C, quaternary C, C_5H_4), 69.1 (8C, C_5H_4), 70.5 (20H, C_5H_5), 76.9 (8H, C_5H_4), 89.3 , 117.4 and 130.9

Synthesis of 5,10,15,20-*tetra*-pyridin-4-yl-porphyrin 56.

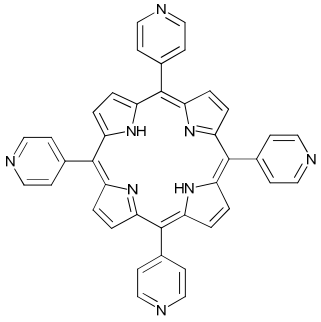

To a refluxing mixture of propanoic acid (50 ml) and glacial acetic acid (0.7 ml) was added dropwise pyrrole (0.28 ml, 4 mmol) and 4-pyridylcarboxaldehdye (0.35 ml, 3.7 mmol). The mixture was refluxed for 1 h and then cooled and the solvent removed under reduced pressure. The residue was washed with distilled water (100 ml) followed by ammonium hydroxide (3M, 2 x 500 ml). The residue was then suspended in MeOH (300 ml) heated gently and then stored in the fridge overnight. The mixture was then filtered under gravity to isolate the crude product which was further purified by filtering through a silica plug ($CHCl_3$). Removal of the solvent under reduced pressure yielded the product as a purple solid.

Yield: 0.09 g, 0.15 mmol, 4%.

^{1}H NMR (250.1 MHz, $CDCl_3$):
δ_H -2.93 (s, 2H, NH), 8.14-8.19 (m, 8H, pyridyl), 8.88 (s, 8H, pyrrole) and 9.03-9.10 (m, 8H, pyridyl).

$^{13}C\{^1H\}$ NMR ($CDCl_3$, 75.5 MHz):
δ_C 77.5, 118.0, 129.5, 148.6 and 148.9.

Attempted synthesis of [$Ru_4(\eta^6$-*p*-Pri($C_6H_4Me)_4$(5,10,15,20-*tetra*-pyridin-4-yl-porphyrin)Cl_8

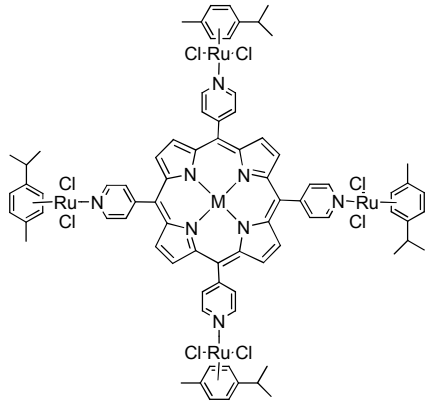

A solution of 5,10,15,20-*tetra*-pyridin-4-yl-porphyrin (0.06 g, 0.1 mmol) in DCM (30 ml) was added to a solution of ruthenium(*p*-cymene)dichloride (0.12 g, 0.2 mmol) in DCM (10 ml). The solution was stirred under an inert atmosphere for 24 h. The solvent was then removed under reduced pressure and the residue was washed with dry toluene until the solution was colourless (60 ml).

Yield: 15 mg, 0.008 mmol, 8.1%.

^{1}H NMR (250.1 MHz, $CDCl_3$):
δ_H 1.47 (d, 24 H,(C<u>H</u>$_3$)CH, $^3J_{H-H}$ 6.9), 2.39 (s, 12H), 3.16-3.27 (sept, 4H, (CH_3)C<u>H</u>), 5.54 (d, 8H, C_6H_4 $^3J_{H-H}$ 5.7), 5.71(d, 8H, C_6H_4 $^3J_{H-H}$ 5.7), 8.14 (d, 8H, pyridyl, $^3J_{H-H}$ 5.6), 8.84 (s, 8H, pyrrole) and 9.52 (d, 8H, pyridyl, $^3J_{H-H}$ 5.5).

Unable to obtain a satisfactory ^{13}C NMR due to solubility.

6 References

[1] J. M. Tour, Molecular Electronics: Commercial Insights, Chemistry, Devices, Architecture and Programming, World Scientific, London, 2003.

[2] G. E. Moore, *Electronics*, 1965, **38**, 114.

[3] P. Ball, *Nat. Mater.*, 2000, **206**, 118.

[4] M. B. Robin and P. Day, *Adv. Inorg. Chem. Radiochem.*, 1967, **10**, 247.

[5] D. O. Cowan, C. LeVanda, J. Park, and F. Kaufman, *Acc. Chem. Res.*, 1973, **6**, 1.

[6] S. B. Braun-Sand and O. Wiest, *J. Phys. Chem. B*, 2003, **107**, 285.

[7] A. Klein, O. Lavastre, and J. Fielder, *Organometallics*, 2006, **25**, 635.

[8] P. Zanello, Inorganic electrochemistry; theory, practise and application., Royal Society of Chemistry, Cambridge, 2003.

[9] M. C. B. Colbert, J. Lewis, N. J. Long, P. R. Raithby, M. Younus, A. J. P. White, D. J. Williams, N. N. Payne, L. Yellowlees, D. Beljonne, N. Chawdhury, and R. H. Friend, *Organometallics*, 1998, **17**, 3034.

[10] Z. Li, A. M. Beatty, and T. P. Fehlner, *Inorg. Chem*, 2003, **42**, 5707.

[11] M. J. Powers and T. J. Meyer, *J. Am. Chem. Soc.*, 1978, **100**, 4393.

[12] M. J. Powers and T. J. Meyer, *Inorg. Chem.*, 1978, **17**, 2955.

[13] S. B. Colbran, B. H. Robinson, and J. Simpson, *Organometallics*, 1983, **2**, 952.

[14] B. S. Brunschwig, C. Creutz, and N. Sutin, *Chem. Soc. Rev.*, 2002, **31**, 168.

[15] C. Creutz, *Prog. Inorg. Chem.*, 1983, **30**, 1.

[16] E. W. Weiss, M. J. Tauber, R. F. Kelley, M. J. Ahrens, M. A. Ratner, and M. R. Wasielewski, *J. Am. Chem. Soc*, 2005, **127**, 11842.

[17] C. E. B. Evans, M. L. Naklicki, A. R. Rezvani, C. A. White, V. V. Kondratiev, and R. J. Crutchley, *J. Am. Chem. Soc.*, 1998, **120**, 13096.

[18] P. J. Low, *J. Chem. Soc., Dalton Trans.*, 2005, 2821.

[19] C. Petzold, Code : The Hidden Language of Computer Hardware and Software, Microsoft Press, Washington, 2000.

[20] http://www.intel.com/education/transworks/flat3.htm.

[21] http://connectors.tycoelectronics.com/glossary/glossary-l.stm.

[22] N. Dale and J. Lewis, Computer Science Illuminated, 2nd, Jones and Barlett Publishers, Sudbury, 2004.

[23] C. S. Lent, *Science*, 2000, **288**, 1597.

[24] C. S. Lent and B. Isaksen, *IEEE Trans. Electronic Dev.*, 2003, **50**, 1890.

[25] G. L. Snider, A. O. Orlov, I. Amlani, X. Zuo, G. H. Bernstein, C. S. Lent, and J. L. Merz, *J. Appl. Phys.*, 1999, **85**, 4283.

[26] G.L.Snider, A.O.Orlov, I.Amlani, X.Zuo, G. H. Bernstein, C.S.Lent, J.L.Merz, and W.Porod, *J. Vac. Sci. Technol. A,*, 1999, **17**, 1394.

[27] G. L. Snider, A. O. Orlov, I. Amlani, G. H. Bernstein, C. S. Lent, J. L. Merz, and W. Porod, *J. Vac. Sci. Technol. A*, 1999, **17**, 1394.

[28] C. S. Lent, B. Isaksen, and M. Lieberman, *J. Am. Chem. Soc.*, 2003, **125**, 1056.

[29] G. L. Snider, A. O. Orlov, I. Amlani, G. H. Bernstein, C. S. Lent, J. L. Merz, and W. Porod, *Microelectronic Eng.,*, 1999, **47**, 261.

[30] M. Macucci, Quantum Cellular Automata: Theory, Experimentation and prospects, Imperial College Press, 2006.

[31] H. Qi, S. Sharma, Z. Li, G. L.Snider, A. O. Orlov, C. S.Lent, and T. P. Fehlner, *J. Am. Chem. Soc*, 2003, **125**, 15250.
[32] S. B. Braun-Sand and O. Wiest, *J. Phys. Chem. B*, 2003, **107**, 9624.
[33] J. Jiao, G. J.Long, F. Grandjean, A. M. Beatty, and T. P. Fehlner, *J. Am. Chem. Soc*, 2003, **125**, 7522.
[34] A. Aviram, *J. Am. Chem. Soc.*, 1988, **110**, 5687.
[35] N. S. Hush, A. T. Wong, G. B. Bacskay, and J. R. Reimers, *J. Am. Chem. Soc.*, 1990, **112**, 4192.
[36] C. S. Lent, M. Liu, and Y. Lu, *Nanotechnology*, 2006, **17**, 4240.
[37] M. Colbert, S. Ingham, J. Lewis, N. Long, and P. Raithby, *J. Chem. Soc., Dalton Trans.*, 1994, 2215.
[38] M. Colbert, J. Lewis, N. Long, P. Raithby, A. White, and D. Williams, *J. Chem. Soc., Dalton Trans.,*, 1997, **99**.
[39] M. Manimaran, G.L.Snider, C.S.Lent, V.Sarveswaran, M. Lieberman, Z. Li, and T. P. Fehlner, *Ultramicroscopy*, 2003, **97**, 55.
[40] Z. Li and T. P. Fehlner, *Inorg. Chem*, 2003, **42**, 5715.
[41] A. J. Bard and L. R. Faulkner, Electrochemical Methods, Wiley, New York, 2001.
[42] H. Qi, A. Gupta, B. C. Noll, G. L. Snider, Y. Lu, C. Lent, and T. P. Fehlner, *J. Am. Chem. Soc.*, 2005, **127**, 15218.
[43] S. Rigaut, J. Perruchon, L. Le Pichon, D. Touchard, and P. H. Dixneuf, *J. Organomet. Chem.*, 2003, **670**, 37.
[44] H. Qi, A. Gupta, B. C. Noll, G. L. Snider, Y. Lu, C. Lent, and T. P. Fehlner, *J. Am. Chem. Soc.*, 2005, **127**, 15218.
[45] M. D. Rausch, F. A. Higbie, G. F. Westover, A. Clearfield, R. Gopal, J. M. Troup, and I. Bernal, *J. Organomet. Chem.*, 1978, **149**, 245.
[46] J. Kotz, G. Neyhart, W. J. Vining, and M. D. Rausch, *Organometallics*, 1983, **2**, 79.
[47] J. Jiao, G. J. Long, L. Rebbouh, F. Grandjean, A. M. Beatty, and T. P. Fehlner, *J. Am. Chem. Soc.*, 2005, **127**, 17819.
[48] J. A. Kramer and D. N. Hendrickson, *Inorg. Chem.*, 1980, **19**, 3300.
[49] T. Y. Dong, T. Kambara, and D. N. Hendrickson, *J. Am. Chem. Soc.*, 1986, **108**, 4423.
[50] M. E. Wright, G. J. Long, D. E. Tharp, and G. O. Nelson, *Organometallics*, 1986, **5**, 779.
[51] Y. Yamamoto, T. Arakawa, R. Ogawa, and K. Itoh, *J. Am. Chem. Soc.*, 2003, **125**, 12143.
[52] E. Rüba, K. Mereiter, R. Schmid, V. N. Sapunov, K. Kirchner, H. Schottenberger, M. J. Calhorda, and L. F. Veiros, *Chem. Eur. J.*, 2002, **8**, 3948.
[53] M. D. Rausch and R. A. Genetti, *J. Org. Chem.*, 1970, **35**, 3888.
[54] H. Sakurai and J. Hayashi, *J. Organomet. Chem.*, 1972, **39**, 365.
[55] M. D. Rausch, I. Bernal, B. R. Davies, A. Siegel, F. A. Higbie, and G. F. Westover, *J. Coord. Chem.*, 1973, **3**, 149.
[56] M. S. Lim, J. Y. Baeg, and S. W. Lee, *J. Organomet. Chem.*, 2006, **691**, 4100.
[57] W.-S. Lee and H. H. Brintzinger, *J. Organomet. Chem.*, 1977, **127**, 93.

[58] C. Schaefer, D. B. Werz, T. H. Staeb, R. Gleiter, and F. Rominger, *Organometallics*, 2005, **24**, 2106.
[59] L. F. Veiros, G. Dazinger, K. Kirchner, M. J. Calhorda, and R. Schmid, *Chem. Eur. J.*, 2004, **10**, 5860.
[60] J. March, Advanced Organic Chemistry, 4th, Wiley Interscience, New York, 1992.
[61] U. H. F. Bunz and V. Enkelmann, *Organometallics*, 1994, **13**, 3823.
[62] D. W. Clack and K. D. Warren, *Structure and Bonding*, 1980, **39**, 1.
[63] D. W. Clack and K. D. Warren, *Inorg. Chim. Acta*, 1978, **27**, 105.
[64] P.R.Raithby, A. L. Johnson, S. Brayshaw, and H. M. Davies, Unpublished, 2008.
[65] M. J. Frisch, in 'Gaussian 03', Wallingford CT, 2004.
[66] S. M. Waybright, K. McAlpine, M. Laskoshi, M. D. Smith, and U. H. F. Bunz, *J. Am. Chem. Soc*, 2002, **124**, 8661.
[67] R. M. Harrison, T. Brotin, B. C. Noll, and J. Michl, *Organometallics*, 1997, **16**, 3401.
[68] J. Clayden, N. Greeves, S. Warren, and P. Wothers, Organic Chemistry, Oxford University Press, Oxford, 2001.
[69] R. P. Hsung, C. E. D. Chidsey, and L. R. Sita, *Organometallics*, 1995, **14**.
[70] W. D. Wulff, K. A. Korthals, R. Martinez-Alvarez, M. Gomez-Gallego, I. Fernandez, and M. A. Sierra, *J. Org. Chem.*, 2005, **70**, 5269.
[71] J. Ohshita, R. Taketsugu, K. Hino, and A. Kunai, *J. Organomet. Chem.*, 2006, **691**, 3065.
[72] C. D. Simpson, J. D. Brand, A. J. Berresheim, L. Przybilla, H. J. Räder, and K. Müllen, *Chem. Eur. J.*, 2002, **8**, 1424.
[73] U.-M. Wiesler, A. J. Berresheim, F. Morgenroth, G. Lieser, and K. Mullen, *Macromolecules*, 2001, **34**, 187.
[74] G. Doisneau, G. Balavoine, and T.Fillebeen-Khan, *J. Organomet. Chem.*, 1992, **425**, 113.
[75] B. Pedersen, G. Wagner, R. Herrmann, W. Scherer, K. Meerholz, E. Schmälzlin, and C. Bräuchle, *J. Organomet. Chem.*, 1999, **590**, 129.
[76] H. Nock, M. Buchmeiser, J. Polin, J. Lukasser, P. Jaitner, and H. Schottenberger, *Mol. Cryst. Lig. Cryst.*, 1993, **235**, 237.
[77] H. Fink, N. J. Long, A. J. Martin, G. Opromolla, A. J. P. White, D. J. Williams, and P. Zanello, *Organometallics*, 1997, **16**, 2646.
[78] M. B. Zaman, M. D. Smith, D. M. Ciurtin, and H.-C. zur Loye, *Inorg. Chem.*, 2002, **41**, 4895.
[79] B. T. Holmes, W. T. Pennington, and T. W. Hanks, *Synth. Commun.*, 2003, **33**, 2447.
[80] B. J. Coe, J. l. Harries, J. A. Harris, B. S. Brunschwig, S. J. Coles, M. E. Light, and M. B. Hursthouse, *Dalton Trans.*, 2004, 2935.
[81] S. Dixon and R. J. Whitby, *Tetrahedron Letters*, 2006, **47**, 8147.
[82] M. Gerloch and R. Mason, *Proc. R. Soc. London. Ser. A.*, 1964, **279**, 170.
[83] L. F. Dahl and D. L. Smith, *J. Am. Chem. Soc.*, 1961, **83**, 753.
[84] D. B. R. Boese, R. L. Halterman, K. P. C. Vollhardt, *Angew. Chem. Int. Ed. Engl.*, 1988, **27**, 553.

[85] E. Pretsch, P. Buhlmann, and C. Affolter, Structure Determination of Organic Compounds, Springer, Berlin, 2000.
[86] S. Guesmi, D. Touchard, and P. H. Dixneuf, *Chem. Commun.*, 1996, 2773.
[87] O. Lavastre, J. Plass, P. Bachmann, S. Guesmi, C. Moinet, and P. H. Dixneuf, *Organometallics*, 1997, **16**, 184.
[88] D. Touchard, P. Haquette, S. Guesmi, L. Le Pichon, A. Daridor, L. Toupet, and P. H. Dixneuf, *Organometallics*, 1997, **16**, 3640.
[89] N. J. Long, A. J. Martin, F. Fabrizi de Biani, and P. Zanello, *J. Chem Soc., Dalton Trans.*, 1998, 2017.
[90] I.-Y. Wu, J. T.Lin, and Y. S.Wen, *Organometallics*, 1999, **18**, 320.
[91] S. K. Hurst, M. P. Cifuentes, J. P. L. Morrall, N. T. Lucas, I. R. Whittal, M. G. Humphrey, I. Asselberghs, A. Persoons, M. Samoc, B. Luther-Davies, and A. C. Willis, *Organometallics*, 2001, **20**, 4664.
[92] H. L. Bozec, K. Ouzzine, and P. H. Dixneuf, *Organometallics*, 1991, **10**, 2768.
[93] M. A. Fox, R. L. Roberts, W. M. Khairul, F. Hartl, and P. J. Low, *J. Organomet. Chem.*, 2007, **692**, 3277.
[94] M. I. Bruce, B. C. Hall, B. D. Kelly, P. J. Low, B. W. Skelton, and A. H. White, *J. Chem. Soc., Dalton Trans*, 1999, 3719.
[95] M. Uno and P. H. Dixneuf, *Angew. Chem. Int. Ed.*, 1998, **37**, 1714.
[96] D. Touchard, P. Haquette, S. Guesmi, L. L. Pichon, A. Daridor, L. Toupet, and P. H. Dixneuf, *Organometallics*, 1997, **16**, 3640.
[97] J. L. Fillaut, J. Perruchon, P. Blanchard, J. Roncali, S. Golhen, M. Allain, A. Migalsaka-Zalas, I. V. Kityk, and B. Sahraoui, *Organometallics*, 2005, **24**, 687.
[98] W. M. Khairul, D. Albesa-Jové, D. S. Yufit, M. R. Al-Haddad, J. C. Collings, F. Hartl, J. A. K. Howard, T. B. Marder, and P. J. Low, *Inorg. Chim. Acta*, 2008, **361**, 1646.
[99] R. Packheiser, A. Jakob, P. Ecorchard, B. Walfort, and H. Lang, *Organometallics*, 2008, **27**, 1214.
[100] K. R□ßler, T. Rüffer, B. Walfort, R. Packheiser, R. Holze, M. Zharnikov, and H. Lang, *J. Organomet. Chem.*, 2007, **692**, 1530.
[101] I. E. Pomestchenko, D. E. Polyansky, and F. N. Castellano, *Inorg. Chem.*, 2005, **44**, 3412.
[102] I. R. Whittall, M. G. Humphrey, S. Houbrechts, J. Maes, A. Persoons, S. Schmid, and D. C. R. Hockless, *J. Organomet. Chem.*, 1997, **544**, 277.
[103] M. Jura, 'Synthetic and spectroscopic studies of platinium and gold acetylide complexes with conjugated ligands', PhD thesis, University of Bath, Bath, 2006.
[104] E. L. Sharp, 'Synthesis of transition metal acetylide complexes and studies into their electronic properties.' PhD thesis, University of Bath, Bath, 2007.
[105] R. J. Cross and M. F. Davidson, *J. Chem. Soc. Dalton Trans*, 1986, 411.
[106] J. Vicente, M.-T. Chicote, and M. M. Alvarez-Falcon, *Organometallics*, 2005, **24**, 5956.
[107] I. R. Whittall, M. G. Humphrey, S. Houbrechts, A. Persoons, and D. C. R. Hockless, *Organometallics*, 1996, **15**, 5738.
[108] K. Onitsuka, M. Fujimoto, H. Kitajima, N. Ohshiro, F. Takei, and S. Takahashi, *Chem. Eur. J.*, 2004, **10**, 6433.
[109] S. Leininger, P. J. Stang, and S. Huang, *Organometallics*, 1998, **17**, 3981.

[110] S. Leininger and P. J. Stang, *Organometallics*, 1998, **17**, 3981.
[111] N. Ohshiro, F. Takei, K. Onitsuka, and S. Takahashi, *J. Organomet. Chem.*, 1998, **569**, 195.
[112] M. S. Khan, M. K. Al-Suti, M. R. A. Al-Mandhary, B. Ahrens, J. K. Bjernemose, M. F. Mahon, L. Male, P. R. Raithby, R. H. Friend, A. Kohler, and J. S. Wilson, *Dalton Trans.*, 2003, 65.
[113] S. O. Grim, R. L. Keiter, and W. McFarlane, *Inorg. Chem.*, 1967, **6**, 1133.
[114] A. Pidcock, *Chem. Comm.*, 1968, 92.
[115] C. E. Wayne and R. P. Wayne, Photochemistry, Oxford University Press, Oxford, 1996.
[116] D. H. Williams and I. Fleming, Spectroscopic methods in organic chemistry, 3rd, McGraw-Hill, London, 1980.
[117] S. C. Johannessen, R. G. Brisbois, J. P. Fischer, P. A. Grieco, A. E. Counterman, and D. E. Clemmer, *J. Am. Chem. Soc.*, 2001, **123**, 3818.
[118] D. C. Caskey and J. Michl, *J. Org. Chem.*, 2005, **70**, 5442.
[119] D. K. Gupta, A. N. Sahay, D. S. Pandey, N. K. Jha, P. Sharma, G. Espinosa, A. Cabrera, M. C. Puerta, and P. Valerga, *J. Organomet. Chem.*, 1998, **568**, 13.
[120] M. Auzias, B. Therrien, G. Suss-Fink, P. Stepnicka, W. H. Ang, and P. J. Dyson, *Inorg. Chem.*, 2008, **47**, 578.
[121] P. Rothemund, *J. Am. Chem. Soc.*, 1939, **61**, 2912.
[122] P. Govindaswamy, G. Süss-Fink, and B. Therrien, *Organometallics*, 2007, **26**, 915.
[123] M. B. Zaman, M. D. Smith, and H.-C. z. Loye, *Chem. Mater.*, 2001, **13**, 3534.
[124] T. M. Fasina, J. C. Collings, D. P. Lydon, D. Albesa-Jove, A. S. Batsanov, J. A. K. Howard, P. Nguyen, M. Bruce, A. J. Scott, W. Clegg, S. W. Watt, C. Viney, and T. B. Marder, *J. Mater. Chem.*, 2004, **14**, 2395.
[125] F. Paul and C. Lapinte, *Coord. Chem. Rev.*, 1998, **178-180**, 431.
[126] C. Engtrakul and L. R. Sita, *Organometallics*, 2008, **27**, 927.
[127] M. I. Bruce, P. J. Low, F. Hartl, P. A. Humphrey, F. d. Montigny, M. Jevric, C. Lapinte, G. J. Perkins, R. L. Roberts, B. W. Skelton, and A. H. White, *Organometallics*, 2005, **24**, 5341.
[128] C. Patoux, C. Coudret, J.-P. Launay, C. Joachim, and A. Gourdon, *Inorg. Chem.*, 1997, **36**, 5037.
[129] T. Weyland, K. Costuas, L. Toupet, J.-F. Halet, and C. Lapinte, *Organometallics*, 2000, **19**, 4228.
[130] T. Weyland, C. Lapinte, G. Frapper, M. J. Calhorda, J.-F. Halet, and L. Toupet, *Organometallics*, 1997, **16**, 2024.
[131] M. Linseis, R. F. Winter, B. Sarkar, W. Kaim, and S. Záliš, *Organometallics*, 2008, **27**, 3321.
[132] Y. Tanaka, A. Inagaki, and M. Anita, *Chem. Comm.*, 2007, 1169.
[133] Á. Díez, J. Fernández, E. Lalinde, M. T. Moreno, and S. Sánchez, *Dalton Trans.*, 2008, 4926.
[134] Á. Díez, J. Fernández, E. Lalinde, M. T. Moreno, and S. Sánchez, *Dalton Trans.,*, 2008, 4926.
[135] K. Axel, O. Lavastre, and J. Fiedler, *Organometallics*, 2006, **25**, 635.

[136] M. J. Plater, J. P. Sinclair, S. Aiken, T. Gelbrich, and M. B. Hursthouse, *Tetrahedron*, 2004, **60**, 6385.
[137] G. J. Bodwell, D. O. Miller, and R. J. Vermeij, *Org. Lett.*, 2001, **3**, 2093.
[138] C. Olivier, B. Kim, D. Touchard, and S. Rigaut, *Organometallics*, 2008, **27**, 509.
[139] R. B. King and F. G. A. Stone, *Inorg. Synth.*, **VII**, 99.
[140] E. Viola, C. Lo Sterzo, R. Crescenzi, and G. Frachey, *J. Organomet. Chem.*, 1995, **493**, C9.
[141] M. Akita, M.-C. Chung, A. Sakurai, S. Sugimoto, M. Terada, M. Tanaka, and Y. Moro-oka, *Organometallics*, 1997, **16**, 4882.
[142] L.-K. Liu, K.-Y. Chang, and Y.-S. Wen, *J. Chem. Soc., Dalton Trans.*, 1998, 741.
[143] M. L. H. Green and T. Mole, *J. Organomet. Chem.*, 1968, **12**, 404.
[144] L. Medei, L. Orian, O. V. Semeikin, M. G. Peterleitner, N. A. Ustynyuk, S. Santi, C. Durante, A. Ricci, and C. L. Sterzo, *Eur. J. Inorg. Chem.*, 2006, 2582.
[145] M. I. Bruce, B. D. Kelly, B. W. Skelton, and A. H. White, *J. Chem Soc. Dalton Trans.*, 1999, 847.
[146] O. F. Koentjoro, P. Zuber, H. Puschmann, A. E. Goeta, J. A. K. Howard, and P. J. Low, *J. Organomet. Chem.*, 2003, **670**, 178.
[147] E. C. Constable, D. Gusmeroli, C. E. Housecroft, M. Neuburger, and S. Schaffner, *Polyhedron*, 2006, **25**, 421.
[148] S. M. Draper, M. Delamesiere, E. Champeil, B. Twamley, J. J. Byrne, and C. Long, *J. Organomet. Chem.*, 1999, **589**, 157.
[149] N. Duffy, J. McAdam, C. Nervi, D. Osella, M. Ravera, B. Robinson, and J. Simpson, *Inorg. Chim. Acta*, 1996, **247**, 99.
[150] K. Noack, *Spectrochim. Acta*, 1963, **19**, 1925.
[151] G. Bor, *Spectrochim. Acta*, 1963, **19**, 2065.
[152] C. J. McAdam, N. W. Duffy, B. H. Robinson, and J. Simpson, *Organometallics*, 1996, **15**, 3935.
[153] M. Arewgoda, P. H. Rieger, B. H. Robinson, J. Simpson, and S. J. Visco, *J. Am. Chem. Soc.*, 1982, **104**, 5633.
[154] D. Osella and J. Fiedler, *Organometallics*, 1992, **11**, 3875.
[155] B. L. Guennic, K. Costuas, J.-F. Halet, C. nervi, M. A. J. Paterson, M. A. Fox, R. L. Roberts, D. Albesa-Jove, H. Puschmann, J. A. K. Howard, and P. J. Low, *C. R. Chimie* 2005, **8**, 1883.
[156] F. Barr-Taylor, 'Novel Compounds for Application as Quantum Cellular Automata Molecular Electronics', University of Bath, Bath, 2003.
[157] J. C. Torres, R. A. Pilli, M. D. Vargas, F. A. Violante, S. J. Garden, and A. C. Pinto, *Tetrahedron*, 2002, **58**, 4487.
[158] K. C. Nicolaou, P. G. Bulger, and D. Sarlah, *Angew. Chem. Int. Ed.*, 2005, **44**, 4442.
[159] M. Vollmann and H. Butenschon, *Chimie*, 2005, **8**, 1282.
[160] O. L. Tok, E. Klimkina, Y. N. Bubnov, and B. Wrackmeyer, *Inorg. Chim. Acta.*, 2000, **300-302**, 169.
[161] R. H. Wopschall and I. Shain, *Anal. Chem.*, 1967, **39**, 1514.
[162] B. C. Berris, G. H.Hovakeemian, Y.-H. Lai, H. Mestdagh, and K. P. C. Vollhardt, *J.Am.Chem*, 1985, **107**, 5670.

[163] E. C. Constable, D. Gusmeroli, C. E. Housecroft, M. Neuburger, and S. Schaffner, *Polyhedron*, 2007, **26**, 1222.
[164] I. Aujard, J.-P. Baltaze, J.-B. Baudin, E. Cogné, F. Ferrage, L. Jullien, E. Perez, V. Prévost, L. M. Qian, and O. Ruel, *J. Am. Chem. Soc.*, 2001, **123**, 8177.
[165] J.-J. Hwang and J. M. Tour, *Tetrahedron*, 2002, **58**, 10387.
[166] D. Touchard, C. Morice, V. Cadierno, P. Haquette, L. Toupet, and P. H. Dixneuf, *J. Chem. Soc., Dalton Trans.*, 1994, 859.
[167] K. M.-C. Wong, L.-L. Hung, W. H. Lam, N. Zhu, and V. W.-W. Yam, *J. Am. Chem. Soc.*, 2007, **129**, 4350.
[168] M. B. Zaman, K. Udachin, J. A. Ripmeester, M. D. Smith, and H.-C. zur Loye, *Inorg. Chem.*, 2005, **44**, 5047.
[169] M. B. Zaman, M. D. Smith, and H.-C. zur Loye, *Chem. Mater.*, 2001, **13**, 3534.
[170] A. J. Amoroso, A. M. W. Cargill Thompson, J. P. Mahr, J. A. McCleverty, and M. D. Ward, *Inorg. Chem.*, 1995, **34**, 4828.
[171] E. Bosch, N. Schultheiss, N. Rath, and M. Bond, *Crystal Growth and Design*, 2003, **3**, 263.
[172] B. Manimaran, P. Thanasekaran, T. Rajendran, R.-T. Liao, Y.-H. Liu, G.-H. Lee, S.-M. Peng, S. Rajagopal, and K.-L. Lu, *Inorg. Chem.*, 2003, **42**, 4795.
[173] M. Ohkita, C. Adachi, M. Kawano, and T. Suzuki, *Heterocycles*, 2004, **63**, 1537.
[174] A. Guenet, E. Graf, N. Kyritsakas, L. Allouche, and M. W. Hosseini, *Chem. Commun.*, 2007, 2935.
[175] M. R. Detty, S. L. Gibson, and S. J. Wagner, *J. Med. Chem.*, 2004, **47**, 3897.
[176] R. Ackroyd, C. Kelty, N. Brown, and M. Reed, *Photochem. Photobiol.*, 2001, **74**, 656.
[177] A. D. Adler, F. R. Longo, J. D. Finarelli, J. Goldmacher, J. Assour, and L. Korsakoff, *J. Org. Chem.*, 1967, **32**, 476.
[178] J. S. Lindsey, I. C. Schreiman, H. C. Hsu, P. C. Kearney, and A. M. Marguerettaz, *J. Org. Chem.*, 1987, **52**, 827.
[179] R. G. Wollmann and D. N. Hendrickson, *Inorg. Chem*, 1977, **16**, 3079.
[180] S. J. Narayanan, S. Venkatraman, S. R. Dey, B. Sridevi, V. R. G. Anand, and T. K. Chandrashekar, *Synlett*, 2000, **12**, 1834.
[181] P. D. W. Boyd, A. K. Burrell, W. M. Campbell, P. A. Cocks, K. C. Gordon, G. B. Jameson, D. L. Officer, and Z. Zhao, *Chem. Commun.*, 1999, 637.
[182] S. Venkatraman, V. Prabhuraja, R. Mishra, R. Kumar, T. K. Chandrashekar, W. Teng, and K. R. Senge, *Indian Journal of Chemistry*, 2003, **42A**, 2191.
[183] S. Venkatraman, R. Kumar, J. Sankar, T. K. Chandrashekar, K. Sendhil, C. Vijayan, A. Kelling, and M. O. Senge, *Chem. Eur. J.*, 2004, **10**, 1423.
[184] Z. Gershman, I. Goldberg, and Z. Gross, *Angew. Chem. Int. Ed.*, 2007, **46**, 4320.
[185] J.-Q. Wang, C.-X. Ren, L.-H. Weng, and G.-X. Jin, *Chem. Commun.,*, 2006, 162.
[186] V. N. Memykin, M. McGinn, A. Y. Koposov, I. N. Tretyakova, E. V. Polshin, N. M. Loim, and N. V. Abramová, *Ukrainskii Khimiheskii Zhural*, 2005, 79.
[187] V. N. Nemykin, C. D. Barrett, R. G. Hadt, R. I. Subbotin, A. Y. Maximov, E. V. Polshin, and A. Y. Koposov, *Dalton. Trans.,*, 2007, 3378.
[188] Z. Lin, K. Nolan, C. R. McArthur, A. B. P. Lever, and C. C. Leznoff, *J. Organomet. Chem.*, 1994, **468**, 205.

[189] S. Barlow and D. O'Hare, *Chem. Rev.*, 1997, **97**, 637.
[190] P. Gütlich and J. Ensling, ed. E. I. Solomon and A. B. P. Lever, New York, 1999.
[191] V. N. Nemykin, M. McGinn, A. Y. Koposov, I. N. Tretyakova, E. V. Polshin, N. M. Loim, and N. V. Abramová, *Ukrainskii Khimiheskii Zhural*, 2005, 79.
[192] C. Ruzié, L. Michaudet, and B. Boitrel, *Tetrahedron Letters*, 2002, **43**, 7423.
[193] H. M. A. Herath, V. Karunaratne, R. M. G. Rajapakse, and A. Wickramsinghe, *Journal of Porphyrins and Phthalocyanines*, 2005, **9**, 155.
[194] S. G. Pukhovskaya, L. Z. Guseva, S. V. Makarov, A. S. Semeikin, and O. A. Golubchikov, *Russ. J. Coord. Chem.*, 2006, **32**, 563.
[195] S. George and I. Goldberg, *Acta Cryst. E*, 2005, **61**, 1973.
[196] F. Schmitt, P. Govindaswamy, G. Süss-Fink, W. H. Ang, P. J. Dyson, L. Juillerat-Jeanneret, and B. Therrien, *J. Med. Chem.*, 2008, **51**, 1811.
[197] J.-Q. Wang, C.-X. Ren, and G.-X. Jin, *Eur. J. Inorg. Chem.*, 2006, 3274.
[198] W. L. F. Armarego and C. L. L. Chai, Purification of Laboratory Chemicals, 5th Edition, Butterworth Heinemann, Amsterdam, 2003.
[199] H. E. Gottlieb, V. Kotlyar, and A. Nudelman, *J. Org. Chem.*, 1997, **62**, 7512.
[200] D. L. Musso, M. J. Clarke, J. L. Kelley, G. E. Boswell, and G. Chen, *Org. Biomol. Chem.*, 2003, **1**, 498.
[201] M. R. Mason and J. G. Verkade, *Organometallics*, 1992, **11**, 2212.
[202] D. L. Mattern, *J. Org. Chem.*, 1983, **48**, 4772.
[203] E. R. Pérez, R. M. Carvalho, R. H. A. Santos, M. T. P. Gambardella, and B. S. Lima-Neto, *Polyhedron*, 2003, **22**, 3289.
[204] N. Mantovani, M. Brugnati, L. Gonsalvi, E. Grigiotti, F. Laschi, L. Marvelli, M. Peruzzini, G. Reginato, R. Rossi, and P. Zanello, *Organometallics*, 2005, **24**, 405.
[205] M. I. Bruce, B. K. Nicholson, and O. Bin Shawkataly, *Inorg. Synth.*, 1989, **26**, 325.
[206] K. Siegmann, P. S. Pregosin, and L. M. Venanzi, *Organometallics*, 1989, **1989**, 2659.
[207] M. A. Bennett, T. N. Huang, T. W. Matheson, and A. K. Smith, *Inorg. Synth.*, 1982, **21**, 74.
[208] A. D. Becke, *Phys. Rev. A*, 1988, **38**, 3098.
[209] J. P. Perdew, *Phys. Rev. B*, 1986, **33**, 8822.
[210] M. Dolg, U. Wedig, H. Stoll, and H. Preuss, *Theor. Chem. Acta.*, 1987, **28**, 866.
[211] P. C. Hariharan and J. A. Pople, *Theor. Chem. Acta.*, 1973, **28**, 213.